LEVEL II

AD-A057599

PROCEEDINGS
FOURTH INTERNATIONAL PYROTECHNICS SEMINAR

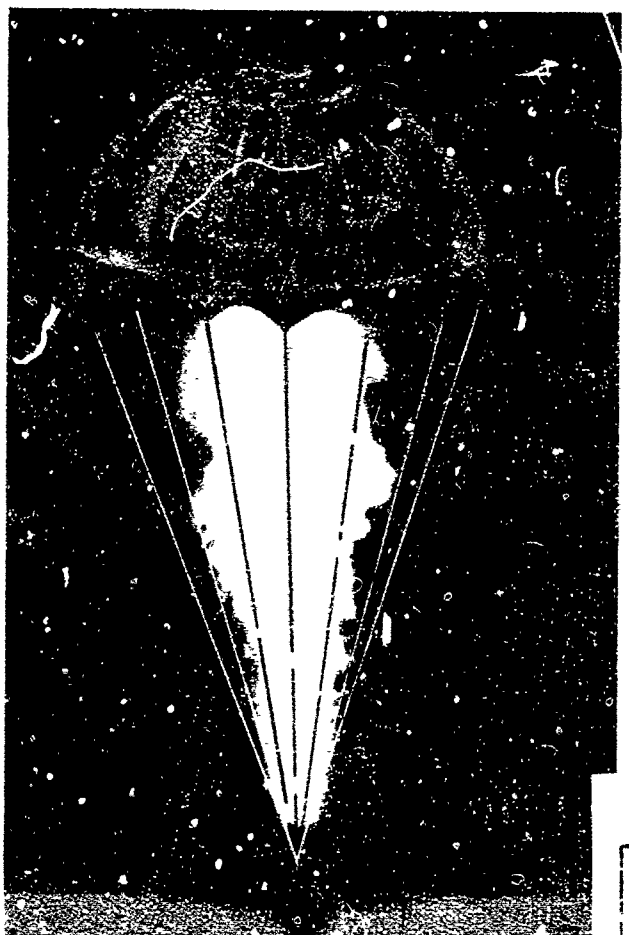

APPROVED FOR PUBLIC RELEASE
DISTRIBUTION UNLIMITED

DDC
AUG 17
D

STEAMBOAT VILLAGE INN
STEAMBOAT VILLAGE, COLORADO
22-26 JULY 1974

HOSTED BY

DENVER RESEARCH INSTITUTE/UNIVERSITY OF DENVER

AD-A057599

LEVEL III

PROCEEDINGS
OF THE
FOURTH INTERNATIONAL PYROTECHNICS SEMINAR

22-26 JULY 1974

Chairman
R.M. Blunt, Mechanical Sciences & Environvental Engineering Division

APPROVED FOR PUBLIC RELEASE
DISTRIBUTION UNLIMITED

Denver Research Institute
University of Denver
Denver, Colorado
80210

DDC
RECEIVED
AUG 17 1978
D

PAGES _____

ARE

MISSING

IN

ORIGINAL

DOCUMENT

FOURTH SEMINAR PROCEEDINGS

INTRODUCTION

As the papers began to come in for the Fourth Seminar, I looked over the Proceedings of the Third for comparison and noted with dismay that the introduction there was labelled "Fourth Seminar Proceedings"! I don't recall anyone bringing this to my attention and, therefore, draw the obvious conclusion that no one reads introductory remarks anyway. That's probably as it should be, because the real purpose of these Seminars is to provide an opportunity for the participants to exchange information and not to justify introductory comments.

It is a pleasure to acknowledge the support of the session chairmen, all of whom accepted their assignments without a quibble. The pyrotechnics community owes a real debt to the authors of the papers that will be presented; their willingness to share their knowledge provides the basis of the informational exchange that justifies these Seminars. The continuing active interest and cooperation of the Naval Air Systems Command and the Applied Sciences Department, Naval Ammunition Depot, (Crane) is also deeply appreciated.

At the time this is written, it appears that the Fourth Seminar has all the material to be a fitting successor to the three previous meetings. I hope you will find it to be so. You may be interested to learn that proceedings of the first three seminars can be obtained from the Defense Documentation Center, Cameron Station, Alexandria, Virginia 22314, by requesting AD 679911 (1st), AD 913407L (2nd) or AD 913408L (3rd).

To all of you who attend and by your presence support these Seminars, sincere thanks; your participation is essential to a successful meeting.

As always, your comments and suggestions are welcomed. If they indicate sufficient support exists for it. there may be a Fifth Seminar in 1976.

R.M. Blunt
General Chairman

June 17, 1974
Denver, Colorado

The Proceedings of the past three seminars can be obtained from:
NATIONAL TECHNICAL INFORMATION SERVICE
U.S. DEPARTMENT OF COMMERCE
5285 PORT ROYAL ROAD
SPRINGFIELD, VA 22161

Their Ordering identification is:
First -- AD 679911
Second -- AD 913407
Third -- AD 913408

ACCESSION for
NTIS White Section
DDC Buff Section
UNANNOUNCED
JUSTIFICATION
Per DDC Form 50 on file
DISTRIBUTION/AVAILABILITY CODES
Dist. AVAIL. and/or SPECIAL
A

78 08 08 148

TABLE OF CONTENTS

Paper		Page
1.	Radiative Transfer Model of a Pyrotechnic Flame, B.E. Douda	1-1
2.	Illuminant Performance in Inert Atmospheres; D.R. Dillehay	2-1
3.	Spectral Characteristics of Flares Containing Sodium Iodate as an Oxidizer, Henry A. Webster III and Clarence W. Gilliam	3-1
4.	A Mathematical Model of Flare Plume Combustion & Radiation, John E. Tanner, Jr.	4-1
5.	Flare Liner Materials, J.D. Gilbert	5-1
6.	A Comparison of the Spectra from Navy & Air Force Aircraft Parachute Flares; Henry A. Webster III	6-1
7.	The Effect of Thermal Conductivity and Gaseous Permeability on the Burning Rate of Pyrotechnic Flare Compositions; Pat Farnell and Tony Beardell	7-1
8.	A Tamp Castable Composition for Illuminating Flares, R.F. Eather	8-1
9.	Substitution of Aluminum for Magnesium as a Fuel in Flares; Bossie Jackson, Frank Taylor et al.	9-1
10.	Improved Red Tracer Flares, D.C.A. Izod, R.F. Eather	10-1
11.	Burning Rate Modifiers; D.R. Dillehay	11-1
12.	Spectroscopic Analysis of Azide Decomposition Products for use in a Pyrotechnically Initiated Carbon Dioxide Laser; Carl E. Dinerman	12-1
13.	Atmospheric Properties & Their Effect on Target Acquisition Under Flare Illumination, Gerald Bradley	13-1
14.	The Effect of Angular Velocity on Pyrotechnic Performance W.J. Puchalski	14-1
15.	Small Arms Tracer Studies Using a Rapid Scanning Spectrometer; P.N. Keliher, W.J. Puchalski	15-1
16.	Radiation Polymerization of Pyrotechnic Compositions, G.B. Franklin, C.F. Parrish	16-1
17.	NonExplosive Destruction of TNT with Hypergols, A.J. Tulis, J.N. Keith, W.K. Sumida, D.C. Heberlein	17-1
18.	Dispersion and Detonation of Explosive Dusts, A.J. Tulis, R.F. Remaly	18-1
19.	Ignition by Shock, Paul Chotard	19-1

20. Thru Bulkhead Ignition of Pyrotechnics: An Analytical & Experimental Investigation, E.A. Kjeldgaard, D.W. Larson, D.J. Gould 20-1

21. Thresholds for the Initiation of Pyrophoric Sparking, Warren W. Hillstrom 21-1

22. A Study of Fast Burning Tungsten Delay Compositions in Small Column Diameters, Scranton G. Nesbitt 22-1

23. A Pyrotechnic Fuze Timer With Selectable Settings, W. Keith Gallant 23-1

24. Tracer Munitions Using Intermetallic Reactions, A.P. Hardt 24-1

25. Pollution Abatement Reclamation of Red Phosphorous Smoke Compositions, Clarence Gilliam, Duane Johnson 25-1

26. Development of Pour Castable Smoke Compositions, G. Couture, R.E. Kluchert 26-1

27. Chemical Effects of Doping on the Litharge Silicon System, Charles A. Lipscomb, Jr. 27-1

RADIATIVE TRANSFER MODEL OF A PYROTECHNIC FLAME

Bernard E. Douda
Naval Ammunition Depot, Crane, Indiana 47522
and
Edward J. Bair
Chemistry Department, Indiana University
Bloomington, Indiana 47401

ABSTRACT

A two-line radiative transfer model for predicting the spectral radiant flux of pyrotechnic illuminating flares over a wide range of system variables such as formula, size, and ambient pressure, has been formulated and validated.

To solve the transfer equation for observed radiant intensity, the flame is represented by a model whose main characteristics are (a) the flame is a homogeneous gaseous atmosphere with plane-parallel stratification, (b) the gas consists of inert molecules plus sodium atoms which can be excited to the $^2P_{\frac{1}{2}}$ or $^2P_{\frac{3}{2}}$ level, (c) there is local thermodynamic equilibrium governed by the local temperature, (d) the temperature gradient can be represented by a parabola whose vertex is at the center of the flame, (e) the dispersion profile and number density of sodium atoms have average values, inside the flame, that are independent of depth, and (f) the individual line dispersion profile is replaced with a two-line function to simultaneously describe the spectral distribution of both of the sodium D lines.

The parameters of the radiative transfer theory were supplied from calculated thermodynamic properties of the flare. Optical thickness as a function of position in the flame was determined using computed sodium atom densities and physical flame size obtained photographically. A flame temperature gradient was constructed numerically as a function of temperature in the flame using the computed temperature at the flame center and the boundary. The two-line dispersion profile was constructed as a function of line broadening. The shape and intensity of the broadened flare spectrum was computed without introducing further assumptions.

INTRODUCTION

Illuminating flares are typically made from a mixture of magnesium, sodium nitrate, and a binder. Light is emitted from these flares at a luminous efficiency of about 50,000 candle-seconds/gram. To satisfy the continuing need to generate light more efficiently, the specific objective of this research was directed toward determining the mechanisms by which light is emitted from illuminating flames, the new knowledge providing the basis for future improvements. In this paper, I will give a summary of the recently completed work during which we developed and validated a radiative transfer model of a pyrotechnic flare. The model allows us to make predictions of the flux emitted from the flame. Further details concerning this research can be found in the final report.[1]

In this paper, I will first present the model and its theoretical basis, next experimental data needed for the model validation, and finally a comparison of experiment with the model.

THEORETICAL

It was hypothesized that the flux radiated from a flame of burning magnesium, sodium nitrate, and binder consists mainly of photons from the resonance transition of the sodium D lines. If this were the case, we should be able to predict radiative output by treating only the sodium D radiation. It is on this basis that the radiative model was developed.

We know that the total radiant intensity $I_{\nu\mu}(\tau)$ at frequency ν in a direction described by $\mu = \cos\Theta$ and issuing from a volume element at optical depth τ is given by the radiative-transfer equation[2]

$$dI_{\nu\mu}(\tau)/d\tau = \phi_{\nu a}[I_{\nu\mu}(\tau) - S_{\nu}(\tau)] . \qquad (1)$$

The optical depth τ is related to the physical depth z by $\tau_{\nu} = \int k_{\nu} dz$, where k_{ν} is the linear absorption coefficient of the flame. The normalized spectral two-line profile of the absorption coefficient $\phi_{\nu a}$ is a function which takes account

on flame line broadening mechanisms. The line-source function $S_\nu(\tau)$ accounts for increments or decrements in the radiant intensity from a volume element at optical depth τ due to emitters and absorbers within that volume element. It is defined at a given frequency by $S_\nu \equiv \varepsilon_\nu / k_\nu$, where ε_ν is the monochromatic volume emission coefficient.

Formal integration of the transfer equation yields the expression

$$I_{\nu 1} = I_{\nu 2} \exp[-(\tau_2 - \tau_1)\phi_{\nu a}/\mu] + \int_{\tau=\tau_1}^{\tau=\tau_2} [S_\nu(\tau)\phi_{\nu a}/\mu] \exp[-(\tau-\tau_1)\phi_{\nu a}/\mu] d\tau, \quad (2)$$

where τ_1 and τ_2 are the optical depth integration limits from front to the rear of the atmosphere respectively, and $I_{\nu 1}$ and $I_{\nu 2}$ are the spectral intensity at optical depths τ_1 and τ_2 respectively. In order to solve the transfer equation, for the observed radiant intensity, the flame is represented by the following model.

(1) The flame is a homogeneous gaseous atmosphere with plane-parallel stratification.

(2) The gas consists of inert molecules plus sodium atoms which can be excited to the $^2P_{\frac{1}{2}}$ or $^2P_{\frac{3}{2}}$ level.

(3) There is local thermodynamic equilibrium LTE governed by the local temperature.

(4) Energy exchange by radiation leads to radiative equilibrium.

(5) The refractive index of the medium is unity.

(6) The radiation is unpolarized when emitted and remains unpolarized in its interactions with flame species.

(7) The temperature gradient can be represented by a parabola whose vertex is at the center of the flame.

(8) The absorption profile $\phi_{\nu a}$ and number density of sodium atoms N_0 have average values, inside the flame, that are independent of τ.

The form of Eq. (2) has been simplified for the present case, namely (a) the observed flux is that emerging normal to the surface (μ=1), (b) no flux is incident on the rear surface of the atmosphere ($I_{\nu 2}$=0), and (c) $S_\nu(\tau) = B_\nu(T')$ for the LTE case where $B_\nu(T')$ is the Planck function. Under these conditions, integrating from the front surface, where z and τ_1 are 0, to the rear surface where $\tau_2 = T$, the total optical thickness, the monochromatic emergent intensity is

$$I_\nu^\circ = \phi_{\nu a} \int_{\tau=0}^{\tau=T} B_\nu(T') \exp(-\tau\phi_{\nu a}) d\tau . \qquad (3)$$

The theoretical relative spectral radiant power $\phi_{\nu a}$, proportional to spectral emergent intensity I_ν° for a particular model, was found by numerical integration of Eq. (3) using Simpson's rule of 2m intervals. Each computed spectrum Φ_λ, normalized to a power maximum of unity, is plotted for comparison with the corresponding experimental flare spectrum Φ_λ' in Figs. 1 and 2.

Parameters of the theory that must be supplied from properties of the flame are (1) optical thickness $\tau(z)$ as a function of position in the flame, (2) a flame temperature gradient $T'(z)$ as a function of position in the flame, and (3) the scattering profile a parameter in $\phi_{\nu a}$.

EXPERIMENTAL

The test flares were composed of 50 g of a magnesium-sodium nitrate-binder mixture compressed into 3.3 cm i.d. by 5.5 cm long paper tubes, having formulas shown in Table 1. Formula groups 1, 2, and 3 are nearly stoichiometric mixtures, the sodium nitrate in groups 2 and 3 being .1 and .01 of group 1 respectively. Stoichiometry was maintained in groups 2 and 3 by addition of potassium nitrate chosen because it reacts with magnesium at about the same rate as sodium nitrate and because of its low-emissivity in the neighborhood of the sodium D lines, the region of interest for these studies.

Each of three different illuminating composition formulas was tested in air at 8 levels of pressure; namely 760, 630, 300, 225, 150, 75, 30 and 6 torr. For each pressure-formula combination, the burning time, flame size, and relative spectral radiant power distribution in the visible region were recorded.

Relative radiant power spectra Φ_λ' of typical flares for each pressure-formula combination are plotted in Figs. 1 and 2. The solid curves in Figs. 1 and 2 are the experimental data. These spectra are normalized to a peak value of unity for convenience in the first step of the theoretical comparison. Spectra were not obtained for formula groups 2 and 3 at 6 torr because the flares did not sustain combustion at this pressure. Group 1 flares at 6 torr barely burned. Combustion difficulty was visually observable for all flares tested at 75 torr or less.

Values of the physical flame depth z' range from 6 cm for formula group 1, 760 torr to 2.5 cm for formula group 3, 30 torr, a rather narrow range considering the large range of experimental conditions.

DISCUSSION

Visual comparison of the theoretical Φ_λ and experimental Φ_λ' relative radiant power spectra, plotted in Figs. 1 and 2, shows that the distribution computed from theory agrees quite well with the experimental distribution for each pressure-formula combination.

In summary, it has been shown that the spectral radiant power distribution of a pyrotechnic illuminating flare flame can be predicted by a two-line radiative transfer model which has been described. This can be done without introducing assumptions which require *ad hoc* modifications of the model to describe different flares. Known system variables such as flare formula, flare size, and ambient pressure are the necessary and sufficient input needed for the theoretical prediction.

REFERENCES

1. B. E. Douda, *Radiative Transfer Model of a Pyrotechnic Flame*, RDTR No. 258, Naval Ammunition Depot, Crane, Indiana (1973). Available from National Technical Information Service, 5285 Port Royal Road, Springfield, Virginia 22151. AD# 769237.

2. D. G. Hummer, J. Quant. Spectrosc. Radiat. Transfer 8, 193 (1968).

TABLE 1. Flare Formulations

Ingredients	Formula Groups 1	2	3
Magnesium	44.0[a]	40.4	40.04
Sodium nitrate	51.5	5.15	0.515
Potassium nitrate	--	49.95	54.945
Epoxy binder mix	4.5	4.5	4.5

[a]Percent by weight

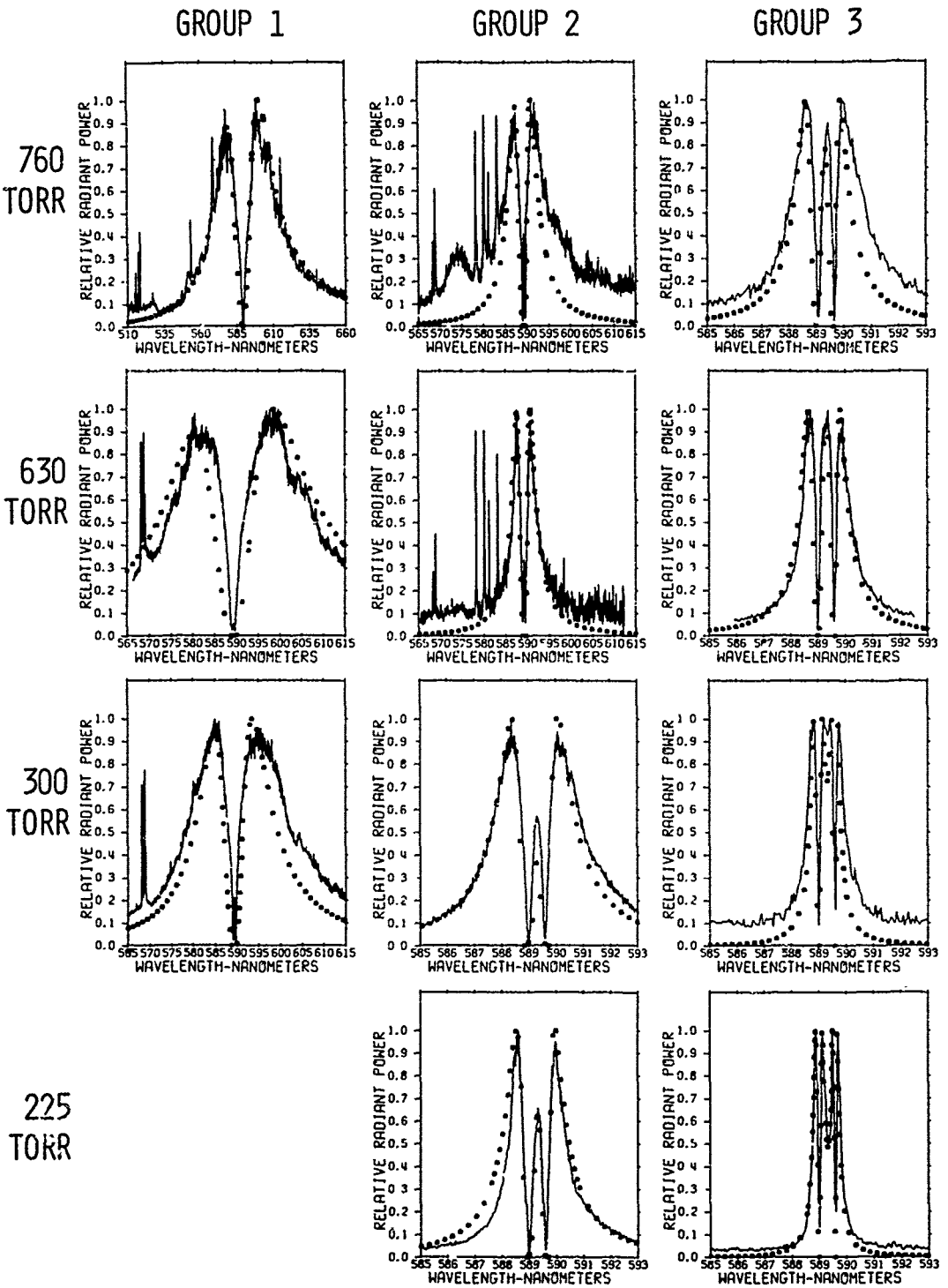

Fig. 1. Illuminating Flare Flame Spectra for formula groups 1, 2, and 3 at 4 levels of ambient pressure. Theoretical relative radiant power values Φ_λ are indicated by boxes ( ). Experimentally determined relative radiant power values Φ_λ' are shown by the solid line.

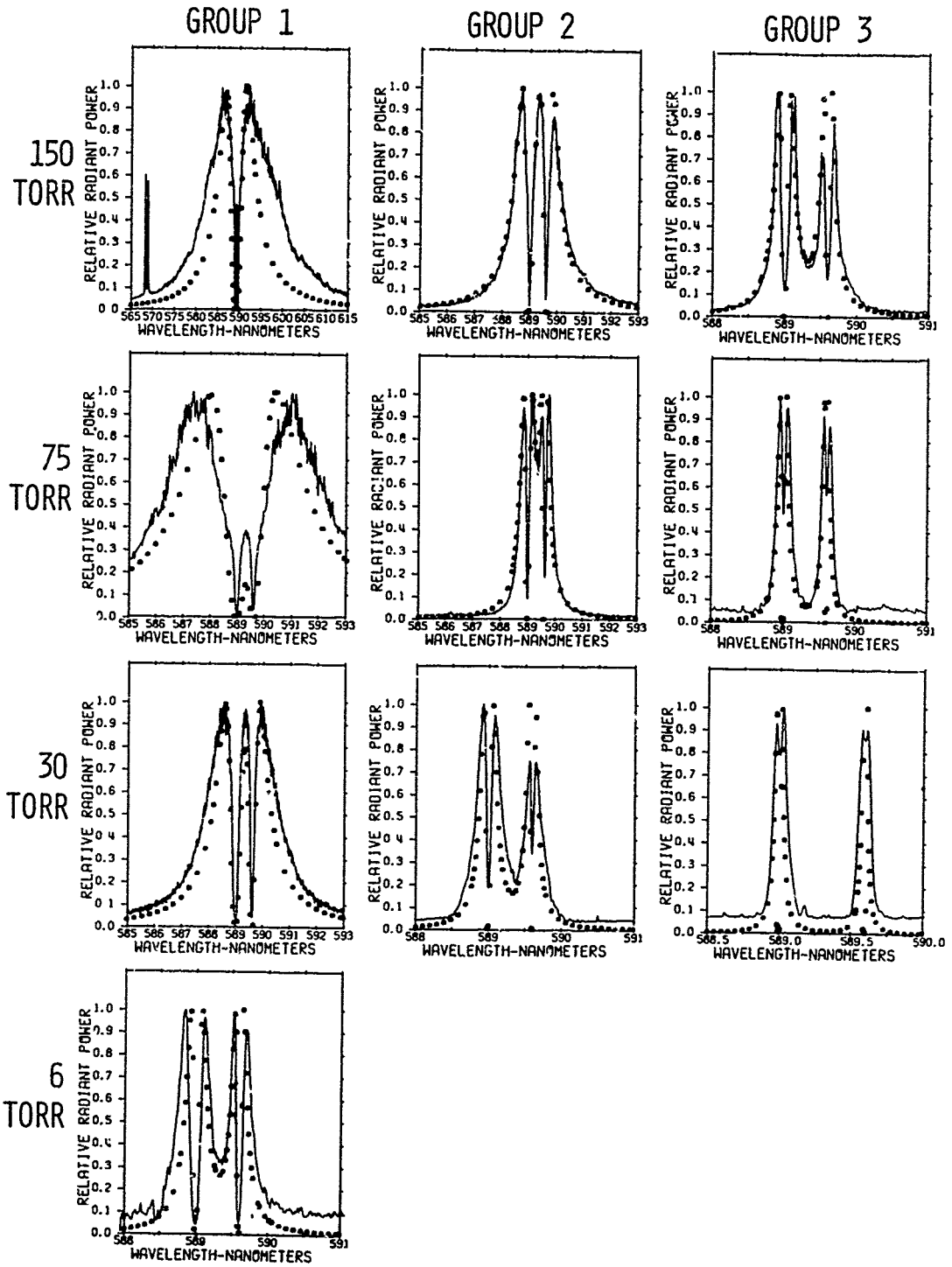

Fig. 2. Illuminating Flare Flame Spectra for formula groups 1, 2, and 3 at 4 levels of ambient pressure. Theoretical relative radiant power values Φ_λ are indicated by boxes (□). Experimentally determined relative radiant power values Φ_λ' are shown by the solid line.

ILLUMINANT PERFORMANCE IN INERT ATMOSPHERES

David R. Dillehay

Thiokol Corporation
Longhorn Division
Marshall, Texas

ABSTRACT

As part of the continuing investigation of illuminant combustion processes, three sets of candles were burned in air, argon, and nitrogen at a pressure of 760 torr. The mixes included a near-stoichiometric formulation and fuel rich formulation. The performance variations and outputs may shed some new light on the complexity of the combustion reactions and aid in modifying models of luminance production.

INTRODUCTION

Although illuminant compositions have been in use for many years, the details of the physical and chemical processes which result in the spectral output are not well understood. In the last few years, several researchers have started to delve into the theoretical aspects of illuminant combustion. Part of the problem has revolved around lack of sufficient data on illuminant formulations burned under carefully controlled and variable conditions. The work reported by Douda[1] on the effect of pressure on the sodium D-line profile is an excellent example of the type of data that will finally lead to an acceptable model of a flare plume. This report will describe data gathered as part of a study on illuminant burning rates. The data suggests some interesting hypotheses for consideration in illuminant combustion problems.

EXPERIMENTAL PROGRAM

The experimental data was developed at Denver Research Institute. Most of the test candles were manufactured at Longhorn Army Ammunition Plant. The formulations and physical dimensions of the candles tested are given in Table I.

A cylindrical chamber approximately two meters in both length and diameter with a volume of about 6.28 m^3 was used to contain the flare in the desired atmosphere during combustion. The chamber is equipped with several windows that permit the flare plume to be observed simultaneously with spectrographs, radiometer/photometer devices and cameras for a variety of characteristics. The chamber was evacuated to less than 1 torr and refilled to 760 torr from a compressed gas manifold and tanks of commercial argon or nitrogen, or locally compressed air.

The interior of the chamber and the permanent fixtures were painted a high reflectance white. A baffle prevented direct radiation from reaching the E.G.& G. Model 580 Photometer; and the effect was essentially that of an integrating photometric sphere. This arrangement of photometer and chamber was calibrated by placing a standard lamp in the spot usually occupied by the flare and recording the reading of the photometer on a strip chart. The deflection of the recording pen was adjusted to a constant value regardless of variations in the lumens/ft^2 read by the meter on the photometer. Small changes in the chamber wall reflectance were removed by this procedure. Frequent cleaning of the chamber was essential, however.

The flame was positioned with respect to a base-line established by a He/Ne laser beam that also served to align the camera and the spectrograph.

[1]Douda, B.E., "Radiative Transfer Model of a Pyrotechnic Flame", RDTR No. 258, Naval Ammunition Depot; Crane, Indiana. Sept. 26, 1973.

The candle was located 51mm below this reference line, which passed through the center of the spectrograph slit and the camera lens. A beam divider was used to insure the same viewpoint for camera and spectrograph.

The spectrograph was a 3 meter grating instrument with a reciprocal dispersion of 11A/mm that can record on a 35mm strip the region from 3500 A to 7000 A. The glass windows on the test chamber limited the short wavelength record to about 4000 A and the Linagraph Shellburst film response limited the long wavelength record to roughly 6500 A. Processing the film in Ek Co. Type 448 Monabath minimized the effects of variations in time and temperature on film density.

Still pictures were taken with a Rolleicord camera at f/22, 1/30 second on Plus X film through a neutral density of 3.0. This exposure produced a range of photographic densities at the position of the most intense region of the flame that are in the linear region of the H & D curve. Motion pictures were made at 150 to 250 frames per second with a Locam camera on 16mm Plus X Negative stock; the 1/900 - 1/1500 second exposure required a change to N.D. 2.0 filtration and f/5.6 to produce densities similar to those in the still photographs.

Ignition of the flare candles was accomplished by passing a low voltage current through an "Atlas" electric match that had been fixed to the top of the candle with masking tape.

RESULTS

Combustion in air in the chamber gave results similar to candles burned at Longhorn for controls. A summary of the burning rate and candlepower of each of the formulations is given in Table II.

Combustion in both nitrogen and argon showed marked decreases in candlepower although the burning rate was not significantly affected. In all cases, the flames in air are larger than the flames in nitrogen or argon. Table III summarizes the results in nitrogen and argon normalized to the results in air. (See Figures 1-14)

In examination of the results, it is apparent that the oxygen in the air must contribute significantly to the production of light in magnesium-sodium nitrate flares. Further, removal of the oxygen from the air, as in the nitrogen tests, results in reduction of light output greater than for substitution of the inert gas, argon. The complexity of the combustion problem is evident. However, a hypothesis may be offered for further testing. Consider the flame as composed of three basic zones. The central zone is a region assumed to be roughly in thermodynamic equilibrium as defined

by the calculated thermodynamic reactions of the NASA-Lewis SP-273 Complex Equilibrium Program. The second zone is the radiation volume, limited on the interior by the optical depth for a radiation wavelength under consideration and on the exterior by the lower temperature limit for Plankian radiation. The third zone is the outer reactive envelope where external mixing with the atmosphere occurs. In the case where the external atmosphere is air, the oxygen in the air reacts with the combustion products and provides two benefits. First, the temperature of the third zone is increased, thereby creating an insulative layer of hot gas which reduces the heat loss of the central zone and produces additional thermal excitation of sodium. The radiative volume is increased since the lower temperature limit is moved further out. Secondly, the oxidation of sodium vapor to sodium oxide will proceed at approximately 2040°K. Unless it is oxidized and removed, the cooler sodium vapor will absorb a significant amount of visible radiation.

Consider the results from the tests for 5% binder and 40, 47.5, and 55% magnesium summarized below.

	BR, in/sec			Candlepower, $X10^{-3}$		
% Mg	Air	Argon	Nitrogen	Air	Argon	Nitrogen
40	.062	.061	.063	80	50	38
47.5	.074	.071	.076	137	42	28
55	.086	.088	.094	178	26	20

The 40% magnesium formulation is close to the theoretical stoichiometric formulation. The candlepower in argon would be expected to be the same as in air since there is little non-combusted material available for reaction with the oxygen in the air. The enhancement realized on burning in air can, however, be explained as the combustion of the excess sodium vapor, removing the sodium as sodium oxide and reducing absorption. Some effect on temperature in the outer zone may also be postulated. On the other hand, in nitrogen the candlepower is reduced because of the very efficient quenching cross-section of nitrogen relative to sodium. It may be noted that this effect undoubtedly occurs in air but is overcome by the effect of the oxygen.

The burning rate of the illuminant is the same regardless of the external atmosphere. This implies that the physical plume is about the same size for a candle whether burned in air, argon, or nitrogen. However, it may be seen in the photographs that the visible plume decreases in size as the external atmosphere goes from air to argon to nitrogen. This effect is in keeping with the postulate.

It is felt that significant improvement in theory will result from additional tests covering a broader range of test conditions.

TABLE I

COMPOSITION OF FLARES

Flare Type	% Mg	% $NaNO_3$	% Binder	Type Binder	Wt. in grams	Lengt cm.	Mg in.	Dia. cms	Area cm^2
1	40.0	52.0	8.0	A	58	4.0	X	3.1	7.55
2	47.5	44.5	8.0	A	66	4.8	X	3.1	7.55
3	55.0	37.0	8.0	A	70	5.4	X	3.1	7.55
4	60.0	32.0	8.0	A	59	4.6	X	3.1	7.55
5	40.0	55.0	5.0	A	59	4.2	X	3.1	7.55
6	55.0	40.0	5.0	A	59	4.6	X	3.1	7.55
7	47.5	47.5	5.0	A	59	4.4	X	3.1	7.55
31	44.0	51.5	4.5	B	50	3.0	Y	3.45	9.35
32	58.0	37.5	4.5	B	50	3.0	Y	3.45	9.35

A ERL 2774 50% DMP 30 7.5% LP 33 42.5%

B DER 321 61% DER 732 25% CX 3482.1 14%

X WASATCH 30/50 Ball Milled

Y JAN-M-382A TYPE III Gran 18

TABLE II

SUMMARY OF RESULTS

	Air			Argon			Nitrogen		
Flare Type	KCDLA	Rate	KCPS/GM	KCDLA	Rate	KCPS/GM	KCDLA	Rate	KCPS/GM
1	82	.052	43.1	26.0	.048	14.7	23.0	.048	12.9
2	133	.060	63.5	14.7	.064	6.4	10.7	.063	4.9
3	177	.076	67.8	5.0	.075	2.0	4.8	.075	2.0
4	160	.076	65.2	2.4	.084	0.9	2.7	.098	0.8
5	80	.062	36.0	50.0	.061	23.0	37.8	.063	16.9
7	137	.074	54.0	41.5	.071	17.3	28.0	.076	10.8
6	178	.086	63.5	25.8	.088	8.9	20.0	.094	6.4
31	60	.042	33.6	22.0	.045	11.5	20.0	.044	10.8
32	140	.060	55.0	12.0	.062	4.8	13.3	.061	5.2

Where: KCDLA = Kilocandela
Rate = Linear burning rate, in/sec.
KCPS/GM = Kilocandela - seconds per gram of mix

TABLE III

RESULTS NORMALIZED TO AIR

Flare Type	Argon		Nitrogen	
	KCDLA	Rate	KCDLA	Rate
1	.313	0.904	.242	0.923
2	.118	1.100	.086	1.050
3	.031	1.000	.025	1.000
4	.015	1.100	.017	1.290
5	.625	0.984	.472	1.010
7	.302	0.960	.220	1.030
6	.146	1.020	.112	1.090

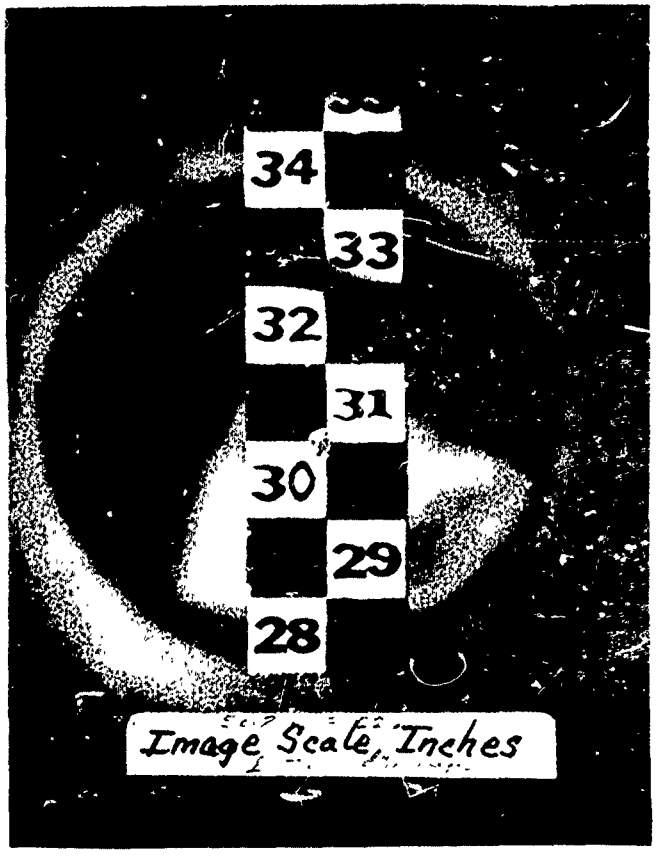

Figure 1

Figure 2

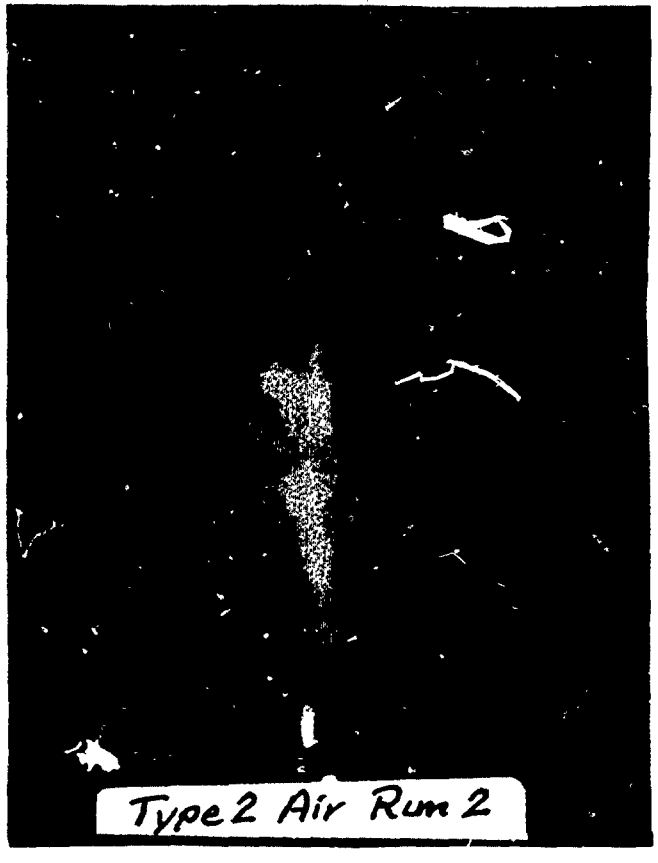

Figure 3

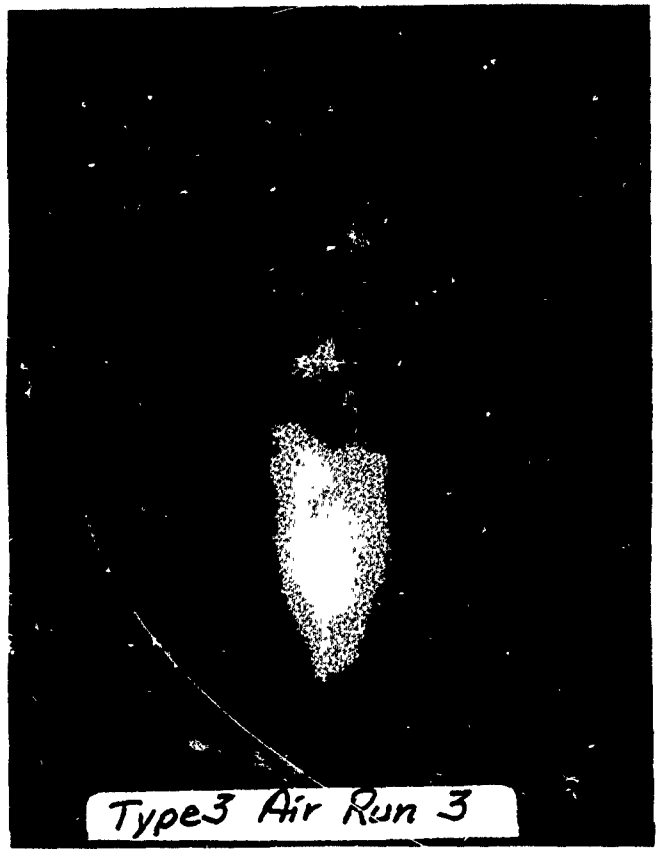

Figure 4

Figure 5

Figure 6

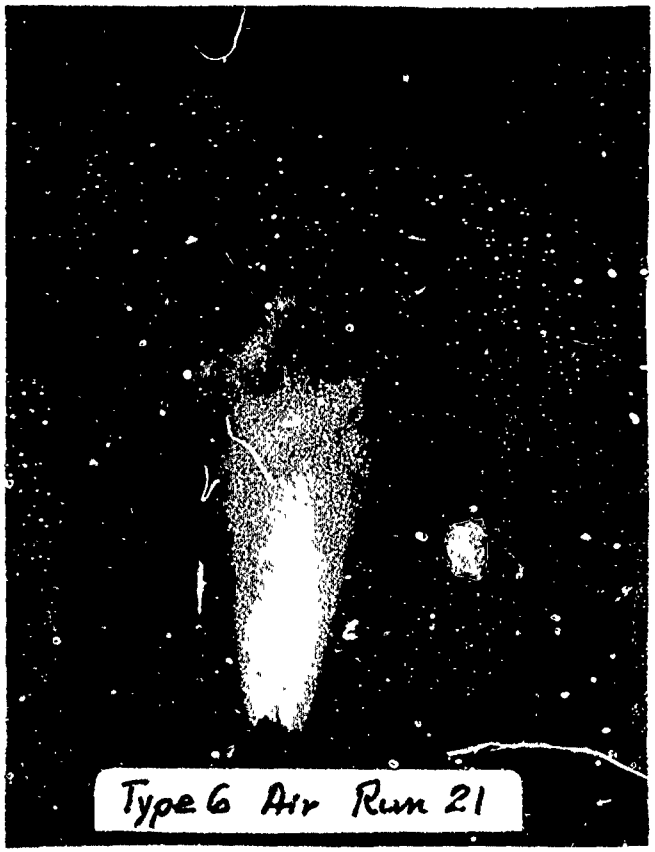

Figure 7

Figure 8

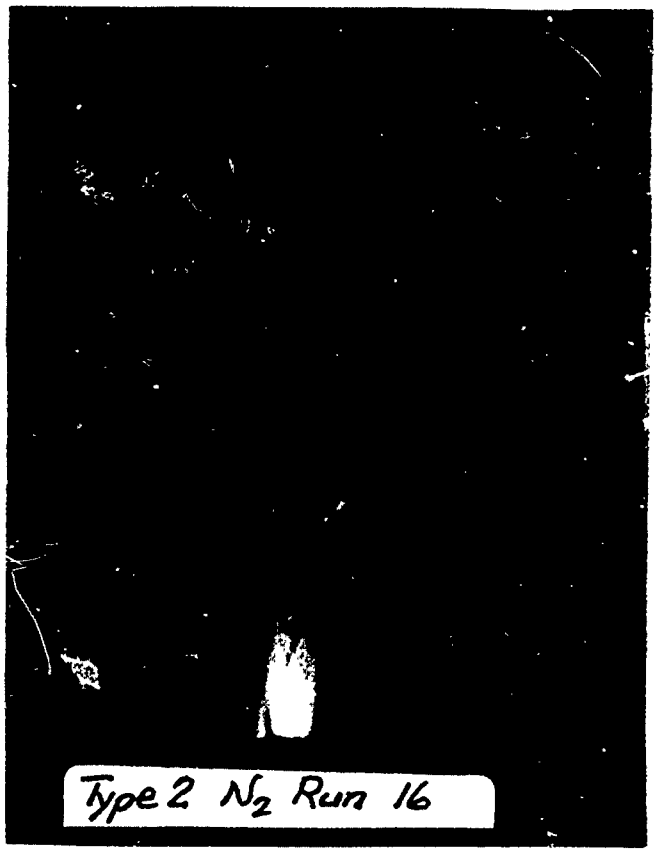

Figure 9

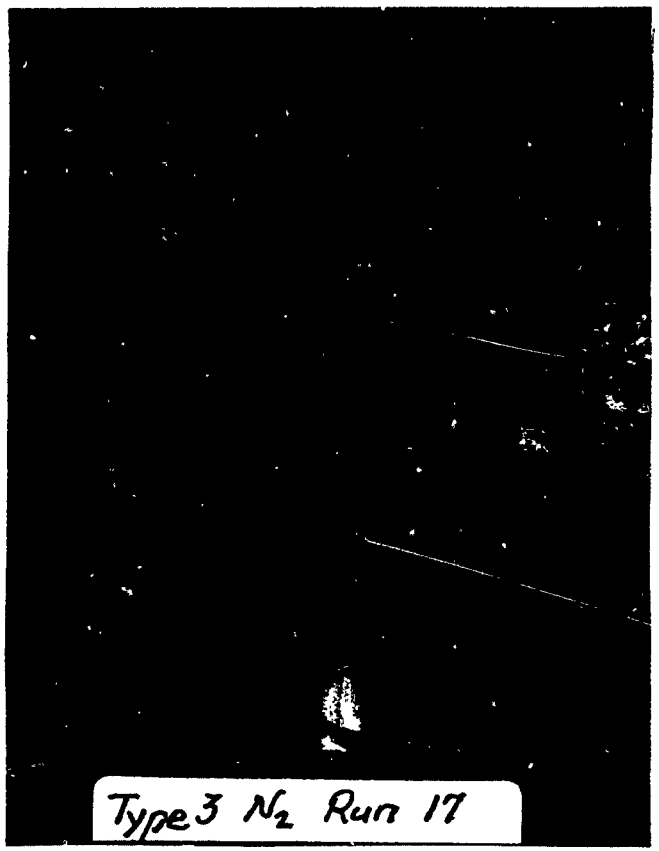

Figure 10

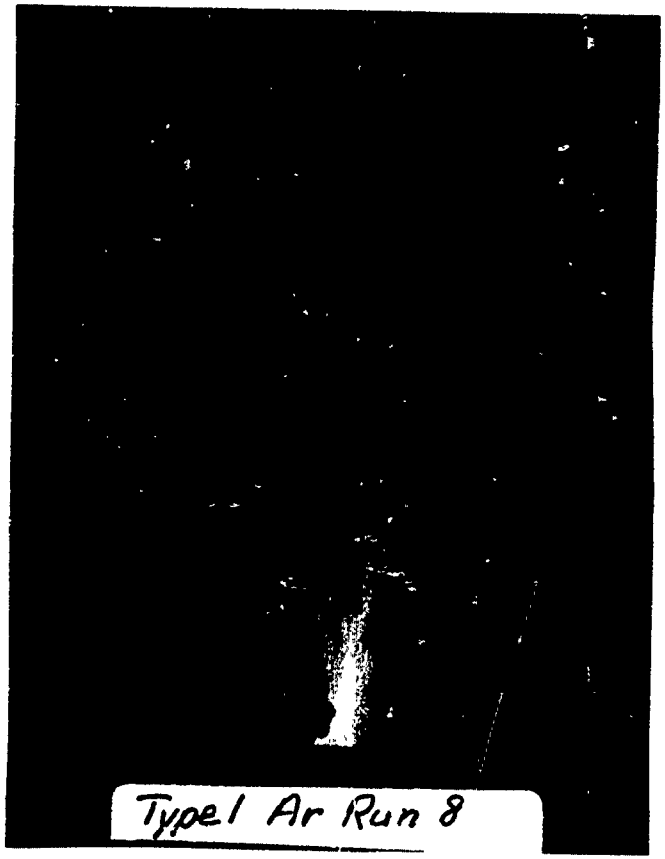

Figure 11

Figure 12

Figure 13

Figure 14

SPECTRAL CHARACTERISTICS OF FLARES CONTAINING SODIUM IODATE AS AN OXIDIZER

Henry A. Webster III
and
Clarence W. Gilliam
Applied Sciences Department
Naval Ammunition Depot, Crane, Indiana 47522

ABSTRACT

Spectra are presented for several flare formulations which incorporated sodium iodate as the oxidizer and magnesium as the fuel. While the flares containing iodate did not produce increased candlepower, several new spectral features were observed. One of the most interesting features was increased emission in the blue region of the spectrum over that obtained from the typical magnesium-sodium nitrate formulations. This emission is attributed to the recombination of iodine atoms in the $^3\pi_{o^+u}$ electronic state of molecular iodine followed by emission from this state. Other emission features are discussed. Color measurements indicate that the iodate flares are more "white" possibly making them better for target acquisition than sodium nitrate flares.

INTRODUCTION

Obtaining high light output efficiency from pyrotechnic devices has always been a major problem and it would be a tremendous advantage if the efficiency could be improved substantially.

Light output from the chemical reactions in flares originates by atoms or molecules in an excited state dropping to the ground state, emitting radiation. Traditional pyrotechnic reactions produce species in their ground state. Some of these species are then excited to an upper electronic state by a purely thermal mechanism. Thermal excitation, however, is a very inefficient method of producing excited species.

If the emitting species in a pyrotechnic reaction could be formed directly in an excited state, the efficiency could be greatly improved. If the excited state molecule can also be chosen to emit in specific wavelength regions, the regions of interest would be from 430-570 nm, i.e. that region where sodium does not emit strongly.

Arnold, Finlayson and Ogryzlo discovered an intense iodine chemiluminescence in the yellow region of the spectrum and attributed it to iodine atom recombination.[1] As far as can be determined, iodine compounds have not been considered for illuminating compositions.[2]

EXPERIMENTAL

In order to test the applicability of using sodium iodate as an oxidizer and to obtain specific emission from iodine, flares were made with the formulas shown in Table 1. Control flares composed of magnesium-sodium nitrate were also prepared. The flares were 33 mm in diameter, 25 mm long and contained 50 grams of composition. In addition, two grams of boron-barium chromate were pressed on the candles as a first fire.

The flares were burned face up at a distance of 400 cm from the measuring instruments. Relative luminous energy and burning times were monitored by recording the output of an EG&G Model 580 radiometer equipped with a photometric filter on an x-y plotter. Table 2 contains a summary of the relative powers and burning times.

TABLE 1

FLARE COMPOSITIONS

Ingredient	Group 101	102	103	104	105
Mg	28.5	38.5	48.5	58.0	44.0
$NaIO_4$	67.0	57.0	47.0	--	--
$NaNO_3$	--	--	--	37.5	51.5
Binder	4.5	4.5	4.5	4.5	4.5

TABLE 2

RELATIVE POWERS AND BURN TIMES

Group	Relative Power	Burn Time
101	0.17	20 sec.
102	0.32	26 sec.
103	0.28	28 sec.
104	1.00	23 sec.
105	0.93	25 sec.

To prevent confusion over actual candlepower values which would obviously be different for these small diameter flares when compared with full size illuminating flares, the data are all normalized relative to the fuel-rich magnesium-sodium nitrate formulation, Group 104.

At the same time that the power measurements were made, spectra were taken in the visible region from 380 nm - 680 nm. The spectra were taken on a Bausch and Lomb 1.5-m grating spectrograph using Linagraph Shellburst film. The instrument is equipped with a 450 groove/mm grating blazed at 490 nm and has a dispersion of 15 Å/mm in the first order. The flare was masked in such a way that the light hitting the spectrometer was from the region of the flame approximately two flare diameters above the burning surface.

After each flare spectrum was taken, several spectra of a 200 watt quartz iodine lamp were taken on the same film. These spectra were used to correct the flare spectra for the film response.

In an effort to study the new emission features apparent in the sodium iodate flares, spectra were taken at higher resolution with a 1-m Spex grating spectrograph. This spectrograph is equipped with a 1200 g/mm grating blazed at 500 nm. To provide the higher resolution, spectra were taken in the second order over the limited wavelength region from 515-580 nm. The spectrograph dispersion in this region in the second order is 2.7 Å/mm. Kodak Tri-X glass plates were used for recording the spectra.

Microdensitometer traces of all spectra were made on an Optronics densitometer. For the low resolution results, digital readings of film density were recorded at 100 micron, i.e. 1.5 Å, intervals along the entire wavelength region. For the high resolution spectra, digital readings were recorded at 12.5 micron, i.e. 0.03 Å, in the wavelength region used. The density readings were converted to radiant power by applying the film correction function generated from the quartz-iodine lamp spectra. These spectra were then converted to luminous power spectra by multiplying the radiant power by the photopic luminous efficiency function, i.e. the eye response curve.[3]

The resulting spectra normalized to a value of one at the maximum emission are shown in Figs. 1-11. Figure 11 is the high resolution spectra of Group 101 magnesium-sodium iodate.

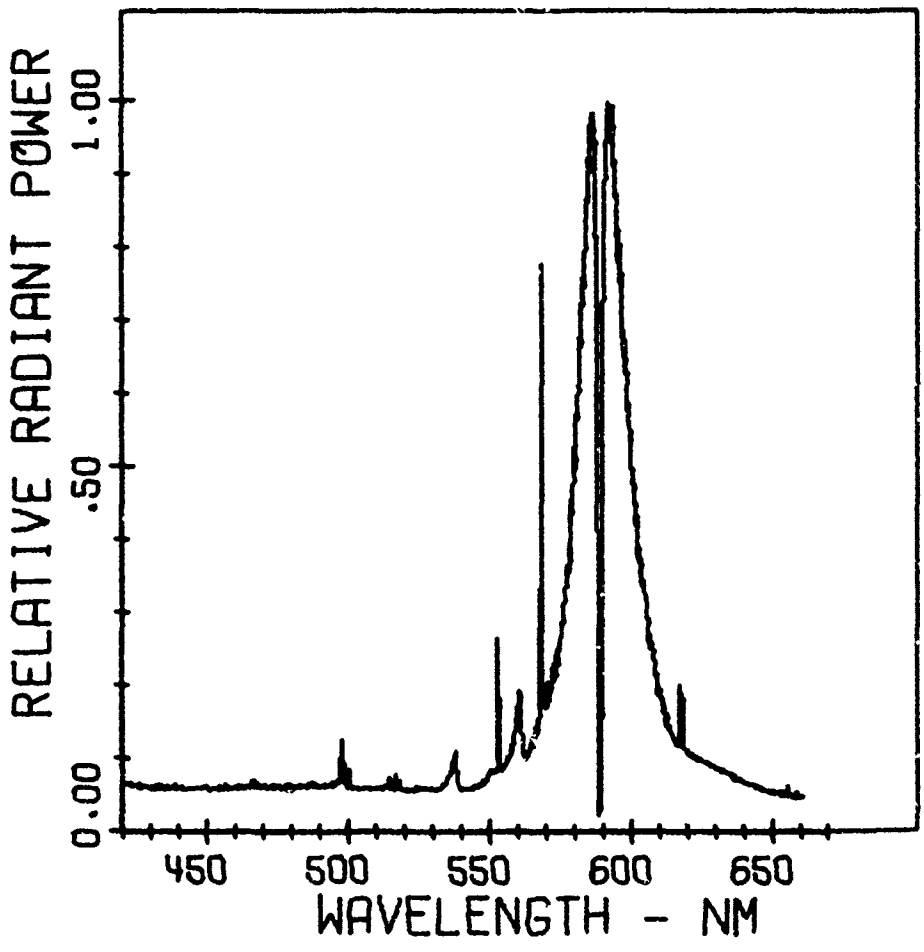

FIGURE 1. Group 101

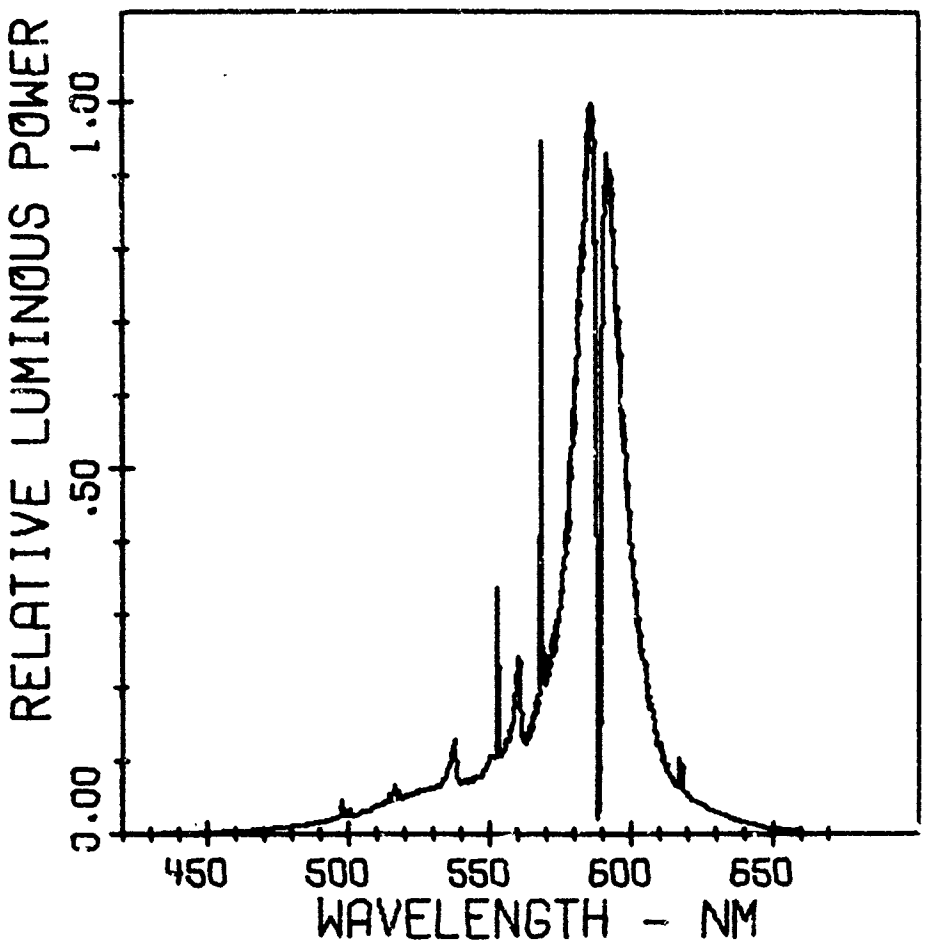

FIGURE 2. Group 101

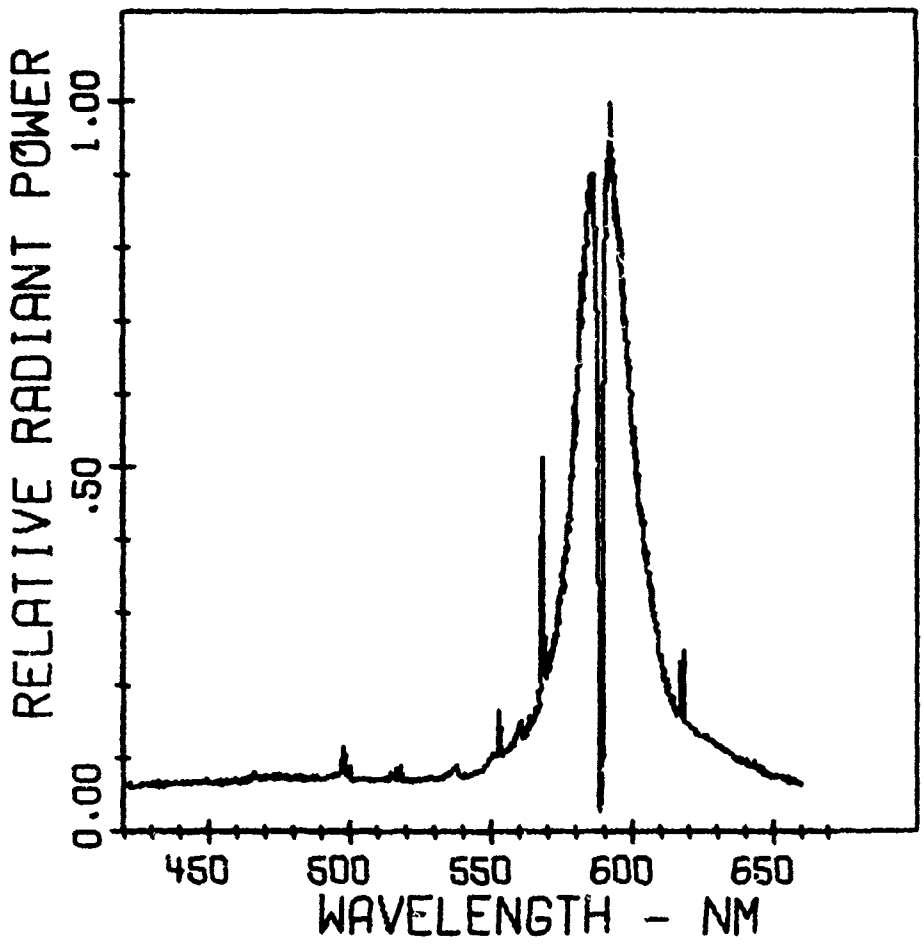

FIGURE 3. Group 102

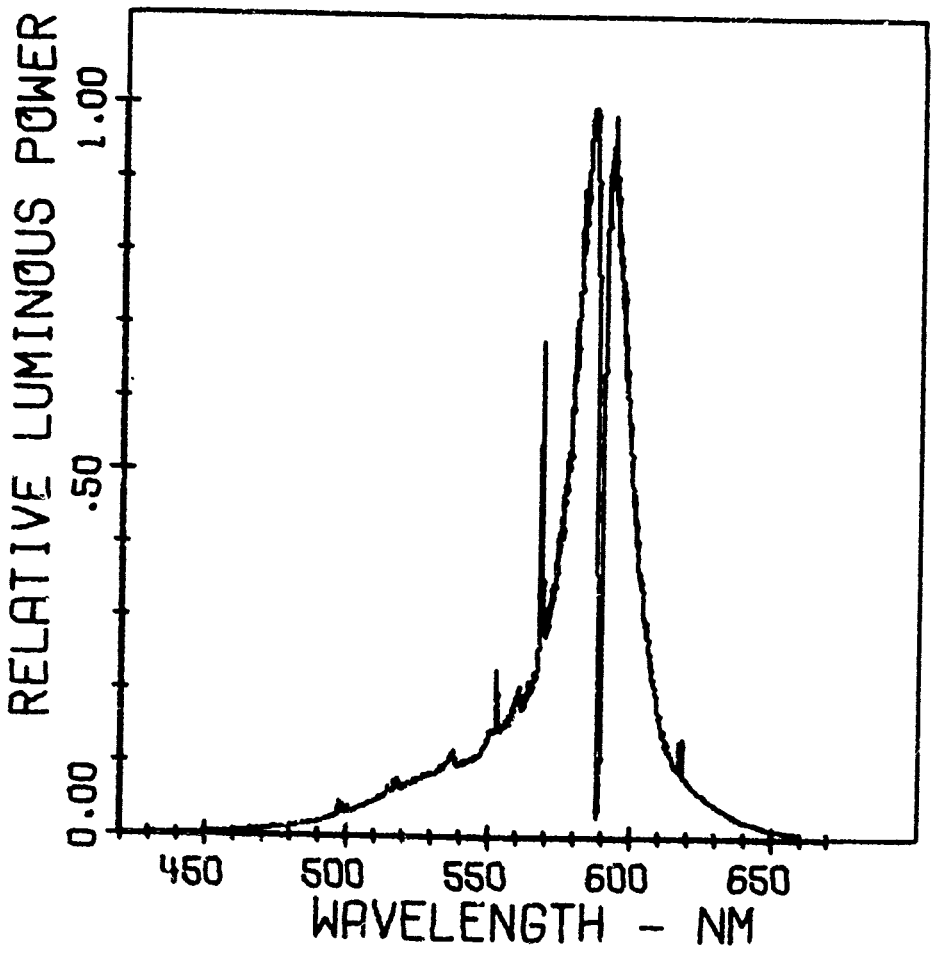

FIGURE 4. Group 102

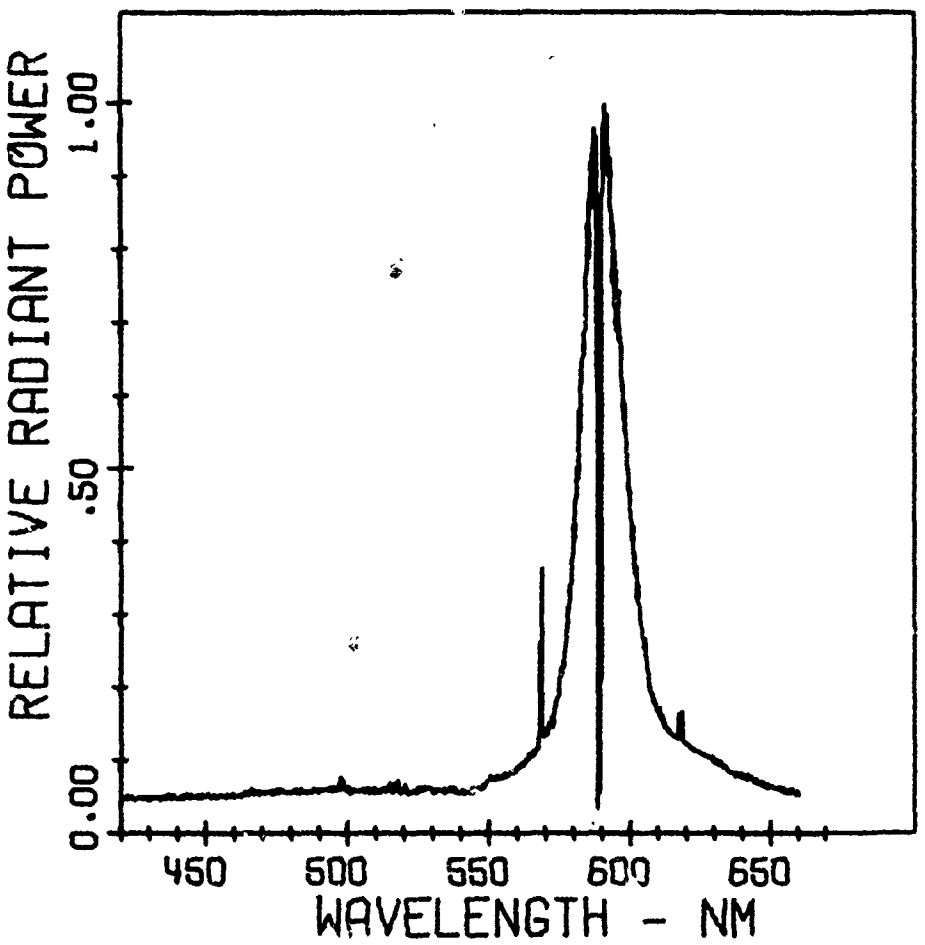

FIGURE 5. Group 103

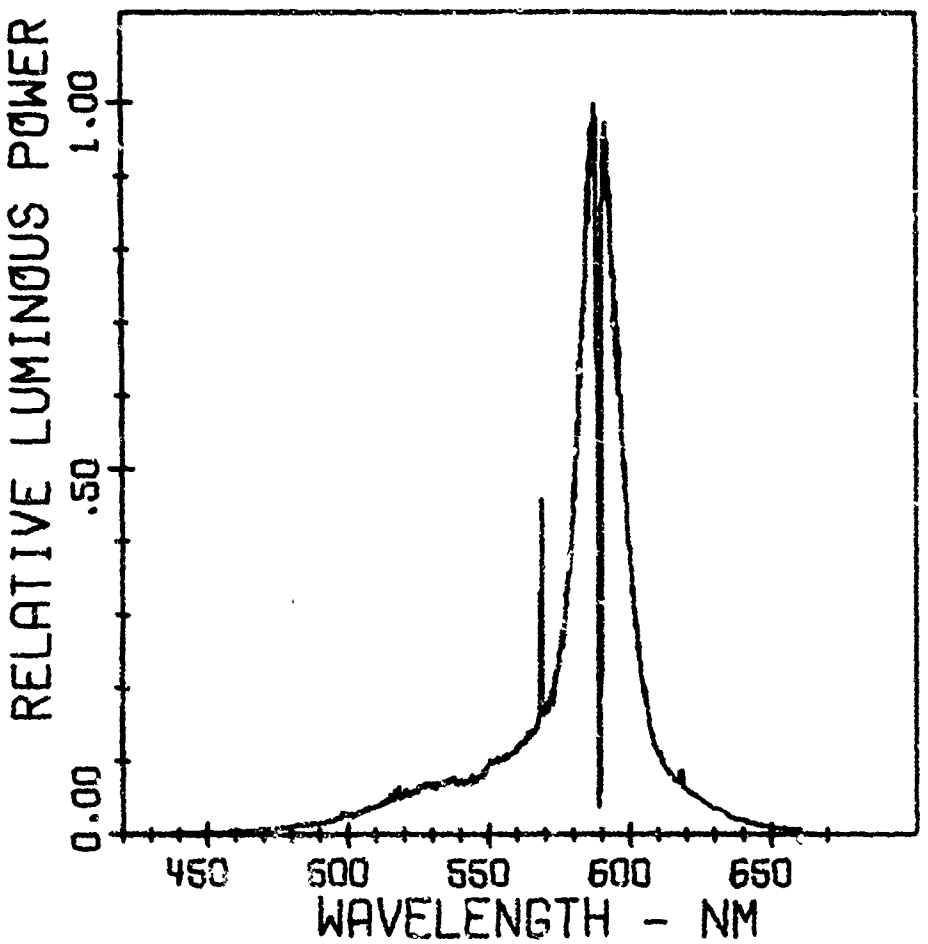

FIGURE 6. Group 103

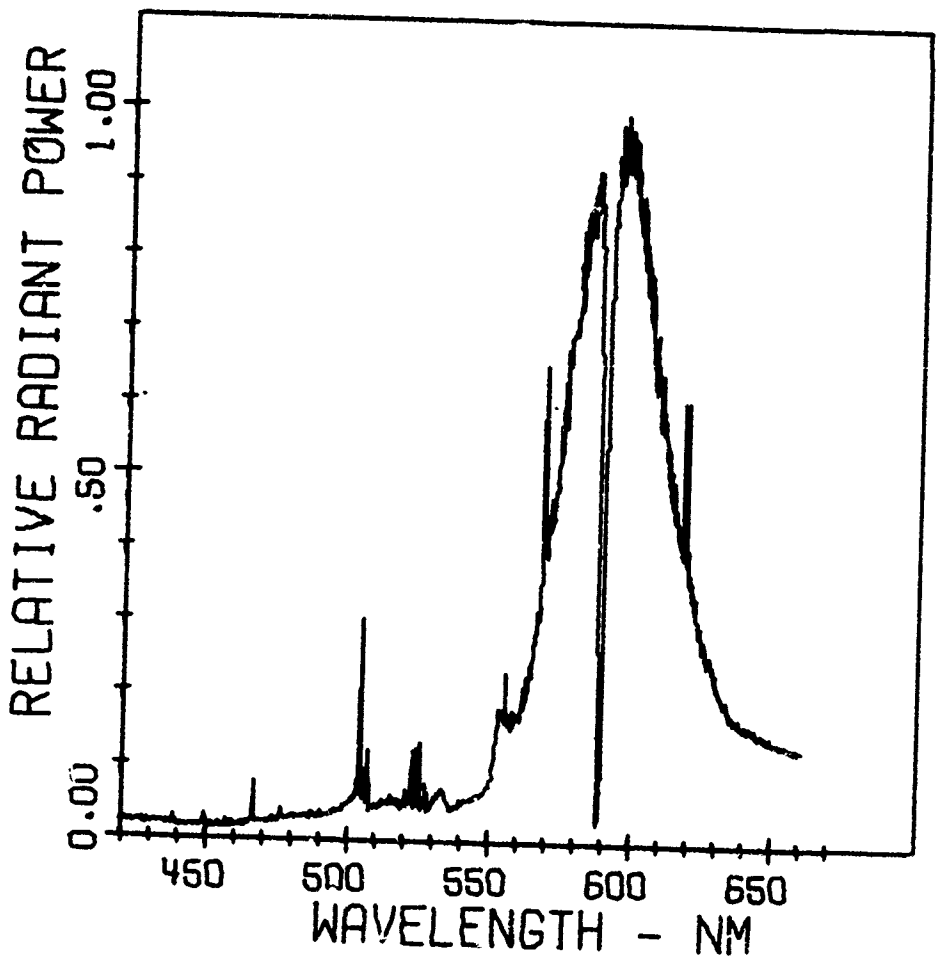

FIGURE 7. Group 104

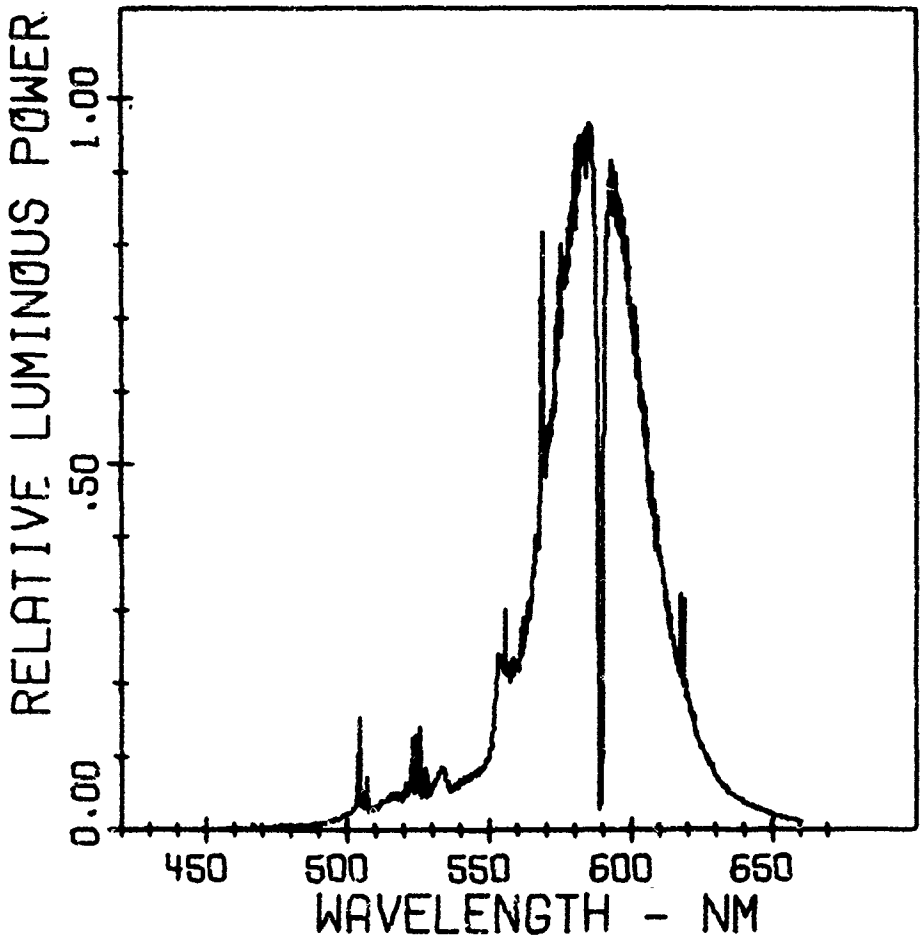

FIGURE 8. Group 104

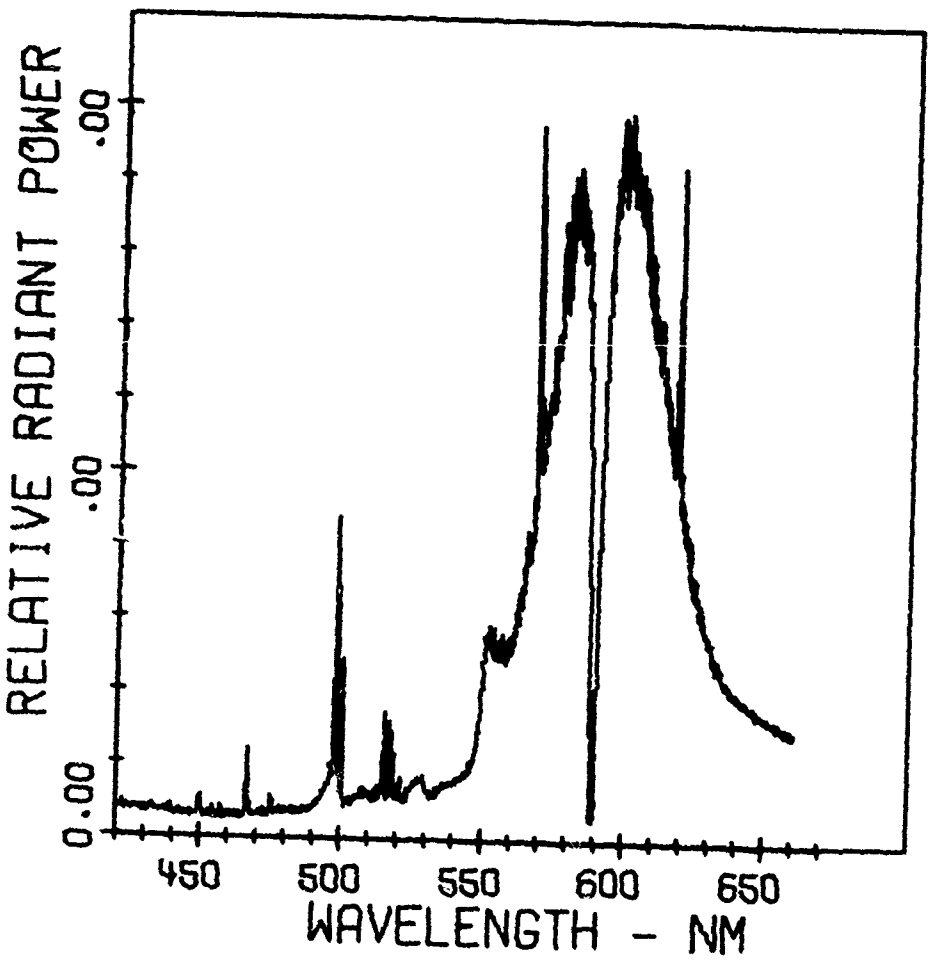

FIGURE 9. Group 105

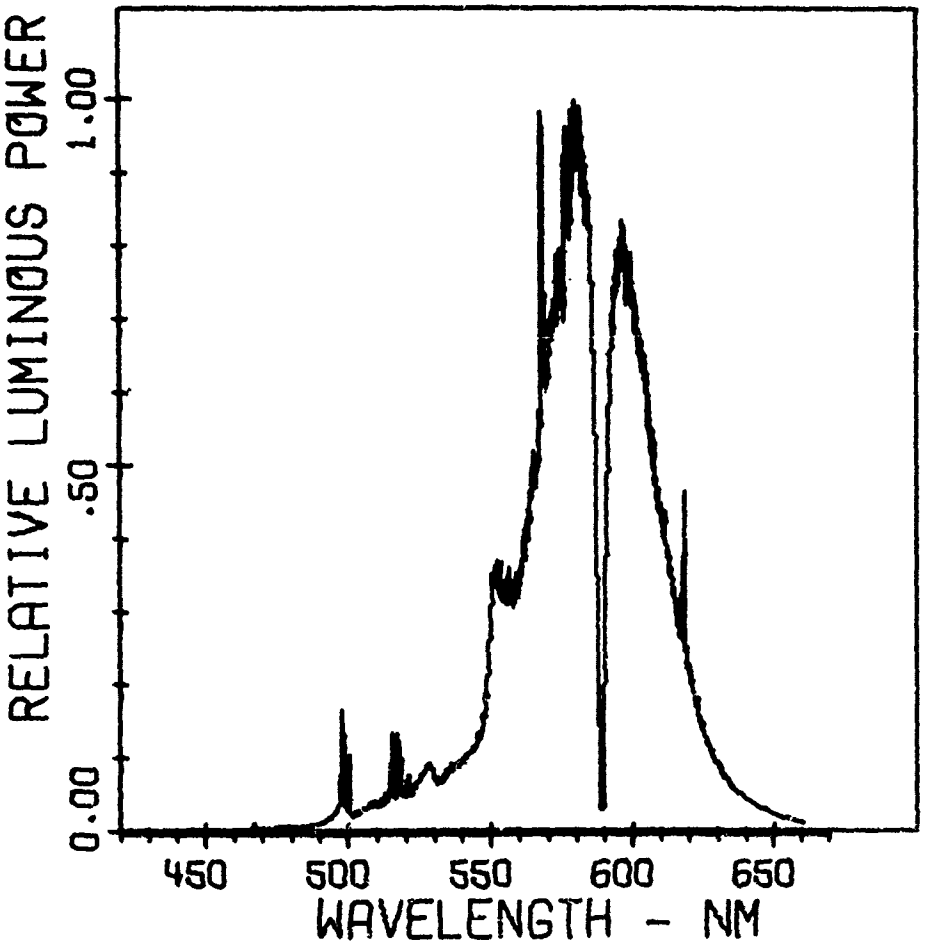

FIGURE 10. Group 105

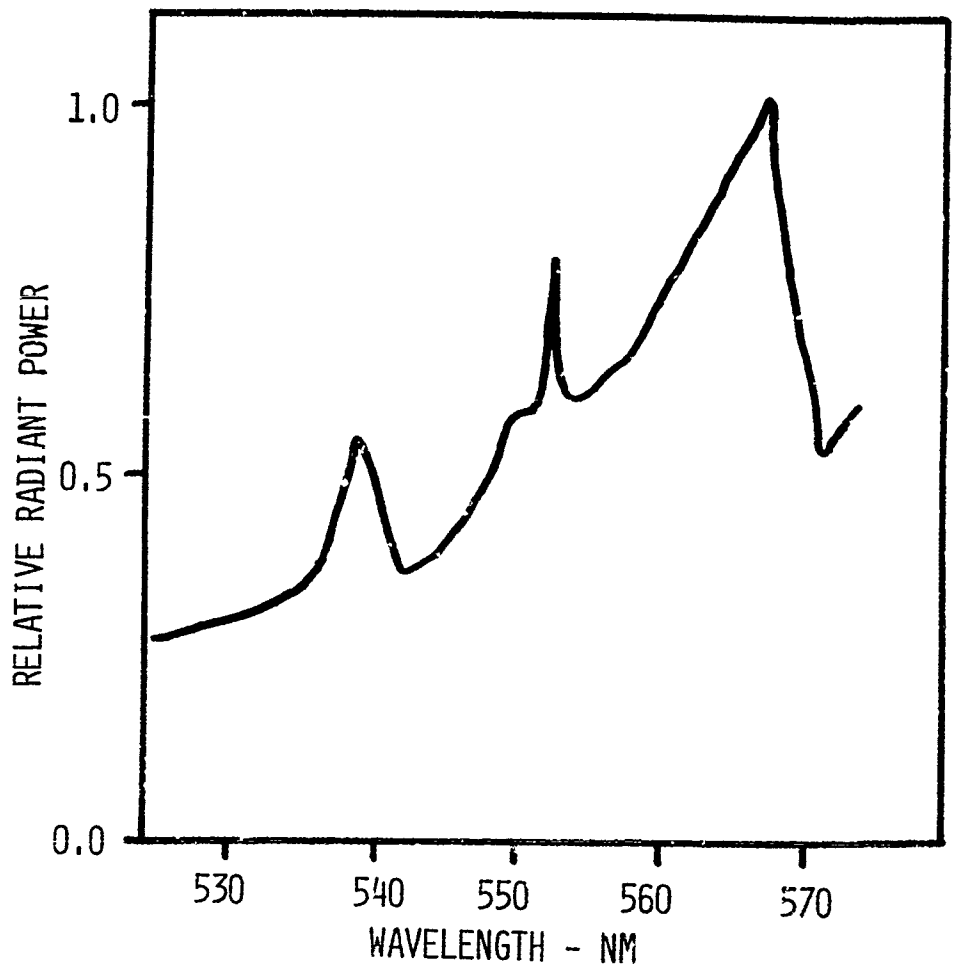

FIGURE 11. Group 101 - High Resolution

DISCUSSION

The compositions of the flare Groups 101 and 105 shown in Table 1 were chosen by adjusting the fuel to oxidizer ratio in the NASA thermodynamics program until the maximum flame temperature was found.[4] This optimum formula was used as a starting point for formulations. It is a known fact that fuel rich formulas tend to produce more light than the so-called optimum formula.[5] Thus, Groups 102 and 103 were arbitrarily selected as fuel-rich sodium iodate formulas. Group 104 is a fuel-rich formula similar to the current Mk 45 aircraft parachute flare formula.

The data presented in Table 2 clearly show that the use of sodium iodate as an oxidizer causes a decrease of about a factor of three in both candlepower and efficiency. This loss in output is probably a result of the reduction in the sodium atom concentration. Due to the high molecular weight of sodium iodate, the sodium concentration in Group 101 is 24% less than in Group 104. The reduction in concentration means that there are not only less sodium atoms to emit but it has been shown that a reduction in sodium atom concentration also causes a narrowing of the broadened sodium D resonance lines.[6] Sodium D emission accounts for most of the light output in magnesium-sodium nitrate illuminating flares. Fig. 12 shows a superposition of the spectra of the iodate containing flares and the nitrate containing flares. The half-width of the sodium D region in the nitrate flares is 400 Å while the half-width in the iodate is only 160 Å. The calculation of the resonance broadening using Douda's method and lowering the sodium atom density by 25% reduces the broadening to only 300 Å. In order to fit the data, it is necessary to adjust the Voigt function a parameter. A value of the Voigt a parameter of 0.20 gives a good fit to the experimental data. Reducing the a parameter is equivalent to reducing the broadening due to like and unlike species in the flame. The resonance broadening half-width, i.e. broadening of sodium resonance lines by sodium atoms, is reduced because there are fewer sodium atoms in the system. The collisional broadening half-width, i.e. broadening due to collisions between sodium and unlike species, is reduced due to the increased reduced mass of the system because of the added iodine. Order of magnitude calculations show that these reductions in half-widths are not entirely sufficient to account for the reduction in the a parameter. A detailed treatment, however, to explain these differences is beyond the scope of this paper. Arguments can be made to show that the broadening and the a parameter are very sensitive functions of temperature and concentration of species in the flame. The problem of

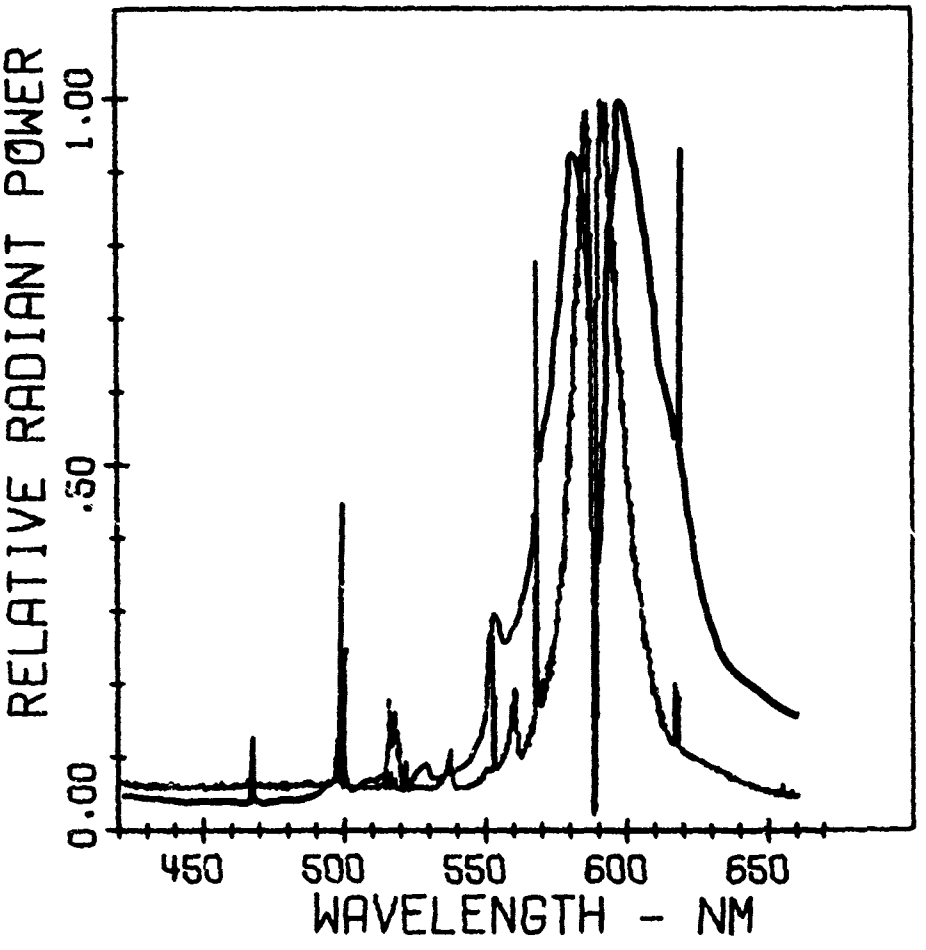

FIGURE 12. Comparison of broadening between 101 and 105

mapping temperature and concentration gradients in a pyrotechnic flame is at the present time very difficult. Much more experimental work in this area is necessary in order to resolve the fine points in a calculation such as the one done by Douda.

The decreased luminous output in the sodium iodate flares would tend to rule out the use of the iodate as an oxidizer. There are, however, interesting features in the spectra which should be pointed out for use in special applications where the high intensity of the magnesium-sodium nitrate formula is not necessary.

The two most striking features in the spectra of the magnesium-sodium iodate flares, see e.g. Fig. 2, are the strong band emission at 538 and 560 nm and the increased continuum in the blue region from 400 - 530 nm. In addition to those shown, there is band emission at 380 nm similar in size and shape to that at 538 and 560.

The observed blue continuum is assigned to the molecular iodine $B\ ^3\pi_{0^+u} \leftrightarrow X\ ^1\Sigma_g^+$ transition.[7] Figure 13 shows the two potential energy surfaces responsible for this transition. There are two possible mechanisms for the production of this emission. The emitting iodine molecule is formed by recombination of iodine atoms.

$$I + I + M \rightarrow I_2 + M$$

In a thermal excitation model, the ground state iodine molecule formed by this reaction would be thermally excited to the upper electronic state which would then emit. Another mechanism would be for the iodine recombination reaction to form the excited state directly followed by the observed emission. Either of these two mechanisms is reasonable due to the high temperatures in the flame. Based on the results which have been obtained, it is impossible to distinguish between the two mechanisms. More detailed studies would be required to observe the molecular and the atomic iodine emission and absorption simultaneously. This type of information would be required to completely determine the reaction mechanism.

The band emissions at 380, 538 and 561 nm have been identified as barium iodide $A^2\pi \leftrightarrow X^2\Sigma$ transition.[7] Barium emission is also seen as atomic emission at 554 nm. The barium in the flare comes from the barium in the boron barium chromate first fire. The barium emission is seen throughout the entire burning time and not just at the start of the burn.

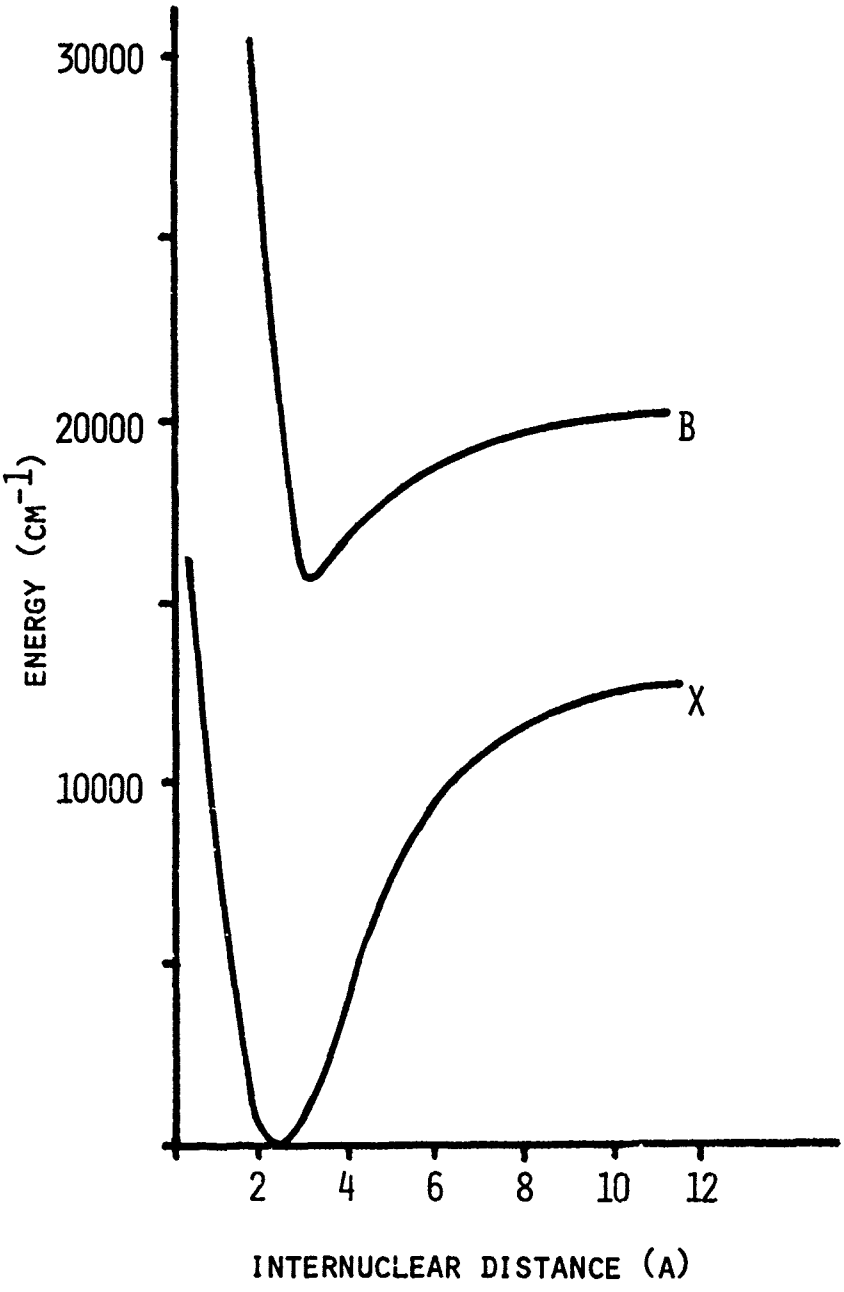

FIGURE 13. Iodine Potential Energy Surfaces

The spectra shown in Fig. 11 unfortunately was not sufficiently resolved to allow calculation of any molecular constants for BaI.

While the spectra were being taken, visual observations of the flares indicated that the sodium iodate flares appeared to be whiter in color than the sodium nitrate. In an effort to quantify this observation to some extent, the spectral information obtained on Group 101 and 104 flares, Figs. 2 and 10, was converted to the tristimulus color values X, Y and Z from which one can obtain the dominant wavelength and purity of each flare.[3] Fig. 14 shows a chromaticity diagram with the points marked for Groups 101 and 104. As can be seen, the iodate are rendered more nearly white than the sodium nitrate flares. For the iodate flares, the dominant wavelength is 583 nm and the purity is 81%. For the nitrate flares, the dominant wavelength is 584 nm and the purity is 94%. The fact that the sodium iodate flares are more nearly white is due to the increased emission in the blue region of the spectrum.

Although little work has been done in the area of the effect of color on target acquisition, it would seem that a source with a more uniform distribution of light would be preferable to a highly monochromatic source. Thus, if one were interested in white flare light of moderate intensity, the magnesium-sodium iodate composition would provide a reasonable system.

CONCLUSIONS

Flares composed of magnesium and sodium iodate show increased emission in the blue region of the spectrum. While the total luminous power is a factor of three less in the iodate flares than in magnesium-sodium nitrate flares, the increased blue emission makes the output of the iodate flares appear whiter. The blue emission is assigned to the $A \rightarrow X$ transition of molecular iodine.

Band systems due to barium iodide formed by the reaction of the iodine atoms with the barium first fire were identified. The systems at 538 and 561 nm were observed under moderate resolution to determine molecular constants. Due to a lack of resolution, this was not possible. The emission bands are very specific and seem to be reasonably strong based on the fact that they are due to a barium impurity.

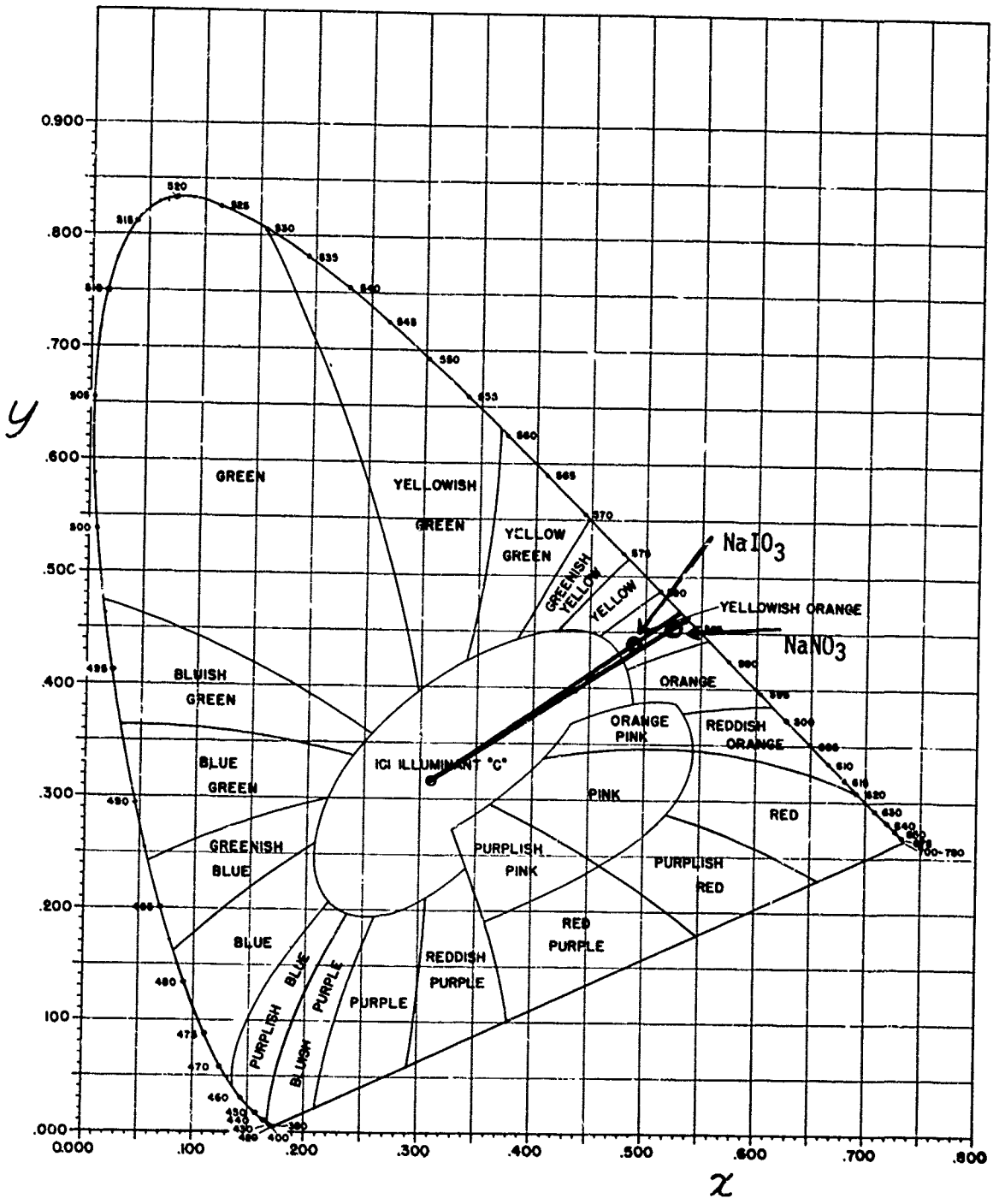

FIGURE 14. Chromaticity Diagram - Comparison of Color of 101 and 104.

Magnesium-sodium iodate flares could be used as a moderate intensity white light source for better target acquisition. The use of barium and iodine containing flares might provide increased specific emission at 538 and 560 nm.

REFERENCES

1. B. Arnold, S. Finlayson, and E. A. Ogryzlo, J. Chem. Phys. 44, 2529 (1966).

2. H. Ellern, *Military and Civilian Pyrotechnics* (Chemical Publishing Company, New York, 1968), p. 337.

3. OSA Committee on Colorimetry, *Science of Color* (Crowell Company, New York, 1953), Chap. 8.

4. S. Gordon and B. J. McBride, *Computer Program for Calculation of Complex Chemical Equilibrium Compositions, Rocket Performance, Incident and Reflected Shocks, and Chapman-Jouquet Detonations*, NASA SP-273, Lewis Research Center (1971). N71 37775.

5. R. M. Blunt, *Flare Flame Phenomena*, RDTR No. 186, Naval Ammunition Depot, Crane, Indiana (1971). AD No. 729 104.

6. B. E. Douda, *Radiative Transfer Model of a Pyrotechnic Flame*, RDTR No. 258, Naval Ammunition Depot, Crane, Indiana (1973). AD No. 769 237.

7. G. Herzberg, *Spectra of Diatomic Molecules* (D. Van Nostrand Co., Inc., Princeton, N. J., 1966).

A MATHEMATICAL MODEL OF FLARE PLUME COMBUSTION AND RADIATION

John E. Tanner, Jr.
Naval Ammunition Depot
Applied Sciences Department
Crane, Indiana 47522

ABSTRACT

A mathematical model of the temperature, composition and radiation profiles along the length of the plume of a pyrotechnic flare is constructed based on observations and on relevant radiation and thermodynamic theory, taking the magnesium/sodium nitrate/binder flare as an example.

Predicted changes in luminous output due to changes in fuel percent, pressure, and ambient oxygen content correlate moderately well with observations.

It is shown that a significant amount of air augments combustion and that this air has a large effect on flame temperature and on luminous output. It is also shown that the smoke is a very weak gray body, much less than 1% of a blackbody.

Particle burning times are shown to be considerably shorter than those predicted from single particle burning experiments. There is also some indication that when a fuel-rich flare burns in an oxygen-poor environment, much of the stoichiometric excess magnesium does not vaporize.

The results show that the maximum temperatures are probably within 200 degrees of computed adiabatic temperatures for all but the most fuel-rich flares.

INTRODUCTION

Many experimental and theoretical studies of the combustion of flares have been made to determine the details of the combustion and light emission processes so that a better understanding of their operation could point the way to devising flares of greater luminosity or color purity.[1-7]

The purpose of the present study has been to construct a theoretical model of flare combustion which would incorporate all the experimental observations and at the same time test them for consistency. The goal is to predict other results which have not yet been determined with accuracy, in particular, luminosities from untried compositions.

Therefore, a computer program has been constructed which models combustion, radiation, and flow of material in the plume of a pyrotechnic flare. This is done by following a fixed amount of the original composition as it leaves the burning surface and progresses toward the tail of the plume.

The flow is modeled in one dimension only. No movement or variation in properties perpendicular to the plume axis is considered, except for the spreading out of the gases to fill a cone-shaped plume. Ambient air (or other gas) is assumed to mix in continuously along the plume.

The slow step in the combustion reaction is taken to be the vaporization and combustion of the metal particles, which begins when they are ejected from the flare body surface and continues to completion in the plume, with a constant, arbitrarily predetermined rate.

The binder and oxidizer are assumed to decompose completely to gaseous products at the flare surface. Chemical equilibrium among these gases and the available metal vapor is assumed to instantaneously follow changes in local temperature.[8]

Radiative loss to the outside is the only macroscopic energy transfer considered. Heat feedback within the plume is ignored.

Three types of radiative energy loss are modeled: (1) gray body radiation proportional to T^4, (2) simple line emission proportional to the concentrations of the relevant species and to the Boltzmann factors and transition lifetimes for their excited states, and (3) strong resonance line emission producing a very high optical density. For this latter case, a simple two-temperature radiative transfer process is constructed.

BASIC EXPERIMENTAL FACTS

In an initial test of the model, we have taken the magnesium/sodium nitrate/organic binder flare composition as an example, since this represents the most common military flare, and the one most thoroughly observed.

Various evidence as follows indicates a temperature of about 1000°K at the burning surface: It has been observed,[7] using high speed photography, that most magnesium particles (m.p. 922°K) melt only a millisecond before ejection from the solid, and that they ignite a short distance from the surface. Furthermore, decomposition of sodium nitrate, which produces the gas to blow the magnesium out of the flare, has been shown to take place rapidly enough at or above 1000°K.[9] Finally, ignition temperatures of magnesium dust in air have been reported to be about 900°K.[10]

Plume temperatures have been determined by thermocouples[11] and by absolute brightness measurements[12] at a frequency in the sodium D line. Both types of measurements yield maximum temperatures in the vicinity of the computed adiabatic temperature, although they are uncertain by several hundred degrees. The position of the maximum temperature is found within a few inches of the surface in the thermocouple measurements cited.

Observations[13] indicate that the region of greatest brightness begins about one diameter from the surface. For stoichiometric mixes, the brightest region is fairly concentrated, whereas for fuel-rich mixes it is well spread out along the length of the plume.

The shape of the flame and smoke plume depends on the orientation of the flare and on the surrounding air flow. For a flare burning upright in still air, the plume can be approximated

as cone shaped, with an apex angle of 15-30°. Plumes of large diameter (4-1/4") flares may be luminous a distance of 4-6 feet, to a point where the photometric brightness has decreased by a factor of about 10^8 from the maximum value.

Power spectra indicate that most of the luminous intensity is from the sodium D radiation,[1,2] a doublet of frequency 5890 Å. This radiation accounts for about 8% of the total heat of combustion in flares which have been optimized for efficiency of luminous output.

THE MODEL

The heart of the model is the NASA computer program for complex equilibria.[14] This program computes equilibrium compositions and temperatures from a given set of reactant materials and their enthalpies. Modifications were added to cause the program to automatically recompute equilibrium a specified number of times to represent closely spaced points along the plume. At each point, increments of air and of magnesium are added to the amount of initial reactants, to represent the continual mixing in of air and vaporization of magnesium. Radiation losses are computed based on temperature and emitter (sodium atom) concentrations at each point. These losses are subtracted from the enthalpy used in computing equilibrium at the next point. In this way, a temperature, composition and radiation profile are constructed along the length of the

plume. The radiant outputs are added up for all of the points, separately for each emission process, to obtain the total output of the amount of material considered.

Details of the addition of materials and of the energy losses in the case of the magnesium/sodium nitrate flare are as follows:

The rate of vaporization of magnesium is in reality dependent on local temperature and oxygen concentration. To properly take this into account would have introduced considerable complexity into the calculation. Therefore, the vaporization of magnesium is assumed to proceed linearly with time, such that the magnesium will all be consumed near the expected point of maximum brightness.

The air (or other gas) is added linearly with distance, the adjustable proportionality constant being referred to as the "air mixing rate". This rate was made proportional to the flare candle diameter and to the 2/3 power of ambient pressure for simulating altitude effects.

The only radiation modeled was the sodium D line and gray body radiation. Radiation losses for most processes involving small molecules in the gas phase could be calculated as directly proportional to the species concentration, the Boltzmann factor for the excited state (not the energy difference between states) and the radiation lifetime of that transition.

However, in the special case of sodium D radiation, the extreme optical density makes the final brightness highly non-linear in sodium concentration. Therefore, a simple two-temperature radiative transfer model was postulated. The line was taken to have a Lorentzian profile with half width computed from a standard formula.[15] The emerging radiant exitance, I', was then assumed equal to

$$I' = pI^\circ \int_{-\infty}^{\infty} [1-\exp(-\ell\, k_\lambda)] \exp(-\ell'\, k_\lambda) d(\lambda-\lambda_o)$$

where I° is the radiant exitance from a blackbody at thermodynamic equilibrium as given by the Planck formula. The first factor in the integral represents emission in the hot region; the second factor is absorption in an outer cold region of the flare plume; k_λ is the optical density, which is a function of the species concentration, the transition lifetime, the Lorentz half width, and the distance from line center, $(\lambda-\lambda_o)$.[15] ℓ and ℓ' are total path lengths in the hot and cold regions, respectively. ℓ is equated to the plume diameter, and ℓ/ℓ' is an adjustable input parameter. An adjustable proportionality constant, p, (hereafter referred to as the "sodium radiation constant") is also included.

Gray body radiation losses were calculated proportional to T^4 with a simple adjustable constant, referred to as the "gray body radiation constant".

Some of the omissions and approximations made deserve further comment. The consequence of neglecting heat feedback within the plume is that the effects of composition, ambient pressure, and other variables on burning rates cannot be estimated even to a first approximation. Also, a consideration of heat feedback is necessary in order to take into account the effect of local temperature on metal particle burning rates.

Since the effects of local temperature and oxygen content on particle vaporization were not taken into account, the model predicts continuing vaporization of all magnesium where the local plume temperature exceeds its boiling point. If not enough oxygen is present, the vaporization of the excess magnesium severely depresses the computed flame temperature, possibly leading to too low a predicted luminous output for fuel-rich flares burning in an oxygen-poor environment.

In spite of these omissions, and the approximations with which other aspects were modeled, it is believed that the model can make useful predictions.

RESULTS

Predicted temperature and flame brightness lengthwise along the plume are compared in Fig. 1 for the reference flare--58% Mg/37-1/2% $NaNO_3$/4-1/2% epoxy binder of 4-1/4" diameter.

The adjustable parameters, which are the radiation constants, the rate of air mixing, and the particle burning time have been chosen after a number of trial calculations on this flare so as to give the best fit to experiment, and to be reasonable theoretically.

Trial calculations used to help determine the air mixing rate constant are shown in Fig. 2a, where the temperature is plotted for various assumed values of this rate. The value two parts air to one part solid at 200 cm is a compromise which produces nearly the maximum total luminous output and satisfactory flight times.

For comparison, the adiabatic temperatures which would be attained during combustion and mixing with air are shown in Fig. 2b.

The adjustable gray body radiation constant turned out to be about 0.1% of the corresponding blackbody coefficient, a small value but perhaps reasonable considering the high reflectivity of magnesium oxide.

The sodium radiation constant was a factor of 4, which is not unreasonably larger than the hoped-for value of unity. The ratio of hot to cold optical path lengths, ℓ/ℓ', was arbitrarily taken as 10.

The particle burning time for 400 microns (30/50) particle size was chosen as 0.1 sec, a compromise between single particle experiments which indicate longer burning times[16] and modeling of the observations of the position of luminous intensity, which indicates shorter burning times.

Having chosen these parameters, we may examine the manner in which temperature, flame brightness, and total luminous output are predicted to vary as the experimentally-controllable parameters are varied. These parameters include the fuel (magnesium) content, ambient pressure, and percent ambient oxygen. Illustrations of their effects are presented in Figs. 3 and 4, and in Table I, respectively.

The remainder of the results presented here consist of comparisons of predicted temperatures and luminous output with specific experimental observations reported in the pyrotechnic literature.

The effect of flare candle diameter on the optimum fuel content has been studied by Douda.[17] Predicted luminous outputs are compared with his results in Table II.

The effect of pressure on luminous output is shown in Table IV, where predicted values are compared with observations of several experimenters.[3,18]

The effect of a nitrogen environment on flare output has been observed both by Waite and Weaver,[13] and by Hamrick and Rose.[11]

Waite and Weaver burned flares of various sizes face downward in an upward flowing stream of air or of nitrogen gas which, however, was not partitioned from the surrounding air. Comparisons of predicted luminous output with their results for 4-1/4" flares of 55% magnesium content are presented in Table III.

Hamrick and Rose used thermocouples to determine flame temperatures at a number of points simultaneously both on and off the plume axis. Their flares of 4-1/4" diameter were burned face upward in an open cylinder supplied with nitrogen at the bottom. Predicted temperatures are compared with their measurements at two different magnesium contents in Fig. 5.

DISCUSSION

In most respects, the model predictions agree qualitatively and semi-quantitatively with expectations and with the specific experimental results presented.

The model correctly predicts a decrease in flame brightness and total luminous output with decreasing atmospheric pressure. This effect is predicted to increase greatly as fuel content is increased. The observations of luminous output presented

in Table IV do show this effect of fuel content, though it is not as large or as consistent as is predicted. The lack of consistency among the different experimenters could be due simply to the well known erratic performance of pyrotechnic flares, particularly non-standard items produced in small quantities. That the predicted effect of fuel percent is larger than that observed could be due to the manner in which the magnesium was assumed to burn, as was discussed in a previous section.

Observations indicate an increase in the length of the visible portion of the plume as pressure is decreased. The model also predicts this effect, of a magnitude similar to that actually observed, see Fig. 4.

A variable similar to atmospheric pressure is atmospheric oxygen content. Flares can be burned in an atmosphere of nitrogen instead of in air. One expects the same deleterious effect of lack of oxygen on fuel-rich flares in both cases. However, a low ambient pressure causes a large increase in dissociation of combustion products, which further lowers the flame temperature.

The model predicts a much more severe effect of a nitrogen environment on flame temperature and luminous output of fuel-rich flares than has been observed experimentally, as can be seen in Table III and Fig. 5, respectively. The discrepancies

between prediction and the observations of Waite and Weaver (Table III) may be in part due to a lack of rigorous exclusion of air in their experimental setup. The apparatus of Hamrick and Rose was probably much better for excluding air.

The bulk of the discrepancy may well be due to the lack of consideration of the effect of local oxygen concentration on vaporization of the magnesium. The magnitude of this effect was checked in a few cases by making the calculation under the assumption that only as much magnesium vaporizes as there is oxygen available to react with it. The results in Table III and Fig. 5b show that the effect is large, and so the detailed behavior of the burning process is an important question.

A question of considerable practical importance is the optimum fuel/oxidizer ratio, the criteria being the total output (luminous efficiency) and the burning rate. For candles burning in an inert environment, a nearly stoichiometric fuel/oxidizer ratio would be expected to give greatest efficiency. Experiments in air show that quite fuel-rich mixtures are the most efficient. The experiments by Douda,[17] cited in the previous section, show how the optimum fuel/oxidizer ratio decreases with increasing candle size. Several factors could contribute: As plume diameter increases (1) efficiency of mixing with air could decrease, necessitating that the candle contain more of its own oxidizer and, (2) the efficiency of

Secondly, it should be possible with a reasonable effort to improve the basic model itself by including the effects of heat feedback within the plume and by including a particle burning model which contains a dependence on local temperature and oxygen content. This would allow at least a first approximate prediction of burning rates. It would also remove the arbitrariness in the way the particle burning is described and would improve the predictions for fuel-rich compositions burning in an oxygen-poor environment.

REFERENCES

1. B. E. Douda, R. M. Blunt and E. J. Bair, J. Opt. Soc. Am. 60, 1116-1119 (August 1970).

2. B. E. Douda and E. J. Bair, J. Opt. Soc. Am. 60, 1257-1261 (September 1970).

3. R. M. Blunt, *Spectral Distribution of Different Regions of Illuminating Flare Flames*, RDTR No. 220, Naval Ammunition Depot, Crane, Indiana (December 1972). AD No. 757663. The author does not give values for luminous intensity, but his raw data permit an estimate of these values.

4. D. R. Dillehay, *Possible Mechanisms for Burning Rate/ Candlepower Enhancement in Illuminants* in *Proceedings - Third International Pyrotechnics Seminar* held at Colorado Springs, Colorado, 21-25 August 1972. (Sponsored by Denver Research Institute, University of Denver), p. 1. AD No. 913408L.

5. R. L. Tischer, *Effect of Entrained Air in Determining Optimum Flare Compositions* in *Proceedings - Second International Pyrotechnics Seminar* held at Snowmass-at-Aspen, Colorado, 20-24 July 1970. (Sponsored by Denver Research Institute, University of Denver), p. 425. AD No. 913407L.

6a. *Exploratory Development of Illuminating Flares*, AFATL-TR-68-91, Air Force Armament Laboratory, Eglin AFB, Florida (August 1968). AD No. 848086.

6b. *Exploratory Development of Illuminating Flares - Phase II*, AFATL-TR-69-107, Air Force Armament Laboratory, Eglin AFB, Florida (August 1969). AD No. 872686.

7. J. Eisel, *Improved Flare Efficiency* in *Pyrotechnic Research and Development January - June 1973*, NWC TP 5551, NWC China Lake, California (June 1973), p. 13. (CONFIDENTIAL).

8. The thickness of the flame reaction zone in high velocity propellant plumes is usually calculated to be of the order of millimeters. See e.g. M. W. Beckstead, R. L. Derr, and C. F. Price, *A Model of Composite Solid-Propellant Combustion Based on Multiple Flames*, AIAA Journal 8, 2200 (1970).

9. J. W. Mellor, *A Comprehensive Treatise of Inorganic and Theoretical Chemistry* (John Wiley and Sons, Inc., New York, N. Y., 1961), Supplement II, Vol. II, p. 1243.

10. H. Ellern, *Military and Civilian Pyrotechnics* (Chemical Publishing Co., Inc., New York, 1968), p. 296.

11. J. T. Hamrick and L. C. Rose, *Temperature Distribution in the Plume* in *Exploratory Development of Illuminating Flares - Phase II*, AFATL-TR-69-107, Air Force Armament Laboratory, Eglin AFB, Florida (August 1969), p. 50-64. AD No. 872686.

12. P. L. Blackshear, et. al., *Flame Characteristics and Spectral Analysis* in *Exploratory Development of Illuminating Flares*, AFATL-TR-68-91, Air Force Armament Laboratory, Eglin AFB, Florida (August 1968). AD No. 848086.

13. H. R. Waite and R. R. Weaver, *Luminous Intensity Distribution* in *Exploratory Development of Illuminating Flares - Phase II*, AFATL-TR-69-107, Air Force Armament Laboratory, Eglin AFB, Florida (August 1969), p. 98. AD No. 872686.

14. S. Gordon and B. J. McBride, *Computer Program for Calculation of Complex Chemical Equilibrium Compositions, Rocket Performance, Incident and Reflected Shocks, and Chapman-Jouquet Detonations*, NASA SP-273, Lewis Research Center (1971). N71-37775.

15. A. Mitchell and M. W. Zemansky, *Resonance Radiation and Excited Atoms* (Cambridge University Press, New York, N. Y., 1971). See especially equations 25, 92 and 104.

16a. H. M. Cassell and I. Liebman, *Combustion and Flame* 6, 153 (1962).

16b. R. P. Wilson and F. A. Williams, *Thirteenth Symposium (International) on Combustion* (The Combustion Institute, Pittsburg, Pa., 1971), p. 833.

16c. J. R. Richard, R. Delbourgo and P. Laffitte, *Twelfth Symposium (International) on Combustion* (The Combustion Institute, Pittsburg, Pa., 1969), p. 39.

17. B. E. Douda, *25 Million Candle Cast Flare, Diameter and Binder Study (Summary Report June 66 to June 67)*, RDTR No. 105, Vol. I, Naval Ammunition Depot, Crane, Indiana (January 1968). AD No. 665301.

18a. S. Resnick, *Simulated High Altitude Tests of Illuminating Compositions*, TR No. 2166, Samuel Feltman Ammunition Labs., Picatinny Arsenal, Dover, N. J. (April 1955).

18b. J. A. Carrazza, Jr., B. Jackson, Jr. and S. M. Kaye, *New Flare Formulations for High Altitude Application*, TR No. 3360, Picatinny Arsenal, Dover, N. J. (October 1966). AD No. 641957.

19a. R. A. Awcock, E. R. Camplin and S. Harrison, *The Spectral Distribution of Radiant Power Emitted by Some Standard SR Pyrotechnic Illuminating Compositions in the Wavebands 0.4-6.0 microns, Part 1. Lantex Cases*, RARDE Memo 47/68, Royal Armament Research and Development Establishment, England (December 1968). AD No. 398909.

19b. R. A. Awcock, E. R. Camplin and S. Harrison, *The Spectral Distribution of Radiant Power Emitted by Some Standard SR Pyrotechnic Illuminating Compositions in the Wavebands 0.4-6.0 microns, Part 2. Composite Curves for Lantex Cases*, RARDE Memo 5/69, Royal Armament Research and Development Establishment, England (February 1969). AD No. 398896.

19c. R. A. Awcock and S. Phillips, *The Spectral Distribution of Radiant Power Emitted by Some Standard SR Pyrotechnic Illuminating Compositions in the Wavebands 0.4-6.0 microns, Part 3. Paper Cases*, RARDE Memo 7/72, Royal Armament Research and Development Establishment, England (March 1972). AD No. 521728.

19d. R. A. Awcock and S. Phillips, *The Spectral Distribution of Radiant Power Emitted by Some Standard SR Pyrotechnic Illuminating Compositions in the Wavebands 0.4-6.0 microns*, RARDE Memo 13/72, Royal Armament Research and Development Establishment, England (April 1972). AD No. 521731.

TABLE I

Predicted Luminous Efficiencies (cd-sec/g) of Flares Burned in Various Atmospheres. Epoxy Binder 4.5%.

Percent Magnesium	Environment		
	Nitrogen	Air	Oxygen
41%	14,000	21,600	22,000
58%	3,900	43,900	66,000
58%, 1/4 unburned		20,700	

TABLE II

Predicted versus Observed Effect of Fuel Percent on Efficiency. Efficiencies Listed in cd-sec/g.

Diameter	Magnesium	55%	62%	70%
2.0"	predicted	43,600	52,500	62,200
	observed	31,100	37,800	35,900
4.25"	predicted	42,300	42,300	45,300
	observed	46,000	44,600	36,900
7.33"	predicted	38,800	31,200	28,800
	observed	40,200	36,300	32,500

TABLE III

Comparison of Predicted and Observed[13] Luminous Efficiencies of 4.25" Mg/$NaNO_3$/Laminac Flares of Composition 55%/40%/5% respectively.

Magnesium Particle Size	Environment	Efficiency, cd-sec/g predicted	observed
30/50	Nitrogen	3,350	22,500
50/100	Nitrogen	1,930 3,470*	28,400
50/100	Air	38,400	47,700

*Assumption that excess magnesium is not vaporized.

TABLE IV

Effect of ambient pressure. Comparison of predicted and observed luminous efficiencies, cd-sec/g, for magnesium, sodium nitrate/binder flares. From left to right the mixtures are increasingly fuel-rich.

Author	Resnick[18]		Blunt[3]		Carrazza et.al.[18]		Blunt		Resnick	
Magnesium	31.8%		44 %		60%		58 %		59.1%	
Binder	9.1%		4.5%		0%		4.5%		9.1%	
Pressure	Calc.	Obs.	Calc.	Obs.	Calc.	Obs.	Calc.	Obs.	Calc.	Obs.
1 atm	15,900	38,000	29,200	26,000	20,200	13,700	45,700	44,000	45,100	45,000*
0.45 atm= 20,000'		17,000							40,200	32,000
0.2 atm= 40,000'	12,200	12,100	20,400	24,000			20,000	33,000	11,100	25,000
0.395 atm			11,700	11,000			5,600	11,400		
0.295 atm= 80,000'					11,500	230				

*Candle weights were not given; therefore, this observation of Resnick's was arbitrarily equated to the predicted value and his other observation set relative to this one.

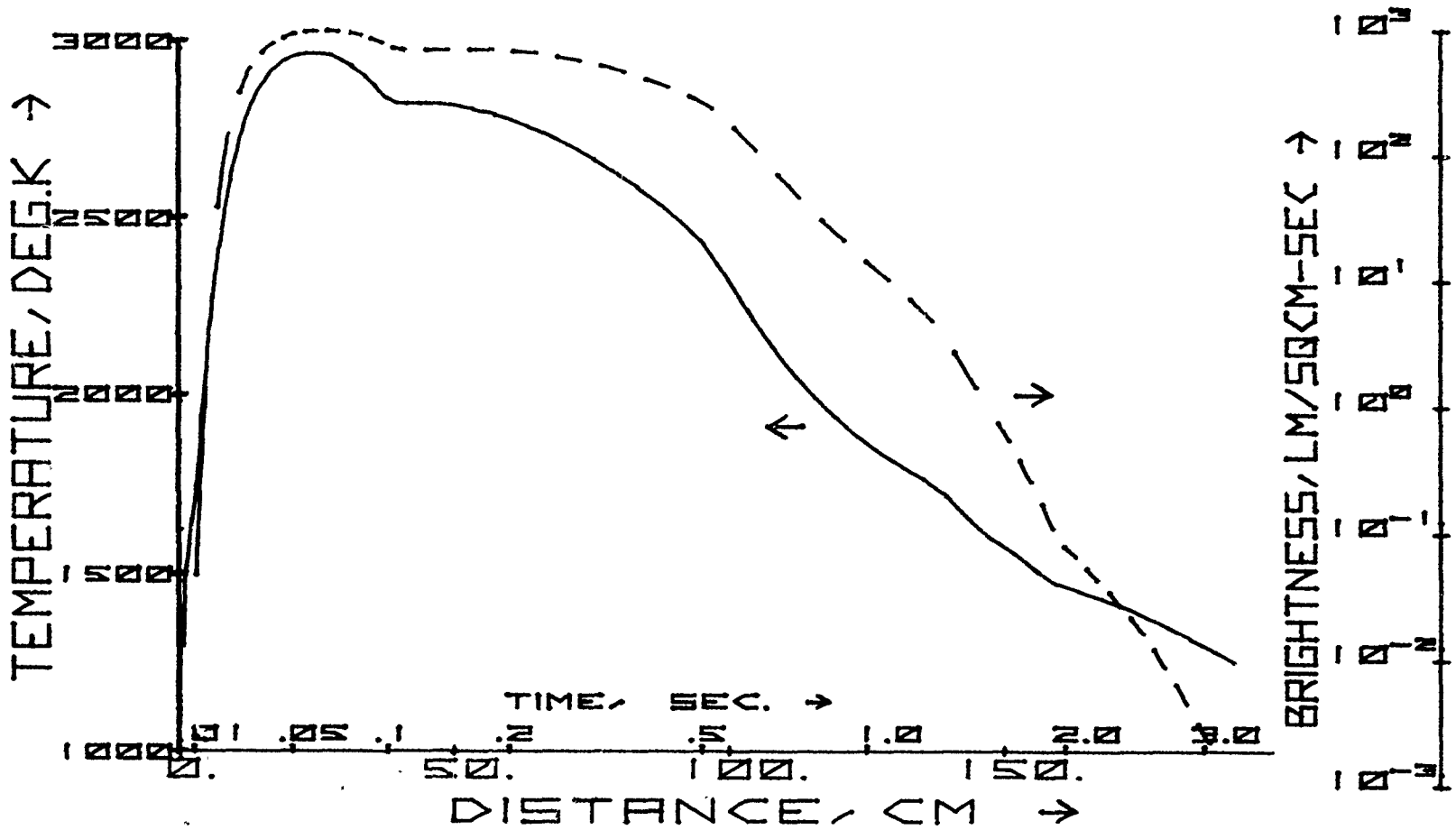

Fig. 1. Computed flame temperature and flame brightness along the plume of a 4.25" diameter, 58% Mg, 4.50% binder, 37.50% $NaNO_3$ flare. Times of flight are indicated along the abscissa.

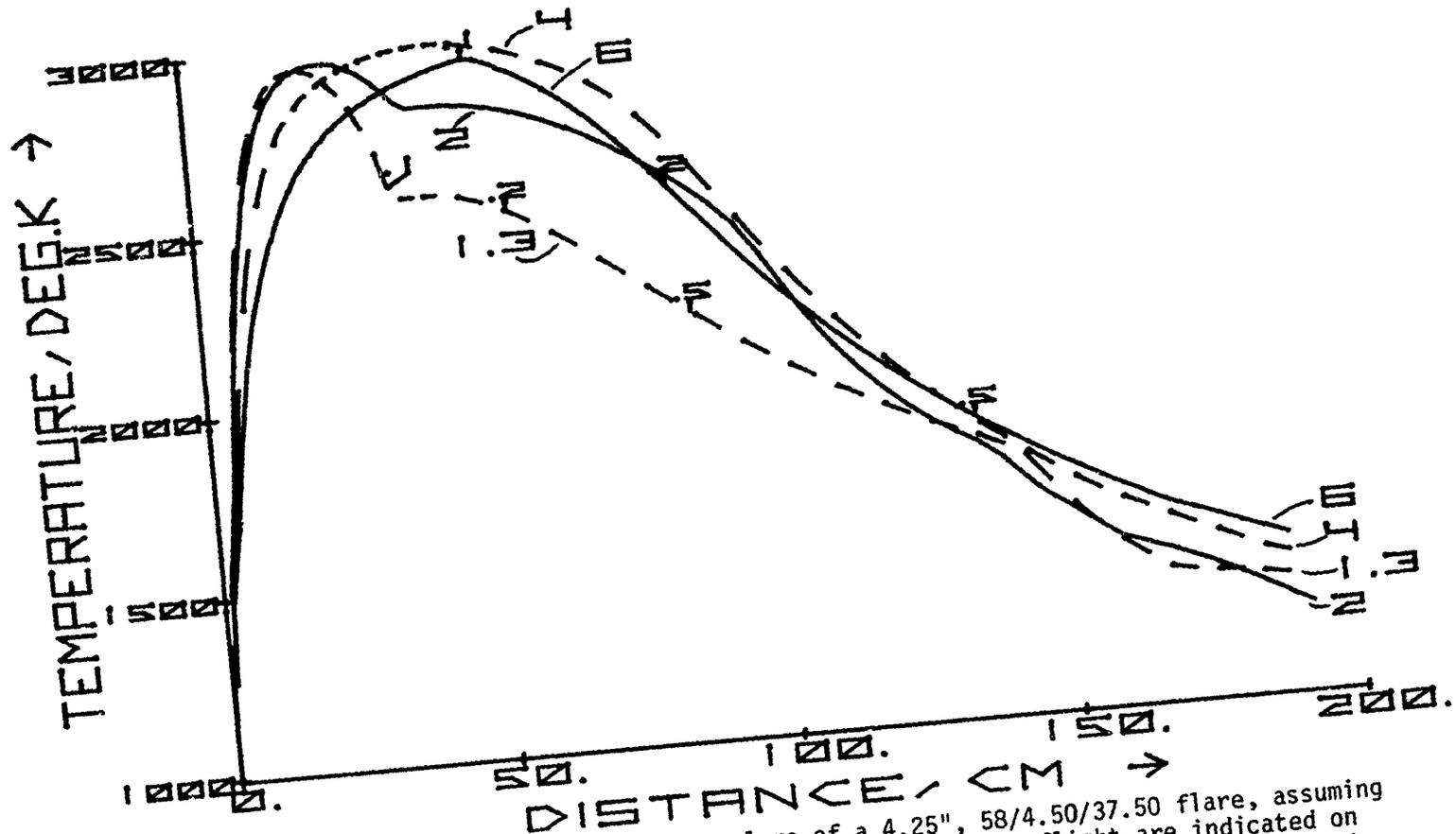

Fig. 2a. Computed flame temperature along the plume of a 4.25", 58/4.50/37.50 flare, assuming air/composition ratios of 1.3, 2, 4, and 6 @ 200 cm. A few times of flight are indicated on the curves. The total integrated luminous outputs are computed to be 22,800, 43,900, 46,900, and 30,200 cd sec/g, respectively, for increasing amounts of air.

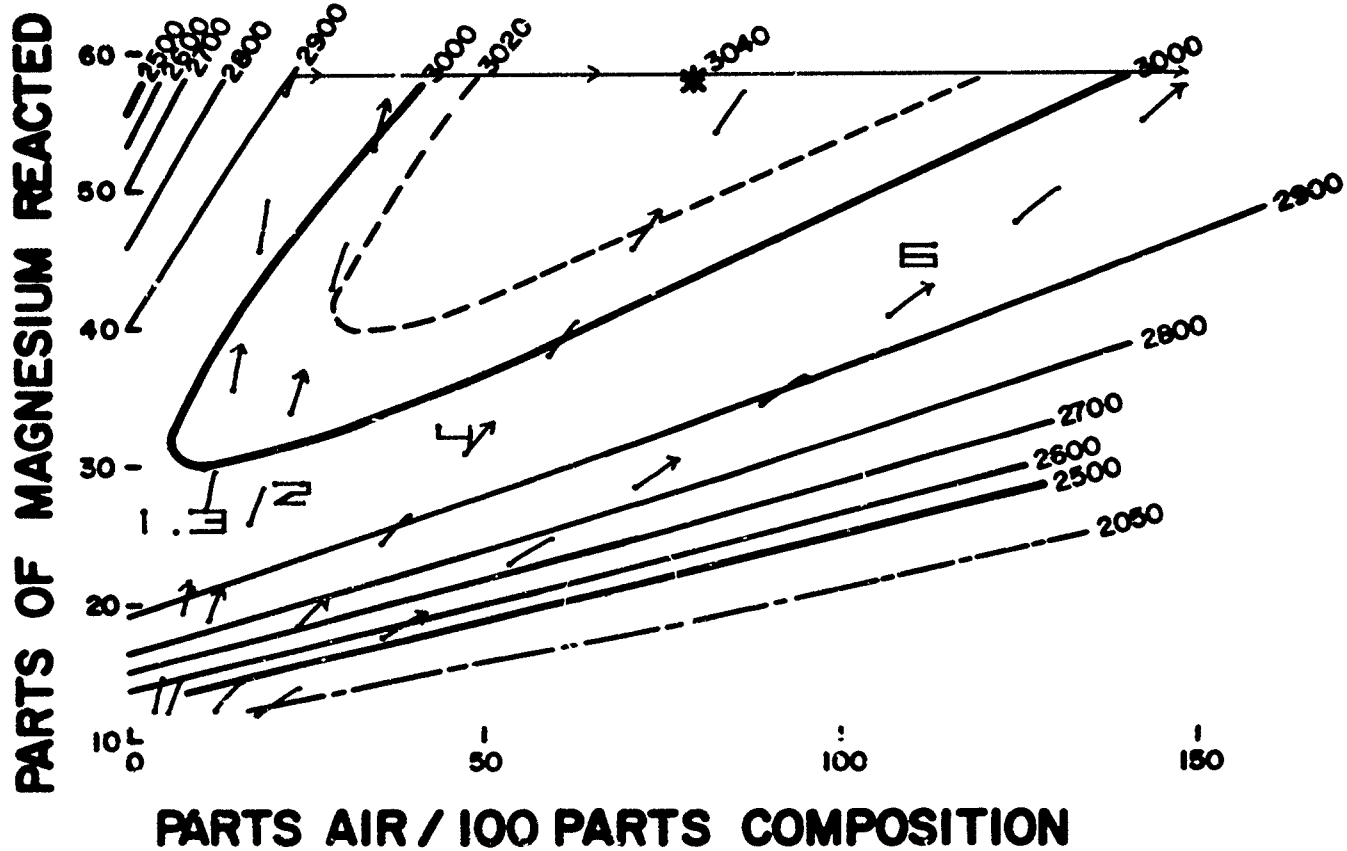

Fig. 2b. Amounts of admixed air and of vaporized magnesium during the course of burning for the air/composition ratios assumed in Fig. 2a. Contour lines for the adiabatic flame temperature (degrees Kelvin) are also shown.

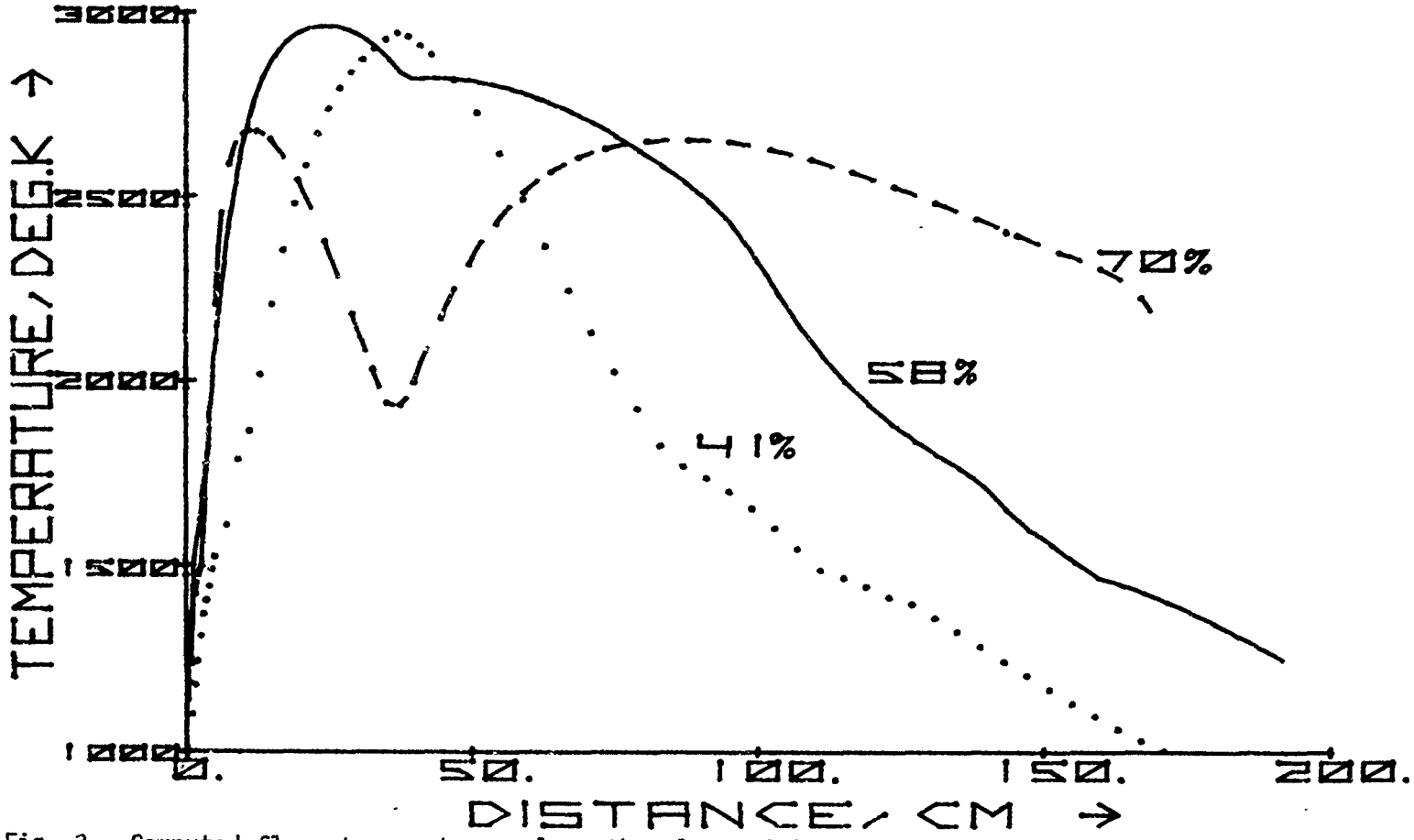

Fig. 3. Computed flame temperatures along the plume of 41%, 58% and 70% Mg flares, 4.25" diameter, approx. 5% binder. Total luminous outputs are computed to be 21,600, 43,900, and 45,300 cd sec/g, respectively. Maximum adiabatic temperatures are computed to be 3085K, 3040K, and 3026K, respectively, for the optimum amounts of air.

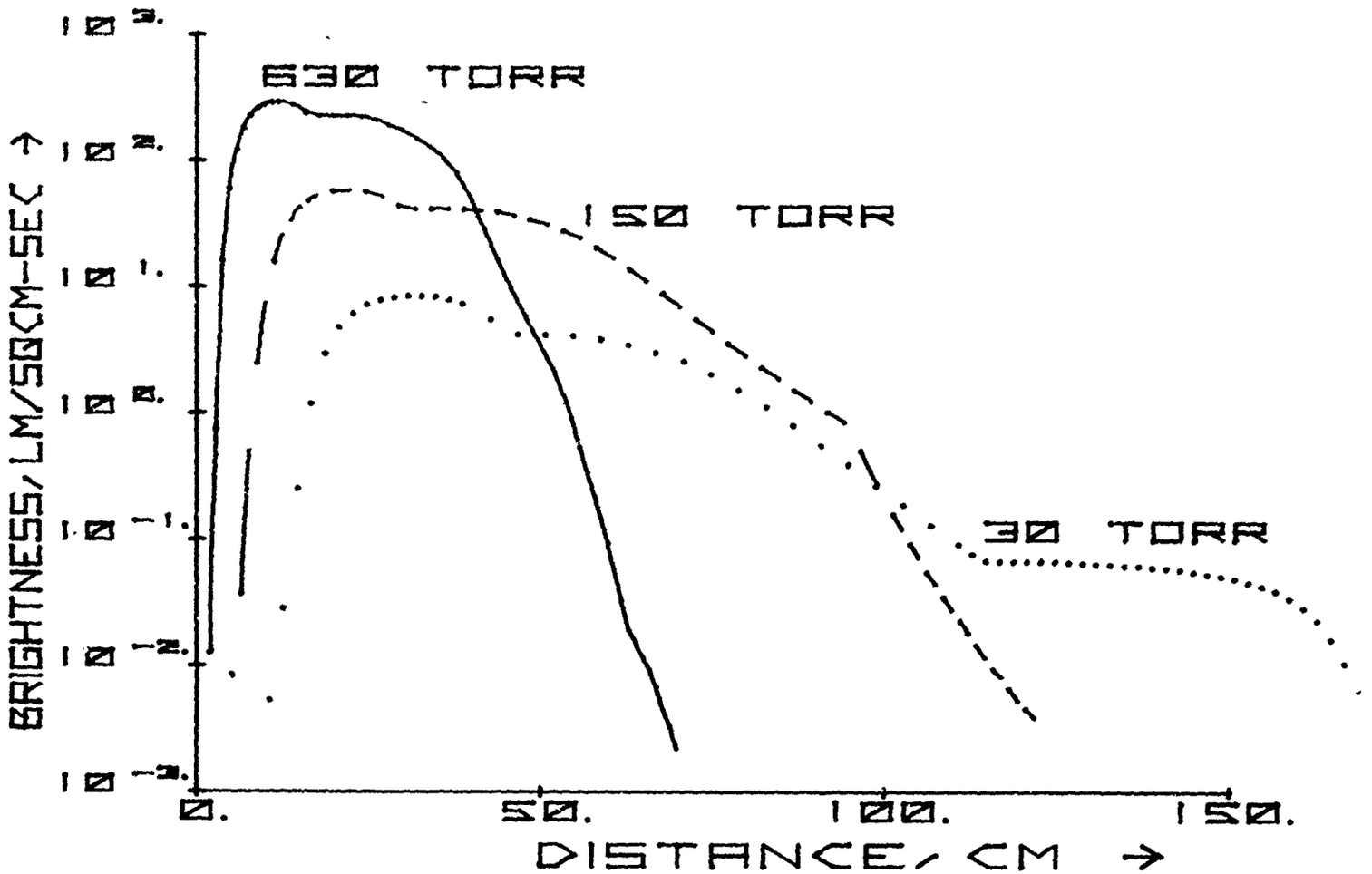

Fig. 4. Computed flame brightness along the plume of a 58% Mg, 1" diameter flare at 630, 150, and 30 Torr ambient pressure. The limit of visibility is probably about 10^{-3} lm/sec-sq. cm. Total computed luminous outputs are those predicted for the 58% flares of R. Blunt in Table IV.

Fig. 5. Computed flame temperatures (nitrogen atmosphere) for flares of 4.25" diameter, compared with thermocouple measurements.[11] Straight line segments connect values measured simultaneously on a single flare. The dotted line assumes that no excess magnesium vaporizes.

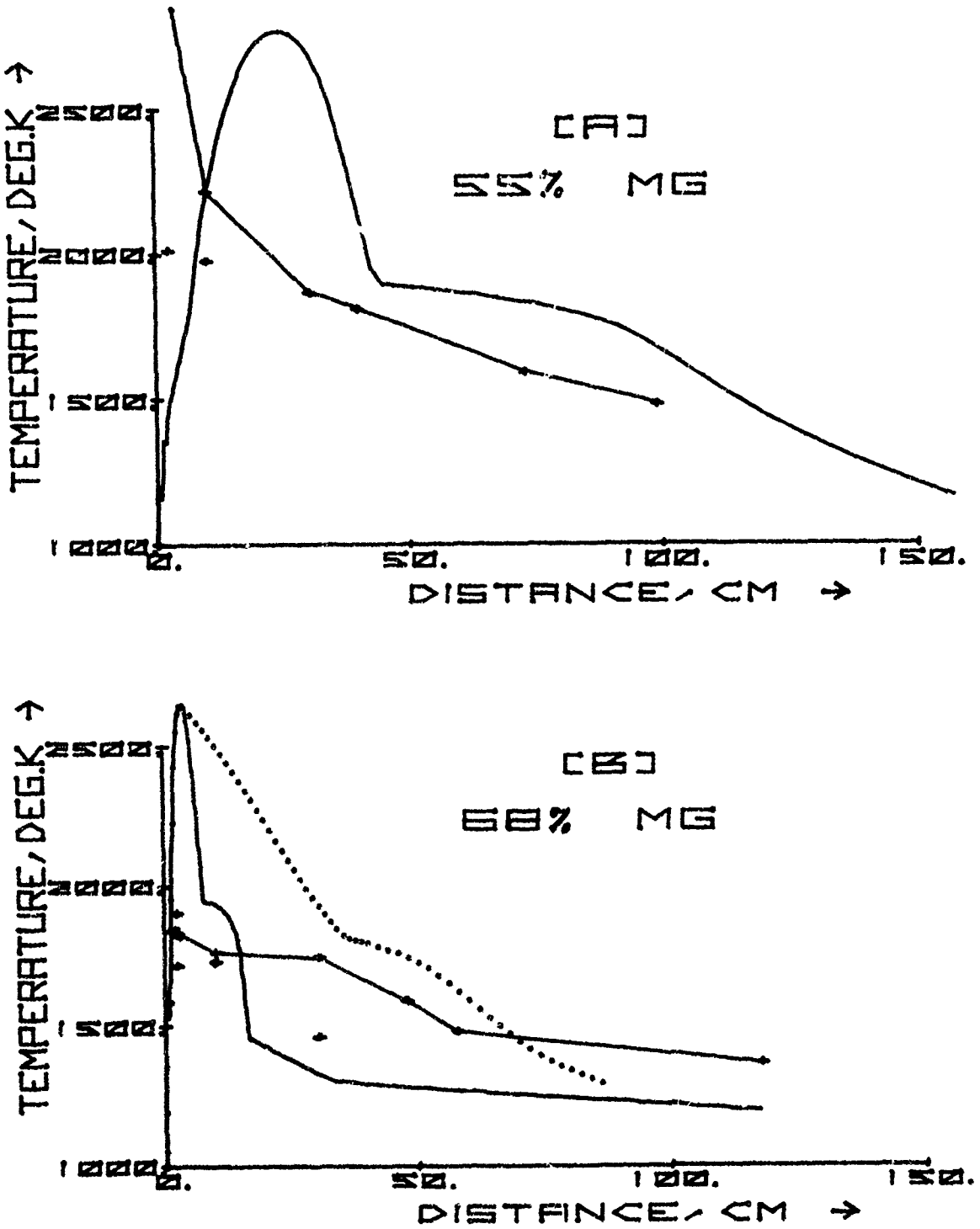

WALLOP INDUSTRIES LTD.

FLARE LINER MATERIALS

by - Dr. J. D. Gilbert

Wallop Industries Limited, Middle Wallop, Hampshire, England

ABSTRACT

For some time it has been felt that the use of traditional materials such as paper and more recently Lantex, a phenolic bonded paper or fabric material, might be replacable with advantage by plastic.

Plastics offer a cheap, lightweight varied range of materials with the possibility of forming fittings, lugs, following ogive shapes et cetera.

A summary of the work carried out at Wallop into the suitability of different liner materials will be given. All the readily available plastics at the commencement of this work were considered although some were rejected on various grounds. This work showed that Kematal and paper, with some reservations, were the most generally useful materials. It was found that the type of flare composition determines the most suitable liner material.

Introduction

Flare composition pressed into metal tubes presents problems due to such factors as the difficulty of removing the flare from the pressing bolster and the fast, often explosive burning of the filled item. The fast burning can be reduced or prevented by using an inhibiting liner or by coating the inside of the metal tube with an inhibiting material.

Most illuminating flare compositions are pressed into a tube, normally of paper or phenolic resin impregnated paper or fabric, (Lantex). The filled liner is then fixed into the metal case which protects the flare composition during storage and handling.

For a long time it has been felt that Lantex may not be the most suitable material for flare liners. This feeling is given substance by the

continued use of paper flare tubes within the pyrotechnic industry.

Lantex tubes whilst reasonably priced become expensive when grooves, slots, et cetera are required. The increased cost is due to both machining and to the increased rejection rate due to the more frequent splitting of the tubes when the composition is pressed into them. At the present time the only alternative to Lantex in wide use is paper. Paper tubes can be easily fabricated but suffer from the disadvantage of having a high, up to 10%, moisture content, and the impossibility of machining grooves et cetera to them. Some initial observation had shown that for a given flare composition the luminous efficiency and burning time were greater for flares burnt in paper tubes than those burnt in Lantex.

We thought that plastics offered an attractive alternative to paper or Lantex. Plastics are easy to fabricate, most are chemically inert and they allow moulded lugs, grooves etcetera to be provided during the initial fabrication.

Plastics Choice

All the moulding plastics available at the time were considered. Some plastics were rejected at this stage on various ground. For example:- (1) chemical degradation on storage e.g. Delrin an homopolymer of formaldehyde decomposes to formaldehyde, and polyvinylacetate gives some acetic acid. (2) High equilibrium water content e.g. Nylon (10%). (3) Poor physical properties e.g. P.T.F.E. with poor dimensional stability especially at the crystallinity changes. (4) Failures found in previous work were not considered further e.g. polycarbonate tubes were found to grow during the burning of the flare. (5) Plastics that might present moulding difficulties were rejected.

The materials finally chosen for investigation were Kematal, polypropylene, glass filled polypropylene, high density polythene, and styrene acrylonitrile. For comparison purposed Lantex, paper and aluminium tubes were included.

The plastics were moulded into tubes of approximate 1" inside diameter and 3½" long. Some variation in size was found, due to the moulding characteristics of the individual plastics. These were expected and for the purpose of this work were ignored (the differences found were up to 0.012 inch on diameter). The other materials, Lantex, paper and aluminium were also used in tubes of this size. The flare compositions were pressed into the tubes in several increments under a load of 4 tons/ square inch. The lower ends of the flares were sealed and the flares ignited with an electric fuze. The light output was measured with an eye response photoelectric cell and recorded on a U.V. oscillograph recorder. In all cases the flares were burned vertically flame upwards.

Compositions Choice

The flare composition used covered as wide a range of materials and burning rates as was feasible. The fuels used were coarse and fine magnesium in varying proportions, and titanium. The oxidants used were sodium, and strontium nitrates in different proportions, calcium oxalate was present in some composition as a rate modifier. The details of the compositions used are given in Table 1.

Results

Quantitatively, Kematal, polyproplylene, H.D. polythene and styrene acrylonitrile burnt away at approximately the same rate as the flare composition. The paper and Lantex tubes burnt more slowly. The glass of the glass filled polypropylene remained as a chimney. The flares in aluminium burnt very fast and erratically and the tubes tended to melt rapidly down one side. Only two flares were burnt in styrene acrylonitrile tubes due to the difficulties found in moulding the plastic.

The burning rates and photometric data for the flare candles are given in Table 2.

From this work the following observation can be made:-

1. Generally the flares in aluminium tubes burnt very fast and did not have very good efficiencies. This reduction in efficiency is however less pronounced with the faster burning composition, such as the titanium based compositions.

2. Styrene acrylonitrile was only used in two tests but as the efficiences were poor no further work was done with this material.

3. The luminous efficiencies of the compositions based on the coarser grades of magnesium with sodium nitrate as oxidant were affected by the liner materials in the following order:- paper, Kematal, H.D. polythene, glass filled polypropylene, polypropylene, aluminium, Lantex and the worst was styrene acrylonitrile.

   Compositions using the finer grades of magnesium were still the most efficient in paper and Kematal but the order of superiority for the other liner materials varied.

4. Trials with faster burning compositions have shown that these are less sensitive to the liner material.

5. It seems likely that as long as a minimum thickness of liner is between the composition and the outer case the results are independent of the material of the outer case but dependent on the liner material. The minimum thickness of liner depends on both the flare composition and the liner material. In parrallel with

the photometric work an X-ray study of burning flares was carried out.

The film to be shown was taken from the X-ray fluorescence screen. The flare candles were rotated at about $\frac{1}{4}$ rev/s about their vertical axes on a turntable. The rotation enable the distinction to be made between the formation of a cone or a tilted plane surface during the burning of the flare. The compositions used were those that were used for the photometric work; and the liners used were paper, Kematal, Lantex, high density polythene and glass filled polypropylene. The flare compositions, liners and comments on the X-ray film are given in Table 3.

Conclusions

On the basis of this work some firm and some tentative conclusions can be drawn:-

1. The most suitable liner for a given composition is not necessarily best for any other composition. The results obtained give an indication of the most likely material in a given case.

   From an efficiency point of view paper or Kematal are the most satisfactory materials for liner construction. The disadvantage of paper is its high equilibrium water value and the ensuing shrinking and stretching that occurs with the change in its water content. This becomes a problem if cracks can occur between the flare and the liner allowing the flame to burn ahead of the compositions surface, rapid and often explosive burning can then occur. However, a flare pressed into a paper tube and potted into a metal outer case soon reaches equilibrium and becomes stable. Kematal or any thermoplastic suffers from the disadvantage of requiring a moulding tool but once fabricated the cost per flare liner is low.

2. Intuitively the conductivity of the liner material plays some part in the burning characteristics of the flares.

TABLE 4

Thermal Conductivity

paper	3×10^{-4}	cal/cm°C
Lantex	7×10^{-4}	"
Kematal	5.5×10^{-4}	"
Polypropylene	5×10^{-4}	"
H.D. polythene	8.7×10^{-4}	"
Aluminium	.57	"

As the conductivity of aluminium is several orders of magnitude greater than the others, different behavious might be expected. That a high conductivity effects the burning rate is shown by the data in Table 5 for a magnesium/sodium nitrate flare of 2.5" diameter and about 5" long.

A further effect of the liner material might be due to its heat capacity and latent heat of fusion both of which might be expected to reduce a flares' efficiency by removing energy and reducing the flame temperature. This effect would be offset by the heat of burning of the flare tube. Unfortunately data is difficult to obtain to substantiate or disprove this theory.

Summing up, the material surrounding a flare is very important as far as the suitability of a particular flare composition is concerned for a given application. The final choice of liner material will still have to be based on the off setting of one factor e.g. cost and quantities required, against such things as desired light output and speed of burning, but at least now a more informed choice can be made.

TABLE 1

Details of Composition Used

Composition	'Speed'	Ingredients :				
A	slow	Mg 49%	Varnish 5%	$NaNO_3$	39%	$Ca(OOC)_2$ 7%
B	slow	Mg 50%	Varnish 4%	$NaNO_3$	46%	
C	slow	Mg 55%	Varnish 2.5%	$NaNO_3$	42.5%	
D	medium	Mg 58%	Polyester epoxy 8%	$NaNO_3$	34%	
E	fast	Mg 50%	Varnish 4%	$NaNO_3$	40%	$Ca(OOC)_2$ 6%
F	fast	Mg 50%	Varnish 5%	$NaNO_3$	35%	$Ba(NO_3)_2$ 10%
G	fast	Ti 48%	Boiled Linseed Oil 4%	$Sr(NO_3)_2$	45%	Chlorinated rubber 3%
H	fast	Mg 55%	Viton 5%	polytetrafluoroethylene	40%	

TABLE 2

The effect of liner materials on the pyrotechnic performance of various compositions

Composition	Tube material	Burning rate in/s	Light output kcd/in^2	Efficiency kcd s/g
A	paper	0.055	47	29
	Lantex	0.13	51	14
	Kematal	0.055	40	26
	polypropylene	0.06	40	23
	glass filled p.p.	0.11	81	25
	H.D. polythene	0.07	54	27
	styrene acrylonitrile	0.06	18	11
	aluminium	0.27	106	16
B	paper	0.07	47	26
	Lantex	0.19	60	11
	Kematal	0.07	50	26
	polypropylene	0.07	29	17
	glass filled p.p.	0.08	40	18
	H.D. polythene	0.07	42	21
	aluminium	0.26	120	16
C	paper	0.07	86	41
	Lantex	0.20	72	12
	Kematal	0.07	80	41
	polypropylene	0.07	42	21
	glass filled p.p.	0.08	75	34
	H.D. polythene	0.07	75	37
	aluminium	0.27	138	18
D	Kematal	0.09	149	39
	paper	0.09	59	29
	Lantex	0.17	116	30
	aluminium and asbestos paper	0.15	92	41

Table 2 Continued.....

TABLE 2 (continued)

Composition	Tube material	Burning rate in/s	Light output kcd/in^2	Efficiency kcd s/g
E	paper	0.15	95	26
	Lantex	0.16	84	20
	Kematal	0.13	76	22
	polypropylene	0.13	48	13
	glass filled p.p.	0.14	77	21
	H.D. polythene	0.13	58	16
	styrene acrylonitrile	0.15	51	13
	aluminium	0.39	145	14
F	paper	0.17	113	20
	Lantex	0.22	78	14
	Kematal	0.15	77	20
	polypropylene	0.16	87	19
	glass filled p.p.	0.13	65	15
	H.D. polythene	0.15	46	13
	aluminium	0.54	250	17
G	paper	0.16	36	5.0
	Lantex	0.21	46	4.9
	polypropylene	0.25	32	2.9
	glass filled p.p.	0.26	40	3.6
	Kematal	0.24	56	5.4
	H.D. polythene	0.25	21	2.9
	aluminium	0.36	62	3.8
H	paper	0.18	38	4.7
	Lantex	0.19	22	3.8
	Lantex with thin coat of Viton	0.18	21	3.7
	Lantex with thick coat of Viton	0.18	19	3.6
	polypropylene	0.18	14	2.4
	glass filled p.p.	0.18	16	2.9
	glass filled p.p. with thin coat of Viton.	0.19	19	3.2
	glass filled p.p. with thick coat of Viton	0.17	17	3.2
	H.D. polythene	0.17	8	1.4
	aluminium	0.67	21	1.1
	Kematal	0.18	20	3.5

TABLE 3

Flares noted in the order they appear on the film

Flare No	Mix	Tube	Efficiency of light production in this tube material	Shape of burning surface
29	F	glass filled polypropylene	poor	some sloping
28	C	Lantex	very poor	some coning
27	C	paper	good	slight saucer
26	C	H.D.polyethylene	good	slight saucer
25	C	Kematal	good	slight saucer
24	D	Lantex	fair	some coning
22) 21)	D	paper	good	flat
20) 19)	D	Kematal	very good	very slight saucer
18) 17)	A	Lantex	poor irregular	irregular burning, coned and sloped.
16) 15)	A	paper	good	slight saucer
14) 13)	A	Kematal	good	some saucer
12	H	Lantex	fair	turbulent but flat
9	H	paper	good	turbulent but flat
8)	H	Kematal	fair	turbulent but flat
7)			fair	turbulent some saucer.
6) 5)	G	Lantex	light intensity very low at start, rose for first third then irregular.	coning getting progressively worse slag left in tube.
4) 3)	G	paper	good from start but irregular.	flat.
2) 1)	G	Kematal	good from start, fairly regular	quite flat, some turbulence.

TABLE 5

Results from flares burnt in 2.5" diameter tubes

Liner	Centre Rod	Burning time	Light output kcd	Efficiency kcds/g
2 layers Delrin '20 thou'	absent	54	529	49.6
2 layers Kematal "	steel tube $\frac{3}{8}$" diameter	24.5	861	36.4
2 layers Kematal "	steel tube $\frac{3}{8}$" diameter	29.2	554	28.0
2 layers Kematal "	viton coated steel tube	49.9	534	45.9
4 layers polythene "	absent	42.5	613	44.1
4 layers polythene "	steel tube $\frac{3}{8}$" diameter	28.9	723	35.0

Composition pressed into an unlined aluminium tube burnt explosively giving a meaningless light output trace.

A COMPARISON OF THE SPECTRA FROM NAVY AND AIR FORCE AIRCRAFT PARACHUTE FLARES

Henry A. Webster III
Applied Sciences Department
Naval Ammunition Depot, Crane, Indiana 47522

ABSTRACT

Spectra have been obtained in the visible and near infrared spectral region from the Navy Mk 45 and the Air Force LUU-2B/B aircraft parachute flares. Marked differences are noted particularly in the region of the sodium D resonance line radiation and in the red region of the spectrum. The broadening of the sodium resonance lines is considerably less in the LUU-2B/B than in the Mk 45. There is also considerably less radiation in the red spectral region from the LUU-2B/B. Color data and candlepower are presented for both flares. An explanation of the differences in the spectra is given in terms of the radiative transfer model.

BACKGROUND

There is currently under consideration a proposal to adopt the Air Force LUU-2B/B Aircraft Parachute Flare as the Tri-Service illuminating flare.

In tests of the LUU-2B/B and in actual use it is often reported that the LUU-2B/B is more yellow in color than the Mk 45. Whether or not the color of the light is important in target acquisition has yet to be determined. The purpose of this work is to determine if there is a color difference in the LUU-2B/B and Mk 45 and to determine the origin of the difference.

EXPERIMENTAL

These experiments were carried out in the photometric burning chamber at NAD Crane. The flares were burned face down at a distance of 400 cm from the spectrographs. The wind speed in the tunnel was 18 mph, the air flow being in the same direction as the mass flow in the burning flare. The flares were positioned and masked so that the light being measured came from a position two flare diameters (8.5 inches) above the burning surface.

Spectra were taken on a Bausch and Lomb 1.5-m spectrograph equipped with Linagraph Shellburst film. The spectrograph has a 450 line/mm grating blazed at 490 nm. The spectral range from 380-680 nm was covered with a dispersion of 15 Å/mm in the first order.

After each flare spectrum was taken, several spectra of a 200 watt quartz-iodine standard lamp were taken on the same film. These spectra from a source with a known output were used to correct the flare spectra for film response. Wavelength calibration was obtained from the known emission features in the flare spectrum.

Microdensitometer traces of all spectra were made on an Optronics densitometer. Readings of film density were made at 100 micron intervals across the entire spectrum. These density readings were converted to radiant power by applying the film correction function generated from the quartz-iodine lamp spectra. The radiant power spectra were converted to luminous power spectra by applying the photopic luminous efficiency function, i.e. the eye response curve.[1]

The resulting spectra normalized to a value of one at the maximum emission are shown in Figs. 1-4.

Intensity measurements based on film density and exposure time indicate that the Mk 45 flares have about 25% more output than the LUU-2B/B. Power measurements made at NAD Crane MAPI site indicate equal intensities and burn times for the Mk 45 and LUU-2B/B flares.

DISCUSSION

Figures 1-4 show that there are two obvious differences between the spectra of Mk 45 and LUU-2B/B Aircraft Parachute Flares. The region of the sodium D resonance line broadening is greatly reduced in the LUU-2B/B and the background continuum and emission from molecular and atomic species other than the sodium is essentially non-existent in the LUU-2B/B.

There are basic differences between the Mk 45 and LUU-2B/B in terms of composition and design. The LUU-2B/B is a tamp-cast flare composed of 61% magnesium, 20% fine sodium nitrate, 10.9% coarse sodium nitrate and 8.1% binder. The flare is cast into an aluminum case. The Mk 45 is a pressed flare composed of 58% magnesium, 37.5% sodium nitrate and 4.5% binder and pressed into a paper case.

The drastic differences in these two spectra are difficult to reconcile on theoretical grounds. If the resonance broadening model developed by Douda[2] is used, the only parameter which is adjustable for two flares with essentially the same composition and burning at the same temperature is the Voigt a parameter. The Voigt function is given by the expression

$$a = [(\Delta\lambda_N + \Delta\lambda_L + \Delta\lambda_R + \Delta\lambda_Q)/\Delta\lambda_D](\ln 2)$$

where $\Delta\lambda_N$, $\Delta\lambda_L$, $\Delta\lambda_R$, $\Delta\lambda_Q$ and $\Delta\lambda_D$ are the natural, Lorentz, resonance, quenching and Doppler broadening half-widths respectively. In order to fit the LUU-2B/B spectrum, it is necessary to reduce the Voigt function a parameter to a value of $a = 0.2$. While this value produces the correct value of the half-width for the sodium resonance radiation, there is no simple reason for obtaining this value of a in the LUU-2B/B case and not in the Mk 45 case since the gross features of sodium atom density, flare temperature and flame size do not change significantly.

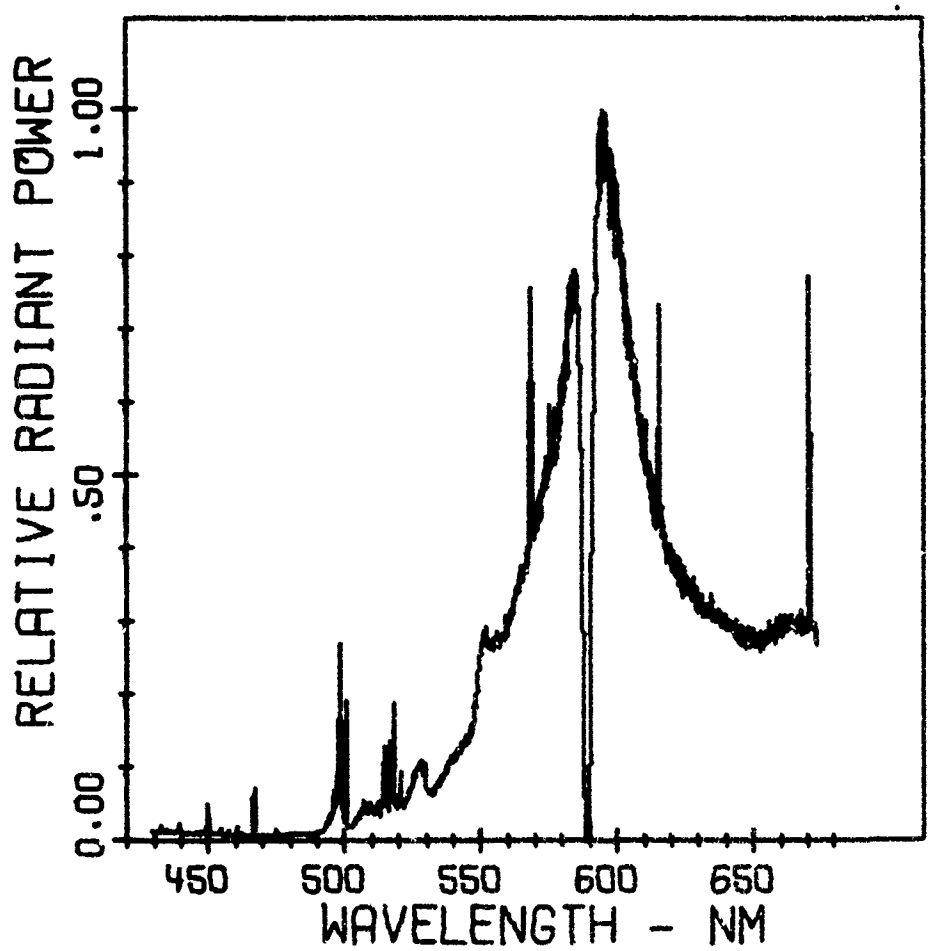
RELATIVE RADIANT POWER
1.00
.50
0.00
450
500
550
600
650
WAVELENGTH - NM

FIG. 1. Mk 45

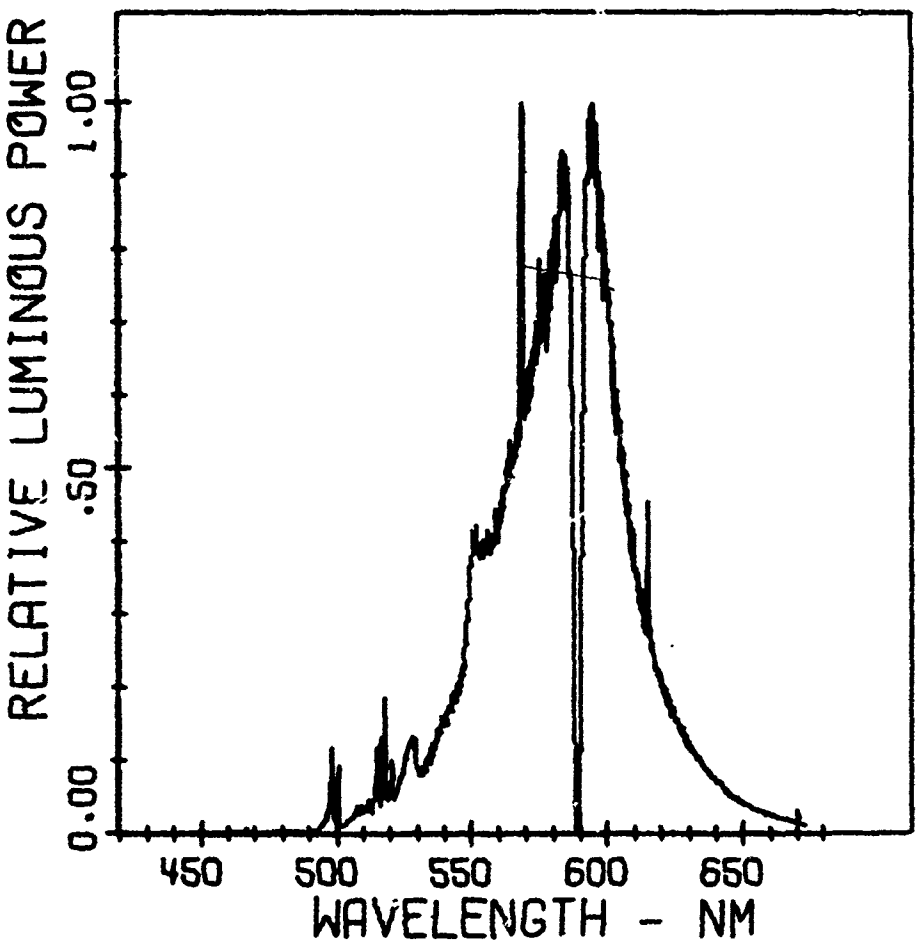
RELATIVE LUMINOUS POWER
0.00
.50
1.00
450
500
550
600
650
WAVELENGTH - NM

FIG. 2. Mk 45

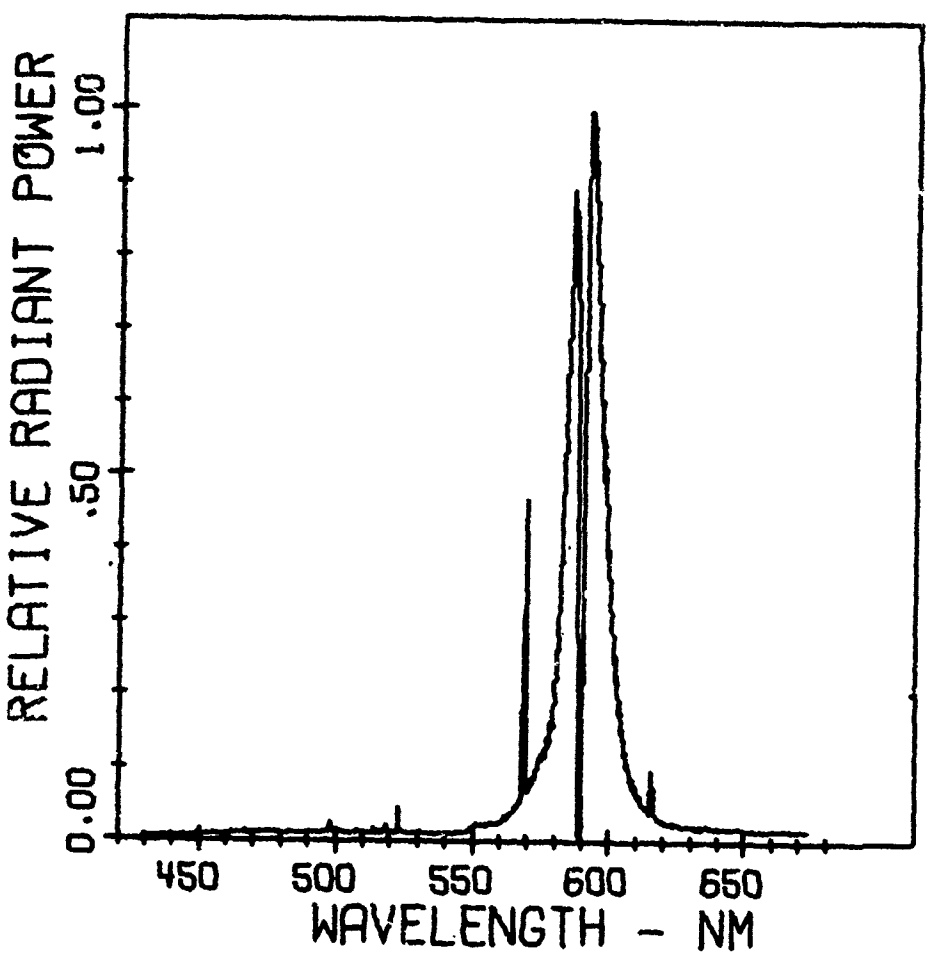
RELATIVE RADIANT POWER
1.00
.50
0.00
450
500
550
600
650
WAVELENGTH - NM

FIG. 3. LUU-2B/B

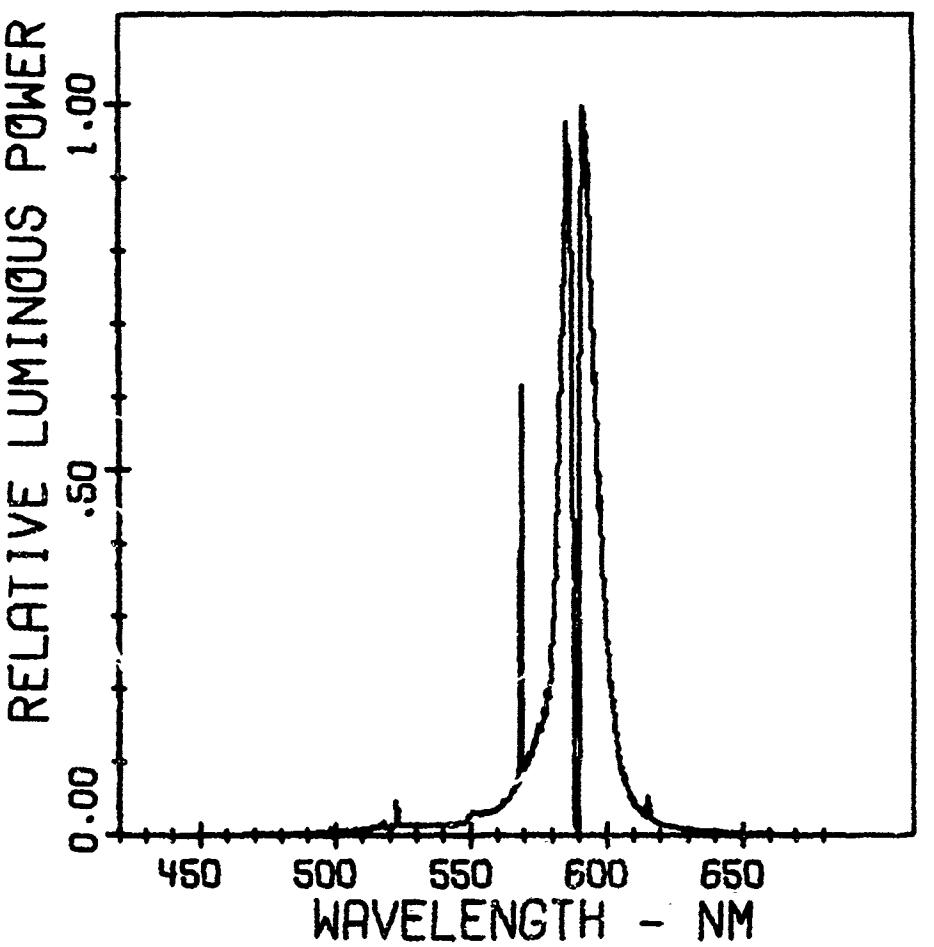
RELATIVE LUMINOUS POWER
1.00
.50
0.00
450
500
550
600
650
WAVELENGTH - NM

FIG. 4. LUU-2B/B

The explanation for a different a parameter has to be on a smaller scale, perhaps microscopic in the flame. The over-simplification of Douda's model makes it impossible to account for these differences. Detailed maps of temperature and specie concentration in the flame are needed in order to discuss the variation in the a parameter. These computations and experiments designed to test them will have to be done in order to unravel some of the problems associated with illuminating flares.

It has recently been shown by Blunt[3] that there are specific regions in the flame where the various atomic and molecular species emit. It is possible that in the LUU-2B/B the magnesium and magnesium oxide emission is stronger in some region other than two flare diameters above the burning surface. This would account for the lack of emission observed in the region 430-550 nm.

In an effort to determine if there is a color difference in the two flare compositions, the radiant power data shown in Figs. 1 and 3 were converted to the tristimulus color values x, y, and z. From these values, the tristimulus coordinates x and y and hence the dominant wavelength and purity can be obtained. The tristimulus coordinates are $x = 0.552$ and $y = 0.427$ for the LUU-2B/B and $x = 0.525$ and $y = 0.452$ for the Mk 45. These values are plotted in Fig. 5 to obtain the dominant wavelength and purity of the flare. For the LUU-2B/B, the dominant wavelength is 589 nm and the purity is 95%. For the Mk 45, the dominant wavelength is 584 nm and the purity is 94%. While the values for the dominant wavelength are different by 50 Å it is difficult to imagine that this difference could be distinguished visually.

CONCLUSIONS

The radiant power and luminous power spectra for LUU-2B/B and Mk 45 Aircraft Parachute Flare are found to be different. The output from the LUU-2B/B is narrower than the Mk 45 in sodium D region. The background continuum and molecular and atomic emission from magnesium oxide and magnesium are absent in the LUU-2B/B spectrum. The dominant wavelength in the LUU-2B/B is 589 nm and 584 nm in the Mk 45. This is not enough difference to account for the so-called yellow color in the LUU-2B/B. The purity of the two flares is also the same indicating that this is not the reason for the color difference.

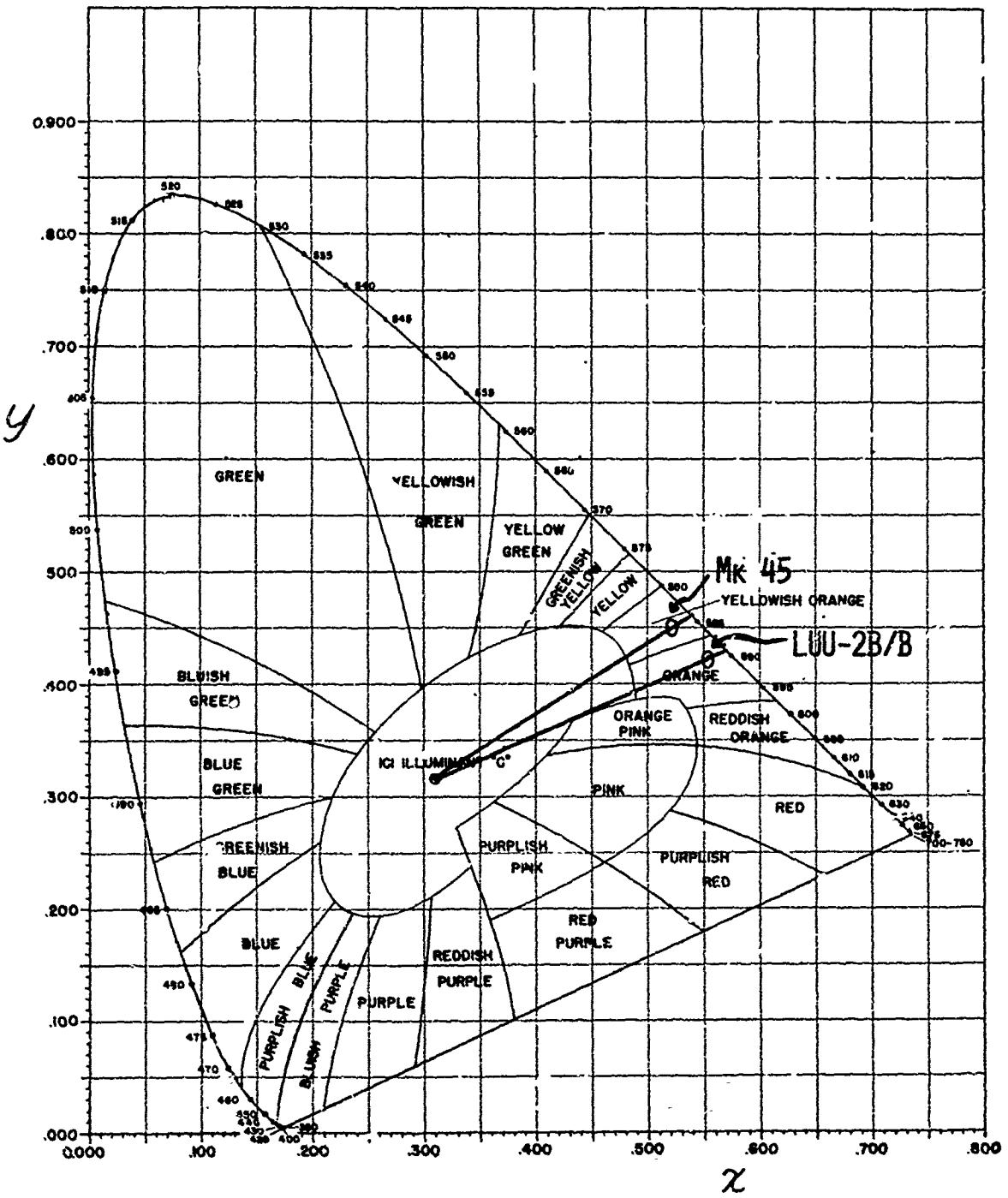

FIG. 5. Chromaticity Diagram

REFERENCES

1. OSA Committee on Colorimetry, *Science of Color* (Crowell Company, New York, 1953), Chap. 8.

2. B. E. Douda, *Radiative Transfer Model of a Pyrotechnic Flame*, RDTR No. 258, Naval Ammunition Depot, Crane, Indiana (1973). AD No. 769 237.

3. R. M. Blunt, *Spectral Distribution of Different Regions of Illuminating Flare Flames*, RDTR No. 220, Naval Ammunition Depot, Crane, Indiana (1973). AD No. 757 663.

ABSTRACT

An experimental investigation has been made to determine quantitatively the effect of thermal conductivity (λ) and gas permeability (κ) on the burning rates of magnesium-sodium nitrate and aluminum-sodium nitrate flare compositions. Measurements of λ and κ were made as a function of composition variation, loading pressure and metal particle size.

In general λ increases with increasing metal content and loading pressure while it decreases with increasing particle size. The burning rate is approximately proportioned to the square root of λ.

The change in the gas permeability with metal content, particle size and loading pressure appears to be quite complex as is the relation of burning rate to gas permeability. These effects are examined and the possibility of heat feedback from the flame to the burning flare via hot gas permeation is discussed.

NOTE: Copies of this paper will be distributed by the author at the seminar.

A TAMP CASTABLE COMPOSITION FOR ILLUMINATING FLARES

By R. F. Eather

Royal Armament Research and Development Establishment,
Fort Halstead, Sevenoaks, Kent, UK

Summary:

Studies have recently been carried out of the factors which influence the luminous efficiency of compositions based on Magnesium, Sodium Nitrate and a polyester/epoxy resin binder. The formulation was optimised with respect to binder level, fuel/oxidant ratio and particle size of ingredients. It was found that by a judicious selection of liner material and tamping load luminous efficiencies in excess of 50 Kcd. secs. gm^{-1} could regularly be achieved.

1. Introduction

Binding or pelleting materials have been incorporated into pyrotechnic compositions for a good many years although the emphasis placed on the reasons for so doing has altered from time to time. The principal functions are as follows:-

a) to increase cohesion between the particulate ingredients when consolidated under pressure

b) to protect the ingredients from moisture, etc.

c) to enable rigid pellets to be obtained with lower pressing loads.

In the past few years particular attention has been paid to the last of these functions. Resin bonded compositions offer an opportunity to reduce both the manpower and machinery involvement in flare production and at the same time enable a greater variety of configurations to be produced. These compositions lend themselves to the type of mass production technique used in the plastics industry since they can often be mixed, moulded or extruded with similar equipment. The composition can be considered as an uncured, fluid plastic to which solid powdered ingredients are added in calculated proportions thereby increasing the viscosity. This gives rise to a series of mixtures which at one end of the spectrum can be pour-cast and at the other end tamp-cast or machine pressed using a small load. The proportion of resin present in final mixture is necessarily higher than the binder level in a pressed composition in order to maintain fluidity and the pyrotechnic properties of the cured filling are correspondingly different. The challenge is then to modify the character of the ingredients so as to match as closely as possible the pyrotechnic properties of conventional fillings.

A newcomer to this branch of pyrotechnics is faced with a bewildering choice of possible binder materials. In order to reduce the workload to managable proportions it was decided, as a result of a literature survey, to base a programme on the Formrez system which has been investigated by Dinsdale et al.

This paper describes the studies that have been done in recent months of the factors which influence the luminous efficiency of this system, with the object of preparing a tamp castable flare composition with maximum luminous efficiency.

2. Flare preparation and evaluation

All the flare compositions were made in a Z-blade mixer. The magnesium, catalyst and resin were blended for 10 minutes with two stops for scraping down. The sodium nitrate was then added and then the machine was run for a further 10 to 20 minutes, depending on the resin content, until a visual examination showed that the mixture was homogeneous.

Various types of flare liner materials were used during this programme; aluminium, paper-phenolic, paper and kematal. The aluminium liners were painted with the resin mixture at least two hours before use. The composition was consolidated in 1.05 inch diameter liners in 20 gram portions under various loads and then the candles were cured in an oven at 60°C before being measured and weighed.

They were all ignited by quickmatch and loose thermite powder and measurements of light output and burning time were done in a standard pyrotechnic tunnel.

3. Variation of consituent proportions

There are obviously a large number of permutations and combinations of fuel/oxidant ratio, binder level and particle size of ingredients and so it was necessary to make certain assumptions regarding the most likely region of interest based on the literature survey and past experience of conventional compositions.

A short programme was carried out based on the following materials

Magnesium Grade 0	75 parts	)
" " 3	25 "	)
Sodium nitrate 60 mesh	50 parts	)
" " 6 micron	50 "	)
Formrez F17-80	)	
ERL 0510	) 9% of the composition	
Iron octoate	)	

Two types of flare tube were used, aluminium and Lantex which is a commercial phenolic impregnated material. Some of the aluminium tubes contained liners of unglazed kraft paper so as to reduce heat conduction down the side of the flare. The inner surfaces of the liners, or the tube if no liner was present, were in all cases painted

with filled resin. In all instances the batches of composition were sufficient for three candles and the candles to any one formula were made from a total of three batches. The results of measurements made on burning flares are given in Table 1.

TABLE 1

$Mg:NaNO_3$:resin	Burning rate (mm/sec)			Light output (cd/mm^2)			Luminous efficiency (Kcd sec/gm)		
	(1)	(2)	(3)	(1)	(2)	(3)	(1)	(2)	(3)
61:30:9	6.1	4.8	4.0	295	172	172	36	25	33
58:33:9	6.5	4.5	4.6	273	175	191	31	29	34
55:36:9	6.6	4.5	4.6	293	178	207	30	29	35

(1) Aluminium tube lined with filled resin
(2) Lantex tube lined with filled resin
(3) Aluminium tube lined with paper and filled resin

The results obtained showed that the variation of fuel to oxidant ratio tried, which were claimed as optimum values by other workers, had no great effect on burning properties when compared with the changes due to different liner materials.

During this series of experiments it was noted that the Type 3 liner, the one with the paper insert, had a much smoother light output curve than the other two types. This is in accordance with our experience on other compositions in paper liners and so it was decided to discontinue the use of aluminium tubes and Lantex liners. Another programme on liner materials which was proceeding concurrently showed that the acetal polymer, marketed under the name of Kematal, gave reproducible pyrotechnic properties with a variety of conventional pressed compositions and so this material was added to the programme.

4. Effect of surfactants

The pyrotechnic properties of resin bonded compositions can be altered by changing the powder to resin ratio. Early work had shown that luminous efficiency increased as the resin content decreased. One way of achieving an increase in powder content, consistent with producing a tamp-castable mix, was to add small quantities of surface active agents to each composition.

For comparison purposes the mixes were classified on an arbitrary scale of 1 to 4 where 1 represents dry sand, 2 damp sand, 3 wet sand and 4 is a putty-like mix.

The most commonly used method of incorporating the surfactant into the mix was to dissolve the material in toluene and add it either to the whole mix or to the sodium nitrate. It was found easier and quicker to do the latter since the toluene could be evaporated off by drying the sodium nitrate in an oven at about 55°C.

Concurrently with the programme on surface active agents a study of the effect of pressing load was carried out. The results in Table 2 indicate that there is not a simple relationship between efficiency and pressing load, in some cases there is even a reversal in the efficiency figures.

The basic formulation used for this series of experiments was:

Magnesium, Grade 0 (75%) / " Grade 3 (25%)	58.5 parts		
Sodium nitrate	33.2	"	
Resin	8.2	"	
Surface active agent	0.1	"	(approx)

The amount of surfactant added to the mix was arbitrary and so recently the quantity of surfactant has been increased. The series of experiments is not yet complete but, as expected, the effect varies according to the particular chemical. It was also found that the liner material affected the result obtained. For instance an increase in Tween 60 reduces the efficiency in Kematal but increases the efficiency in paper, whilst an increase in S101 improves the efficiency of the composition in both.

5. Summary

There is obviously still a large number of experiments to be done before this composition system is fully characterised. All future experiments will be done in Kematal liners since these enable good luminous efficiencies to be achieved. The choice of surfactant is obviously a key area but further work is needed to establish whether the mix consistency can be improved, by increasing the amount of surfactant used, without detriment to the performance of the composition.

When this has been achieved it will be possible to investigate the use of pressing loads of less than $\frac{1}{2}$ ton/sq in. to find the minimum load required to ensure reproducable performances.

British Crown Copyright reserved
Published with the permission of the Controller of Her Brittanic Majesty's Stationery Office

TABLE 2

Surfactant	Pressing load (tons/sq in)	PAPER LINER			KEMATAL LINER			Consistency
		Burning rate (mm/sec)	Light output (cd/mm^2)	Efficiency (Kcd sec/gm)	Burning rate (mm/sec)	Light output (cd/mm^2)	Efficiency (Kcd sec/gm)	
.08% Lecithin	Tamped	3.9	135	29	3.3	178	44	3
	0.5	2.7	128	33	2.5	191	55	
	1	2.6	117	30	2.2	179	51	
	2	2.3	114	30	1.9	157	51	
.08% Tween 60	Tamped	3.4	130	32	3.0	202	56	2
	0.5	2.5	114	31	2.3	184	55	
	1	2.4	104	30	2.1	160	50	
	2	2.2	96	27	2.0	183	57	
.08% Span 80	Tamped	-	-	-	3.3	169	42	2
	0.5	2.6	112	29	2.4	183	52	
	1	2.4	111	29	2.3	181	50	
	2	2.3	109	30	2.0	150	46	
.08% S101	Tamped	4.3	120	20	4.0	217	46	3
	0.5	3.3	136	28	3.1	204	47	
	1	3.0	111	24	2.9	204	46	
	2	2.8	118	27	2.6	204	46	

TABLE 2 (cont'd)

Surfactant	Pressing load (tons/sq in)	PAPER LINER			KEMATAL LINER			Consistency
		Burning rate (mm/sec)	Light output (cd/mm^2)	Efficiency (Kcd sec/gm)	Burning rate (mm/sec)	Light output (cd/mm^2)	Efficiency (Kcd sec/gm)	
.08% Manoxol N60%AG	Tamped	-	-	-	4.5	199	27	2
	0.5	3.3	101	22	3.1	183	43	
	1	3.0	155	35	2.9	204	48	
	2	3.1	127	29	2.5	202	50	
.08% Manoxol 1B	Tamped	4.1	155	35	3.8	212	50	2
	0.5	2.9	134	34	2.8	213	57	
	1	2.7	128	31	2.6	202	54	
	2	2.5	123	30	2.3	188	54	
.08% Manoxol MA60	Tamped	4.7	129	24	3.9	208	50	2
	0.5	3.0	133	32	2.8	196	54	
	1	2.8	76	18	2.6	191	50	
	2	2.5	109	26	2.4	196	52	
.08% Anti-terra P	Tamped	4.5	133	26	3.2	181	48	3
	0.5	2.8	120	29	2.7	172	44	
	1	2.6	125	30	2.5	185	48	
	2	2.5	121	29	2.3	184	49	

TABLE 2 (cont'd)

Surfacant	Pressing load (tons/sq in)	PAPER LINER			KEMATAL LINER			Consistency
		Burning rate (mm/sec)	Light output (cd/mm^2)	Efficiency (Kcd sec/gm	Burning rate (mm/sec)	Light output (cd/mm^2)	Efficiency (Kcd sec/gm)	
.08% Anti-terra U	Tamped	3.5	154	40	3.2	182	52	3
	0.5	2.7	116	29	2.7	183	50	
	1	2.5	110	28	2.4	183	49	
	2	2.4	114	29	2.2	196	52	
.1% Tween 60	Tamped	3.2	137	36	3.5	170	37	3
	0.5	2.5	139	36	3.1	180	41	
	1	2.4	123	32	2.6	180	46	
	2	2.1	113	30	2.4	173	47	
.1% S101	Tamped	3.8	143	33	3.3	195	51	3
	0.5	2.7	130	35	2.6	195	54	
	1	2.5	118	31	2.5	187	52	
	2	2.3	128	33	2.2	183	53	

ABSTRACT

A formulation has been developed for use in the U.S. Army Trip Flare which utilizes aluminum as a substitute for magnesium fuel. Previously aluminum was not considered to be a good fuel for flare applications since mixtures of atomized aluminum (diameter $\geq$ 15 μ) and sodium nitrate are not readily ignitable, propagate poorly, and burn very erratically and inefficiently. One of the reasons for the inefficiency of this system is the considerable loss of fuel as incandescent particles. This Roman Candle effect makes the flare an incendiary device as well as an illumination source. This incendiary aspect is very undesirable causing possible harm to users and danger of starting ground fires. The present study shows how the ignition properties of aluminum-sodium nitrate can be significantly improved and how the production of incandescent particles can be minimized by using small percentages of various additives, such as tungsten metal.

By using these new additive systems, the two basic advantages of aluminum can be used. The first is cost, 38 cents per pound for aluminum as compared to 85 cents for 20/50 mesh atomized magnesium, and the second is its ready availability.

The disadvantages associated with the present aluminum formulation, as well as with other aluminum formulations, when exposed to excess moisture are gassing and self-heating leading to spontaneous ignition in storage. Experimental data is presented showing these interesting phenomena. By careful exclusion of moisture during processing, these effects can be eliminated, as was demonstrated by long term storage stability testing.

INTRODUCTION

The present study was conducted to determine if a composition could be developed for the Army M49A1 Trip Flare containing aluminum as a substitute for magnesium. The primary justification for this program was based on cost and availability of aluminum as opposed to magnesium. Atomized magnesium powder is primarily produced for pyrotechnic applications, while powdered aluminum is mass produced for a host of applications ranging from pigments in paints to energy constituents in propellants and explosives.

Although the present study is directed primarily towards the Trip Flare, it delves into all aspects of flare technology. For example, investigations were made of the effects of particle size, fuel-oxidant ratio, binder concentration, additives, fuel coating, flare case materials, flare case coatings, moisture, and short and long-term stability.

Previously aluminum was not considered to be a good fuel for flare applications since mixtures of atomized aluminum (diameter $\geq 15\ \mu$) and sodium nitrate ignite poorly, propagate poorly, and burn very erratically and inefficiently. One of the reasons for the inefficiency of the Al-$NaNO_3$ system is that it produces a profusion of incandescent particles. This Roman Candle effect makes the flare an incendiary device as well as an illumination source. This incendiary aspect is very undesirable -- causing possible harm to users and danger of starting ground fires.

A few years ago, however, it was demonstrated that powdered aluminum in combination with sodium nitrate (Ref 1, 2) will burn propagatively when small quantities of various transition metals or metal compounds are incorporated into the mixture. These studies showed that the transition metal compounds affecting the Al-$NaNO_3$ reaction fell into five classes.

Class 1 are those which increase the efficiency of the system by decreasing the thermal conductivity of the basic binary. Class 2 compounds, consisting of manganese oxides, catalyze the normal decomposition of sodium nitrate to evolve oxygen at low temperatures. Compounds which cause ignition of aluminum at about 700°C (a value well below its normal ignition temperature of 1000°C) are in Class 3. Class 4 embraces transition metals which all ignite with sodium nitrate at lower temperatures than does aluminum. Finally Class 5 compounds are those which alter the normal decomposition pattern of sodium nitrate, causing the evolution of the oxides of nitrogen at the melting point of the nitrate.

RESULTS AND DISCUSSION

As stated in the Introduction, previous studies showed that the combustion properties of Al-$NaNO_3$ compositions can be dramatically improved by the addition of certain additives (Ref. 2, 3). Since an inefficient Mg-$NaNO_3$-Laminac composition is presently employed in the M49A1 Trip Flare (higher candlepower apparently not required), it was not difficult to meet the basic Trip Flare requirements of 35,000 candles and minimum burning time of 55 seconds.

The performance characteristics of the basic Al-$NaNO_3$-2% $MnCO_3$ (previously found to be the best additive system) and the total system Al-$NaNO_3$ - 2% $MnCO_3$ - 5% Laminac binder 4116 were gathered from Ref 2 and are presented in Table 1. To simplify the analysis of these data, a comparison of the absolute values of the various performance characteristics are presented in Table 2 together with percentage changes in the parameters with respect to the basic binary system. It is seen that the additive $MnCO_3$ produced marked reductions in burning rates, caused sizeable increases in light output, and resulting increases in efficiencies. One interesting and unfortunate finding was that the addition of Laminac binder reduced the beneficial effects of the $MnCO_3$.

A series of Al-$NaNO_3$ - 2% $MnCO_3$ + 5% Laminac compositions were loaded into paper and aluminum Trip Flare cases. The cases were coated internally with a variety of case coatings. The purpose of these experiments were threefold. Firstly, it was desired to see if performance characteristics would be obtained comparable to those previously obtained with flares made in 1968 (Ref 2). Secondly, to determine the effect of case material on performance characteristics. Finally, to determine if the Laminac/asbestos coating is the optimum insulator for use with the metal trip flare case.

TABLE 1

PERFORMANCE CHARACTERISTICS OBTAINED MARCH 1968 FOR AL/$NaNO_3$/ADDITIVE COMPOSITIONS

	PERCENT INGREDIENTS								
ALUMINUM POWDER, ATOMIZED, 6.2 MICRONS	35	45	55	35	45	55	35	45	55
SODIUM NITRATE, USP, 35 MICRONS	65	55	45	63	53	43	58	48	38
MANGANESE CARBONATE, 2 MICRONS				2	2	2	2	2	2
LAMINAC RESIN 4116							5	5	5
PERFORMANCE CHARACTERISTICS									
BURNING RATE, INCHES/MIN	4.7	7.6	8.8	2.6	6.6	10.1	2.0	3.4	4.4
LUMINOUS OUTPUT, KILOCANDLES	30.7	76.5	37.4	50.2	120.8	120.7	18.6	46.6	43.9
EFFICIENCY, KILOCANDLESEC/GM	9.7	14.5	6.2	26.5	26.2	16.9	13.2	18.9	13.2

TABLE 2

EFFECTS OF MANGANESE CARBONATE AND LAMINAC
ON PERFORMANCE CHARACTERISTICS OF
ALUMINUM-SODIUM NITRATE COMPOSITIONS

COMPOSITIONS	BURNING RATE IN./MIN	% Δ	LIGHT OUTPUT KILOCANDLES	% Δ	EFFICIENCY KILOCDLE-SEC GM	% Δ
35/65 AL/NaNO3	4.7		30.7		9.7	
+ 2% MnCO3	2.6	- 44.7	50.2	+ 63.5	26.5	+ 173
+ 2% MnCO3 + 5% LAM	2.0	- 57.4	18.6	- 39.4	13.2	+ 36
45/55 AL/NaNO3	7.6		76.5		14.5	
+ 2% MnCO3	6.6	- 13.1	120.8	+ 57.9	26.2	+ 80.7
+ 2% MnCO3 + 5% LAM	3.4	- 42.1	46.6	- 39.1	18.9	+ 30.3
55/45 AL/NaNO3	8.8		37.4		6.2	
+ 2% MnCO3	10.1	+ 14.8	120.7	+ 222.7	16.9	+ 172.6
+ 2% MnCO3 + 5% LAM	4.4	- 50.0	43.9	+ 17.4	13.2	+ 112.9

The performance characteristics obtained in these tests are presented in Tables 3a through 3d.

As previously stated the first goal was to determine how the characteristics of the present flares compared to those made six years ago. Table 4 makes this comparison and shows that the performance characteristics of the flare are quite comparable, especially in their luminous efficiencies.

The second goal of these experiments was to determine the effects of the two widely different flare cases. Table 5 shows the performance characteristics obtained using Kraft paper cases versus aluminum cases. The metal cases used are those employed to make M49A1 production items. These cases are extruded and have a wall thickness of 1/16 inch. The data in Table 5 shows two extremely interesting facts. Firstly, changing the case from paper to aluminum results in only a 15% reduction in luminous output of the flares. In fact, the luminous output was only minimally affected using aluminum cases, regardless of case liner material. Secondly, and more importantly, nearly equivalent burning rates were realized in both paper and metal cases provided that an excellent insulating liner such as Laminac-asbestos was employed. When either Viton A or Laminac above was used, the total achievable time was reduced from $\cong$ 100 sec to $\cong$ 59 sec. This demonstrates that without an insulator, heat is transferred down the metal tube causing pre-heating and rapid burning of the composition. Furthermore the data of Table 5 presents an unusual case in flare behavior. Normally an increase of nearly 50% in the burning rate of a flare, such as that occurring when going from Kraft paper to Laminac coated aluminum, would have resulted in a significant increase in luminous output. In the present case, however, this did not occur; instead the luminous output remained approximately the same.

TABLE 3A

PERFORMANCE CHARACTERISTICS OF AL/$NaNO_3$ COMPOSITIONS IN VARIOUS COATED FLARE CASES

PARAFFIN COATED KRAFT PAPER CASES

	PERCENT INGREDIENTS		
ALUMINUM POWDER, ATOMIZED 6.2 MICRONS	35	45	55
SODIUM NITRATE, USP, 35 MICRONS	58	48	38
MANGANESE CARBONATE, 2 MICRONS	2	2	2
LAMINAC RESIN 4116	5	5	5
PERFORMANCE CHARACTERISTICS			
BURNING RATE, INCHES/MINUTE	2.5	3.9	6.2
BURNING TIME, SECONDS	100.3	63.2	39.4
LUMINOUS OUTPUT, KILOCANDLES	24.7	49.4	52.1
EFFICIENCY, KILOCANDLESEC/GM	15.1	19.0	12.5

TABLE 3B

PERFORMANCE CHARACTERISTICS OF AL/$NaNO_3$ COMPOSITIONS IN VARIOUS COATED FLARE CASES

VITON A COATED AL TRIP FLARE CASES

	PERCENT INGREDIENTS		
ALUMINUM POWDER, ATOMIZED 6.2 MICRONS	35	45	55
SODIUM NITRATE, USP, 35 MICRONS	58	48	38
MANGANESE CARBONATE, 2 MICRONS	2	2	2
LAMINAC RESIN 4116	5	5	5
PERFORMANCE CHARACTERISTICS			
BURNING RATE, INCHES/MINUTE	3.5	5.4	7.5
BURNING TIME, SECONDS	59.5	37.9	27.1
LUMINOUS OUTPUT, KILOCANDLES	21.4	61.2	67.1
EFFICIENCY, KILOCANDLESEC/GM	7.8	14.2	11.1

TABLE 3c

PERFORMANCE CHARACTERISTICS OF AL/$NaNO_3$ COMPOSITIONS IN VARIOUS COATED FLARE CASES

LAMINAC 4116 COATED AL TRIP FLARE CASES

	PERCENT INGREDIENTS		
ALUMINUM POWDER, ATOMIZED 6.2 MICRONS	35	45	55
SODIUM NITRATE, USP, 35 MICRONS	58	48	38
MANGANESE CARBONATE, 2 MICRONS	2	2	2
LAMINAC RESIN 4116	5	5	5
PERFORMANCE CHARACTERISTICS			
BURNING RATE, INCHES/MINUTE	3.7	6.6	9.3
BURNING TIME, SECONDS	56.2	30.7	21.9
LUMINOUS OUTPUT, KILOCANDLES	23.1	69.8	70.4
EFFICIENCY, KILOCANDLESEC/GM	7.9	13.1	9.4

TABLE 3D

PERFORMANCE CHARACTERISTICS OF AL/$NaNO_3$ COMPOSITIONS IN VARIOUS COATED FLARE CASES

LAMINAC/ASBESTOS COATED AL TRIP FLARE CASES

	PERCENT INGREDIENTS		
ALUMINUM POWDER, ATOMIZED 6.2 MICRONS	35	45	55
SODIUM NITRATE, USP, 35 MICRONS	58	48	38
MANGANESE CARBONATE, 2 MICRONS	2	2	2
LAMINAC RESIN 4116	5	5	5
PERFORMANCE CHARACTERISTICS			
BURNING RATE, INCHES/MINUTE	2.2	4.0	5.3
BURNING TIME, SECONDS	96.8	50.7	38.6
LUMINOUS OUTPUT, KILOCANDLES	20.9	47.3	46.1
EFFICIENCY, KILOCANDLESEC/GM	12.3	14.6	10.9

TABLE 4

COMPARISON OF PAST AND PRESENT PERFORMANCE CHARACTERISTICS
OF AL-$NaNO_3$ - 2% $MnCO_3$ - 5% LAMINAC COMPOSITIONS

PERCENT AL	35		45		55	
	OLD*	NEW	OLD	NEW	OLD	NEW
BURNING RATE, IN/MIN	2.0	2.5	3.4	3.9	4.4	6.2
LUMINOUS OUTPUT, KILOCANDLES	18.6	24.7	46.6	49.4	43.9	52.1
EFFICIENCY, KILOCANDLESEC/GM	13.2	15.1	18.9	19.0	13.2	12.5

*DATA OBTAINED FROM FLARES MADE AND TESTED IN NOV. 1968.
ALL COMPOSITIONS LOADED INTO 1.31 IN. DIAMETER KRAFT
PAPER CASES LINED WITH PARAFFIN.

TABLE 5

EFFECT OF CASE MATERIAL AND CASE LINERS ON
PERFORMANCE CHARACTERISTICS OF ALUMINUM/SODIUM NITRATE/
MANGANESE CARBONATE/LAMINAC 4116 (35/58/2/5) COMPOSITION

CASE MATERIAL:	KRAFT PAPER	M49A1 TRIP FLARE CASE		
CASE LINER:	PARAFFIN WAX	VITON A	LAMINAC	LAMINAC-ASBESTOS
BURNING RATE, INCHES/MINUTE	2.5	3.5	3.7	2.2
TOTAL BURNING TIME, SECONDS	100.3	59.5	56.2	96.8
LUMINOUS OUTPUT, KILOCANDLES	24.7	21.4	23.1	20.9
EFFICIENCY, KILOCANDLESEC/GM	15.1	7.8	7.9	12.3

The next step in the program was to determine if $MnCO_3$ was the best additive for the Al-$NaNO_3$ system when using an aluminum case as it was when using a paper case. Using the efficient 40/48 Al/$NaNO_3$ system as a base, a number of formulations were made and loaded containing the following additives (based on previous studies, Ref 2 and 4): 5% ferric oxide (red), 5% chromium sesquioxide, 7% tungsten powder, and 3% manganese carbonate. The performance characteristics obtained with these formulations are presented in Table 6. The data obtained shows that all of the compositions produced candlepower values in excess of the minimum requirement of 55 seconds. During these tests a significant observation was made. It was noted that the flares containing ferric oxide and tungsten exhibited a marked reduction in the amount of incandescent particles ejected. In view of this result, as well as the candlepowers produced, ferric oxide, tungsten and chromium sesquioxide were selected for further evaluation. New additive formulations were made using reduced percentages of aluminum powder in order to increase the burning time of the systems. The performance characteristics obtained for these new formulations are presented in Table 7 and show that several of the systems give outputs meeting the minimum requirements of the M49A1 flare. Based upon these results as well as visual evaluation, the compositions employing 7% tungsten powder (FY-1639) and 5% ferric oxide (FY-1634) were chosen as prime candidates for the M49A1 flare. Reconfirmation tests of these two systems showed that the tungsten system gave the same results whereas the ferric oxide one did not. It was discovered that the change in the performance

TABLE 6

EFFECT OF VARIOUS ADDITIVES ON PERFORMANCE CHARACTERISTICS OF ALUMINUM/SODIUM NITRATE/LAMINAC 4116 IN M49A1 TRIP FLARE CASE

	PERCENT INGREDIENTS			
ALUMINUM, AT., 6.2 MICRONS	42	42	40	42
SODIUM NITRATE, 35 MICRONS	48	48	48	50
FERRIC OXIDE (RED)	5	-	-	-
CHROMIUM SESQUIOXIDE	-	5	-	-
TUNGSTEN, 4.5 MICRONS	-	-	7	-
MANGANESE CARBONATE, 2 MICRONS	-	-	-	3
LAMINAC RESIN 4116	5	5	5	5
PERFORMANCE CHARACTERISTICS				
BURNING RATE, INCHES/MIN.	4.7	4.0	4.3	3.4
LUMINOUS OUTPUT, KILOCANDLES	61.4	49.8	59.4	36.2
EFFICIENCY, KILOCANDLESEC/GM	15.3	15.1	15.1	13.3
BURNING TIME, SECONDS	43.9	51.4	47.8	60.9

TABLE 7

EFFECT OF ALUMINUM CONTENT ON PERFORMANCE CHARACTERISTICS OF ALUMINUM/SODIUM NITRATE/LAMINAC 4116 WITH OPTIMUM ADDITIVES IN M49A1 TRIP FLARE CASE

	PERCENT INGREDIENTS						
ALUMINUM, AT., 6.2 MICRONS	36	38	40	30	35	38	39
SODIUM NITRATE, 35 MICRONS	54	52	52	58	53	50	51
FERRIC OXIDE (RED)	5	5	3	-	-	-	-
TUNGSTEN, 4.5 MICRONS	-	-	-	7	7	7	-
CHROMIUM SESQUIOXIDE, 2 MICRONS	-	-	-	-	-	-	5
LAMINAC RESIN 4116	5	5	5	5	5	5	5
PERFORMANCE CHARACTERISTICS							
BURNING RATE, INCHES/MIN	3.3	3.4	3.7	3.2	3.5	3.9	3.3
LUMINOUS OUTPUT, KILOCANDLES	42.9	43.9	48.1	29.1	46.7	53.6	44.0
EFFICIENCY, KILOCANDLESEC/GM	15.0	14.9	14.9	10.8	14.1	14.8	15.3
BURNING TIME, SECONDS	61.3	59.7	54.9	71.0	61.1	53.0	61.1

characteristics of the ferric oxide system was due to the use of a new lot of material. From a purely cost advantage, it would be more desirable to use ferric oxide rather than tungsten. Consequently some efforts were expended to characterize the old and new ferric oxides. An x-ray analysis of the original material showed the presence of 10% of silicon dioxide (alpha quartz form), while the new material contained no silicon dioxide.

Table 8 presents the results of experiments to determine if other forms of ferric oxide or ferric oxide plus silicon dioxide (Superfloss, Johns-Manville Company) could be employed to produce desirable performance characteristics. It was found that the Jeweler's rouge form of ferric oxide, as well as silicon dioxide (Superfloss), gave performance characteristics approaching that of the composition containing unknown grade ferric oxide. However, these systems were abandoned because both of them did not reduce the profuse production of incandescent aluminum particles. It was decided to continue the investigation using the tungsten formulation because of its superior performance characteristics.

A comparative investigation was next conducted using a lower cost atomized aluminum obtained from the Alcoa Corporation. This material costs $0.38/lb per 450 lbs whereas the Alcan material previously employed was in excess of $1.00/lb. The results of this comparison are presented in Table 9 and show that the lower cost Alcan aluminum gave performance characteristics comparable to the more expensive 8μ Alcoa aluminum.

Before subjecting the tungsten additive system to the necessary storage and safety tests, a final attempt was made to further improve

TABLE 8

EFFECT OF FERRIC OXIDE ON THE PERFORMANCE CHARACTERISTICS OF ALUMINUM/SODIUM NITRATE/LAMINAC 4116 COMPOSITION (38/52/5) IN M49A1 TRIP FLARE CASE

ADDITIVES	PERCENT				
FERRIC OXIDE, RED, GRADE UNKNOWN	5	-	-	-	-
FERRIC OXIDE, JEWELER'S ROUGE, 0.6 MICRON	-	5	-	-	-
FERRIC OXIDE, REAGENT, 0.5 MICRONS	-	-	5	-	4.5
SUPERFLOSS	-	-	-	5	0.5
PERFORMANCE CHARACTERISTICS					
BURNING RATE, INCHES/MIN	3.7	3.3	3.1	3.5	3.0
LUMINOUS OUTPUT, KILOCANDLES	46.5	40.3	35.3	44.7	34.6
EFFICIENCY, KILOCANDLESEC/GM	15.9	15.3	14.6	16.0	14.6
BURNING TIME, SECONDS	60.4	67.1	72.6	63.0	74.3

TABLE 9

PERFORMANCE CHARACTERISTICS OF ALUMINUM (ALCOA AND ALCAN) - SODIUM NITRATE COMPOSITIONS

INGREDIENTS	FY COMPOSITION NO. 1639	1671
ALUMINUM, ATOMIZED, 6.2 MICRONS, ALCAN, %	35	-
ALUMINUM, ATOMIZED, 8.0 MICRONS, ALCOA, %	-	35
SODIUM NITRATE, USP, 35 MICRONS, %	53	53
TUNGSTEN POWDER, 6.7 MICRONS, %	7	7
LAMINAC RESIN 4116, %	5	5
PERFORMANCE CHARACTERISTICS		
CANDLEPOWER, KILOCANDLES	49.9	47.5
BURNING TIME, SECONDS	65.3	71.6
LUMINOUS EFFICIENCY, KILOCANDLE-SEC/GM	16.9	17.7

the luminous efficiency of the Al-$NaNO_3$-W system by adding small percentages of 20/50 mesh atomized magnesium. As Table 10 shows the addition of 5% or 10% atomized Mg did not produce any increase in the efficiency of the system while resulting in slightly increased burning rates. These data consequently did not indicate any advantage in utilizing Mg in the Al-$NaNO_3$-W system.

The finalized 35/53/7/5 Al/$NaNO_3$/W/Laminac system was loaded into M49A1 flare cases and then incorporated into final end items. Two groups of these end items were subjected to two temperature extremes for sixteen (16) hours. One group was maintained at 75°C (hot), while the other was kept at -54°C (cold). After conditioning at these temperatures the flares were examined visually and their performance characteristics determined. Table 11 shows that no deleterious results occurred due to conditioning at these extreme temperatures.

Standard sensitivity characteristics were determined for the Al/$NaNO_3$/W/Laminac system. The values obtained are as follows:

Impact test, P.A. apparatus → 21 inches

Friction pendulum, steel shoe → no action

Electrostatic initiation, minimum joules → >11.025

Ignition temperature, 5 second value → 564°C

The sensitivity values obtained indicate that only normal safeguards are required during blending and loading operations.

A series of M49A1 trip flares were loaded using the FY-1639 composition (35% atomized Al, 53% $NaNO_3$, 7% W, and 5% Laminac resin binder). This group of flares were placed in storage for an

TABLE 10

EFFECT OF MAGNESIUM AS AN ADDITIVE ON PERFORMANCE CHARACTERISTICS OF ALUMINUM/SODIUM NITRATE/TUNGSTEN/LAMINAC 4116 COMPOSITION IN M49A1 TRIP FLARE CASE

	PERCENT INGREDIENTS		
ALUMINUM, AT, 6.2 MICRONS	35	35	35
MAGNESIUM, AT, 30/50 MESH	-	5	10
SODIUM NITRATE	53	48	50
TUNGSTEN, 6.7 MICRONS	7	7	-
LAMINAC RESIN 4116	5	5	5
PERFORMANCE CHARACIERISTICS			
BURNING RATE, INCHES/MIN	3.6	4.2	4.0
LUMINOUS OUTPUT, KILOCANDLES	50.2	54.2	54.0
EFFICIENCY, KILOCANDLESEC/GM	15.6	15.0	15.9
BURNING TIME, SECONDS	59.1	50.0	54.2

TABLE 11

16 HOUR TEMPERATURE CONDITIONING TEST ON PERFORMANCE CHARACTERISTICS OF OPTIMUM ALUMINUM FUELED COMPOSITION IN ASSEMBLED M49A1 TRIP FLARE

ALUMINUM, AT., 6.2 MICRONS, %	35
SODIUM NITRATE, 35 MICRONS, %	53
TUNGSTEN, 6.7 MICRONS, %	7
LAMINAC RESIN 4116, %	5

STORAGE CONDITIONS	AMBIENT	75°C	-54°C
PERFORMANCE CHARACTERISTICS			
BURNING RATE, INCHES/MIN.	3.3	3.5	3.6
LUMINOUS OUTPUT, KILOCANDLES	43.6	47.2	44.6
EFFICIENCY, KILOCANDLESEC/GM	14.1	13.8	13.7
BURNING TIME, SECONDS	62.2	56.1	59.1

extended period of four (4) months at both ambient and 75°C. Table 12 shows the results obtained at monthly intervals over a four month period. The data obtained clearly indicates that no degradation occurred in the performance characteristics of the Al composition during this extended storage period.

GASSING AND SELF-HEATING OF Al-$NaNO_3$ COMPOSITIONS

One of the basic properties of pyrotechnic compositions leading to instability in storage is their reactivity to moisture. The troublesome gassing occurring in Mg systems is attributable to the well known reaction:

$$5\ Mg + NaNO_3 + 8\ H_2O \rightarrow 5\ Mg(OH)_2 \downarrow + H_2 \uparrow + NH_3 \uparrow + NaOH \qquad \text{(eq 1)}$$

This reaction is the summation of the following two fundamental ones:

$$Mg + 2H_2O \rightarrow H_2 \uparrow + Mg(OH)_2 \downarrow \qquad \text{(eq 2)}$$

and

$$4\ Mg + NaNO_3 + 7\ H_2O \rightarrow 4\ Mg(OH)_2 \downarrow + NH_4OH + NaOH \qquad \text{(eq 3)}$$
$$\downarrow\uparrow$$
$$NH_3\uparrow + H_2O$$

The generation of NH_3 and H_2 gases by (eq 1), of course, is greatly accelerated with increasing temperature. Oftentimes munition items in extended storage will suffer damage such as ruptured closure seals and split cases due to this unwanted generation of gases.

The gaseous as well as thermal output of reaction 1 is moderated by the insolubility of the magnesium oxide in the increasing alkalinity of the medium resulting from the products of NaOH. This growing insolubility follows from the rudimentary equilibrium process shown by the following equation:

$$Mg(OH)_2 \rightleftarrows Mg^{++} + 2OH^{-}. \qquad \text{(eq 4)}$$

TABLE 12

FOUR MONTH STORAGE SURVEILLANCE OF PERFORMANCE CHARACTERISTICS OF OPTIMUM ALUMINUM FUELED COMPOSITION IN ASSEMBLED M49A1 TRIP FLARES

STORAGE PERIOD, MONTHS	BURNING RATE, INCHES/MIN		LUMINOUS OUTPUT, KILOCANDLES		EFFICIENCY KILOCANDLESEC/GM		BURNING TIME, SECONDS	
	AMBIENT	75°C	AMBIENT	75°C	AMBIENT	75°C	AMBIENT	75°C
0	3.5	-	38.8	-	13.5	-	63.3	-
0.5	3.2	3.3	39.8	38.3	14.6	13.6	68.9	66.9
1	3.4	3.3	43.6	41.5	15.2	14.9	65.5	67.3
2	3.5	3.1	46.2	41.4	15.8	15.7	64.3	71.3
3	3.4	3.4	38.9	40.5	13.9	13.9	64.9	64.8
4	3.4	3.4	39.8	39.2	13.7	13.5	64.9	65.1

As the concentration of OH^- ion increases, the equilibrium shifts to the left favoring the formation of the protective coating or at least saturating the solution with $Mg(OH)_2$ thereby preventing dissolution of the metal coating.

Consider now the case of aluminum. The reaction of Al with moisture and sodium nitrate is shown in the following equation:

$$3NaNO_3 + 8\ Al + 18\ H_2O \rightarrow 3NaOH + 8\ Al(OH)_3 + 3NH_3\uparrow \qquad \text{(eq 5)}$$

Unlike the Mg reaction, the aluminum oxide coating and $Al(OH)_3$ formed are quite soluble in the resulting alkaline medium. Consequently, reaction 5 which produces NH_3 (probably also some H_2 by the reaction $2Al + 6H_2O \rightarrow 2Al(OH)_3 + 3H_2\uparrow$) and heat proceeds at an accelerating rate. This latter process eventually causes extensive self-heating and, under certain conditions, spontaneous ignition of the composition.

The Al composition developed in this program, FY-1639, exposed to an uncontrolled ambient environment for a few days, generated 11 + ml. of gas in five (5) minutes duration at 120°C temperature using the standard vacuum stability test. When another sample of this composition was dried at 105°C for sixteen hours prior to conducting the vacuum stability test, only 0.35 ml of gas was produced after forty hours at 120°C. This result demonstrates that a stable Al composition can be processed and loaded by rigorous exclusion of moisture.

Table 13 summarizes data obtained from the Alcoa Corporation which shows the amount of gas produced by refluxing powdered aluminum in a 20% ammonium nitrate solution. This data shows the effect of changing the particle size on gassing and how this gassing can be significantly reduced by coating the metal with isostearic acid. When isostearic acid

TABLE 13

AMOUNT OF HYDROGEN GENERATED BY
POWDERED ALUMINUM

(DATA PROVIDED BY RESEARCH LABS, ALCOA,
NEW KENSINGTON, PENN)

AL, PARTICLE DIAMETER MICRONS	ML GAS PRODUCED* UNTREATED	ML GAS PRODUCED* COATED WITH ISOSTEARIC ACID
25 - 30	8	NEGLIGIBLE
15	10	0 - 0.2**
8	50 - 60	0 - 0.2*

*VOLUME OF GAS PRODUCED BY REFLUXING ONE GRAM AT 93°C FOR 6 HOURS IN A 20% AMMONIUM NITRATE SOLUTION.

**VALUE DEPENDS ON EFFICACY OF COATING.

coated aluminum was employed in the FY-1639 formulation, however, it was found as shown in Table 14 that a marked reduction occurred in both candlepower and efficiency. For example the candlepower was reduced from 50,000 to 31,000 candles and the efficiency went from 17,000 to 12,000 candleseconds/gram. Consequently the more feasible method to eliminate gassing is rigorous drying rather than coating the metal.

Although the gassing of the aluminum/sodium nitrate composition is an annoying problem, the more serious danger is that of self-heating leading to spontaneous ignition. A good discussion of this phenomenon is given by Johansson and Persson in the Swedish journal Pyrotechnikdogen (Ref 3).

Figure 1 shows the DTA of a simple 45/55 Al (6μ)/$NaNO_3$ composition which had been conditioned at 52% RH for 6 days. As is seen, the pattern is quite complex having three primary exotherms at approximately 135, 790, and 915°C. The last exotherm resulted in ignition. When the same Al/$NaNO_3$ composition was conditioned at a higher RH of 79% for the same length of time, 6 days, a different DTA pattern resulted as shown in Figure 2. Here the small exotherm at 135° grew tremendously in intensity and ignition occurred at the second exotherm at 690°C. With increased mass and confinement, ignition occurs easily in the region of the first exotherm, at temperatures as low as 60 to 70°C.

Figure 3 shows that the exotherm at 135°C is solely dependent upon moisture content. In the DTA (a), no exotherm appears for a perfectly dry Al/$NaNO_3$ sample. Some activity begins to appear in run (b) where the same Al/$NaNO_3$ composition is exposed to a 79% RH

TABLE 14

EFFECT OF ISOSTEARIC ACID COATED ALUMINUM POWDER ON PERFORMANCE CHARACTERISTICS IN M49A1 TRIP FLARE CASE

	PERCENT INGREDIENTS		
ALUMINUM, AT., 6.2 MICRONS	35	-	-
ALUMINUM, AT., COATED WITH 4% ISOSTEARIC ACID, 8.5 MICRONS	-	35	-
ALUMINUM, AT., 8 MICRONS	-	-	35
SODIUM NITRATE, 35 MICRONS	58	58	58
TUNGSTEN, 6.7 MICRONS	7	7	7
LAMINAC RESIN 4116	5	5	5
PERFORMANCE CHARACTERISTICS			
BURNING RATE, INCHES/MIN	3.4	3.1	3.1
LUMINOUS OUTPUT, KILOCANDLES	49.9	31.3	47.5
EFFICIENCY, KILOCANDLESEC/GM	16.9	11.7	17.7
BURNING TIME, SECONDS	65.3	72.3	71.6

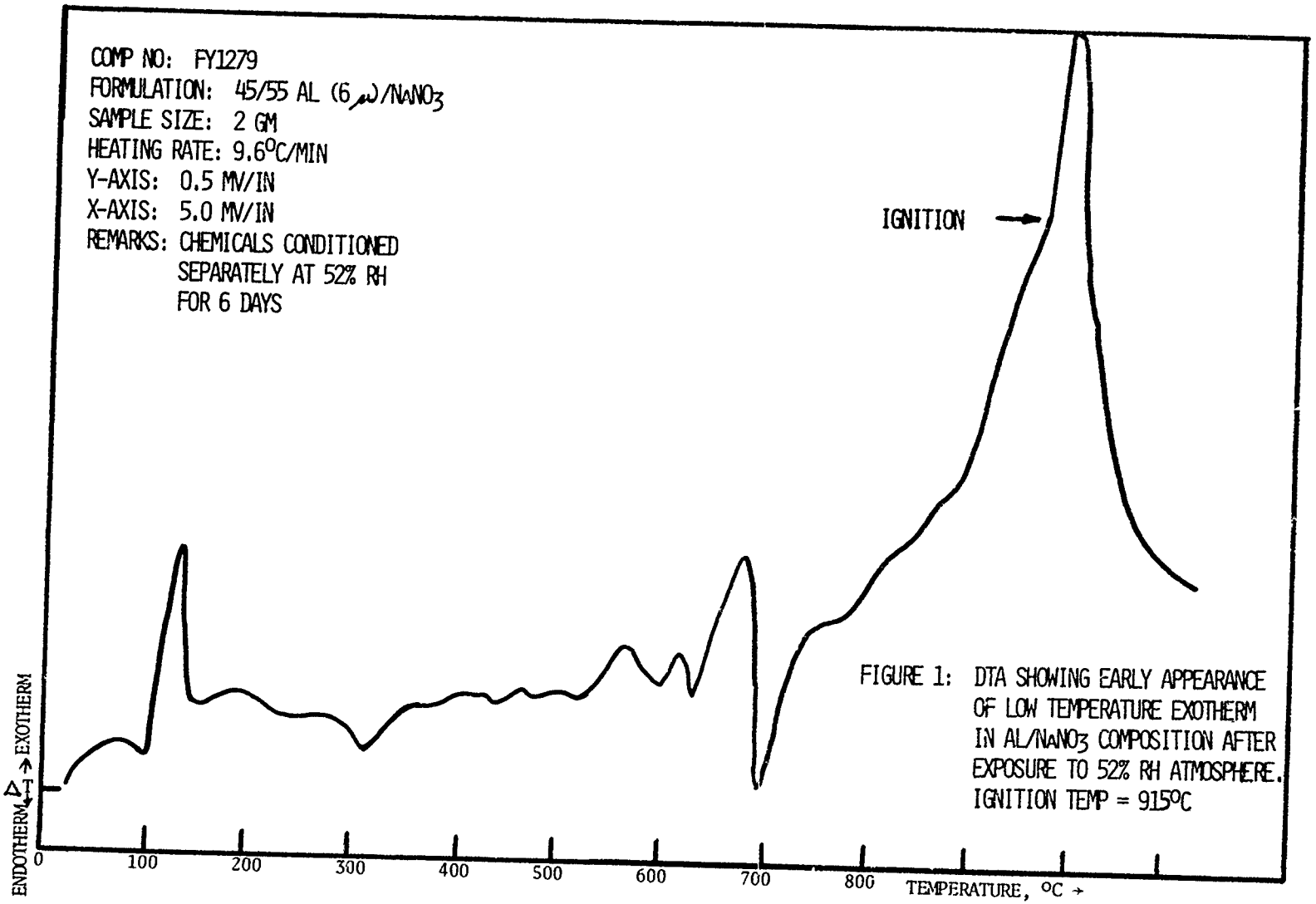

FIGURE 1: DTA SHOWING EARLY APPEARANCE OF LOW TEMPERATURE EXOTHERM IN AL/$NaNO_3$ COMPOSITION AFTER EXPOSURE TO 52% RH ATMOSPHERE. IGNITION TEMP = 915°C

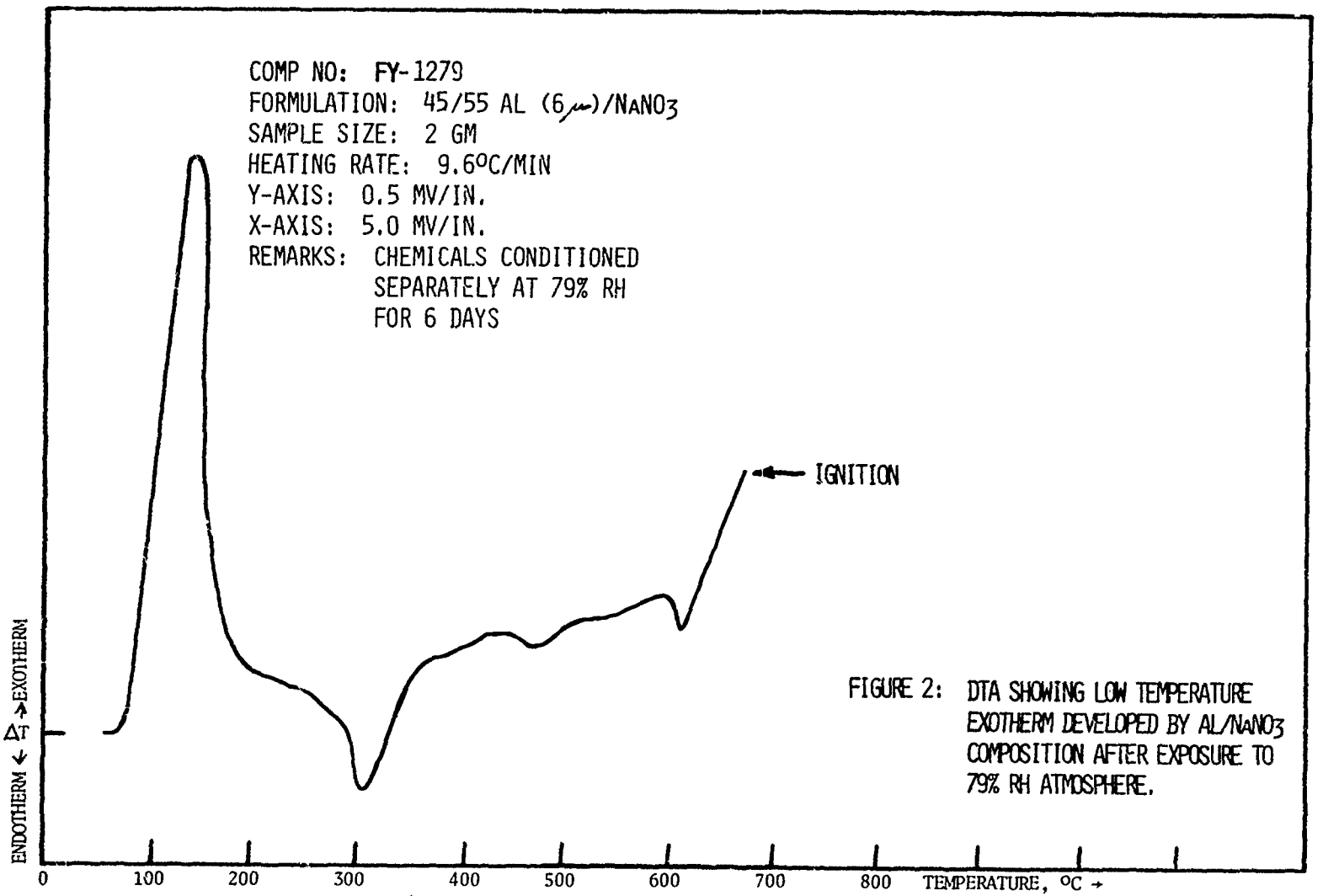

FIGURE 2: DTA SHOWING LOW TEMPERATURE EXOTHERM DEVELOPED BY AL/NaNO3 COMPOSITION AFTER EXPOSURE TO 79% RH ATMOSPHERE.

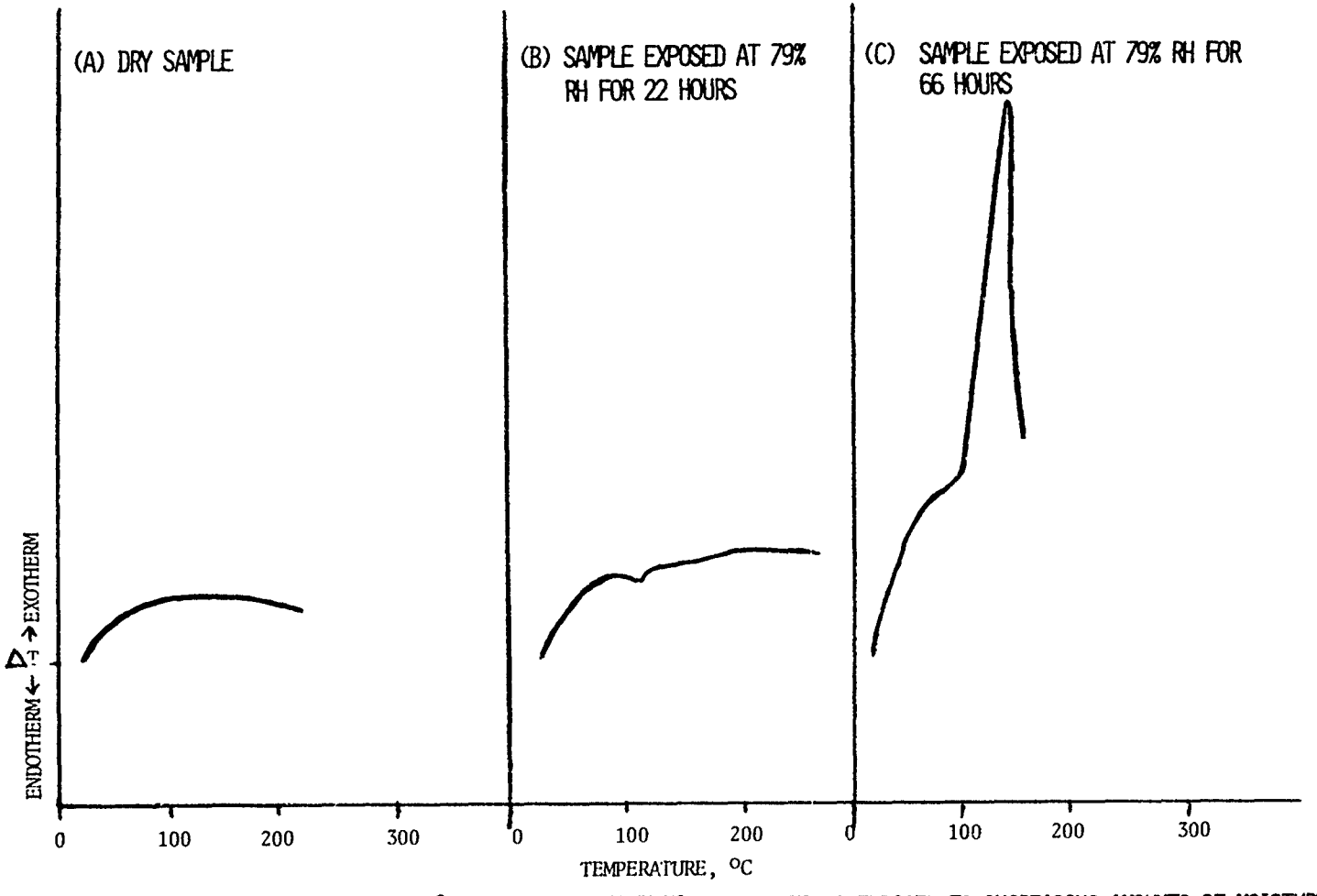

FIGURE 3: DEVELOPMENT OF 135°C EXOTHERM IN AL/$NaNO_3$ COMPOSITIONS EXPOSED TO INCREASING AMOUNTS OF MOISTURE. ALL DTA'S EMPLOYED 2 GM SAMPLES OF 45/55 AL/$NaNO_3$ AT HEATING RATE OF 9.6°C/MIN. X-AXIS = 0.5 MV/IN., XY-AXIS = 5.0 MV/IN

atmosphere for 22 hours. Finally the DTA in (c) clearly shows the dramatic growth of the exotherm using a sample which had been exposed to a 79% RH atmosphere for 66 hours.

In another program designed to furnish a highly exothermic composition for rocket assisted projectiles, an Al composition was developed containing the additive $MnCO_3$. This highly metallized composition contained 85/10/2/5 Al (6μ)/$NaNO_3$/$MnCO_3$/Viton A. Figure 4 presents the DTA behavior for the basic composition which had been conditioned at 50% RH for 5 weeks. This composition exhibited no low temperature exotherm and ignited immediately following the melting of $NaNO_3$ at approximately 300°C. This ignition behavior is peculiar to aluminum/$NaNO_3$ systems containing additives such as transition metal compounds as well as organic and inorganic fluorides. It has been hypothesized by many that at the melting point of $NaNO_3$, the additive either removes and/or makes the aluminum oxide protective coating permeable so that an immediate reaction occurs between the clean Al surface and the molten oxidant.

When this additive composition was exposed to a 90% RH atmosphere for 5 weeks, the same low temperature exotherm occurred as with the Al/$NaNO_3$ binary. This phenomenon is clearly seen in Figure 5. Consequently it appears that the presence of moisture sensitizes simple as well as complex Al/$NaNO_3$ systems. Studies are presently being conducted to determine the nature of the intermediate which causes the low temperature ignition of Al/$NaNO_3$ system. This intermediate is probably NaOH which reacts exothermally with both Al and its protective coating.

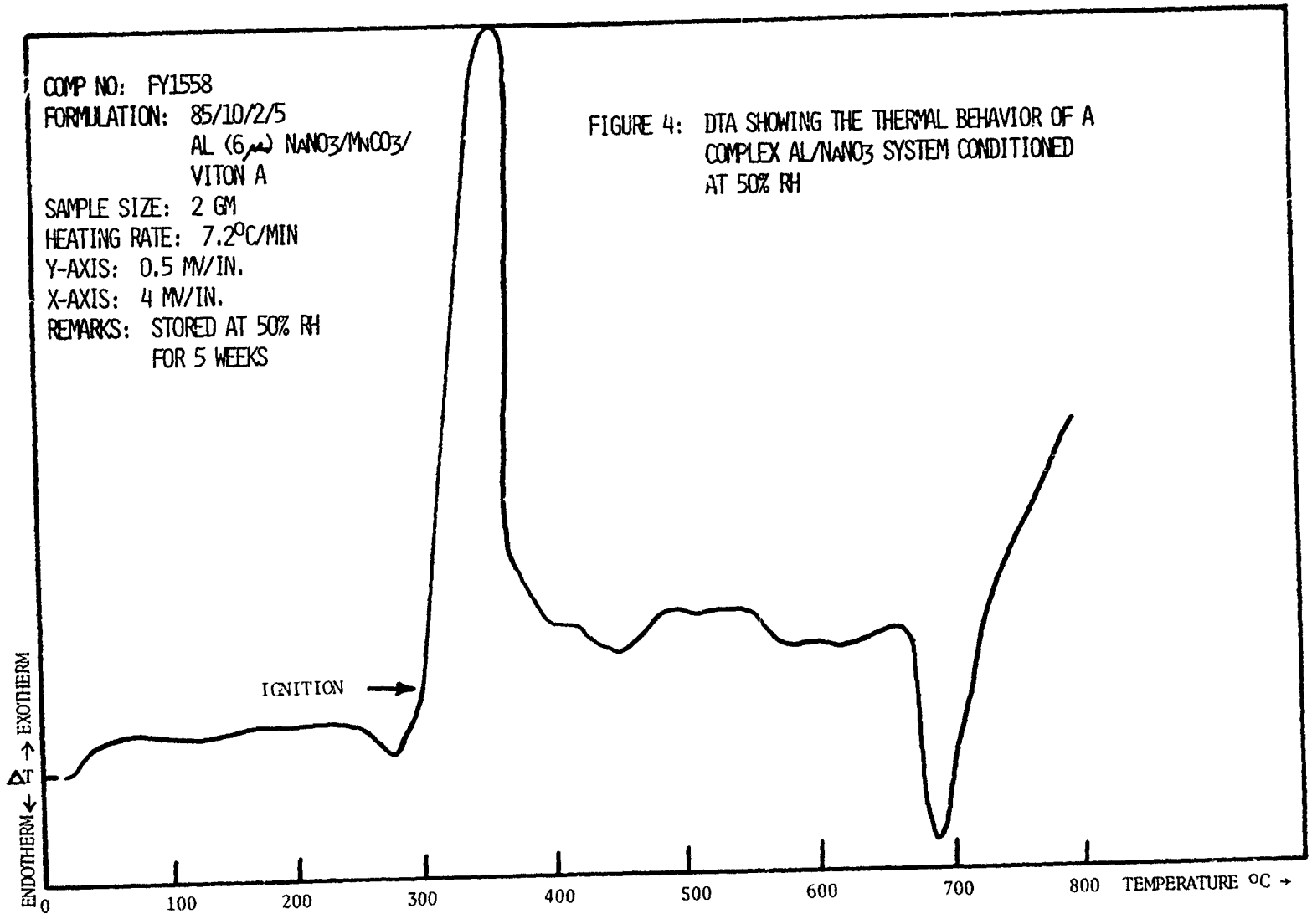

FIGURE 4: DTA SHOWING THE THERMAL BEHAVIOR OF A COMPLEX AL/NaNO3 SYSTEM CONDITIONED AT 50% RH

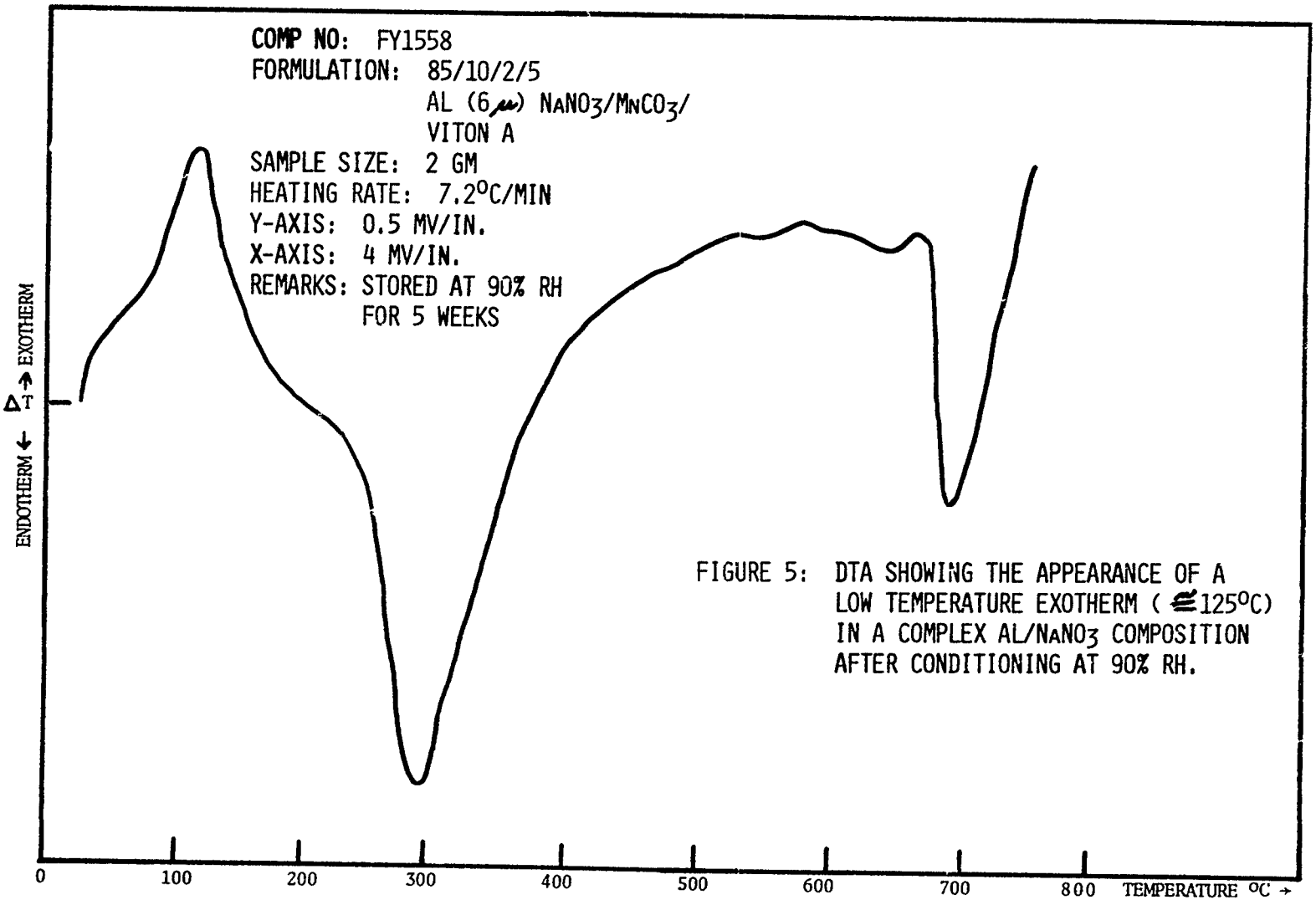

FIGURE 5: DTA SHOWING THE APPEARANCE OF A LOW TEMPERATURE EXOTHERM (≲125°C) IN A COMPLEX AL/$NaNO_3$ COMPOSITION AFTER CONDITIONING AT 90% RH.

CONCLUSIONS:

A formulation has been developed for use in the U.S. Army Trip Flare which utilizes aluminum instead of magnesium for a fuel. This composition contains 35% six micron atomized aluminum, 53% sodium nitrate, 7% seven micron tungsten powder and 5% Laminac 4116 polyester resin.

The two basic advantages of the new aluminum system are cost, 38 cents per pound for aluminum as compared to 85 cents a pound for 20/50 mesh atomized magnesium, and ready commercial availability.

The disadvantages of the aluminum system are gassing and self-heating which occurs when it is exposed to excess moisture. By careful exclusion of moisture during processing, however, these effects can be eliminated as was demonstrated by long term storage stability testing.

REFERENCES

1. Jackson, B., Kaye, S. M., and Taylor, F. R. "Aluminum Powder as an Alternate Fuel for Magnesium in Illuminant Compositions," Picatinny Arsenal Technical Report 3713, November 1968.

2. Leader, P. J., Westerdahl, R. R., and Taylor, F. R., "The Effects of Some Transition Metal Compounds on the Performance Characteristics of Aluminum/Sodium Nitrate Compositions," Picatinny Arsenal Technical Report 3846, May 1969.

3. Johansson, S. R. and Persson, K. G. "Explosion Hazards of Pyrotechnic Aluminum Compositions", Pyroteknikdogen, Stockholm, 10 May 1971, pp 74-90.

EXPERIMENTAL PROCEDURE

Blending

The compositions cited in this report were blended in a Lancaster counter-current mixer, Model PC which imparts a mulling type action to the constituents of the blend. The sodium nitrate was dried for twenty-four hours at 110°C prior to use. The resultant flare compositions were dried in trays containing a one inch thickness of composition for a minimum of sixteen hours at 105°C.

Loading

Each composition was loaded in four equal increments at a pressure of 7,000 psi. Ten (10)grams of DP-1886 igniter composition (65% five micron tungsten powder, 24% barium chromate, 10% potassium perchlorate and 1% Vinyl Alcohol Acetate Resin MA-28-18) was used as the first fire. Ten (10) grams of Laminac coated fireclay was used as an inert charge at the bottom of the Kraft paper cased flares. The interior walls of the flare cases were coated with the materials indicated in the tables.

Testing

Light measurements of the flares were determined in accordance with Mil-P-20464 except that a black background was used instead of a white one.

LIST OF MATERIALS USED

Aluminum powder, atomized, Lot No. 1072, average particle diameter 6.2 microns, Aluminum Company of Canada.

Aluminum powder, atomized, Lot No. 1401, average particle diameter 8.0 microns, Aluminum Company of America.

Sodium nitrate, double refined, USP Grade, average particle diameter 35 microns, Davies Nitrate Company.

Tungsten powder, Lot No. 6154D, average particle diameter 6.7 microns, General Electric Company.

Magnesium powder, atomized, 20/50 mesh, Specification Mil-P-14067B, Hart Metals Incorporated.

Ferric oxide, Red, unknown grade, lot, company.

Ferric oxide, jeweler's rouge, Catalogue No. I-115, average particle diameter 0.6 microns, Fisher Scientific Company.

Ferric oxide, reagent grade, Catalogue No. I-116, average particle diameter 0.5 microns, Fisher Scientific Company.

Chromium sesquioxide, Lot 32194, average particle diameter 2 microns, J. T. Baker Chemical Company.

Sodium fluoride, S-299, average particle diameter 8.6 microns, Fisher Scientific Company.

Superfloss (SiO_2), Johns-Manville Company.

Cab-O-Sil (SiO_2), MS-7, Cabot Corporation.

Magnesium, atomized, 30/50 mesh, Specification Mil-P-14067B, Hart Metals Incorporated.

Laminac polyester resin 4116, American Cyanamid Company.

Vinyl alcohol acetate resin, MA-28-18, Palmer Cement Company.

Viton A fluorocarbon resin, Dupont Chemical Company.

Asbestos powder, technical grade, Lot 61971, Fisher Scientific Company.

IMPROVED RED TRACER FLARES

by

D C A Izod and R F Eather

Royal Armament Research and Development Establishment,
Fort Halstead, Sevenoaks, Kent, United Kingdom

British Crown Copyright reserved. Published with the permission of the Controller of Her Brittanic Majesty's Stationery Office.

Summary

The effect of high spin rates on tracer compositions is to drastically increase the burning rate. This paper describes the work carried out to elucidate the reasons for this effect and reports some steps taken to ameliorate the problem.

Introduction

1. Tracer compositions have been in use now for 60 years and although the conditions under which they have to function have been well described, very little seems to have been reported on the reasons for increased burning rates during flight.

No work on tracer compositions has been done in the UK for at least 10 years but now that more advanced sighting and ranging systems are available for military use there has been a renewed interest in this topic. The primary task is to provide a new tracer filling for an existing capsule with an increased burning time and the same or improved light output.

This paper describes some experiments which have looked at the effect of various spin rates on the burning characteristics of Service and experimental tracer compositions. Spectral power distributions have been recorded in some instances and this basic data will be useful for ensuring that the outputs of new compositions are tailored for optimum response to the human eye and/or optical devices fitted to military vehicles.

2. Experimental details

All current UK tracers are based on the well-known magnesium/strontium nitrate/chlorine donor system. Appendix (1) lists the compositions of some tracer mixtures together with some additional red signal and missile tracking beacon flares. Composition D is commonly used in small arms ammunition, whilst composition F is used in the larger calibre rounds.

The flare mixtures were filled into standard UK tracer capsules, known as "type 33". The diameter of this capsule is approximately 15 mm. The column length was approximately 20 mm. Because of the high set-back forces generally encountered in gun barrels, tracer compositions are consolidated at high pressing loads, and this technique was adopted when filling the compositions into the capsule.

The filled tracer capsules were spun by means of an air turbine. The turbine rotor was mounted on an air bearing and this technique permitted spin rates as great as 50×10^3 revolutions per minute to be attained. The spin rate was determined by means of a light source, photocell and counter/timer arrangement. At zero spin rates, ignition of the composition could be achieved by means of a simple electric squib, but at spin rates greater than this an igniter with a much longer burning duration had to be used.

When the composition was initiated an intense green flash occurred before the take-over of the normal red tracer colour. This was due to the coating of priming material pressed onto the tracer composition to aid in ignition. Part of the art of operating the photometric equipment, which will be described below, was to initialize the timing and integration circuits so as to ignore the initial primer flash. If this were not done then this flash could

contribute to a significant percentage of the integrated light output of the tracer.

The photometric equipment consisted of a UDT 500 detector, corrected to the CIE 2° Observer, which was mounted in a suitable field-defining enclosure having an in-field sub-calibration source, a gating switch, a Hewlett-Packard DVM/Integrater and a Venner timer. The system has been in use for several years and has proved to be rugged and reliable. The typical experimental accuracies achieved with this system have been better than ± 5%.

3. Description of the Effect of Spin on Tracer

When a burning tracer composition is subjected to a high spin condition the primary effect is to increase the burning rate by a factor of 2 to 4 times. In addition, it is usually found for most compositions that both the integrated light output and the average light output are reduced. Tables (1a) to (1c) illustrate the effect for some typical red tracer, red signal and tracking beacon compositions. The recipes for these compositions are given in Appendix 1, and all compositions were filled into a standard type 33 tracer capsule.

TABLE (1a)

Effect of Spin on Burning Rate

Composition	Burning time, seconds		
	Static	30×10^3 rpm	40×10^3 rpm
A	8.6	5.4	4.8
B	9.7	3.6	3.3
C	4.6	2.6	2.4
D	11.8	3.0	3.3
E	9.2	4.0	3.8
F	8.9	2.6	2.6
G	3.5	3.6	3.2

TABLE (1b)

Effect of Spin on Average Luminous Intensity

Composition	Average Luminous Intensity Candelas x 10^3		
	Static	30 x 10^3 rpm	40 x 10^3 rpm
A	1.8	0.5	0.5
B	2.1	1.4	1.3
C	3.2	0.4	0.3
D	1.7	1.6	2.0
E	1.7	1.4	1.5
F	2.6	1.6	1.5
G	3.9	0.5	0.3

TABLE (1c)

Effect of Spin on Integrated Light Output

Composition	Integrated Light Output cd.sec. x 10^3		
	Static	30 x 10^3 rpm	40 x 10^3 rpm
A	15.0	2.4	2.4
B	20.3	5.1	4.2
C	15.0	1.0	0.6
D	20.1	6.4	6.9
E	15.3	5.7	5.6
F	23.0	4.1	3.9

Visually, the flame size of the burning tracer decreases from about 0.5 metres long to about 0.1 metres long for static and spin rates greater than 10,000 rpm respectively.

Measurements of the spectral power distribution statically and at high spin rates show that minor changes occur in the flame. The spectral power distributions for composition F, which is frequently used as a tracer filling, are given in Figures (1) (static) and (2) spun). These are seen to consist of the well-known SrOH and SrCl

bands between 605 and 690 nm, with a small contribution from a continuum emission. The intensity of the 605 nm SrOH band shows a considerable reduction relative to the SrCl bands and the continuum background emission shows an increase in intensity when the tracer is spun at 40,000 rpm. The increase in the intensity of the continuum is in contrast with the values obtained for the correlated colour temperature which shows a drop from 2050°K when burnt statically to 1900°K when burnt at 40,000 rpm. This is probably due to the retention of the incandescant solid products of combustion on the capsule wall through the centrifugal effect.

When combustion has been completed under the spin condition examination of the tracer capsule has shown that the products of combustion have formed a solid throttle at the mouth of the capsule. This material was probably magnesium oxide.

4. A Model to Account for the Decrease in Burning Time

Many pyrotechnic compositions exhibit burning rates which are dependent upon the ambient pressure. It is postulated that the effect of the throttle is to increase the pressure on the burning surface and consequently increase the burning rate. The functional dependence of the burning rate of explosives on pressure was first examined by Veille who found that it followed the general form:

$$r = a\,p^{n} \qquad (1)$$

where r is the burning rate
p " " pressure
a " a constant relating the units
n " a dimensionless constant

Experiments were carried out in a vacuum chamber at RARDE Langhurst to determine the values of these constants for composition F. Unfortunately a pressure chamber was not available to gather observations at pressures greater than atmospheric and this detracts from the confidence one can place in the extrapolation which was used later. Six tracer capsules were tested at each pressure and the average burning times are plotted in figure (3). A least squares fit to the data yields the values a = 148.9 sec., n = -0.423; thus for a burning time of 2.65 the ambient pressure on the burning surface would have to be about 33 atmospheres.

For a given fluid in a rocket chamber, the ratio of the pressure in the chamber to the pressure at the exit $\frac{Pe}{Pc}$ is a function of the ratio of the exit to throat areas $\frac{Ae}{At}$ only. The relationship between these ratios is

$$\frac{Ae}{At} = \frac{\Gamma^{2}}{\left(\frac{Pe}{Pc}\right)^{1/\delta} C^{o}_{F}} \qquad (2)$$

where δ is the ratio of the specific heats at constant pressure and volume

$$\Gamma = \delta^{\frac{1}{2}} \cdot \left[2/(\delta+1)\right]^{\frac{\delta+1}{2(\delta-1)}}$$

$$\text{and } C_F^o = \Gamma \left\{ (2\delta/\delta - 1) \left[1 - \frac{Pe}{Pc} \frac{\delta - 1}{\delta} \right] \right\}^{\frac{1}{2}}$$

The δ value at the flame temperature of this composition was not known due to the lack of thermodynamic data for the reactants and the products. For many commonly encountered rocket propellant δ lies in the range 1.2 to 1.3. However, thermochemical calculations for the magnesium/sodium nitrate system yielded values in the range 1.1 to 1.2. Figures (4) gives the results of the numerical calculations according to equation (2) for the latter two values of δ .

Examination of the burnt tracer capsules after spinning at 40×10^3 rpm showed that the build up of slag resulted in a mean value of the area ratio for twelve firings of 5.5 ± 0.5. Transposing this value onto figure (4) yields a pressure ratio of 30 to 35. Since the exhaust gases were venting into the atmosphere, this implies that the pressure on the burning surface was about 30-35 atmospheres; a remarkably close correlation with the value obtained from the extrapolation of the Vielle plot.

It has not yet proved possible to measure the pressure over a spinning burning tracer directly. The evidence that there is a high pressure comes from indirect sources. Firstly, the spectral power distribution of the spinning tracer shows some broadening of the bands, although with the resolution of the equipment employed it is not possible to quantify this. Secondly, at intermediate spin rates, around 20,000 rpm, the burning composition is often ejected violently from its capsule. It is conjectured that the centrifugal force is insufficient to hold the throttle in place at the mouth of the capsule against the composition when the pressure has reached a level sufficient for the gas to penetrate around the sides of the composition to its base.

5. Attempts to modify the Nature of the Slag

On the assumption that the throttle formed by the slag causes the increased burning rate, experiments were undertaken to determine whether by altering the flow properties of the slag the burning rate could be altered. To this end measurements were made of tracer filled with composition F to which additional quantities of calcium silicide were mixed. The results are presented in Tables 2a and 2b. These data show that whilst $CaSi_2$ speeds up the reaction at zero spin, the burning rate is reduced at 40,000 rpm and also at intermediate rates of spin. In addition the average light output is increased at the 10% weight level of $CaSi_2$. Application of the T-test indicates that the effect on the burning times is only significant at the 10% probability level for the addition of 5% CaSi, but is highly significant at the 1% probability level for the addition of 10% CaSi.

TABLE (2a)

Effect of $CaSi_2$ on Burning Times (seconds)

Spin rpm	Composition F	F + 5% $CaSi_2$	F + 10% $CaSi_2$
0	8.9 ± 0.3	6.3 ± 0.1	6.2 ± 0.1
40K	2.6 ± 0.2	2.8 ± 0.1	3.2 ± 0.2

TABLE (2b)

Effect of $CaSi_2$ on Average Light Output (candelas x 10^3)

Spin rpm	Composition F	F + 5% $CaSi_2$	F + 10% $CaSi_2$
0	2.6 ± 0.4	2.0 ± 0.2	4.5 ± 0.9
40K	1.5 ± 0.2	1.5 ± 0.2	2.0 ± 0.4

6. The effect of the Aperture of the Tracer Retaining Washer

The tracer capsule is normally retained in large calibre shells by a washer with a small orifice. In addition, it is said that the washer protects the tracer composition from erosion by the propellant gases as the shell travels up the barrel of the gun. From the observation that there is a tendency for the tracer composition to be ejected at intermediate rates of spin it may be inferred that the retaining washer may play an additional role in preventing this occurrence. In the past, the size of the orifice in the washer has been small, typically giving an area ratio of about 10, and it could therefore be envisaged that the retaining washer plays a major role in pressurizing the burning surface and consequently reducing the burning time.

To confirm this, live firing trials were carried out using 105 mm ammunition in which a number of retaining washers of different orifice sizes were fitted. The shells were tracked visually and the burning times recorded by a number of observers using stop watches. The tracer composition was composition F. Table (3) lists the predicted burning times based on the above theory and the observed burning times. The observed burning times are the average of the "best" of the observers results for six rounds.

TABLE (3)

Effect of orifice size in Washer on Burning Times (seconds)

Orifice area	.04 sq. in.	.06 sq. in.	.10 sq. in.	.14 sq. in.	.19 sq. in.	.19 sq. in.
Predicted	1.6	1.9	2.4	2.6	2.7	2.7
Observed	1.9	2.2	2.3	2.4	2.5	2.5
Shape	Hex.	Square	Square	Square	Square	Circular
Area ratio	9.6	6.4	3.8	2.7	2.0	2.0

These results show reasonable agreement with the predicted results, particularly when it is remembered that the motion of the shell through the air results in a reduced pressure over the base of the shell, and the lack of knowledge of the precise value of the ratio of specific heats of the combustion products. Note that the theory gives predicted burning times which are less than observed results for orifice sizes of 0.04 and 0.06 sq. inches, yet higher results for the remainder. What probably affects the results are the reduced pressure at the base of the shell and the build-up of slag to form a throttle having an area ratio of about 5 to 6. The throttle formed by the slag then controls the burning times rather than the washer orifice size.

7. Effect of Particle Size on Burning Rate and Light Output

The effect of changing the particle sizes of both the magnesium and the strontium nitrate in composition F has been examined. Tables 4a and 4b show the effect that coarser and finer grades of magnesium have on the burning times and average light output respectively.

TABLE (4a)

Effect of Magnesium Particle Size on Burning Times (seconds)

Spin rate rpm	MAGNESIUM		
	Grade 0	Grade 3	Grade 6
0	11.0 ± 0.3	8.9 ± 0.3	5.8 ± 3.9
40K	3.2 ± 0.2	2.6 ± 0.2	3.4 ± 0.1

TABLE (4b)

Effect of Magnesium Particle Size on Average Light Output (candelas x 10^3)

Spin rate rpm	MAGNESIUM		
	Grade 0	Grade 3	Grade 6
0	1.7 ± 0.6	2.6 ± 0.4	0.8 ± 0.7
40K	1.4 ± 0.3	1.5 ± 0.2	1.0 ± 0.1

It is evident from these data that this composition when filled with the fine grade 6 magnesium burns extremely erratically at zero spin rates. This tendency is reversed when it is burnt under spin. The T-test indicates that the effect of magnesium particle size on the burning time is significant at the 1% and 0.1% levels for grade 0 and grade 6 respectively. Tables 5a and 5b indicate the effect of using 7 micron strontium nitrate compared with the standard size 120 in composition F.

TABLE (5a)

Effect of $Sr(NO_3)_2$ Particle Size on Burning Time (seconds)

Spin Rate rpm	STRONTIUM NITRATE SIZE	
	Standard 120	7 Micron
0	8.9 ± 0.3	7.3 ± 0.3
40K	2.6 ± 0.2	2.9 ± 0.2

Here the action of the finer strontium nitrate has the expected effect on the burning rate at zero spin but slows down the burning rate at 40,000 rpm and intermediate rates of spin. The difference in the mean burning times is significant at the 5% probability level.

TABLE (5b)

Effect of $Sr(NO_3)_2$ Particle Size on Average Light Output (candelas)

Spin rate rpm	STRONTIUM NITRATE SIZE	
	Standard 120	7 Micron
0	2.6 ± 0.4	3.2 ± 0.5
40K	1.6 ± 0.2	2.3 ± 0.3

8. Effect of Proportion of Magnesium in Composition and Pressing Agents

In carrying out the initial study covering a gamut of compositions, it became apparent that the burning rate at high spin rates was decreased when low proportions of magnesium was incorporated into the compositions. This may simply be due to a lack of magnesium oxide to build up the throttle. In order to reduce the number of variables in the study, simplified compositions were mixed and filled into the tracer capsules. These mixtures are listed in Appendix 2.

Figure (5) shows the effect on the burning time as the proportion of magnesium in the composition is changed. It may be seen that the proportion of magnesium has a considerable effect on the burning times at 40K rpm particularly at the lower magnesium concentrations.

Table (6) shows the effect of changing the proportion of magnesium on the average light output, for tracer burnt at 40K rpm.

TABLE (6)

Effect of Proportion of Magnesium on Average Light Output (candelas)

% Weight Magnesium	PRESSING AGENT	
	Beeswax	Boiled Linseed oil
10	200 ± 40	120 ± 40
15	480 ± 50	380 ± 40
20	500 ± 70	400 ± 90
25	690 ± 130	1420 ± 230
30	650 ± 130	1230 ± 190

The above table shows the remarkable increase in the average light output for those compositions utilizing boiled linseed oil as the pressing agent when the magnesium content is increased to about 25%.

The choice of pressing agent apparently seems to have a strong effect on the average light output, yet seems not to significantly effect the burning times of the composition when the magnesium content exceeds 15% by weight. However, the tests so far completed have only investigated two of the many possible materials.

9. Intensity of Tracer Compositions and Sighting Range

Most of the emphasis so far in this paper has been placed upon the requirement that the burning time of the tracer should be increased by at least 20% above its present value. This is related to the fact

that modern tank tactics and advances in ranging equipment require and permit engagements to take place at ever increasing ranges. The fact that the tracer must be observed at greater ranges than in the past raises the question of what is the luminous intensity required to maintain visual contact.

At present there is little data available relating to the characteristics of this problem to enable a good estimate to be made. Figures (5) and (7) are based on the Tiffany data (reference 1) and show the variation of sighting range with the intensity of the light source, with the visibility as parameter, for daylight and moonlight viewing conditions. Taking the daylight viewing condition as being the most difficult to produce a satisfactory tracer it may be seen from figure (6) that a luminous intensity of 2,000 candelas will permit a sighting range of 1500 metres and 3200 metres for visibilities of 5.5×10^3 metres and infinity respectively. The probability of sighting is 95%. Since modern tracers are required to be sighted at ranges greater than 3000 metres, and under visibility conditions which are less than perfect it would seem that the present luminous intensities are not sufficient. On the basis of figure (6) the intensity should be increased to about 10,000 candelas.

However, the Tiffany data is based upon unlimited observation times upon a static target. The tracer problem has a moving target with limited observation time, but most importently the position of the first appearance of the tracer is known and the eye has to perform a tracking task rather than a search task. Hence the values obtained from figure (6) are likely not to apply to this particular situation.

When the eye is adapted to background luminances corresponding to moonlight conditions the Tiffany data predicts much greater sighting ranges for a given luminous intensity and visibility (figure 7) than the daylight case. The same differences in the tasks apply as were outlined above, but in addition the colour of the tracer becomes important as the eye approaches the threshold between scotopic and photopic vision. The threshold value is accepted to be 2×10^{-3} candela/metre^2 below which red signals cannot be detected. Thus for a sighting range of 4000 metres with a perfectly clear intervening atmosphere a luminous intensity of about 30,000 candelas is required. Thus under certain very low background luminances the red colour may be a disadvantage.

The determination of the relative importance of the brightness contrast and colour contrast of a light source against is background is complex. Red has the advantage that it is little changed when observed at small angles of subtense, whereas yellow, green and purple become almost grey in appearance (reference 2). Typically, tracers subtend angles of a few seconds of arc so that this effect is likely to be of major importance. In addition, both red and green have been shown by Hill, (reference 3), to be the most easily recognisable colours at low illuminace levels.

It may be seen from this necessarily brief section that our knowledge of the processes which lead to the ability to follow a tracer is extremely limited.

10. References

1. Blackwell, H. R. J. Opt. Soc. Am. 36, pp 624-643, 1946

2. Middleton, W. E. K. and Holmes, M.C. J. Opt. Soc. Am. 39, 582-592, 1949.

3. Hill, N. E. G. Proc. Phys. Soc. 59, 560-574, 1947.

COMPOSITIONS OF TRACER FILLINGS

A	Magnesium, Grade 0	35 parts
	Boiled Linseed Oil	4 "
	Strontium Nitrate, Size 120	41 "
	Chlorinated Rubber, Size 120	20 "
B	Magnesium, Grade 4	35 parts
	Polymerised Linseed Oil	10 "
	Strontium Nitrate	45 "
	Strontium Peroxide	10 "
	Magnesium Carbonate	5 "
C	Magnesium, Grade 3	48 parts
	Boiled Linseed Oil	4 "
	Potassium Perchlorate, Size 120	38 "
	Strontium Oxalate, Size 120	10 "
D	Magnesium, Grade 4	30 parts
	Polymerised Linseed Oil	12 "
	Strontium Nitrate	53 "
	Strontium Peroxide	5 "
	Talc ($2\frac{1}{2}$ parts mixed with 100 parts of the above prior to pressing)	
E	Magnesium, Grade 4	25 parts
	Strontium Nitrate	58 "
	Strontium Peroxide	5 "
	Polymerised Linseed Oil	12 "
	Talc ($2\frac{1}{2}$ parts prior to pressing)	
F	Magnesium, Grade 3	38 parts
	Beeswax	4.8 "
	Strontium Nitrate, Size 120	42.8 "
	Shellac Size 100	4.8 "
	Chlorinated Rubber	4.8 "
	Magnesium Carbonate	4.8 "
G	Titanium, (8u)	48 parts
	Boiled Linseed Oil	4 "
	Strontium Nitrate, Size 120	45 "
	Chlorinated Rubber, Size 120	3 "

APPENDIX 2

COMPOSITIONS OF EXPERIMENTAL TRACER FILLINGS

	H	J	K	L	M
Magnesium, Grade 3	10	15	20	25	30
Strontium Nitrate, 120	89	83	78	72	66
Beeswax	1	2	2	3	4

	N	O	P	Q	R
Magnesium, Grade 3	10	15	20	25	30
Strontium Nitrate, 120	89	83	78	72	66
Boiled Linseed Oil	1	2	2	3	4

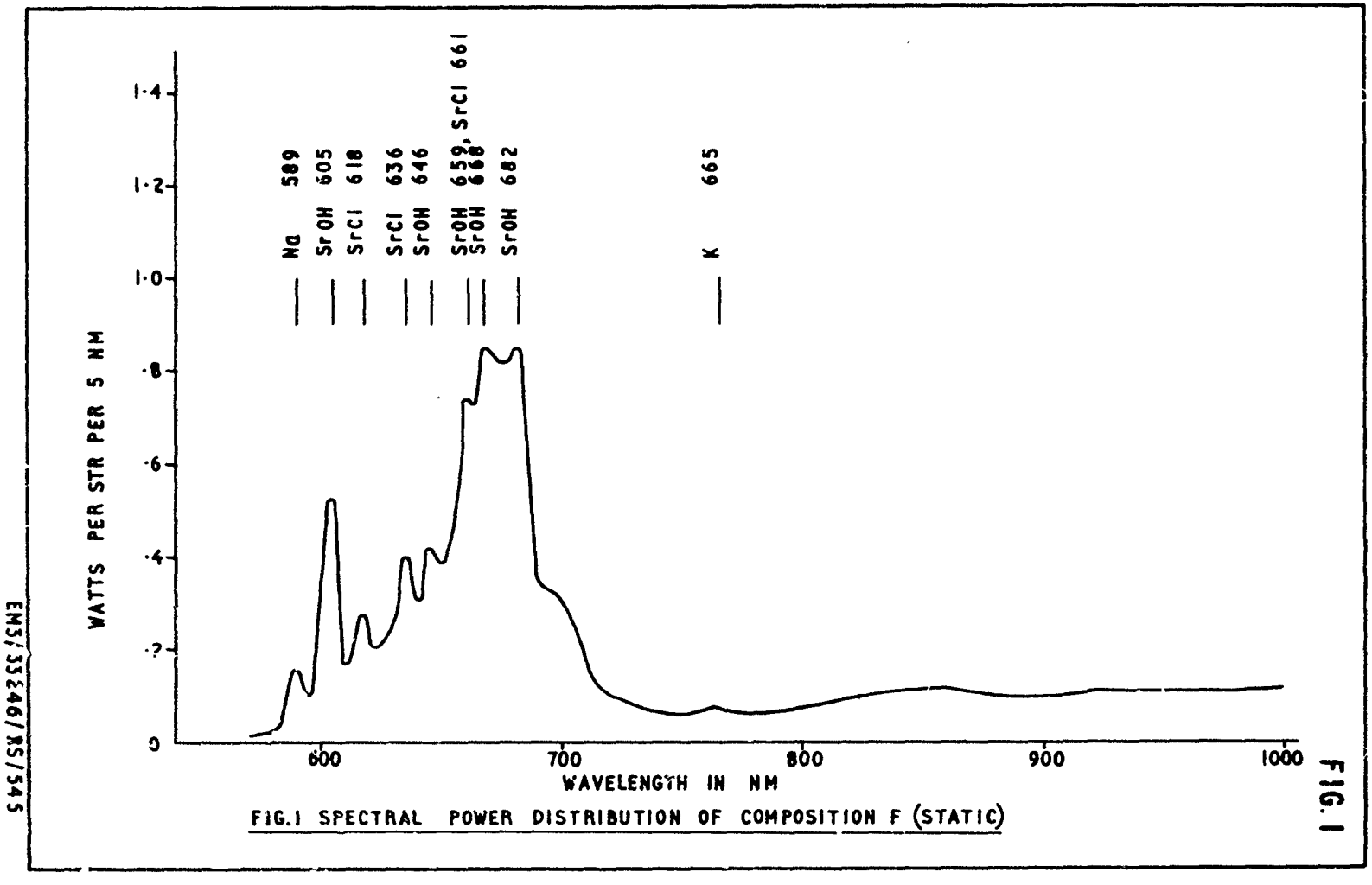

FIG.1 SPECTRAL POWER DISTRIBUTION OF COMPOSITION F (STATIC)

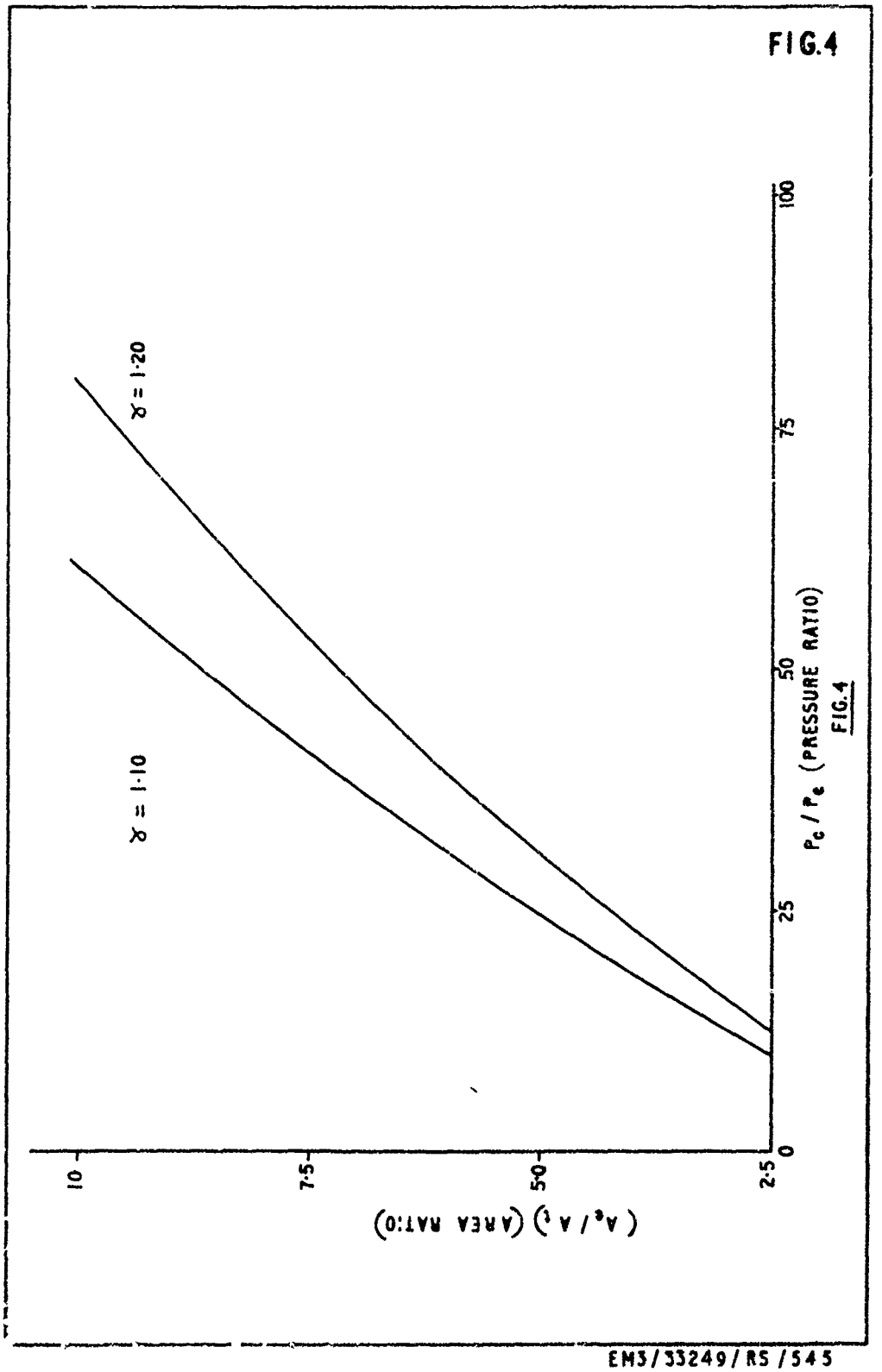
FIG.4
γ = 1·20
γ = 1·10
(Aₑ / A t) (AREA RATIO)
10
7·5
5·0
2·5
0
25
50
75
100
Pc / Pe (PRESSURE RATIO)
FIG.4
EM3/33249/RS/545

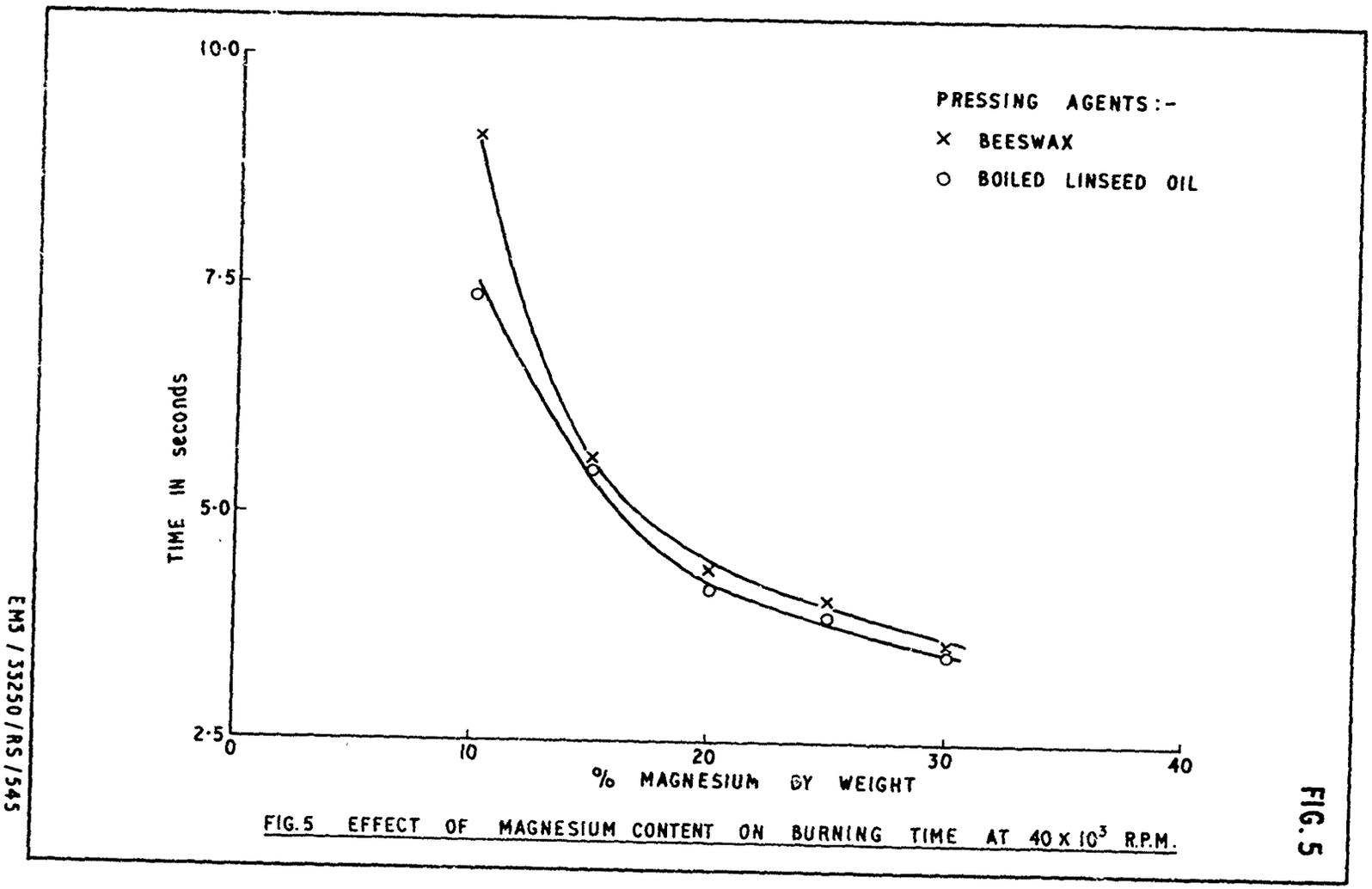

FIG.5 EFFECT OF MAGNESIUM CONTENT ON BURNING TIME AT 40×10^3 R.P.M.

FIG. 5

FIG. 6

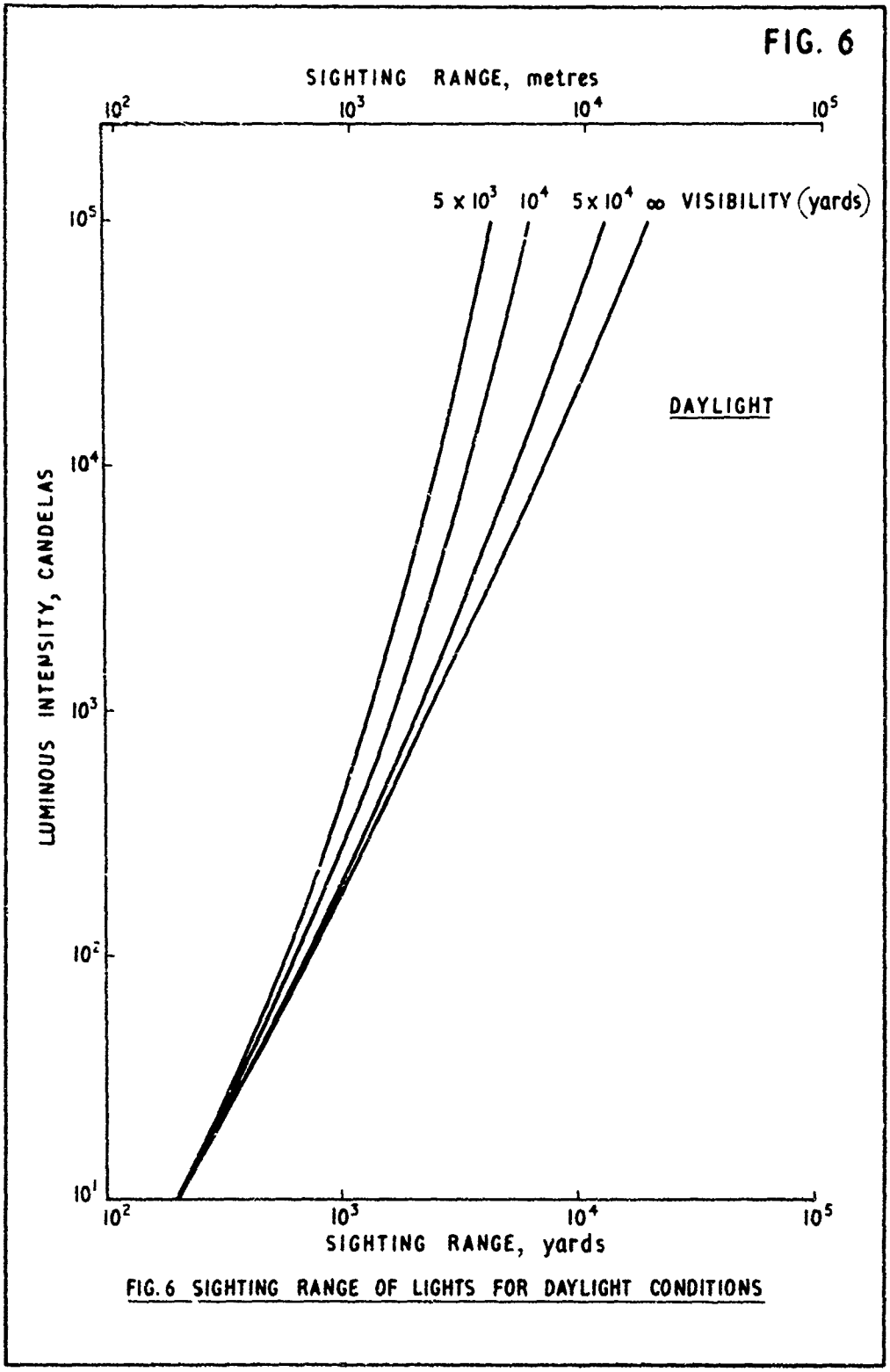

FIG. 6 SIGHTING RANGE OF LIGHTS FOR DAYLIGHT CONDITIONS

EM3/33258/RS/545

FIG. 7

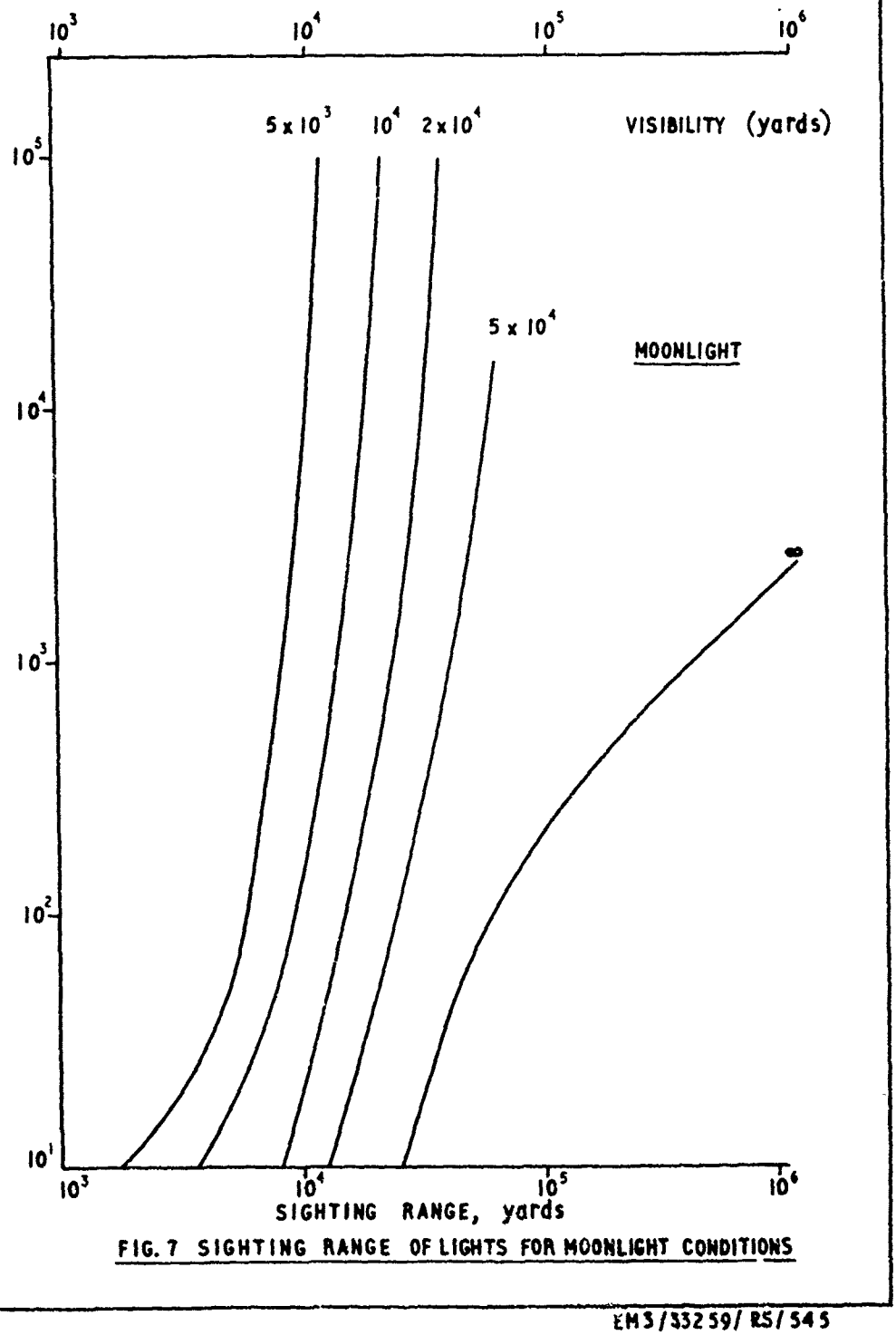

FIG. 7 SIGHTING RANGE OF LIGHTS FOR MOONLIGHT CONDITIONS

EMS/33259/RS/545

BURNING RATE MODIFIERS

David R. Dillehay

Thiokol Corporation
Longhorn Division
Marshall, Texas

ABSTRACT

A study program is currently in progress to investigate additives for altering the burning rate of illuminant compositions. Materials have been found which will increase or decrease the burning rate. This report will outline results obtained to date and describe some of the techniques being used to investigate burning rate controlling reactions.

INTRODUCTION

Current illuminant compositions are based on magnesium/sodium nitrate/binder. Burning rate control is achieved by adjusting the magnesium and/or binder content. The candlepower is then taken as a resultant. Decreasing burning rate in this manner decreases illuminant efficiency and increasing burning rate increases illuminant costs.

Consider the impact of this limitation by comparison of the following examples. The M127A1 candle can tolerate a burning rate of 0.085 in/sec. maximum but requires a candlepower average of at least 145,000. Table I shows results of tests with standard illuminant in M127A1 candles. The data indicates that the magnesium should be increased to 55% to provide the candlepower. Table I also shows that substitution of sodium nitrite for part of the sodium nitrate provides a formulation that meets the requirements with a reduction in magnesium content. The use of a burning rate modifier results in a production cost saving of about $0.03 per pound. In the event of a national shortage of magnesium, the ability to formulate with less magnesium is an obvious advantage.

EXPERIMENTAL RESULTS

A study program is currently in progress at Longhorn Army Ammunition Plant to investigate means for modifying burning rates of illuminant other than varying magnesium content. Candidate materials are screened for general compatability with illuminant ingredients. Laboratory mixes are made in a 12 inch Lancaster muller-type mixer. The illuminant is consolidated in M127A1 candle cases 31mm in diameter and 64mm in length. The candles are cured for 48 hours, minimum, at 140 $\pm$ 10°F.

Some of the results are listed in Table II. The increases and decreases in burning rate appear to be real and reproducible. Figures I and II graphically show the results obtained with two of the additives.

The mechanism of burning rate modification is of great importance and interest. By studying the effects of classes of materials it is hoped that a more complete understanding of the surface kinetics will lead to improved illuminants. The data generated thus far indicates that there is an optimum burning rate for any given formulation. Increasing the burning rate beyond this optimum does not yield any improvement in candlepower. Decreasing the burning rate from above the optimum to near the optimum will improve the candlepower. Also, increasing burning rates from below the optimum to near the optimum will result in improved candlepower.

As part of the current study program, computer calculation of combustion products are being combined with experimental data to find relationships which will predict optimum burning rates for formulations. The computer program is the NASA-Lewis SP-273 Complex Equilibrium Program. The mole fractions of products are converted to moles/second values with the experimental data. This normalization permits examination of the plume products on a real time basis. The effect of normalization on moles of magnesium oxide, magnesium gas, and sodium gas are shown in Figures III and IV for 6% binder and varying percentage of magnesium.

Additional work is planned to relate the computer data and experimental data to improve the illuminant combustion model. In addition, studies of the surface of extinguished illuminant using scanning electron microscopy are planned.

TABLE I

Laminac 4116 Binder Illuminant

% Binder	% Mg	% $NaNO_3$	% $NaNO_2$	Rate	KCDLA	KCPS/GM
6	50	44	--	.060	115.8	54.0
6	53	41	--	.064	135.8	60.2
6	50	28	16	.077	149.2	54.2
6	53	21	20	.083	160.9	54.9

Where: Rate = Linear Burning Rate, in/sec

KCDLA = Kilo candela

KCPS/GM = Kilo candela - seconds per gram of mix

TABLE II

6% Binder Illuminants

% Mg	Additive	Rate	KCDLA	KCPS/GM
40	--	.042	55.7	36.4
45	--	.045	72.2	44.7
50	--	.051	110.2	59.4
55	--	.056	125.4	64.4
60	--	.062	143.3	65.9
50	1% Ammonium Dichromate	.056	117.9	59.2
50	1% Nitron	.057	112.0	55.5
50	1% Sodium Cyanide	.049	102.4	58.2
60	2% Sodium Cyanide	.067	139.2	59.3
40	1% TFE/1% Antimony Oxide	.035	45.2	35.4
45	1% TFE/1% Antimony Oxide	.044	72.8	45.6
50	1% TFE/1% Antimony Oxide	.046	93.2	56.5
55	1% TFE/1% Antimony Oxide	.052	111.9	60.6
50	2% TFE/2% Antimony Oxide	.046	91.6	55.3
60	2% TFE/2% Antimony Oxide	.060	117.4	56.1
45	1% Tetranitrocarbazole	.060	105.7	48.4
50	1% Tetranitrocarbazole	.060	117.2	54.6
55	1% Tetranitrocarbazole	.068	135.0	56.1
60	1% Tetranitrocarbazole	.075	146.9	56.5
50	2% Sodium Metabisulfite	.056	114.5	57.5
60	2% Sodium Metabisulfite	.065	143.3	63.6
50	4% Magnesium Nitrate Hexahydrate	.076	146.3	54.0
50	2% Sodium Fluoride	.056	102.0	51.3
60	2% Sodium Fluoride	.072	134.2	53.7

Where: Binder = 50% Diglycidylether of Bisphenol A;
45% Ethylformal polysulfide polymer
5% Dimethylaminomethyl phenol

Rate = Linear Burning Rate, in/sec

KCDLA = Kilo candela

KCPS/GM = Kilo candela - seconds per gram of mix

Figure 1

Effect of 1% TFE/1% Antimony Oxide

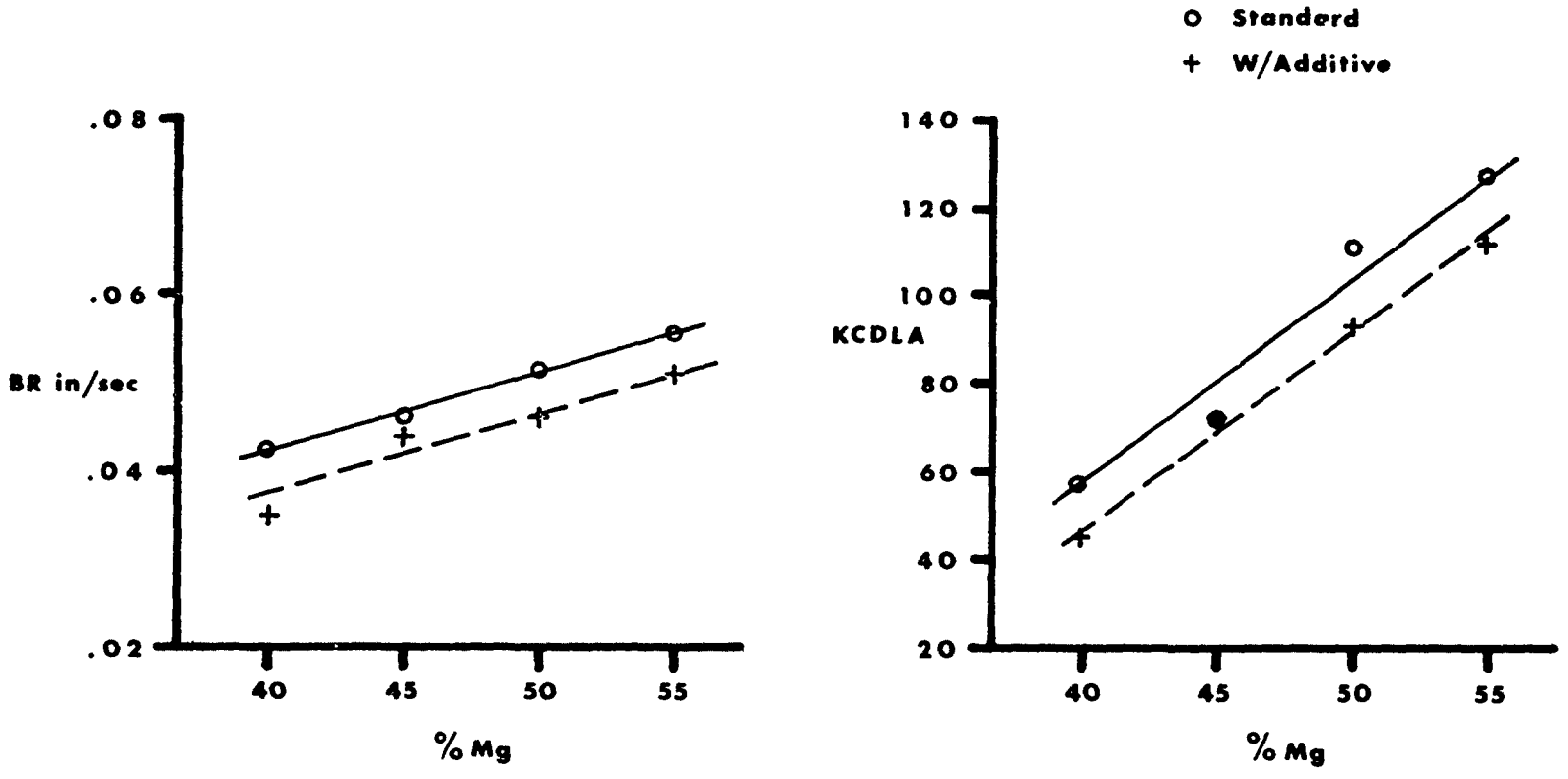

Figure 2

Effect of Tetranitrocarbazole

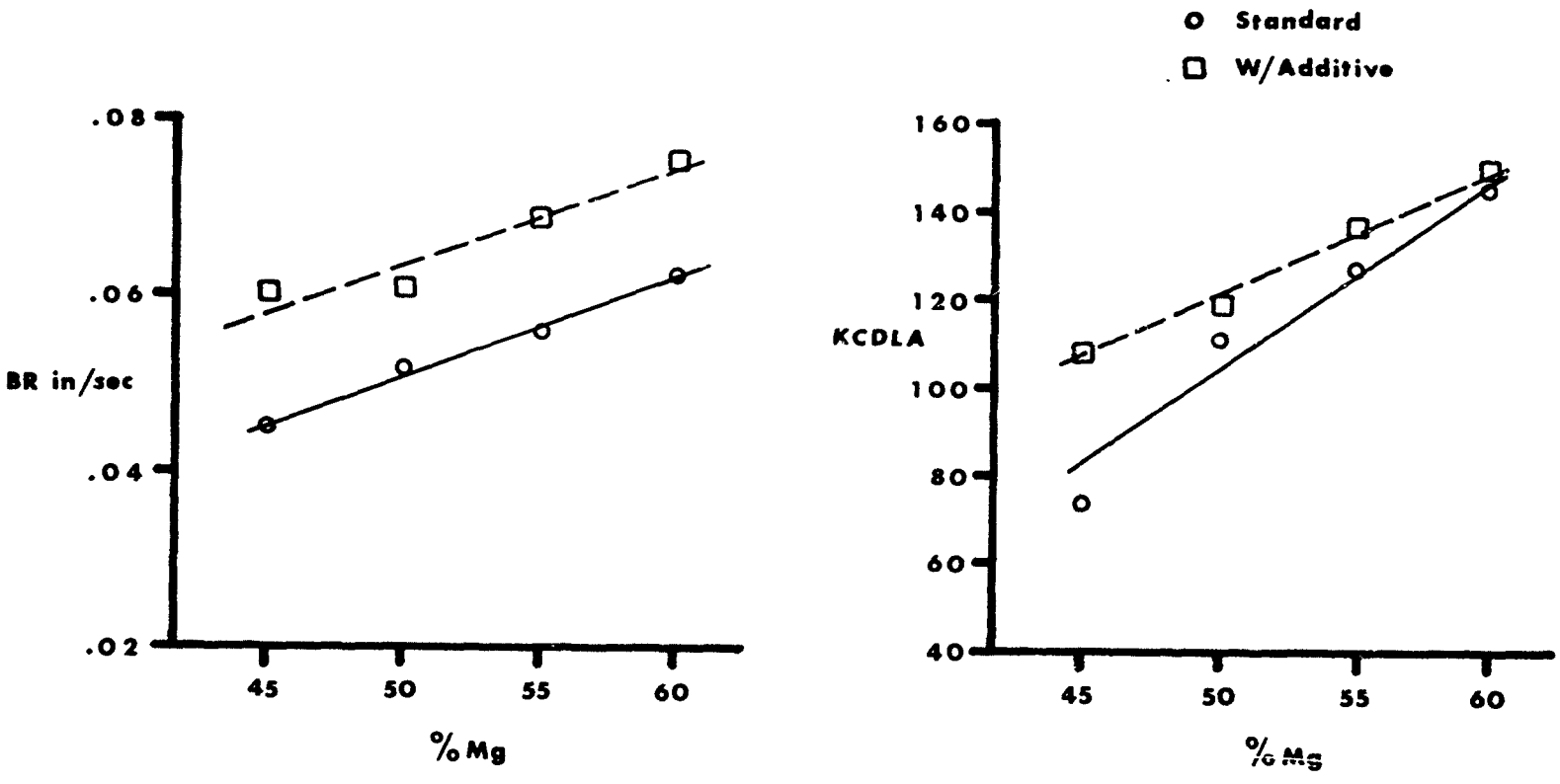

Figure 3

Normalized Moles of MgO(s) and MgO(g)

6% Binder

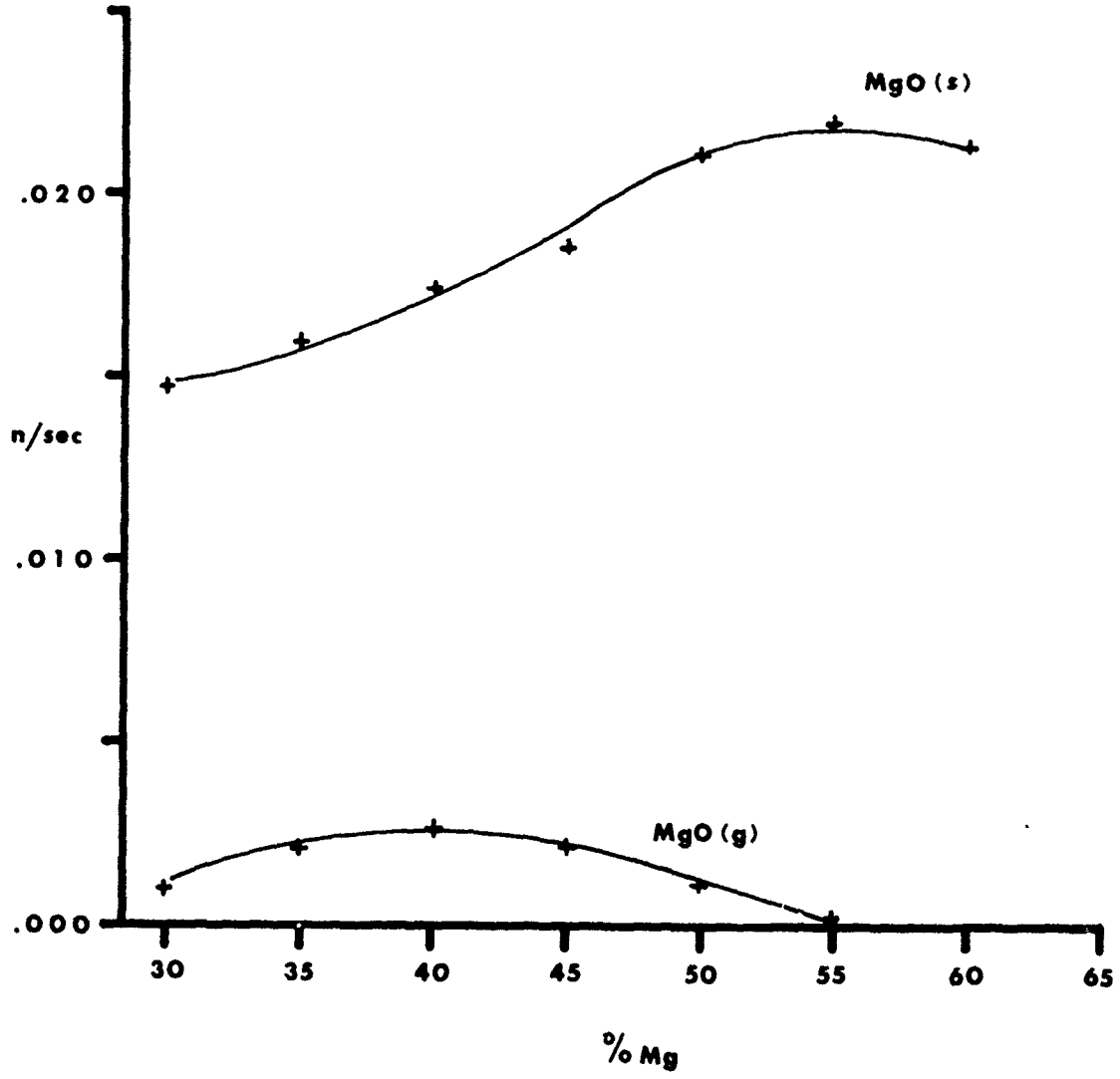

Figure 4

Normalized Moles of Na(g) and Mg(g)

6% Binder

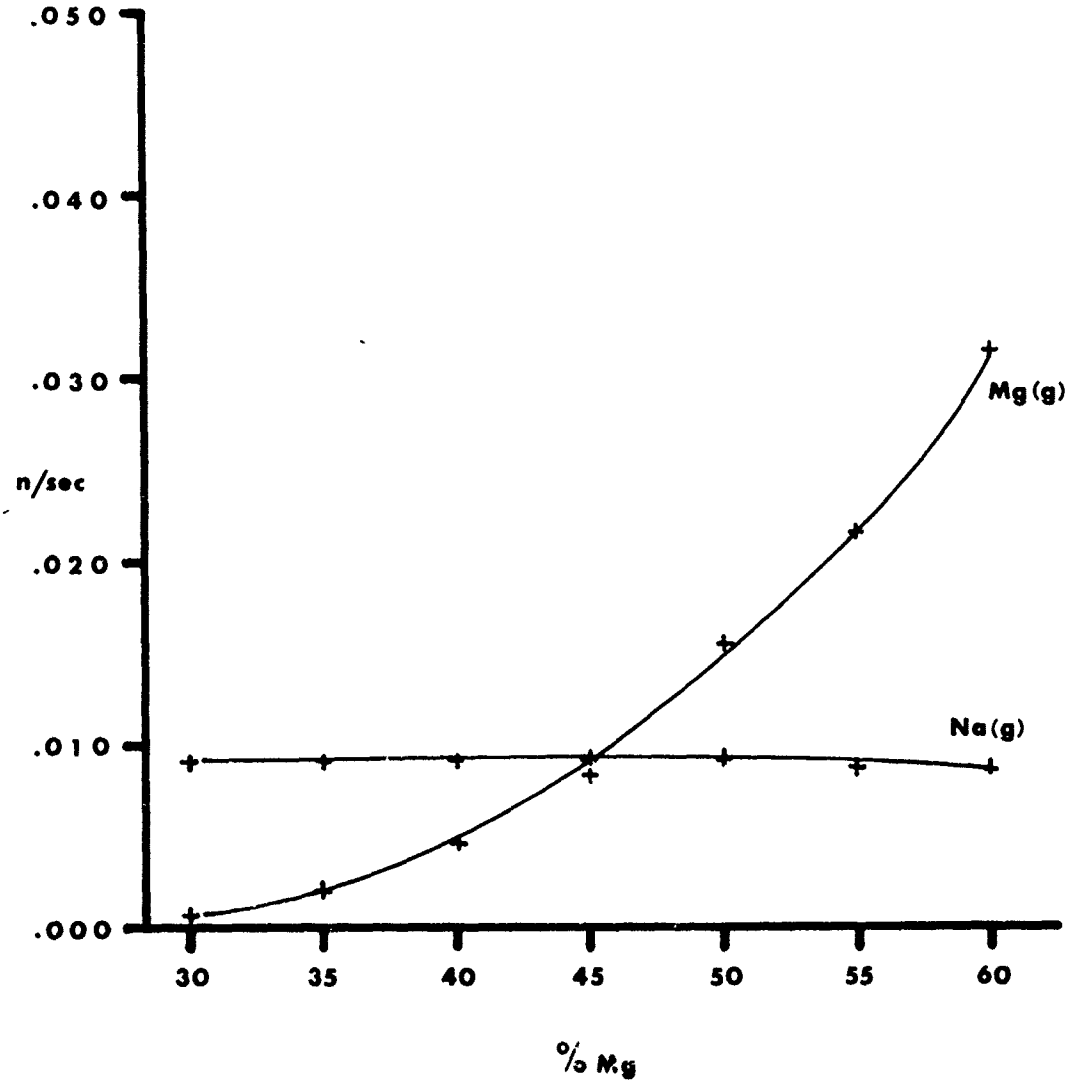

SPECTROSCOPIC ANALYSIS OF AZIDE DECOMPOSITION PRODUCTS FOR USE IN A PYROTECHNICALLY INITIATED CARBON DIOXIDE CHEMICAL LASER

Carl E. Dinerman
Applied Sciences Department
Naval Ammunition Depot, Crane, Indiana 47522

ABSTRACT

In the consideration of sodium azide as a potential nitrogen source for a nitrogen-carbon dioxide chemical laser, it is important to know the fraction of the heat of decomposition of the azide that will appear as vibrational excitation in the nitrogen. To this end, the v"=0, v"=1 and possibly the v"=2 progressions of the Lyman-Birge-Hopfield ($a^2\Pi_g - X^2\Sigma_g^+$) bands of nitrogen will be monitored by means of absorption spectroscopy in the vacuum ultraviolet, upon thermal decomposition of sodium azide. The analyzed data will be in the form of ratios of numbers of molecules in two vibrational levels, such as v"=1 and v"=0: N_1/N_o. This number is shown to be proportional to the ratio of the two vibrational-electronic band absorption intensities, when certain good approximations are made.

The chemical laser system envisioned would have the NaN_3 as a nitrogen source and another compound as a carbon dioxide source, both reactions initiated by pyrotechnic means.

The experimental system is described and results to date are discussed.

BACKGROUND

In the quest for convenient ways to produce a nitrogen-carbon dioxide laser, it was found that gain at 10.6μ was exhibited when hydrazoic acid, a covalent compound, was decomposed in the presence of carbon dioxide[1,2] by nature of the vibrationally excited nitrogen product (in its ground electronic state) being able to transfer its energy to upper vibrational levels of carbon dioxide. This suggests that there is a possibility the decomposition of other covalently bonded azides, e.g., organic azides, may produce vibrationally excited nitrogen as well.

In order to better understand this process, it would be very useful to have an experimental measurement of the degree of vibrational excitation of this nitrogen immediately after decomposition, using a technique such as thermal decomposition of the azide coupled with absorption spectroscopy of an appropriate vibrational-electronic transition in nitrogen, while quickly flowing the evolving nitrogen through the absorption cell.

The objective of this preliminary study is to develop and perfect an experimental method for determining the distribution of vibrational energy in the products of azide decomposition. The initial investigation will be accomplished using sodium azide.

Upon decomposing sodium and potassium azides, investigators[3,4] have described an ultraviolet emission near 2500 Å; this has been interpreted[5] as the result of an electronic transition in nitrogen. Electromagnetic energy with a wavelength of 2500 Å is equivalent to about 120 Kcal/mole. With this much energy available for excitation of the nitrogen, there could be a higher degree of vibrational excitation than that provided by thermal equilibrium.

It is possible to envision a chemical laser system whereby the azide decomposition is initiated by a heat-producing pyrotechnic charge. A conceptual diagram of such an initiator is shown in Fig. 1. The heat source module would be completely separate from the azide to prevent contamination.

EXPERIMENTAL

The experimental arrangement, Fig. 2, is designed around a Spex model 1500 3/4 meter Czerny-Turner vacuum ultraviolet spectrometer with a magnesium fluoride overcoated 1500 Å blazed Bausch and Lomb grating, producing 10 Å/mm dispersion in first order. The spectrometer can be evacuated to 6×10^{-5} mm Hg with a Sargent-Welch model 3120D turbomolecular pump, backed up by a model 1376 roughing pump (Sargent-Welch Co., Skokie, Illinois).

The light source is a sealed krypton or xenon continuum lamp (Ophthos Inc., Rockville, Md.). Both have a magnesium

fluoride window. The lamps are excited by a 2450 MHZ microwave discharge unit (Scintillonics, Inc., Fort Collins, Colorado).

The 25 cm absorption cell has a vacuum ultraviolet quality magnesium fluoride lens (Harshaw Chemical Co., Cleveland, Ohio) at each end in order to collimate the light from the source and to focus it on the entrance slit. Two stainless steel bellows enable minor adjustments to be made in order to maximize energy throughput. A glass vacuum line is employed to evacuate the cell, the space between entrance slit and cell, and the space between light source and cell. A layer of DC 704 diffusion pump oil (Dow Chemical Co., Midland, Mich.) is placed on the mercury in the manometer to prevent any hazard resulting from mercury vapor coming in contact with azides.

Detection is by either photoelectric or photographic means. The first utilizes a Centronic Q4249B photomultiplier (Bailey Instrument Co., Saddlebrook, N.J.). This tube is mounted very close to a sodium salicylate covered quartz window which is sealed onto the exit slit opening. The sodium salicylate, when irradiated by vacuum ultraviolet energy, fluoresces in the blue. This emission is detected by the photomultiplier and the resulting signal displayed on a strip chart recorder (Yokogawa Model 3041-514, Electric Works, Ltd., Tokyo, JAPAN). Visible scattered light, as measured by inserting a pyrex glass section in the light path, was about 1/2%. Any

second order light is eliminated by the MgF_2 absorption cutoff at 1130 Å. The other detection method is via a rackable vacuum camera holding a 35 x 50 mm section of either SWR (Kodak, Rochester, N.Y.) or SC-7 film (Kodak Pathé, FRANCE). The AC power to the electronics is regulated to within .1% by a Sorenson Model ACR 2000 (Raytheon Corp., Norwalk, Conn.).

The azide is decomposed in fused silica combustion boats in a pyrex tube surrounded by a split-tube oven (Lindberg Model 55053, Watertown, Wisconsin) arranged at right angles to the absorption cell. The evolving nitrogen is continually pumped from the decomposition tube through the absorption cell by a liquid nitrogen trapped pump. It is also important to have a fast enough reaction and nitrogen flow rate so that vibrational relaxation and collisional deactivation do not change the vibrational distribution appreciably before entering the absorption cell.

Extreme purity of the azide is necessary, both to control the thermal decomposition and also to minimize impurity absorption in the region 1200 - 2000 Å which would interfere with the nitrogen absorption measurements. Dr. Richter at Picatinny Arsenal has prepared highly purified sodium azide for this project by a 3-step ion exchange process.

Determining the optimum decomposition conditions is a complex problem, for the decomposition rate is influenced by

such factors as particle size, purity, total sample mass, and temperature.[7,8,9,10] Fig. 3 illustrates the variation of decomposition rate with temperature and particle size.[10]

Basically, the project consists of four stages. Stage one involves adding research grade nitrogen gas to the absorption cell and taking its spectrum to determine the best values of the operating parameters, such as slit width, scanning speeds, signal-to-noise ratio, film exposure times, etc. Stage two consists of establishing the NaN_3 decomposition conditions (temperature, particle size, mass, flow rate) that will best suit the spectroscopic observation requirements. In stage three, nitrogen resulting from sodium azide decomposition will be spectroscopically examined in a normal absorption experiment in order to determine which interfering impurities may be present, so that correction may be subsequently made for them. Stage four involves the actual search for the vibrationally excited nitrogen species, using the fast flowing nitrogen system referred to above.

DISCUSSION

The transition in nitrogen that is most appropriate for the study of the vibrational excitation in the electronic ground state is the Lyman-Birge-Hopfield ($a^1\Pi_g \leftarrow X^1\Sigma_g^+$) system, with band origin at 1450 Å, or 68,965 cm^{-1}.[11] Although this is a forbidden transition, it is still the most intense band

in the region above 1000 Å.[12] The potential energy diagram for this band system is reproduced in Fig. 4.[13]

The following relates the experimentally measurable quantities with theory.

The experimental integrated absorption coefficient of a particular vibrational electronic transition of a diatomic molecule can be related to vibrational level populations in the following way:[14]

$$\int k_\nu d\nu = \frac{8\pi^3}{3hc} N_{v''} \nu \bar{R}_e^2 [(\int \psi_{v'} \psi_{v''} dr)^2] \qquad (1)$$

where $\int k_\nu d\nu$ is the integrated absorption coefficient, $N_{v''}$ is the number of molecules in the vibrational level of the lower electronic state, ν is the frequency in cm^{-1}, and $\bar{R}_e^2$ is the square of the average electronic transition moment and can be considered constant to good approximation for this band system.[15] The term in brackets is the Franck-Condon factor, tabulations for which are given.[15]

As an example of the use of equation (1), we can compare the relative intensities of the $a^1\Pi_g \leftarrow X^1\Sigma_g^+$ (3,0) band at 1354 Å or 73,856 cm^{-1} with that of the (1,1) band at 1464 Å or 68,306 cm^{-1}. These are the most intense absorption bands for the v"=0 and v"=1 progressions, respectively. Since we are only interested in relative intensities, it is permissible to form a ratio using equation (1) for the two bands:

$$\frac{\int k_\nu d\nu \quad (1,1)}{k_\nu d\nu \quad (3,0)} = \frac{(N_1)}{(N_0)} \frac{(68,306)}{(73,855)} \frac{(.193)}{(.183)}$$

where constant terms have been dropped and the values for the Franck-Condon factors inserted from reference (15).

Therefore, a determination of the relative band intensities allows the fraction N_1/N_0 to be calculated. Similar considerations apply for N_2/N_0, etc. Dressler[16] did not observe bands with $v''>1$ in an absorption measurement of the Lyman-Birge-Hopfield bands of active nitrogen, so it is possible that the only transitions we will observe will be those originating in $v''=0$ and $v''=1$. In this case, $N_0 + N_1 = N$, the total number of molecules, and N_1/N will be the percentage of molecules in the first vibrational level.

Fig. 5 shows a spectrum of 600 torr of Linde research grade nitrogen through a 25 cm path length using the Krypton continuum. The spectral slit width is .6 Å. The spectrometer vacuum is 1.5×10^{-4} torr, as measured by a Veeco cold cathode gauge. The carbon monoxide Fourth Positive bands are most likely the result of the photolysis of traces of organic material (such as stopcock grease or pump oil) and an ensuing reaction with small amounts of oxygen.

The asterisk at 1464 Å indicates the position of the (0,1) band, which would appear if there were $v''=1$ vibrational excitation as a result of the sodium azide decomposition.

One would not expect to see the (0,1) band at this pressure and path length because, even at 400°C, the maximum temperature at which the nitrogen could conceivably be, the v"=1 thermal equilibrium population is .007 of that of v"=0.

Some results of preliminary sodium azide decompositions in the present apparatus are presented in Fig. 6, with experimental conditions shown in Table I.

TABLE I

Decomp. Number	Azide Source	Mass ±.1gm	Temp. ±4°C	Induction* Period Min.	Max. Press. ±1 mm	Percent Decomp.
3	Fisher	.6	335	19	184	46
4	Fisher	.7	348-355	16	227	49
6	Fisher	.7	362-370	7	256	55
7	Fisher	.7	364-372	6	275	59

*Induction period as used here is the time for the pressure to rise to 1 mm.

CONCLUSION

As of this writing, the work is continuing. Final results are expected within a few months.

REFERENCES

1. N. G. Basov, et. al., J.E.T.P. Lett. 10, 2 (1969).

2. D. Collins, Private Communication.

3. R. Audubert, Trans. Faraday Soc. 35, 197 (1939).

4. G. D. Singer and H. J. Mueller, Nature 207, 1073 (1965).

5. R. W. Nicholls, J. Phys. Chem. 64, 1760 (1960).

6. J. A. Samson, *Techniques of Vacuum Ultraviolet Spectroscopy* (John Wiley & Sons, New York, 1967), p. 214.

7. W. E. Garner and D. J. B. Marke, J. Chem. Soc., 657 (1936).

8. E. A. Secco, J. Phys. Chem. Solids 24, 469 (1963).

9. P. W. M. Jacobs and A. R. Kureishy, J. Chem. Soc., 4718 (1964).

10. R. F. Walker, J. Phys. Chem. Solids 29, 985 (1968).

11. L. Wallace, Astrophysical Journal Supplement Series #62, VI, 445 (1962).

12. Y. Tanaka, M. Ogawa, and A. S. Jursa, J. Chem. Phys. 40, 3690 (1964).

13. J. T. Vanderslice, E. A. Mason, and E. R. Lippincott, Jr. J. Chem. Phys. 30, 129 (1959).

14. G. Herzberg, *Molecular Spectra and Molecular Structure* (Van Nostrand Co., Princeton, N. J., 1966), 2nd ed., Vol. I, pp. 201 and 383.

15. R. W. Nicholls, J. Quant. Spect. Rad. Trans. 2, 449 (1962).

16. K. Dressler, J. Chem. Phys. 30, 1621 (1959).

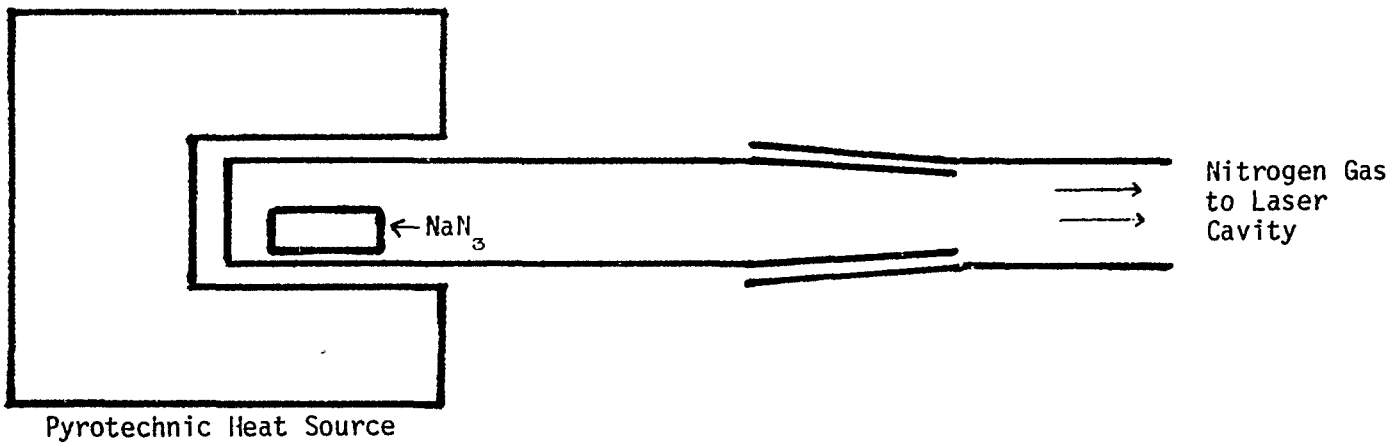

FIG. 1. Concept for pyrotechnic heat source for nitrogen-carbon dioxide chemical laser.

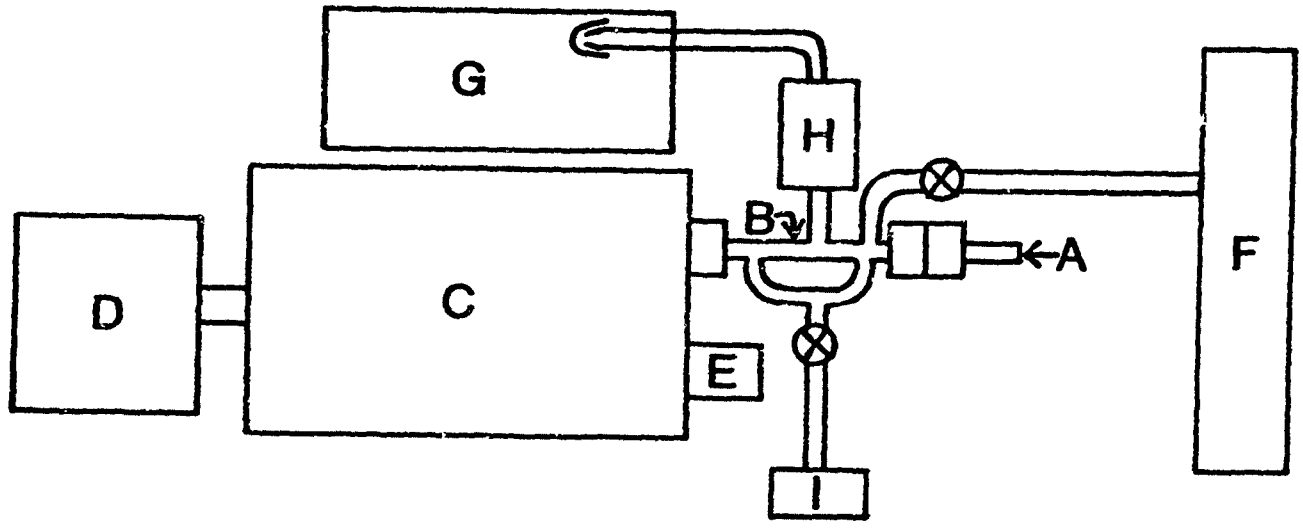

FIG. 2. Experimental Apparatus

(A) Light source
(B) Absorption cell
(C) 3/4 meter vacuum spectrometer
(D) Pump
(E) Detector
(F) Vacuum line
(G) Dry box
(H) Split tube oven
(I) Pump

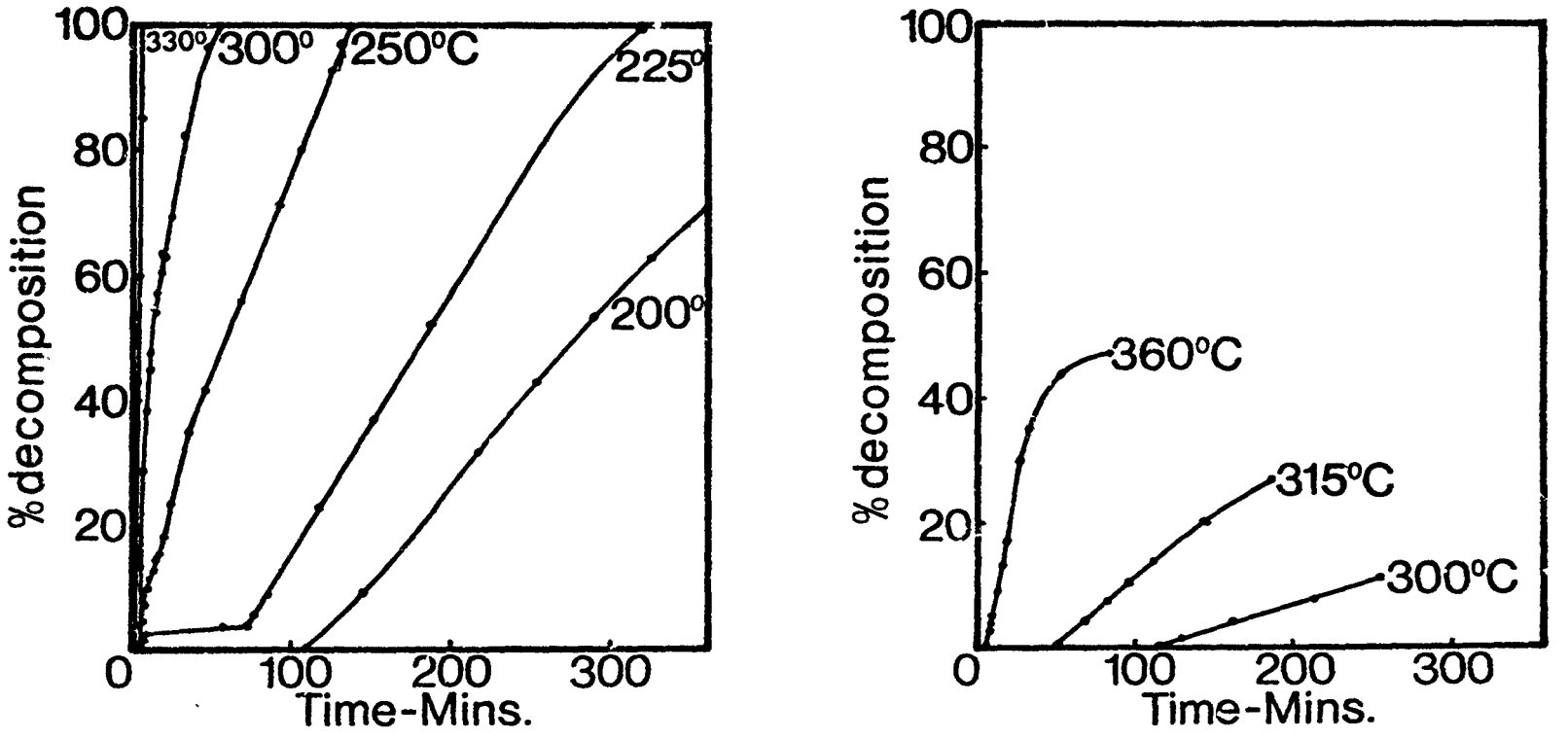

FIG. 3. Thermal decomposition curves for sodium azide (ref. 10).

Left Graph: Sodium azide in form of hexagonal plates, dimensions .2 - 1μ x .1μ, mass .1 - .5μg.

Right Graph: Plates, dimensions 1mm x .01mm, mass .18 - .56 mg.

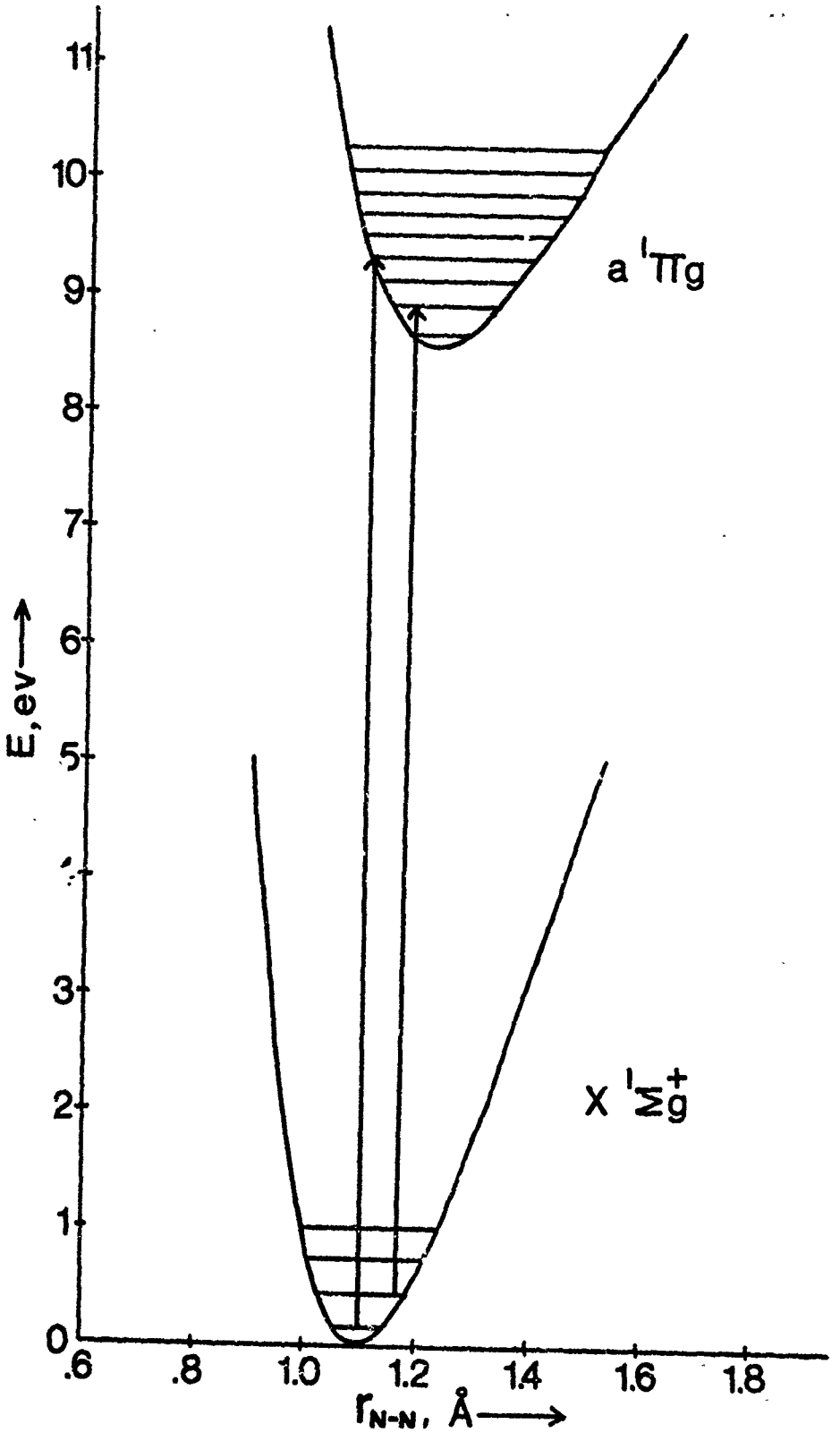

FIG. 4. Potential energy curves for the Lyman-Birge-Hopfield bands of nitrogen (ref. 13). The transitions indicated are the strongest absorption lines that originate from v"=0 and v"=1.

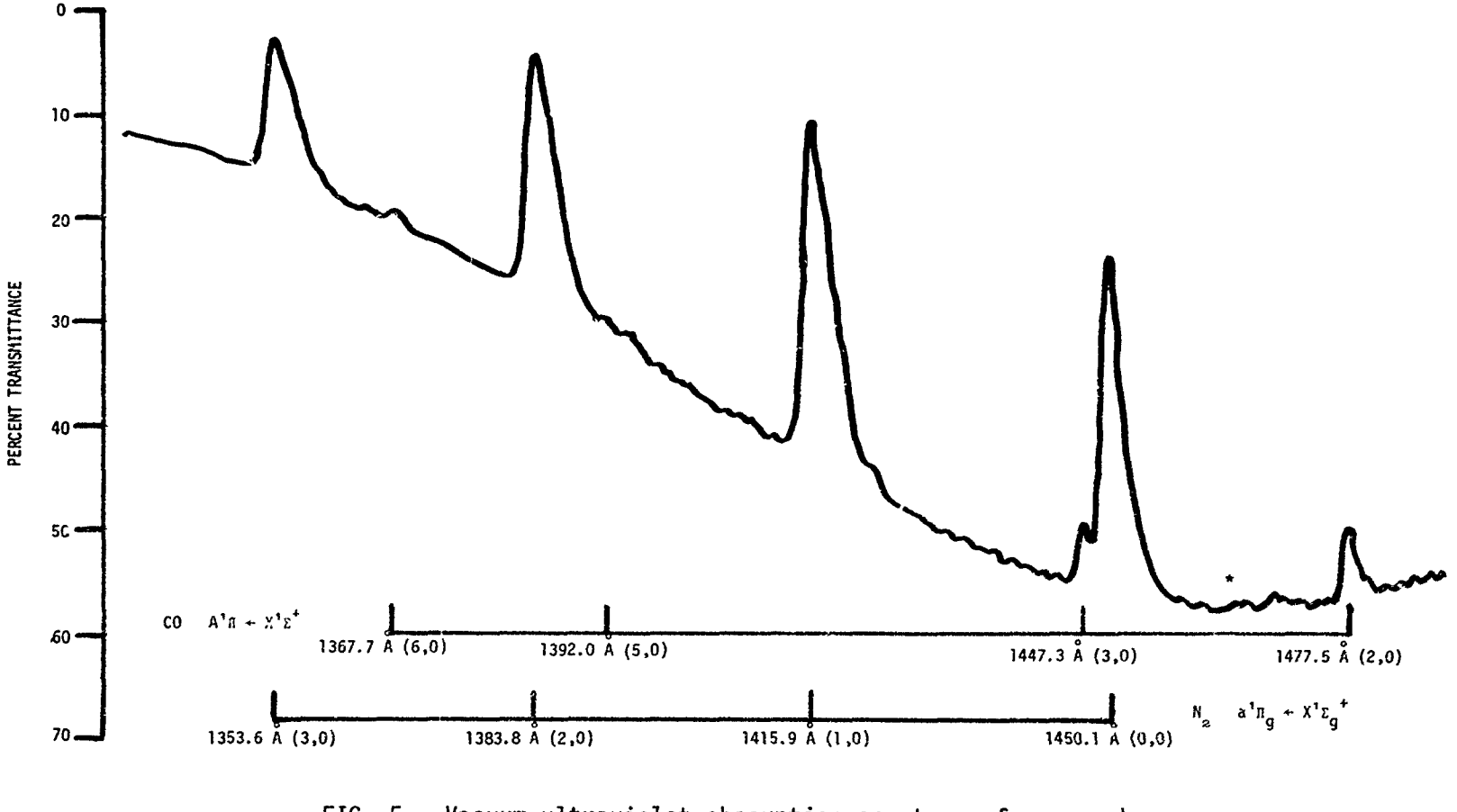

FIG. 5. Vacuum ultraviolet absorption spectrum of research grade nitrogen gas.

Path: 25 cm
Pressure: 600 mm
Spectral Slitwidth: .6 Å
Source: Krypton continuum

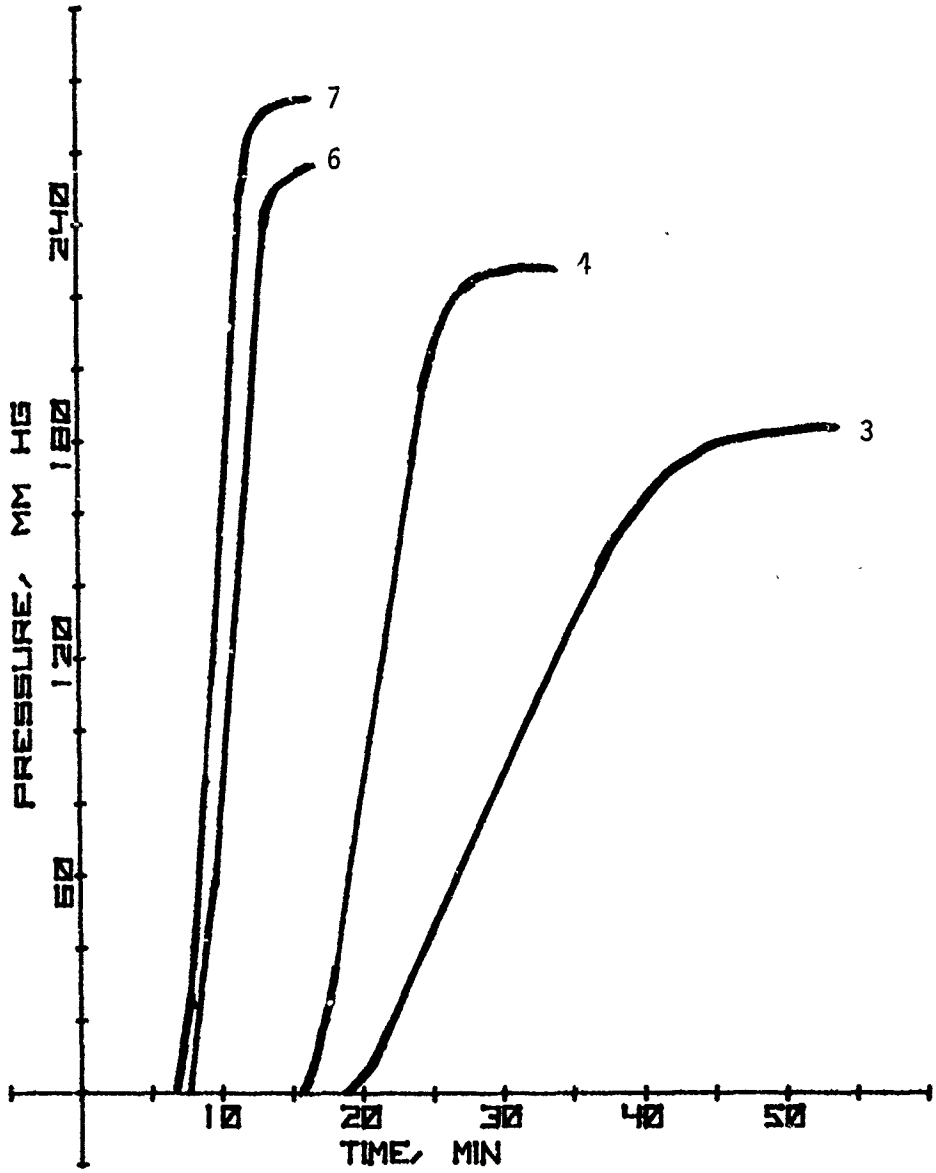

FIG. 6. Sodium azide decomposition curves. See Table I for experimental conditions.

ATMOSPHERIC PROPERTIES AND THEIR EFFECT ON TARGET ACQUISITION UNDER FLARE ILLUMINATION

BY

GERALD S. BRADLEY

INTRODUCTION

This effort was supported by the Target Acquisition Working Group of the Joint Technical Coordinating Group for Munitions Effectiveness.

In order to determine where best to position the flare and aircraft for target acquisition under various atmospheric conditions in Europe, a search was performed to define weather conditions in that area. The search confined itself to defining the atmospheric properties in terms of visibilities, ceilings, and wind velocities. After defining the atmosphere for various areas of Europe, analyses were performed to investigate the effects of ceilings, visibilities, and wind speed on target acquisition.

Current air-launched flares are ignited at 2,000 feet and 2,600 feet depending on the "breed" of the flare. The Navy MK 45 is ignited at 2,000 feet, while the Air Force LUU 2B/B is ignited at 2,600 feet. The burning time of the MK 45 is 180 seconds and of the LUU 2B/B, 240 seconds.

ATMOSPHERIC PROPERTIES

Data has been taken by the U. S. Naval Weather Service Command along the Mediterranean coastal areas and inland areas of different European countries on ceilings, surface visibilities, and wind speeds.

Ceilings

Figure 1 shows the ceiling height distribution of the Eastern coastal region of Spain for January and July. Figure 2

PROBABILITY DISTRIBUTION OF CEILING HEIGHTS
FOR ORAN, SPAIN
DURING NIGHT HOURS

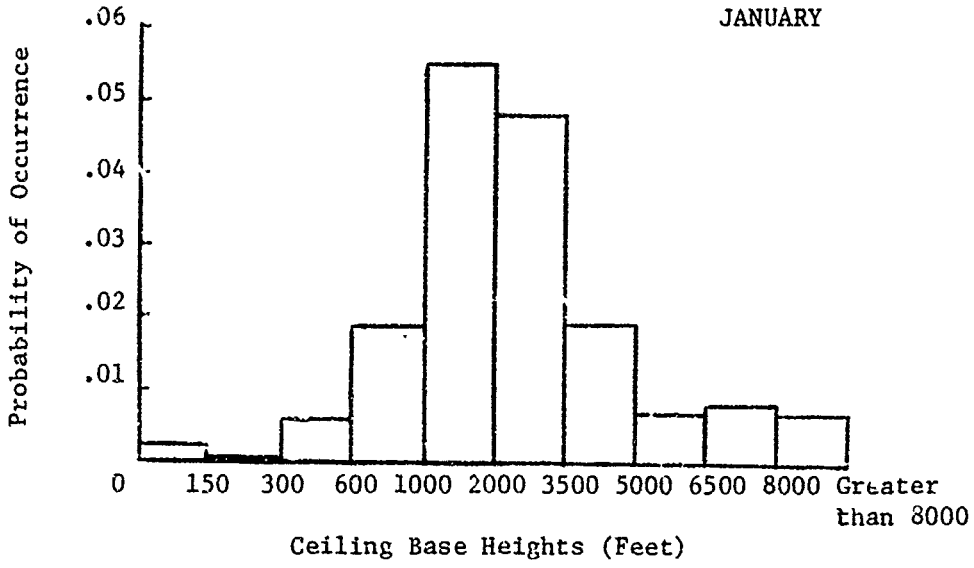

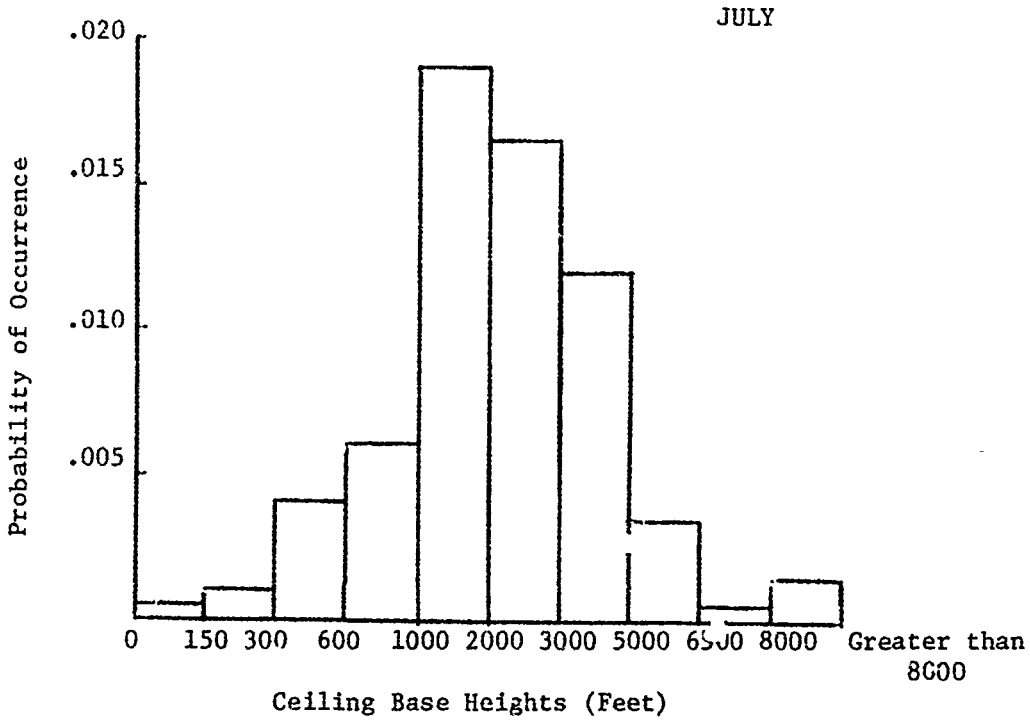

FIGURE 1

PROBABILITY DISTRIBUTION OF CEILING HEIGHTS
FOR N. ADRIATIC SEA
DURING NIGHT HOURS

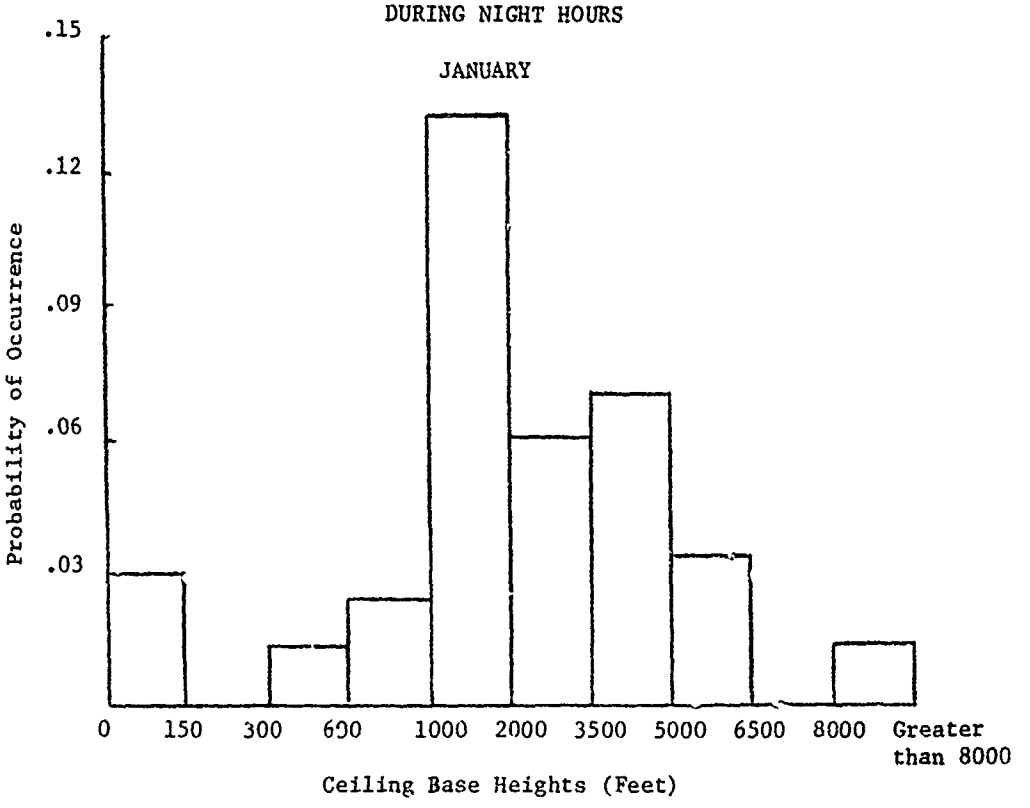

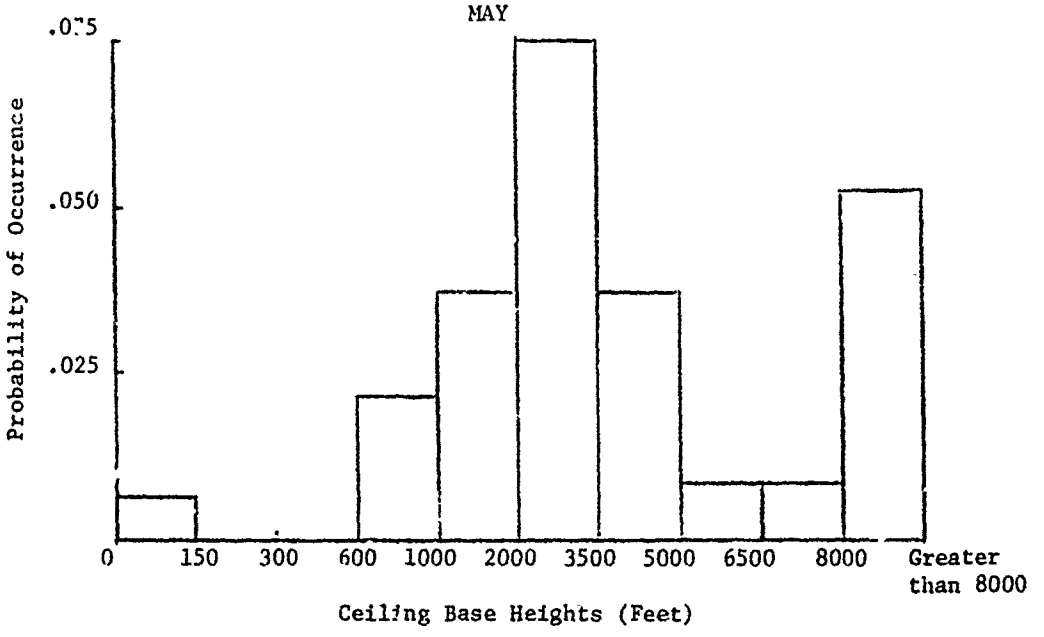

FIGURE 2

shows the frequency distribution of ceilings of the Northern Adriatic Sea for the months of January and May.

For the Northern Adriatic Sea in January, approximately 25 percent of the time ceiling occurred below 2,700 feet, which is the approximate ignition height of the LUU 2B/B. Approximately 12-15 percent of the time ceilings occur below 2,700 feet for Spain's coastal region. As can be observed from Figures 1 and 2, the summer months do not have as many ceilings existing as the winter months. To represent the variability of ceilings with months, the following table is given.

TABLE 1

% Time Ceilings Below 8,000 FT AGL
(Night Time)

Month	N. Adriatic Sea	Oran, Spain
January	38.0	17.0
February	32.4	16.3
March	30.5	14.5
April	27.7	14.9
May	24.7	11.3
June	23.8	8.3
July	11.4	6.4
August	3.3	5.5
September	8.1	9.4
October	17.1	11.6
November	27.0	13.7
December	34.8	14.9

TABLE 2

NUMBER OF NIGHTS PER MONTH AND PER YEAR
HAVING CEILINGS BETWEEN 1000' AND 2500'
WITH 3 MILES OR GREATER SURFACE VISIBILITY

Scandinavia & Northern Europe*

AREA	JAN	NOV	ANNUAL	% ANNUAL
Finland				
01	7.3	6.8	52	14
02	5	6	54	15
Sweden				
01	4.8	6	63	17
02	5.5	6	56	15
03	7	7.3	62	17
Norway				
01	7	7.3	76	20
02	4.8	5.7	63	17
03	-	-	-	-
Denmark				
01	8	9	78	21
02	6	7	51.7	14
03	7.7	7.6	58.1	16
Germany				
01	4.6	4	41	12
02	5	4	36	10
03	5.8	6	52	14
04	4.2	4.2	34	9
05	5.5	5	43.3	12
06	3	2	30	8
West Berlin	6	4	35	9

*0100 nour observation

Table 2 (cont)

Mediterranean

AREA	JAN	NOV	ANNUAL	% ANNUAL
France				
01	2.5	0	36	9
02	5	2.6	31	8
03	5	4	38	10
Italy				
04	4	3	36	10
06	3	2.4	20	5
Sicily	2.5	1.2	25	7
Yugoslavia				
01	2.4	2.5	19	5
02	5	6	41	11
03	3.9	4.8	34	9
04	1	1	7	2
Crete	4.6	4	27	7

Europe (Alps & S.W. Europe)

AREA	JAN	NOV	ANNUAL	% ANNUAL
France				
01	4.8	5.4	42	11
02	4	4.7	36.3	10
04	2	2	18	5
05	1.8	3	27	7
06	3	3	29	7
Switzerland				
01	2.4	3.7	34	9
Austria				
01	3	4	31	8
Spain				
01	6	6	69	19
02	3	2.6	24	7
03	2	1.3	16	4
04	2	1.3	17	5
UK	4	2.5	31.3	8

TABLE 3

CEILING BETWEEN 2500' and 6000'
AND VISIBILITIES > 3 MILES

AREA	JAN	NOV	ANNUAL	% ANNUAL
Finland				
01	2.1	2.6	22	6
02	1.6	1.5	24	6
Sweden				
01	2.8	3.5	37.7	10
02	2.8	2.2	33	9
03	2.5	2.5	23	6
Norway				
01	4.4	5	61	16
02	3	4	46	12
Denmark				
01	2.2	2.8	26.6	7
02	4.4	3.4	30.2	8
03	4.1	3.8	43.4	12
Germany				
01	2.3	4.8	41	11
02	3.7	4.4	49	13
03	3.7	4	45	12
04	2.5	2.8	35	9
05	3.1	3.4	45	12
06	1.9	2.2	33	9
		(ALPS)		
France				
01	3	4.0	44	12
02	3	4.0	44	12
04	4.4	9.7	76	21
05	1.8	1.4	36.6	10
06	4.4	2.4	24	7

It was found by reviewing much of the literature that the winter increase of frequency is characteristic of the entire Mediterranean marine areas. The spread of percentages for different marine areas is fairly well encompassed by the North Adriatic Sea and Oran, Spain, areas.

A well defined frequency distribution of ceiling heights could not be found for the inland areas of Europe. However, a limited amount of data was found and is presented in Tables 2 and 3. From inspection, one can see that the percent of time cloud cover exists is greater in Northern Europe and the Scandanavian countries than in Southwest Europe and the Alps. It should be noted that to obtain the percent of time that ceilings exist, one would have to sum the numbers of Tables 2 and 3 for the corresponding countries and areas. In reality, one could say that 20-25 percent of the time, difficulty in performing attack missions with flares will occur due to ceiling problems on an annual basis.

The following analysis was performed to examine the effect of ceilings, haze and wind speed on target acquisition. The trade-offs of ignition altitude, ceiling height and observer position were analyzed in terms of usable flare light and performance.

Let usable burning time be defined as that time for which the pilot would have a .9 or better probability of a target recognition, with approximate target size being equal to that of a truck. In addition, performance measure is defined as the probability of recognition. In this report, the target is taken as being a truck with dimensions 7 X 8 X 25 feet.

EFFECT OF DIFFERENT CLOUD AND IGNITION ALTITUDES ON FLARE PERFORMANCE

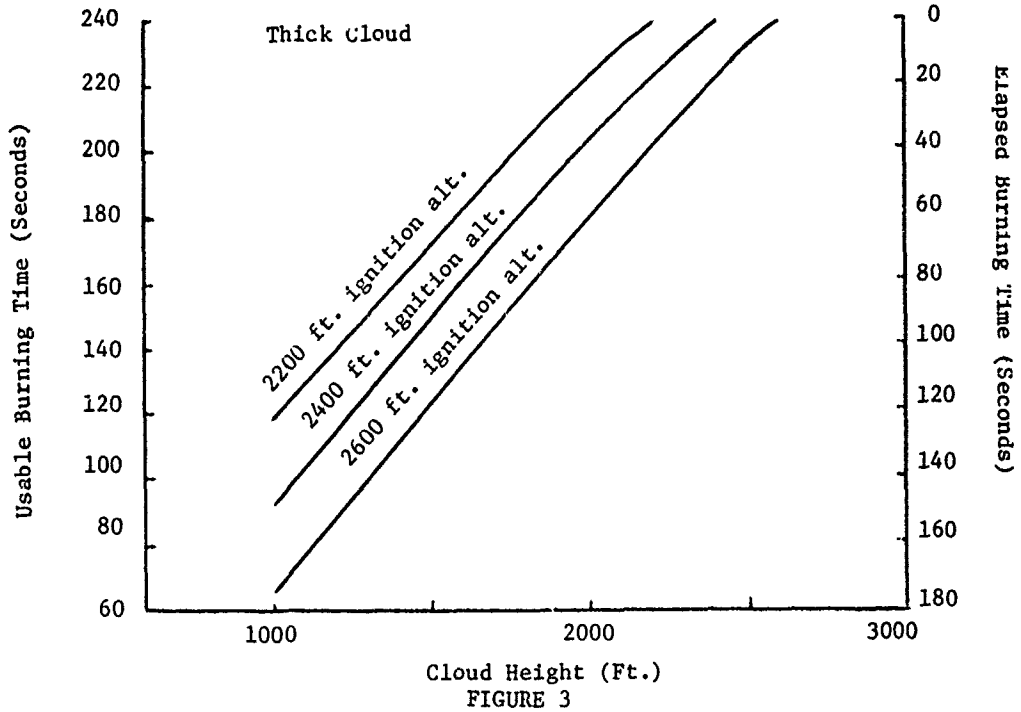

FIGURE 3

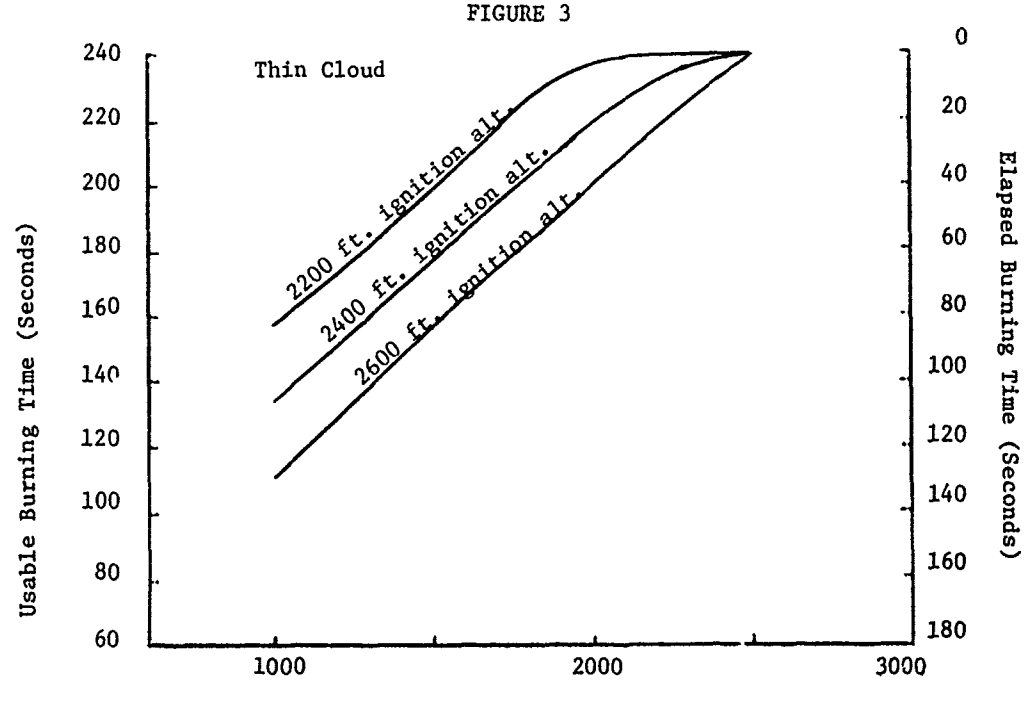

FIGURE 4

PROBABILITY DISTRIBUTION OF VISIBILITY
FOR N. ADRIATIC SEA
DURING NIGHT HOURS

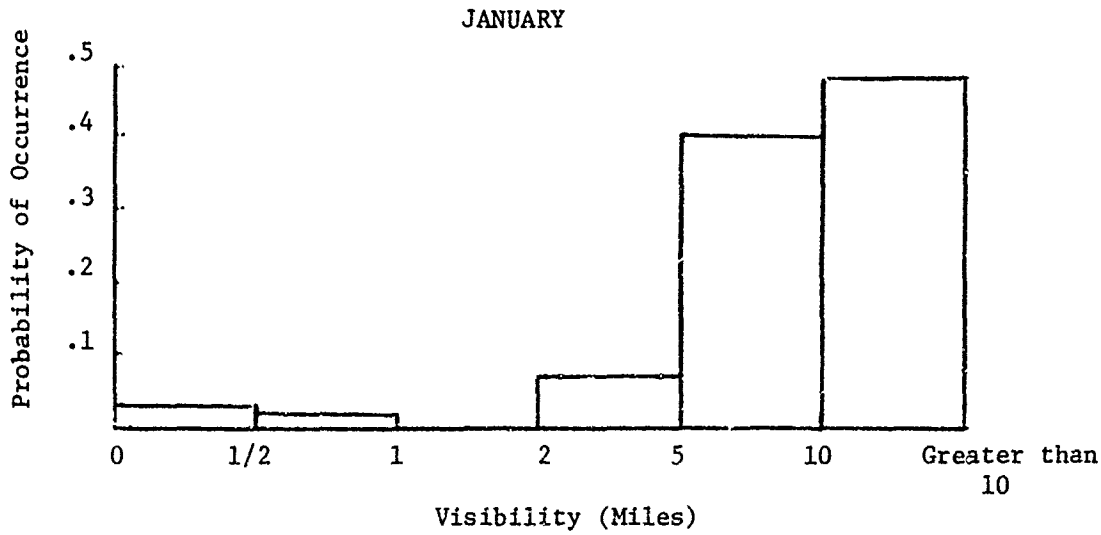

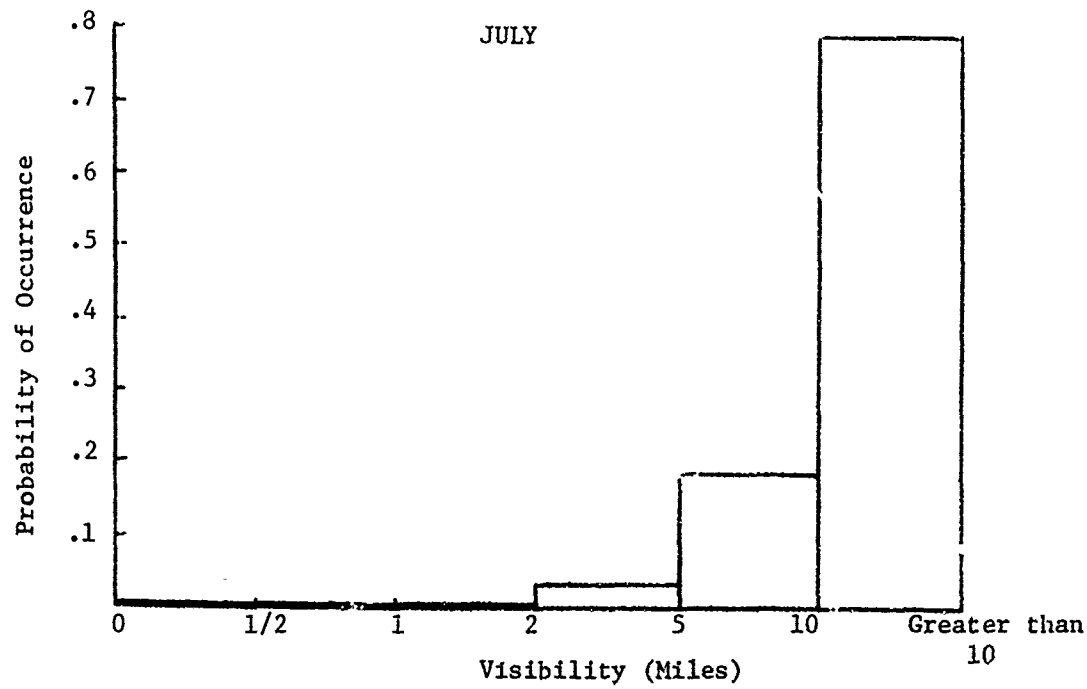

Figure 5

METEOROLOGICAL RANGE PROFILE FOR
DIFFERENT DAYS IN SOUTHERN GERMANY
FOR NON-OVERCAST DAYS

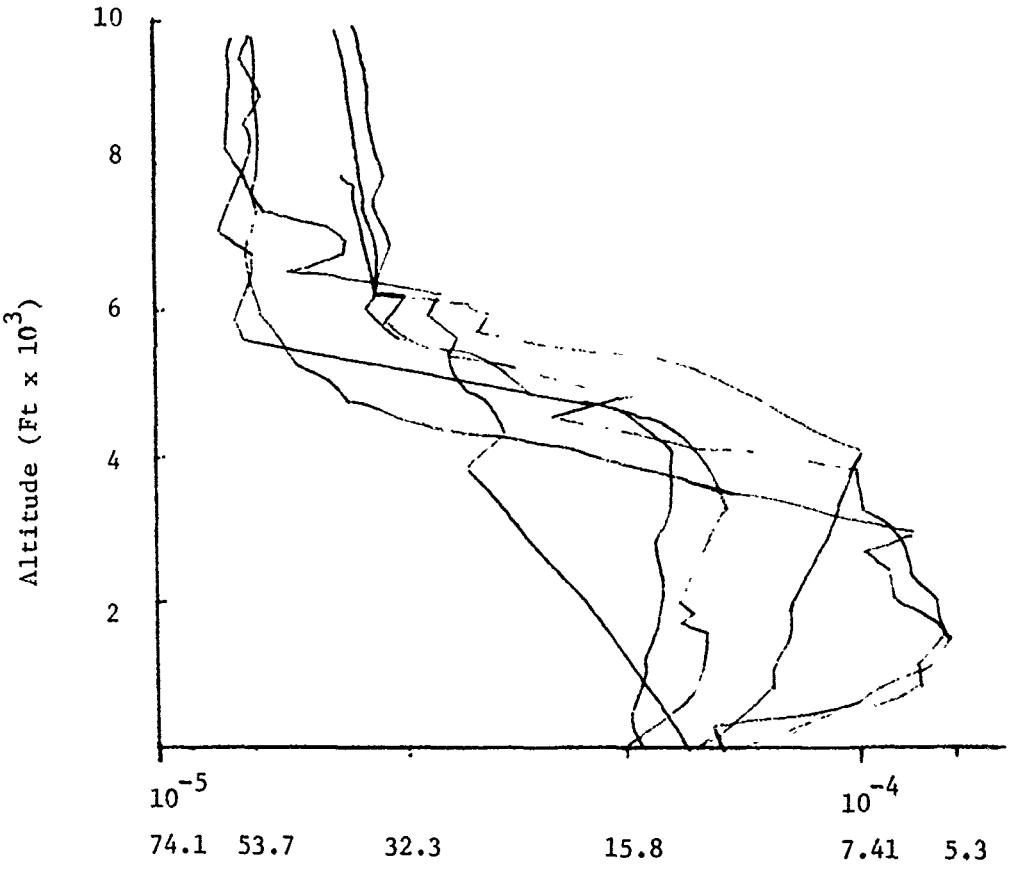

Figure 6

A summary on the effect of the above parameters is given in Figures 3 and 4. Figures 3 and 4 show the usable burning time out of 240 seconds for various cloud heights and ignition altitudes for a thick and thin cloud which correspond to meteorological ranges of 130 feet and 1,300 feet respectively. The pilot was located below the cloud layer. As can be seen for low clouds, as little as 25 percent of the flare burning time may be useful. The usable burning time can, however, be increased as much as 25 percent by igniting the flare at 2,200-foot altitude as shown in Figure 3. From Figures 3 and 4, one could probably apply a rule of thumb that for every 200-foot decrease in ignition altitude, a 20-second increase in usable burning time is gained.

Visibility

A frequency distribution on surface visibilities is presented in Figure 5 for the Northern Adriatic Sea. The probability of the visibility being less than 10 miles is given as approximately .5 for the Northern Adriatic Sea. After inspecting the data for the different marine areas, large visibility variation was not found.

Extinction profile data has been collected for the Air Force-Cambridge Research Laboratory (AFCRL) on Southern Germany. A representative sample is presented in Figure 6. Also shown is a visibility scale which represents the distance over which transmission is two percent. As can be observed, there exists a definite haze up to 3,200-4,900 foot altitude. This haze layer corresponds to a visibility of 5-16 miles. The existence of this haze is quite prevalent in that all of the data collection flights showed the haze layer. Most of the flights were made with non-overcast conditions occurring.

Effect of Aerosol Scattering In a Hazy Atmosphere

The aerosols in the atmosphere degrade the transmission of image forming rays by scattering and absorption. Radiation in the visible wavelength is attenuated almost entirely by scattering. When viewing an object through the atmosphere, the scattered light reduces the contrast. In the use of flares, the amount of direct illumination on the target is reduced and some of the flux which is attenuated is scattered into the sight path of the pilot, thus degrading his ability to see a target.

The scattering degradation is dependent on the distance of the flare from the sight path and the scattering angle. Figure 7 shows the effect of locating the pilot at different distances and scattering angles from the flare for pilot altitudes near that of the flare in a hazy atmosphere. As can be seen, there does not seem to exist much difference for this particular geometry. By locating the pilot at a higher altitude (Figure 8), position 1 shows a 15-20 second burning time difference from position 2 to obtain equal visual performance. This difference is due mainly to forward scattering lobe of the sight path, e.g., 2,600-5,000 foot pilot altitude. The conclusion is, neglecting target aspect angle, and secondary atmospheric scattering effects, that at most, 15-20 seconds burning time is the difference needed to obtain equivalent performances when the pilot is operating completely in the haze. If the haze is below the pilot, the burning time difference is going to be even less.

After investigating the scattering effect in a hazy atmosphere, an analysis was performed to investigate the effect of meteorological range in general. Therefore, a pilot

EFFECT OF AEROSOL SCATTERING ON VISIBILITY FOR DIFFERENT PILOT POSITIONS
METEOROLOGICAL RANGE = 14 MILES

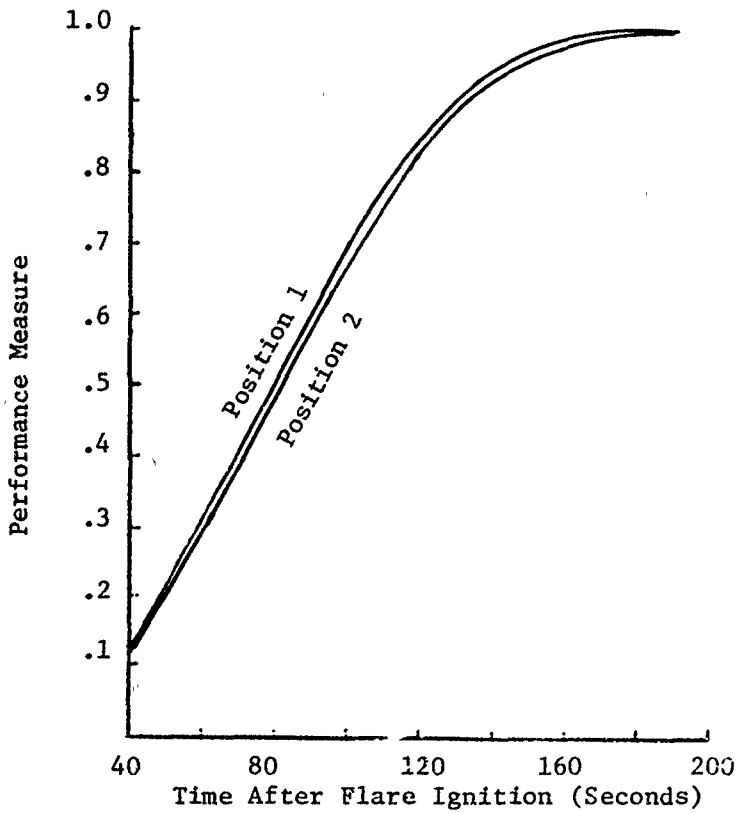

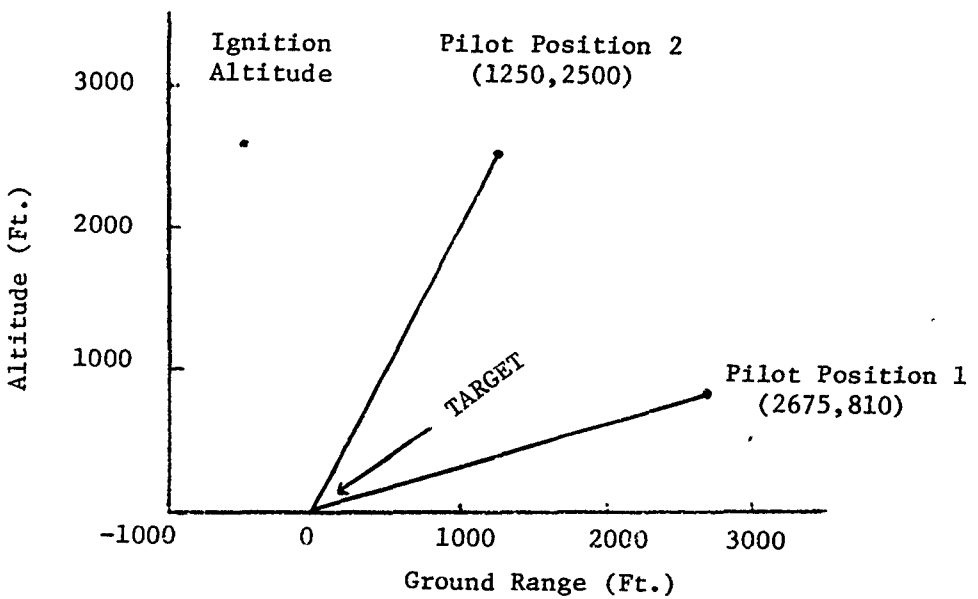

Figure 7

EFFECT OF AEROSOL SCATTERING ON VISIBILITY FOR DIFFERENT PILOT POSITIONS
METEOROLOGICAL RANGE = 1/4 MILES

NOTE: Position 2 assumes the haze continues up to an altitude of 5000 ft.

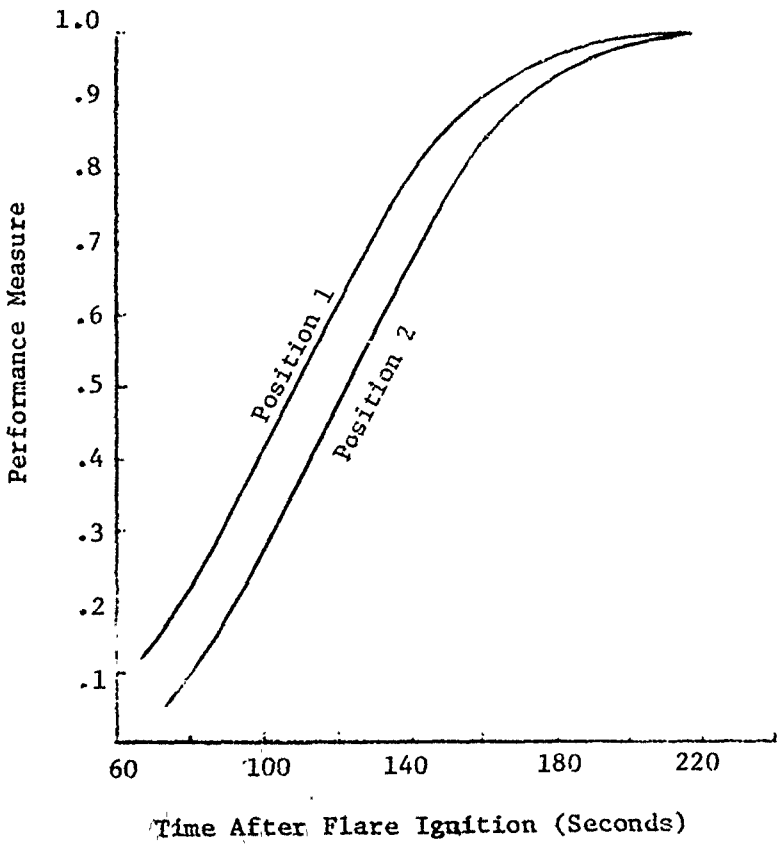

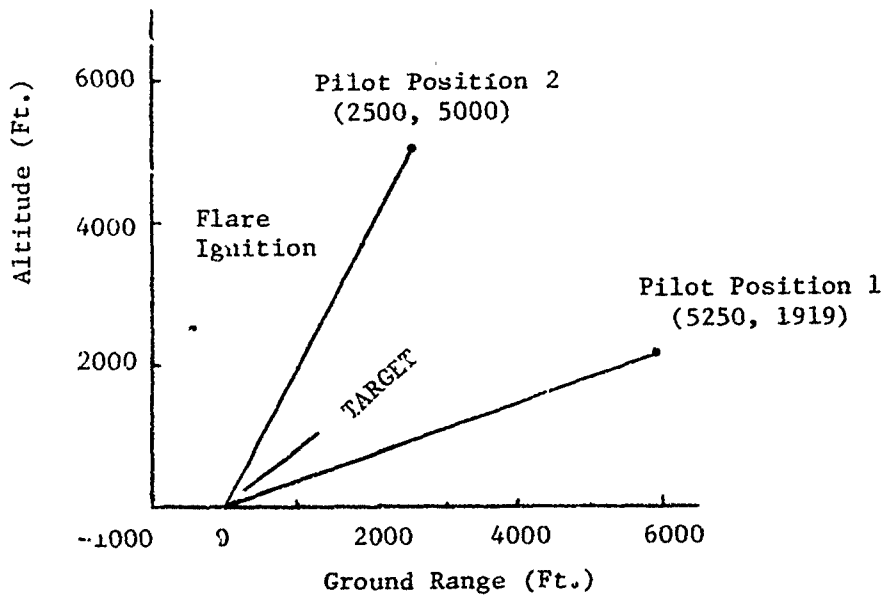

Figure 8

Table 4

COMPARISON OF DIFFERENT METEOROLOGICAL RANGES ON TARGET ACQUISITION

Meteorological Range (Mi)	Recognition Range for .9 Probability of Recognition (Ft)	% Target Acquisition Reduction Relative to 17 Mi. Meteorological Range
17	5400	0.0%
10	4400	18%
5	2900	46%

altitude of 2,000 feet was simulated and the pilot flew a simulated level path toward a vehicular target for different meteorological ranges. The differences in pilot-target ground ranges to obtain equal visual performances were recorded and are shown in Table 4. As can be seen from Table 4, the recognition range can be reduced as much as 46% for the five-mile meteorological range.

Wind Speed

Parachute flares in general will drift with a velocity equal to that of the wind. Another important aspect of flare placement on target acquisition is flare drift. Therefore, the deployment of flares over the target might not be the best location.

Figure 9 represents the wind speed frequency distributions of January and August for the marine area of Spain. Forty percent of the winds fall in the 10-33 knot range in the winter and 30 percent for the summer.

Inland mean wind speeds for cities of various European countries are shown in Table 5. The areas further north have greater wind velocities. For example: Bremen, Germany, has a wind velocity four knots greater than Heidelberg's wind speed. Heidelberg is located south of Bremen. Likewise, Denmark, which is in the northern part of Europe, has higher wind velocities than Germany, Switzerland and France.

Figure 10 shows the cumulative frequency distributions of flare drift for the coastal region of Spain in January. Upon inspection of Figure 10, one can readily see that a flare could drift completely off the target before it burned out. Thirty

WIND VELOCITY PROBABILITY DISTRIBUTION
FOR EASTERN COASTAL REGION OF SPAIN
DURING NIGHT HOURS

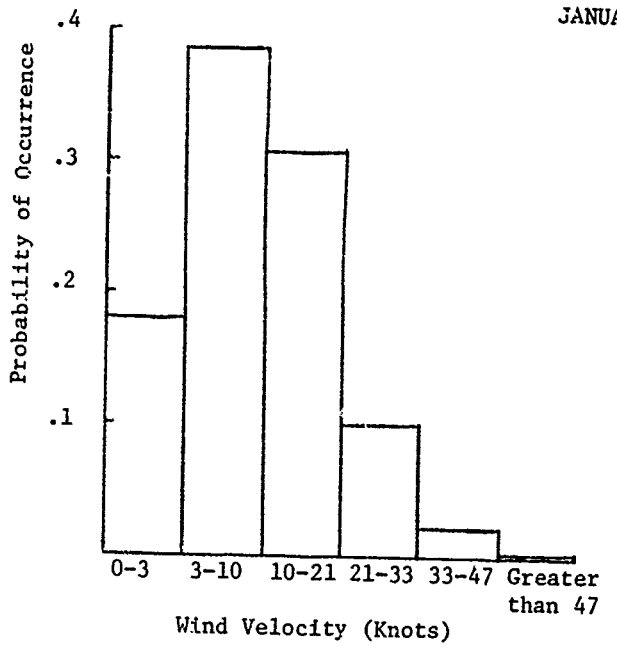

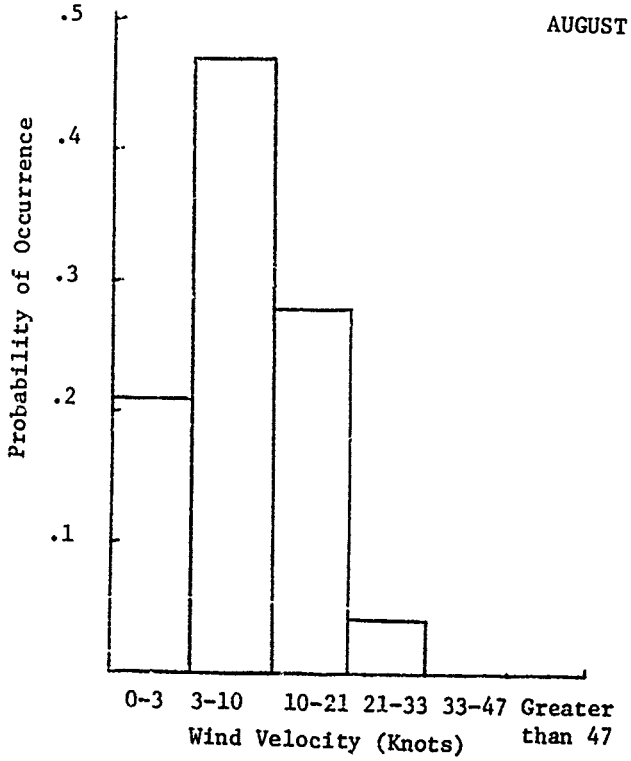

Figure 9

Table 5

SCALAR MEAN WIND SPEEDS (KNOTS)

Switzerland	
Geneva	5.1
Locarno	2.6
Santis	14.0
Zurich	4.2
Denmark	
Blavand	11.9
Fornaes	10.1
Karup	9.8
Skagen	11.5
Germany	
Berlin	7.3
Bremen	7.9
Heidelberg	4.1
France	
Chambley	4.2
Chateauroux	5.5
Orleans	5.7
Paris	7.0

CUMULATIVE FREQUENCY DISTRIBUTION OF TOTAL FLARE DRIFT
OVER 240 SECONDS BURNING TIME FOR LUU-2B/B
FOR COASTAL REGION OF SPAIN

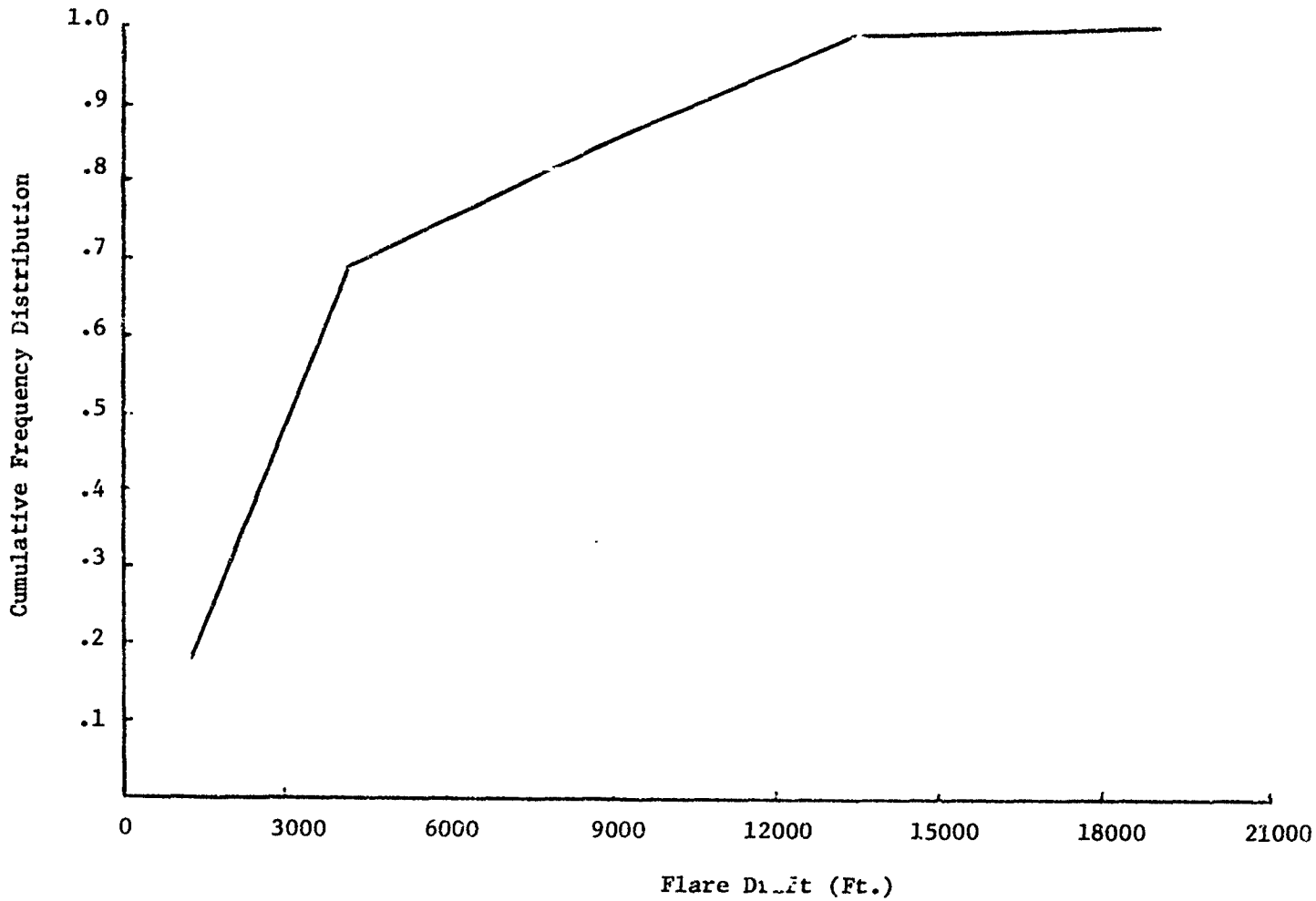

Figure 10

percent of the time, the flare will drift more than 4,000 feet, and 15 percent of the time, the flare will drift more than 9,000 feet. Wind drift, therefore, gives added emphasis to the timing and precision of flare placement in conjunction with acquiring target and possibly delivering ordnance on the target.

SUMMARY

An attempt has been made to define atmospheric environmental conditions for Europe as would be encountered during missions involving flare deployment.

After reviewing the findings, it was concluded that the users of flares should give careful consideration to the atmospheric parameters of ceiling height, visibilities and wind velocities in developing deployment tactics for flares. In addition, the flare designer should be made aware of the environmental parameters that may affect the performance of a flare. Therefore, it may be possible to design the burning time, parachute characteristics, and candlepower in such a manner as to maximize target acquisition capability.

REFERENCES

D. Deirmendjian, *Electromagnetic Scattering on Spherical Polydispersions*, American Elsevier, New York (1969).

S. Q. Duntley, R. W. Johnson, J. I. Gordon, *Airborne Measurements of Optical Atmospheric Properties in Southern Europe*, Scripps Institute of Oceanography (1972).

R. E. Huschke, *Tactical Airpower in NATO Contingencies -- Modeling Weather Constraints on Air Operations: Weather and Warplanes IV(U)*, R-1195-1-PR January, Rand, Santa Monica, California (1974).

W. E. Knowles Middleton, *Vision Through the Atmosphere*, University of Toronto Press, Toronto, Canada (1963).

R. G. Quayle, J. M. Meserve, H. L. Crutcher, *Probability of Penetrable Optical Path for High Intensity, High Contrast Optical Targets*, The National Weather Records Center.

U. S. Naval Weather Service Command, *Summary of Synoptic Meteorological Observations*, Vol. 2, U. S. Naval Weather Service (1970).

U. S. Naval Weather Service Command, *Summary of Synoptic Meteorological Observations*, Vol. 5, U. S. Naval Weather Service Command (1970).

THE EFFECT OF ANGULAR VELOCITY ON PYROTECHNIC PERFORMANCE

by

Walter J. Puchalski
Pyrotechnic Development Branch, Frankford Arsenal, Phila., Pa.

ABSTRACT

The influence of angular velocity on the light output, slag retention, and burning rate of pyrotechnic $Mg/Sr(NO_3)_2$ samples consolidaced into metal cavities is discussed. Stoichiometric as well as non-stoichiometric fuel/oxidizer mixtures were studied at rotational speeds up to 43,000 RPM and a parametric burning-rate equation is developed. In addition, semi-quantitative descriptions of the burning phenomenon and its effects are presented.

INTRODUCTION

Background

Studies to date on the effects of spin rate and cavity geometry on burn time and candlepower output (1,2) had the objective of correlating laboratory performance with field performance. When standard tracer and igniter compositions were used in tracer cavities, results of laboratory testing indicated a direct relationship between burning time and projectile spin rate for the lower spin rates and an asymptotic value of burning time for the higher spin rates. No correlations between burning rate and compositions were reported.

When dealing with a standard tracer mixture, not only is the investigator examining the fuel and oxidizer, but also any binder, burning rate modifier, and/or color agent(s) which were added to meet a specific requirement for a specific round. The many ingredients comprising these mixtures tend to mask the individual roles of the fuel and the oxidizer. With this experiment we have removed all components except the fuel and the oxidizer. This was done so as to examine only the roles of the fuel and oxidizer in a pyrotechnic reaction.

In addition to determining the roles of the fuel and oxidizer, it is also necessary to explain why certain phenomena occur. In past reports there was a tendency to report and not to explain. In this study we hope to present not only the data but at least a semi-quantitative explanation of the factors affecting pyrotechnic performance.

Scope of Work

In the present work, cavities containing binary (fuel/oxidizer) pyrotechnic mixtures were evaluated as to their output characteristics,

with the independent variables being the degree of stoichiometry and cavity spin rate, and the dependent variables being average linear burning rate, candlepower, and percent slag retained in the column after burning.

The average linear burning rate, as well as the intensity of light output, determines the effective range over which a tracer projectile functions -- a performance factor which is related to its fire control effectiveness. The retention of slag products in the tracer cavity undoubtedly contributes to the local burning processes of a pyrotechnic but just as important, however, is the effect of slag retention on the degree of fumer capability or, base drag reduction. As the burning tracer projectile loses mass due to the ejection of product gases and solids, the "dead air" region behind the moving bullet is filled with this ejected material. This ejection changes the flow pattern around the bullet, resulting in less degradation of striking energy at any one point during its flight. By knowing the percent slag, it will be possible to design the optimum fumer composition to reduce the base drag by concentrating on the ejected mass and heat of reaction of the burning pyrotechnic. Hence, a knowledge of how burning rate, light output level and slag retention are influenced by composition and spin will contribute to the design of better tracer ammunition.

EXPERIMENTATION

The experimental arrangement is presented schematically in Figure 1. The major components consist of a spinner (to both hold the capsuled sample and impart a certain rotation); a photocell (to detect light output and to convert it to measurable, electrical signals); and the oscilloscope (to collect and record the data). Peripheral equipment includes a photometer, the pyrotechnic ignition system, a stroboscope, and an oscilloscope recording camera.

The samples were held in an air-driven spinner (Figure 2) patterned after spinners described by Beams and Pickels (3). An exploded view is presented in Figure 3. The spinner is operated by passing air through the inlet port and the holes in the stator. Air jets from the stator provide an air cushion between the stator and the rotor, and strike the flutes along the conical portion of the rotor, causing rotor spin. Air jet velocity (and consequently rotor rotational speed) is controlled by regulating the upstream air pressure.

The photocell and oscilloscope were used to record output from the burning column. Light from the burning sample was picked up by the photocell and transferred to the oscilloscope for photographic recording. Most tests were conducted with the photocell positioned three feet from the spinner; however, this distance was increased for higher candlepower values. To determine the vertical scale on the CRT, a 500 Watt Mazda lamp was placed in the position of the spinner and a Weston Photometer was placed at the position of the photocell. The voltage to the lamp was controlled by a rheostat giving a variable intensity. With this arrangement, lamp output (in foot-candles) could be correlated with beam deflections in the vertical plane of the CRT.

Rotational speeds of the capsules were determined by placing an identifying mark on the rotor surface and noting with a stroboscope the fundamental speed at which the mark appeared stationary.

Ignition was accomplished by means of a spark from a Telsa coil. Each pyrotechnic sample, after being charged into its capsule, had added to it a milligram quantity of a BaO_2/Mg igniter mix and a spark-sensitive Zr/PbO_2 mix, respectively. Upon discharge of the Telsa coil (after the sample was placed in the spinner and brought up to the desired RPM) the Zr/PbO_2 mix was ignited, thereby igniting the sample.

The samples themselves were magnesium/strontium nitrate mixtures prepared by combining granulation 11 magnesium (MIL-M-382) with strontium nitrate (MIL-S-20322) after each was passed through a number 60 sieve. The three compositions prepared for this study were a stoichiometric blend based on the reaction:

$$5Mg + Sr(NO_3)_2 \rightarrow 5MgO + SrO + N_2$$

and blends containing 30 mole percent more and less magnesium from stoichiometric. These three mixes are presented in Table I. These mixes were then pressed with a flat punch at 70,000 psi into 0.375" diameter cavities to individually measured heights of approximately 0.600". A flat punch was used rather than the normal teated punch used in tracer manufacturing so as to provide a flat surface for column length measurements.

Rotational speeds used were 0, 20K, 28K, 35K, and 43K RPM. For angular velocities below 20K, the low pressure air flow resulted in a large variance in speed; therefore, 20K RPM was the lowest rotational speed studied. Also, 43K RPM was the maximum studied, because above this rate, the spinner became unstable.

Data measurements on the samples included total burning time, candlepower, slag percent retained in the cavity, and rotational speed. In order to establish representative candlepower values for the samples tested, the average values for the peaks and troughs were taken. The peaks themselves were not reported because it was believed that they, the peaks, were not representative of the flame phenomenon. For the stoichiometric and the fuel-rich mixtures burned at the higher rotational speeds, candlepower increased as the column burned. For these conditions the maximum candlepower value was the one reported.

The amount of slag retained or slag percent was determined by simply weighing the capsules before and after charging and then again after burning. Weights were obtained only to the nearest decigram because of the handling problems during both the charging and the burning operations.

DISCUSSION

Burning Rate as a Function of Composition and Angular Velocity

The data listed in Table II and plotted in Figure 4 indicate that the average linear burning rate of a $Mg/Sr(NO_3)_2$ binary mixture is directly proportional to the magnesium content of the mixture and also to the rotational speed of the mixture. The excess magnesium composition exhibits the highest burning rate at all rotational speeds and the deficient (from stoichiometric) magnesium composition has the lowest burning rate at all rotational speeds, with the stoichiometric mixture always between the two.

It is interesting to note that, for rotational speeds up to and including 43K RPM and variations of magnesium content of ± 30 mole percent from stoichiometric, the influence of spin on the burning rate can be represented by a simple linear relationship. Using a least squares analysis on each of the data sets the following three equations were obtained:

for the fuel-rich mixture:

$$r = 0.160 + 1.43 \times 10^{-6} \text{ (RPM)} \quad (1)$$

for the stoichiometric mixture:

$$r = 0.122 + 1.54 \times 10^{-6} \text{ (RPM)} \quad (2)$$

for the fuel-deficient mixture:

$$r = 0.059 + 1.84 \times 10^{-6} \text{ (RPM)} \quad (3)$$

where r is the average linear burning rate in inches/second.

Taking these three individual equations and applying the appropriate mathematical techniques, a general virial equation containing both magnesium content and spin rate coefficients results:

$$R = -0.148 + 0.729 \times 10^{-2}(M) - 2.75 \times 10^{-8}(M)(S) + 2.60 \times 10^{-6}(S) \quad (4)$$

where R = linear burning rate in inches/second
M = magnesium percentage
S = spin rate of sample in revolutions per minute.

This equation space is plotted versus the experimental data curves in Figure 5. The parametric equation agrees quite well with the observed data. For example, at the spin, magnesium percentage values of (0,28.8), 43K, 42.8), and (28K, 36.3),the parametric equation burning rates are 0.062, 0.225, and 0.161 in/sec, respectively. These rates compared to

the observed rates of 0.059, 0.227, and 0.160 in/sec, respectively, give corresponding percentage differences of 5.1, 0.6, and 0.9. It was, therefore, not deemed necessary to include a scaling factor to have the termini correspond with the actual data since this would produce larger percentage errors in the middle of the space.

The combustion of a pyrotechnic is the sum total of many exothermic and endothermic reaction processes with their accompanying physical processes of heat transfer. In discussing the data reported here, a rough division of the actual overall combustion process is made, separating the overall reaction into a condensed or solid-solid/liquid phase and a flame or gaseous phase. In the condensed phase, reactions are endothermic or weakly exothermic and are greatly affected by both outside forces (compaction pressures, cavity diameter, spin, etc.) and compositional effects (percent ingredients, thermodynamic properties of ingredients, etc.). In the gaseous phase, however, the reactions are highly exothermic and are less affected by outside forces. With this division, the overall reaction process can be effectively analyzed by regarding the condensed phase as the rate determining phase and the flame phase as a heat reservoir for the condensed phase.

In the stoichiometric, static condition, the reaction proceeds at some linear burning rate, r, not affected by the spin variables ($S = 0$) nor by any excess ingredient variables. This reaction condition produces a laminar burning effect or reaction profile similar to the one outlined in Figure a. Section A represents the unreacted portion of the pyrotechnic composition "unaffected" by outside parameters. Section B is the "pre-heated" portion of the curve in which the heat transfer process is noticeable and results in a raising of the composition temperature. Section C is the reaction zone in the condensed

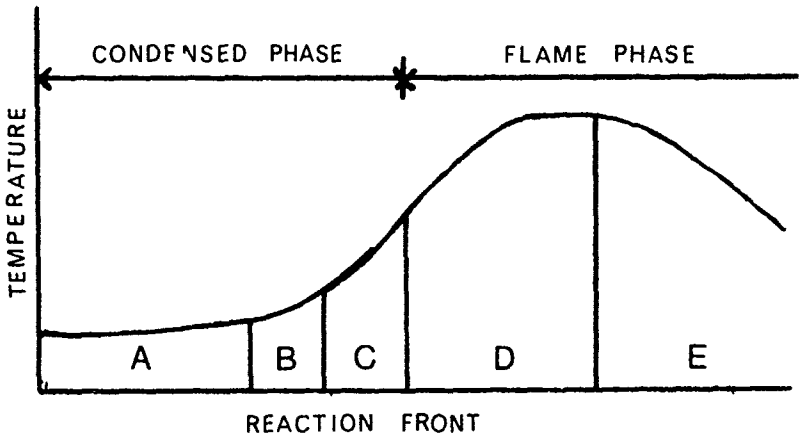

Figure a. Reaction Profile of a Burning Pyrotechnic

phase. This portion represents the melting and thermal decomposition of the oxidizer and the high absorption of heat from the flame phase. Species exist primarily as liquid and not solid in this region and are relatively mobile compared to sections A and B. These three sections together comprise the condensed phase and can be characterized as being generally endothermic and rate-controlling.

The final portion of the reaction profile is the flame phase (D, E). In this phase the temperatures are the highest (D) with all reactions primarily being gaseous. In this last stage of combustion, atmospheric oxygen and nitrogen participate in the oxidation. With this addition, the total caloric level of this already exothermic region is enhanced. Subsequently, these flame phase species combine to form stable oxides and these produce the lowered temperature region (E) with final reaction products.

In the fuel-deficient, static condition (as in all other conditions), there is oxidizer which must decompose first to react with the metal to propagate the reaction. With excess oxidizer, however, the pre-heated zone (B) is greatly reduced in temperature due to an abundance of the $Sr(NO_3)_2$ endothermic agent, and the reaction zone (C) has a lower temperature. This is due to a shifting of "priorities" from the heating of the Mg to facilitate reaction kinetics to the absorption of that heat by the $Sr(NO_3)_2$ (C_p = 38.3 cal/deg-mole) for the decomposition of the excess nitrate which proceeds at a much slower rate and at a higher thermal cost than the magnesium heating process, thus reducing the overall reaction rate. This can be seen from the fact that by reducing the magnesium content 30 mole percent from stoichiometric the reaction rate is lowered 50% from 0.120 in/sec to 0.059 in/sec.

In the excess-fuel, static condition, the larger percentage of magnesium acts as an excellent heat conductor. With the moderately high thermal conductivity of magnesium (0.38 cal/cm^2/°C/(cm/sec) versus 0.18 for iron) the pre-heated zone (B) is extended at a higher temperature further into the unburnt column and the composition as a whole absorbs a greater total quantity of thermal energy. This results in a lesser amount of additional heat needed to raise the temperature of the pre-heated and combustion zones (B-C) for more rapid decomposition of the nitrate.

The imposition of spin to a binary pyrotechnic column introduces a new parameter in the burning process of the mix. As is noticed in the data, burning rates increase linearly for each of the mixes up to 43K RPM. Also, spin has a greater effect on the mixes with lesser percentages of magnesium. This latter fact can be gleaned from the percentage increases in burning rates for each of the mixtures listed in Table II and from the individual slopes of the burning rate Equations 1-3.

Spin has different net quantitative effects on each of the three mixes but qualitatively the effect is the same for each sample type.

The differences in spin effects come from the compositional properties of the mixes themselves and their non-spin burn characteristics. In all cases, the spin effect is most pronounced in the reaction zone of the condensed phase. In this zone, the particle mobility is highest and therefore most susceptible to the radial effects of spin.

Consider the burning pyrotechnic column. A layer of molten reactants exists at the top of the column (zone C). This layer is only several mils thick, consisting of decomposing $Sr(NO_3)_2$ and high temperature (~450-500°C) solid magnesium. With the decomposition of the nitrate, the average molecular weight of this region is considerably lower than the rest of the column. This creates the low density region at the surface of the column to which the addition of spin produces the following:

1. The unburnt portion of the column (A + B) is basically unaffected although the temperature gradient is changed.

2. The flame zone (D - E) is moderately affected but less than the condensed phase reaction zone. It is noticed that, at the higher spin rates, the plume volume is decreased and the flame is closer to the reaction surface.

3. The condensed phase reaction zone particles (C) travel spirally outward, density gradients are formed at and near the surface, heat transfer processes increase in a radial direction, and the burning surface becomes convex in shape.

For the following discussion, the unburnt portion of the column and the flame phase will not be considered, but only the condensed phase reaction zone.

The hot viscous particles at the burning surface are accelerated outward in a spiral-type path. This results in each particle remaining at the surface longer thus increasing the amount of heat it receives from the flame phase (thus increasing its temperature) and also increasing the probability of reaction through both a longer mean path of travel on the reaction surface and a longer time span in which it is in close proximity with other reactants.

While these particles are spinning outward, the tangential component is also forcing these particles to a greater density as the radius increases. And since this layer is molten, the particles on the outward edges of the spinning capsule are closer together increasing their effective collision frequencies and thus their reaction probability. This phenomenon occurs, of course, in a gradient-like fashion and increases reaction rates outward resulting in an overall increase in the linear burning rate of the column.

A third effect of spin is the increase in the conductive heat transfer process. This increase is due to the density gradient at and

near the surface of the column and the fact that the flame is closer to the surface. With the closer flame zone, the heat flux to the column increases. The density gradient then more effectively dissipates this heat to the column because of the nearness of the molecules at the higher densities. These two conditions combine to preheat the unreacted portion of the sample. As the temperature of the sample is increased less heat from the flame zone is required for the reactions in the condensed phase. This factor is quantitatively described by the Arhenius Factor, $e^{-E_a/RT}$. As the temperature increases the negative exponent also increases thus increasing reaction rate.

The final result of spin considered is the change from a "cigarette-type" burning under static conditions to a convex-type while spinning. The convex burning surface is caused by the tangential forces directing the major reaction components towards the circumferential portions of the spinning capsule. Because these effects are increasing with radial distance, the burning rate quite naturally will also increase with radial distance. This produces the convex burning surface sketched in Figure b:

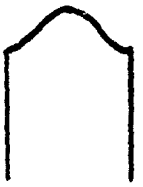

Figure b. Cross-Sectional View of Burning Pyrotechnic (Spinning)

Recent unpublished studies at Frankford Arsenal on the M13 artillery tracer capsule have shown that at 43,000 RPM the burning tracer ejects a pyramided section of unburnt tracer mixture toward the end-of-burn. This section had a base diameter approximately equal to the diameter of the cup with an uncharred portion of mix at the underside base of the mix at the axis. From this test it appears that the above postulations are correct to one degree or another.

Projecting the above hypothesis to other systems, it would be predicted that for identical mixes at identical rotational speeds, a capsule with a larger internal diameter would have a higher burning rate than those with smaller diameters, since the tangential forces would increase as one proceeds radially from the center. Figures 6 and 7 (2) are presented to support this theory. It is noticed that in all cases the greater the diameter of the capsule the greater the burning rate (shorter burning time). The difference in the shapes of the curves is probably due to compositional effects of the multicomponent mixtures

Candlepower as a Function of Composition and Angular Velocity

The light outputs of the pyrotechnic samples are presented in Table III and Figure 8. From these, the general relationships between

magnesium content, spin and candlepower can be seen. As magnesium content is increased the flame intensity also increases. As spin is introduced the greater the magnesium content the greater the increase in illuminosity. Figure 8 shows this general trend.

For the deficient magnesium sample, spin has little effect on light output. This is probably due to the lack of sufficient thermal energy to raise the magnesium to a level of high emission. Most of the heat of reaction is absorbed by the excess $Sr(NO_3)_2$ for decomposition. This produces magnesium particles to be ejected at a much lower temperature and therefore a lower luminous flux.

The stoichiometric mixture has the highest adiabatic flame temperature. This results in the highest intrinsic thermal radiation of the three mixes studied. As the temperature is raised the amount of energy emitted by the flame is increased by a power of four. (Stefan-Boltzman Law). Although the flame is not a black body, one can see that even a first approximation would give copious quantities of light.

At approximately 500°C, luminescence begins to appear due to the atoms and ions in the flame being excited to higher energy levels and then emitting as they return to the ground state. Since pyrotechnic flames are at least five times hotter than this minimum temperature requirement, luminescence can be considered an integral part of flame phenomenon. Therefore, with the addition of luminescence to the already greatly increased thermal radiation of the hotter stoichiometric flame, this mixtures will emit more strongly than the fuel deficient mixture.

The fuel-rich mixture has the highest <u>total</u> light output. Its flame temperature is lower than the stoichiometric mix; but, with the excess magnesium reacting with atmospheric oxygen on the outer edges of the flame the overall light output is greater than either of the two other mixes. Also, since there are these additional reactions occurring at the edges of the flame, the plume of the fuel-rich mixture is larger than the others. This factor causes an increase in total flame volume which in turn increases the total light output.

Figures 9 and 10 present candlepower versus burning time for the three type mixes in a static and spin condition, respectively.

In the first figure, erratic burning conditions are more pronounced as magnesium content increases. This erratic burning is related to the increased burning rate and the greater thermal diffusivity of higher magnesium content mixes. As the magnesium content increases the decomposition of the nitrate in the condensed phase increases which in turn causes greater conglomerates of fuel and oxidizer to be ejected. With these ejected fragments, a portion of the heat from the reaction is lost which causes a reduction in the

heat flux to the pre-heated zones and therefore a reduction in the overall reaction and light output. As more mixture is decomposed on the surface and heat is again being released in large quantities, the reaction increases to the point where another "large chunk" of mix is ejected. This pulsating-type reaction is less noticeable at lower percentages of magnesium because there is less preheating at the lower percentages.

The second figure (Figure 10) demonstrates the effect of spin on light output. At 43,000 RPM, the burning rate is accelerated and as the magnesium content increases both the total light output and the increase in light output increases (Figure 9). This amplification in luminosity is probably due to the same basic reactions occurring in a shorter period of time. This produces the same amount of light energy in less time resulting in an increase in luminosity; also, as the sample spins, greater surface area is created due to the convex burning surface. This could contribute significantly to the differences in light output since the faster the spin, the faster the reaction and the greater the convex surface. As the surface of an emitter increases, the greater is the magnitude of the luminous flux.

Slag as a Function of Composition and Angular Velocity

The slag percentages of the mixes studied appeared to be inversely related to magnesium content at static burn but have no direct relationships to either magnesium content or spin rate at high (> 30K) RPM (Table II, Figure 11). An explanation of this phenomenon might be gleaned from Figures 9 and 10.

As the magnesium content increases at static burn, the light output becomes more irregular due to the expulsion of larger conglomerates of unburnt mix (Figure 9). And since more mix is being expelled there is a lower percent slag retained as the magnesium content increases. (The fuel-deficient mixture has a slag percent of 69.5% while the excess fuel has 49.1%). As the sample is spun (Figure 10) the particles are held in the capsule for a longer period of time during reaction and less variation in light output occurs along with less large particles being ejected. The three mixes tend toward a mean value, because at these spin rates and compositions there is not enough force from the reactions themselves to force their proportionate residues from the capsule. For this reason all three samples will have approximately the same percentage of high density reacted material along the inside edge of the capsule wall.

CONCLUSIONS

1. The burning rate of a $Mg/Sr(NO_3)_2$ system consolidated into a 0.375" ID cylindrical cavity be given by the equation:

$$R = -0.148 + 0.729 \times 10^{-2}(M) - 2.75 \times 10^{-8}(M)(S) + 2.60 \times 10^{-6}(S)$$

where R = burning rate in inches/sec.
M = magnesium percentage between 28.2 and 42.8
S = spin rate of sample in RPM up to 43,000

2. The linear burning rate of a pyrotechnic increases as the tangential moment of the sample increases. The greater the spin rate of the sample or the greater the cavity diameter at the same spin rate, the faster the burning rate.

3. Luminoisity increases with increasing magnesium content and increasing spin rate of the sample.

4. Slag percent is unaffected at high (> 30K RPM) spin rates and is not directly related to the magnesium content of the mixture at these higher rates.

5. The burning surface of a spun pyrotechnic becomes convex rather than the anticipated concave surface.

TABLE I. COMPOSITION OF BINARY FUEL/OXIDIZER MIXTURES

Mixture Description	Wt % Mg	Wt % $Sr(NO_3)_2$
Stoichiometric	36.3	63.7
Fuel Deficient (-30 mole %)	28.8	71.2
Fuel Rich (-30 mole %)	42.8	57.2

TABLE II. BURNING RATE AND SLAG RETENTION DATA

A. Burning Rate and Percent Change

Spin Rate	Deficient Mg	% Change*	Stoichiometric	% Change*	Excess Mg	% Change*
0 RPM	0.059 in/sec	---	0.120 in/sec	---	0.160 in/sec	---
20K	0.094	59.3	0.159	32.5	0.195	21.8
28K	0.117	101.8	0.160	33.3	0.195	21.8
35K	0.118	103.5	0.179	49.1	0.208	30.0
43K	0.139	135.6	0.186	54.9	0.227	41.9

B. Slag Percent and Percent Change

Spin Rate	Deficient Mg	% Change*	Stoichiometric	% Change*	Excess Mg	% Change*
0 RPM	69.5%	---	53.3%	---	49.1%	---
20K	65.6	-5.6	63.0	8.1	57.4	16.9
28K	72.4	4.2	64.5	10.6	62.2	26.6
35K	66.7	-4.1	60.7	4.2	63.7	29.6
43K	70.0	0.1	66.7	13.1	62.5	27.2

* from static condition

TABLE III CANDLEPOWER VERSUS ANGULAR VELOCITY FOR SAMPLE MIXES

Spin Rate	Deficient Mg Maximum Candlepower	Stoichiometric Maximum Candlepower	Excess Mg Maximum Candlepower
0 RPM	180	1400	5100
20K	700	4600	4800
28K	1350	3200	6200
35K	1250	3750	5750
43K	950	4550	9050

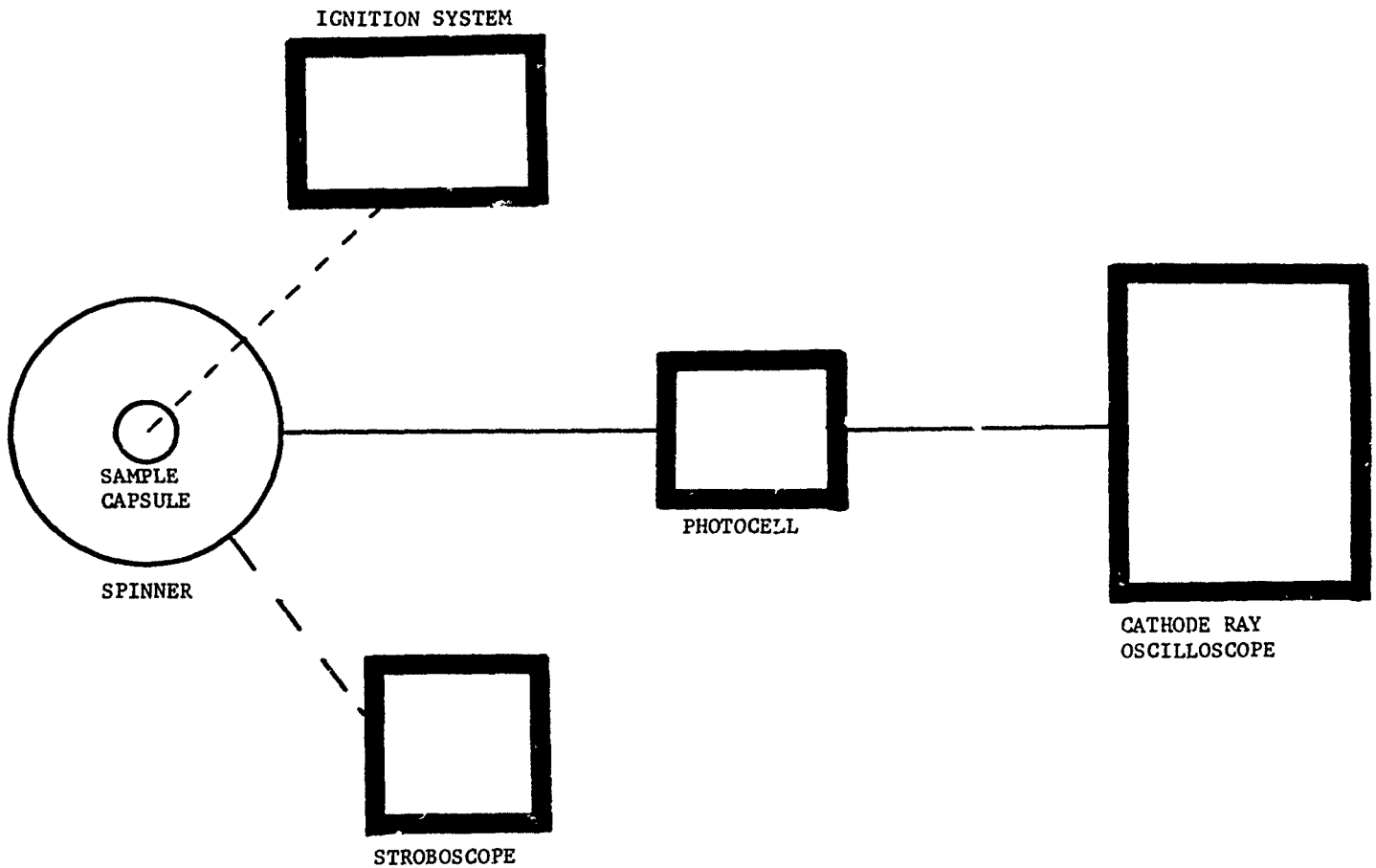

FIGURE 1 PYROTECHNIC PERFORMANCE TEST APPARATUS

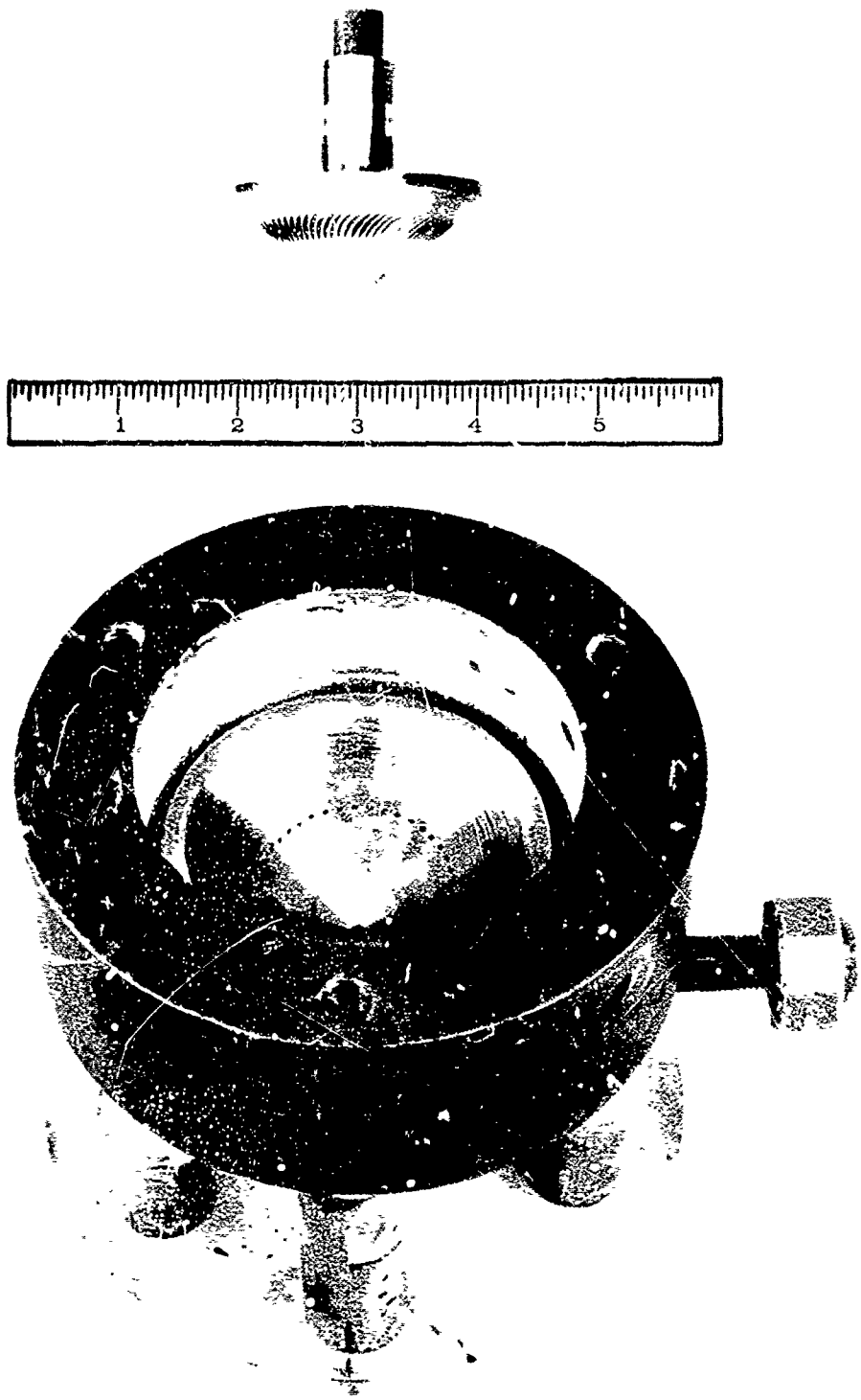

Figure 2. Bullet Spinner

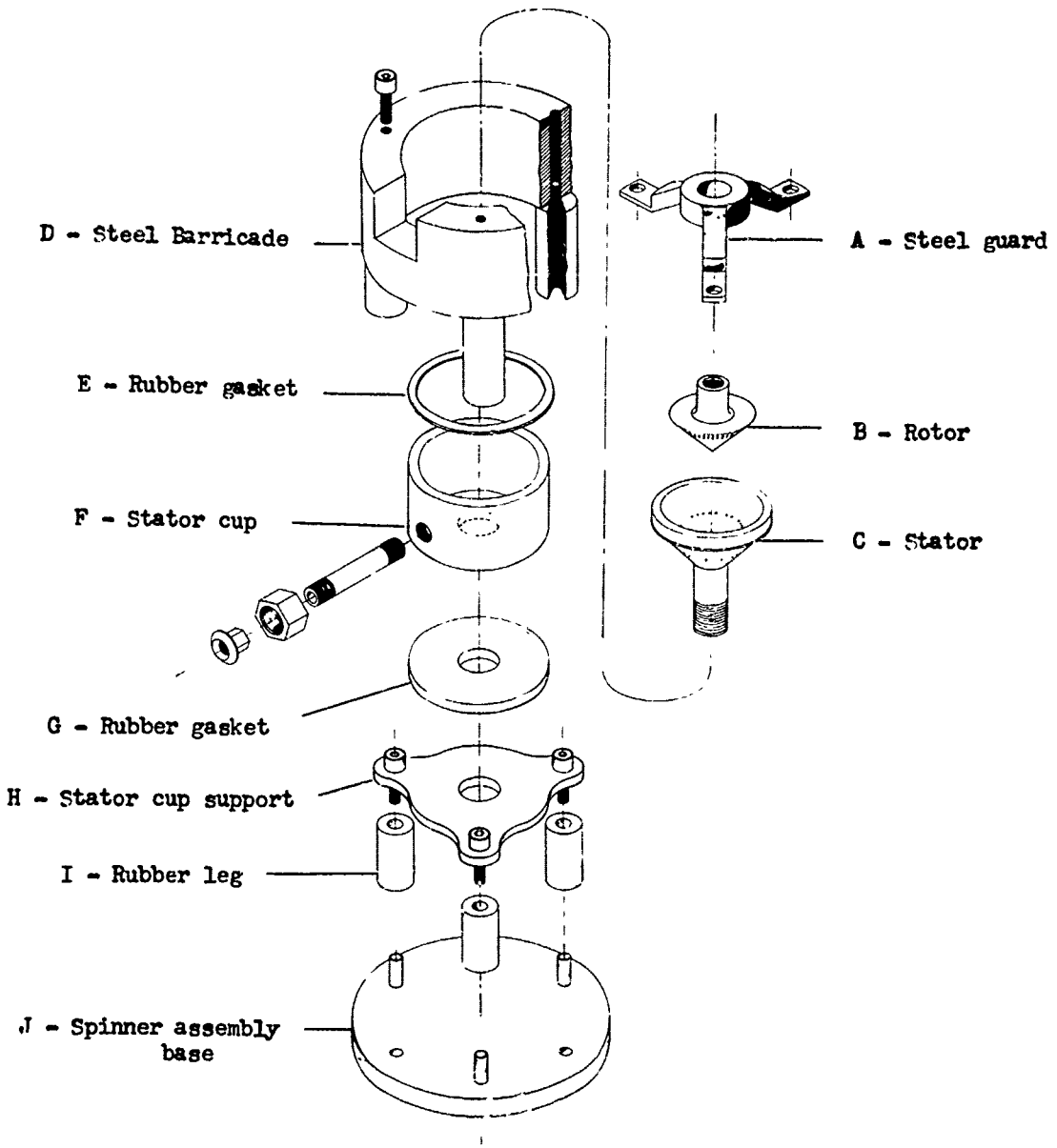

Figure 3. Exploded view of bullet spinner assembly

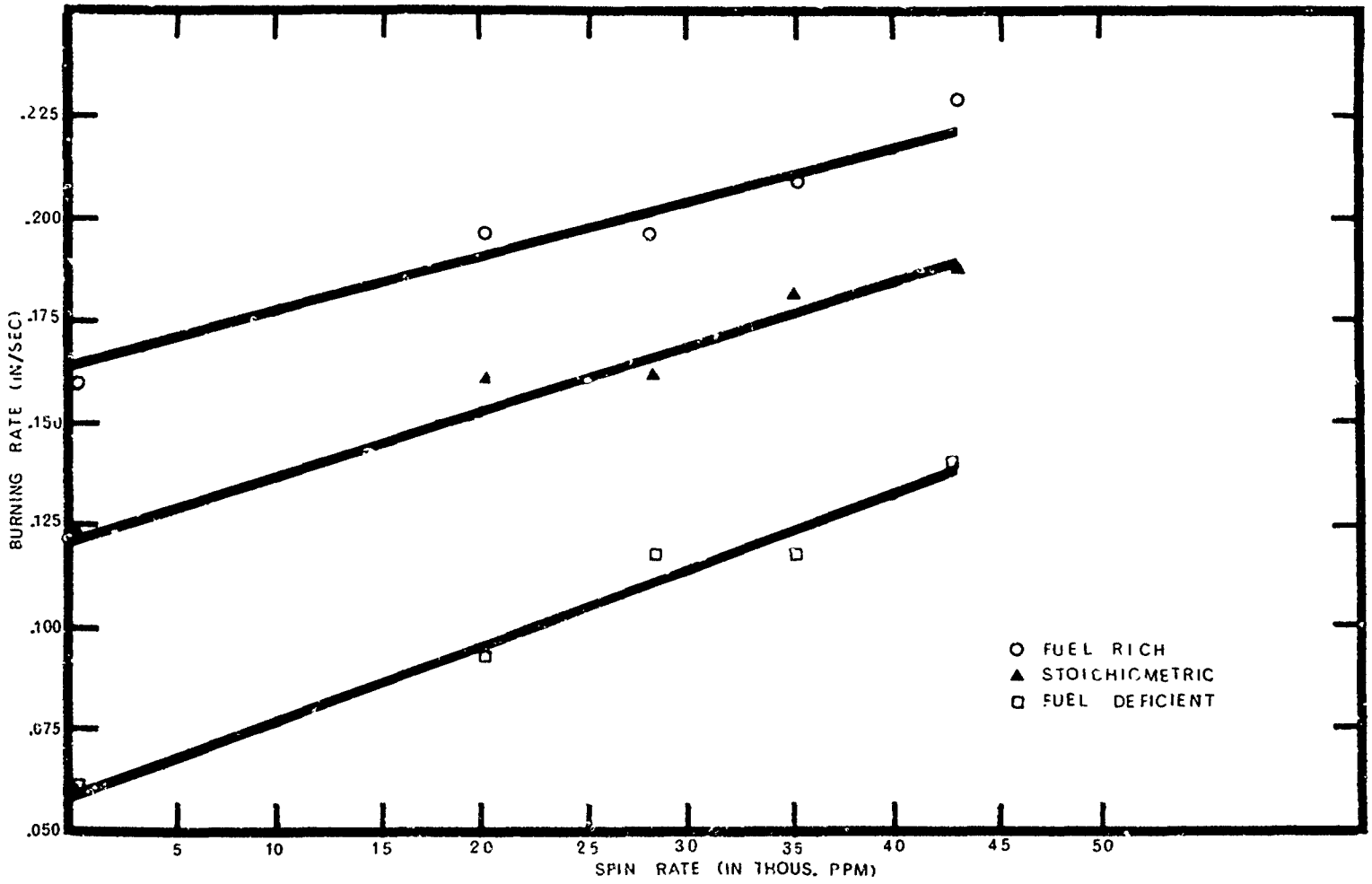

BURNING RATE VS SPIN RATE FOR THREE $Mg\text{-}Sr(NO_3)_2$ MIXES

Figure 4

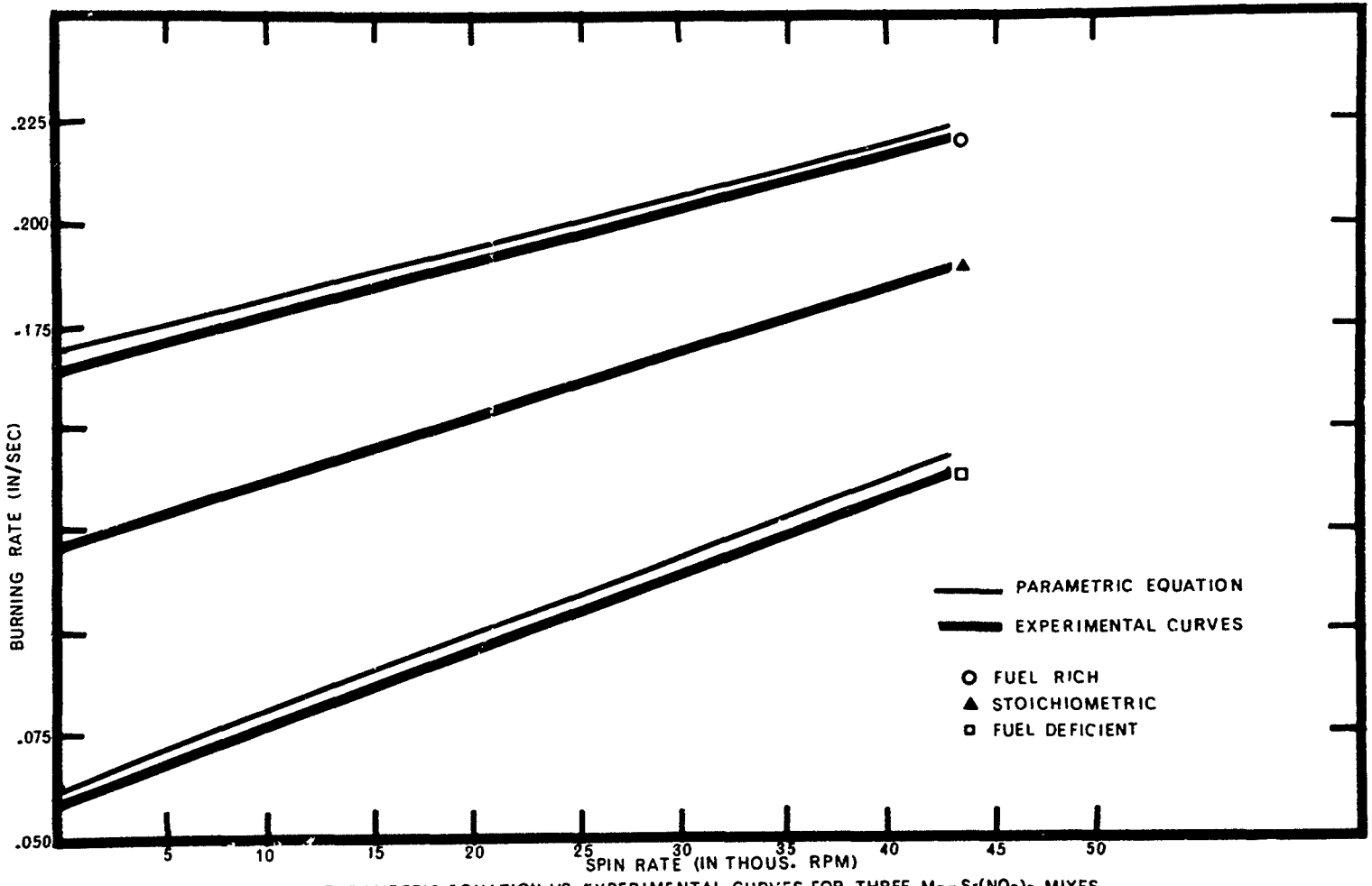

PARAMETRIC EQUATION VS EXPERIMENTAL CURVES FOR THREE $Mg-Sr(NO_3)_2$ MIXES

Figure 5

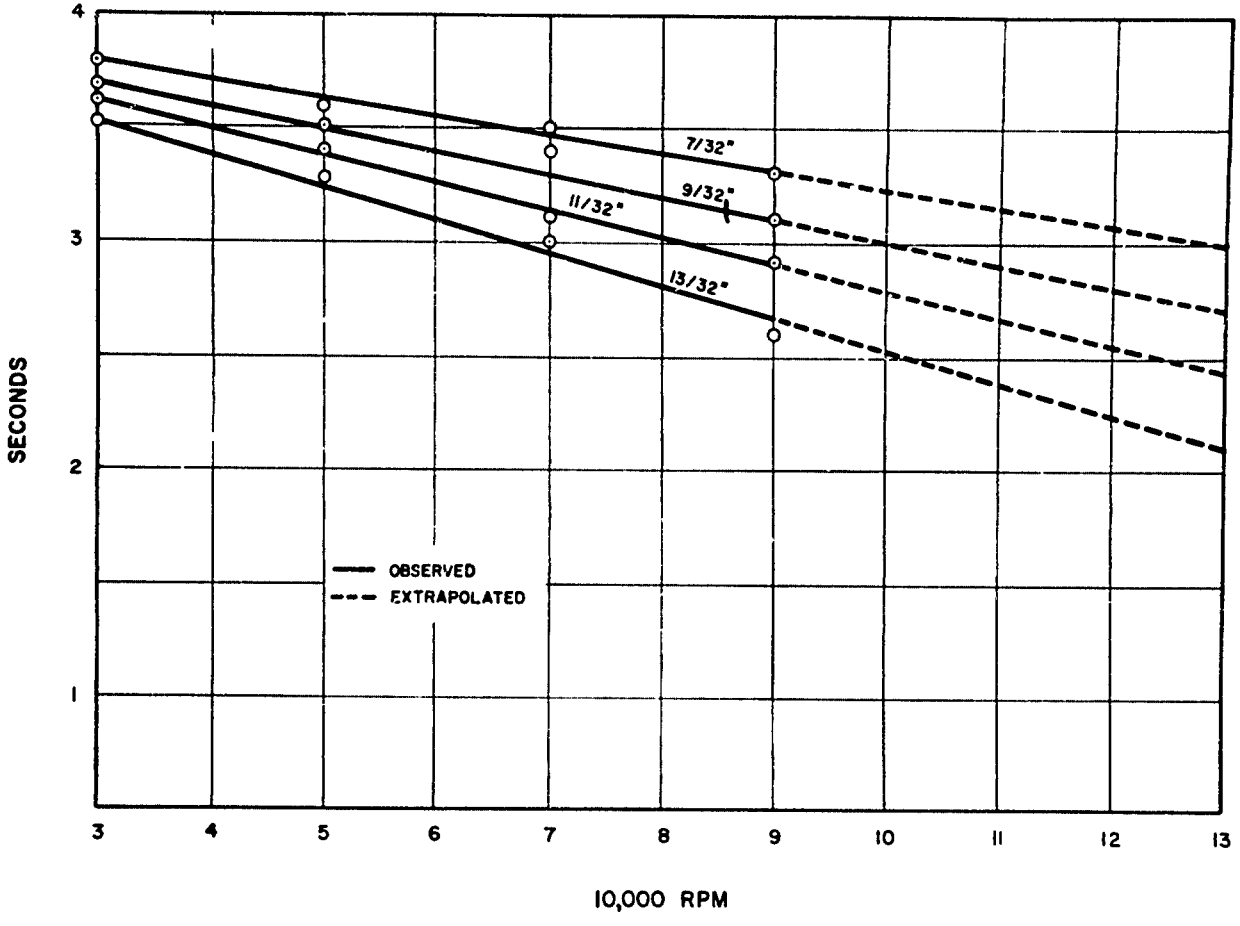

Effect of spin upon trace duration of tracer composition R-256 charged in various diameters in a 9/16 inch column

Figure 6

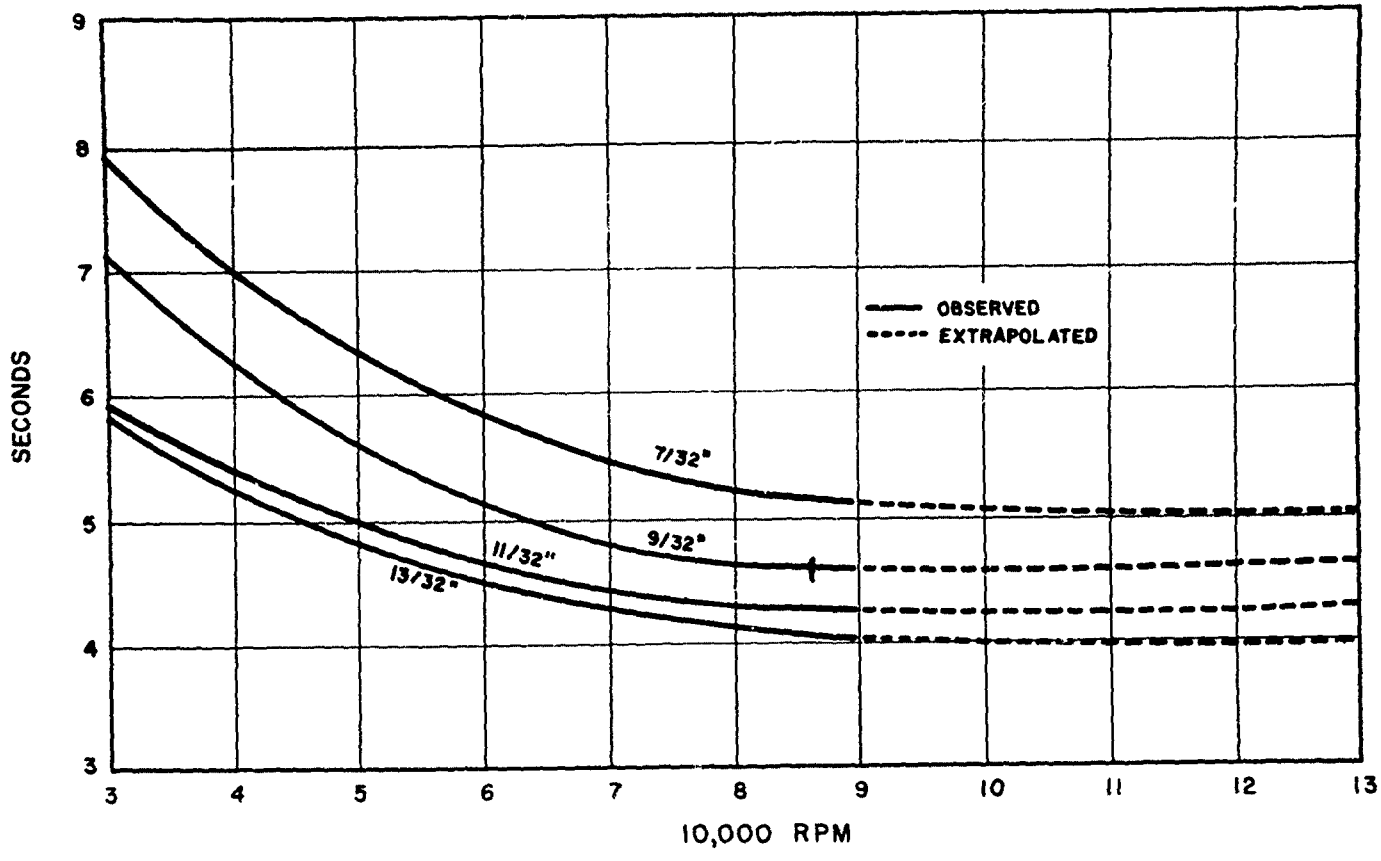

Effect of spin upon trace duration of tracer composition R-257 charged a 9/16 inch column of various diameters

Figure 7

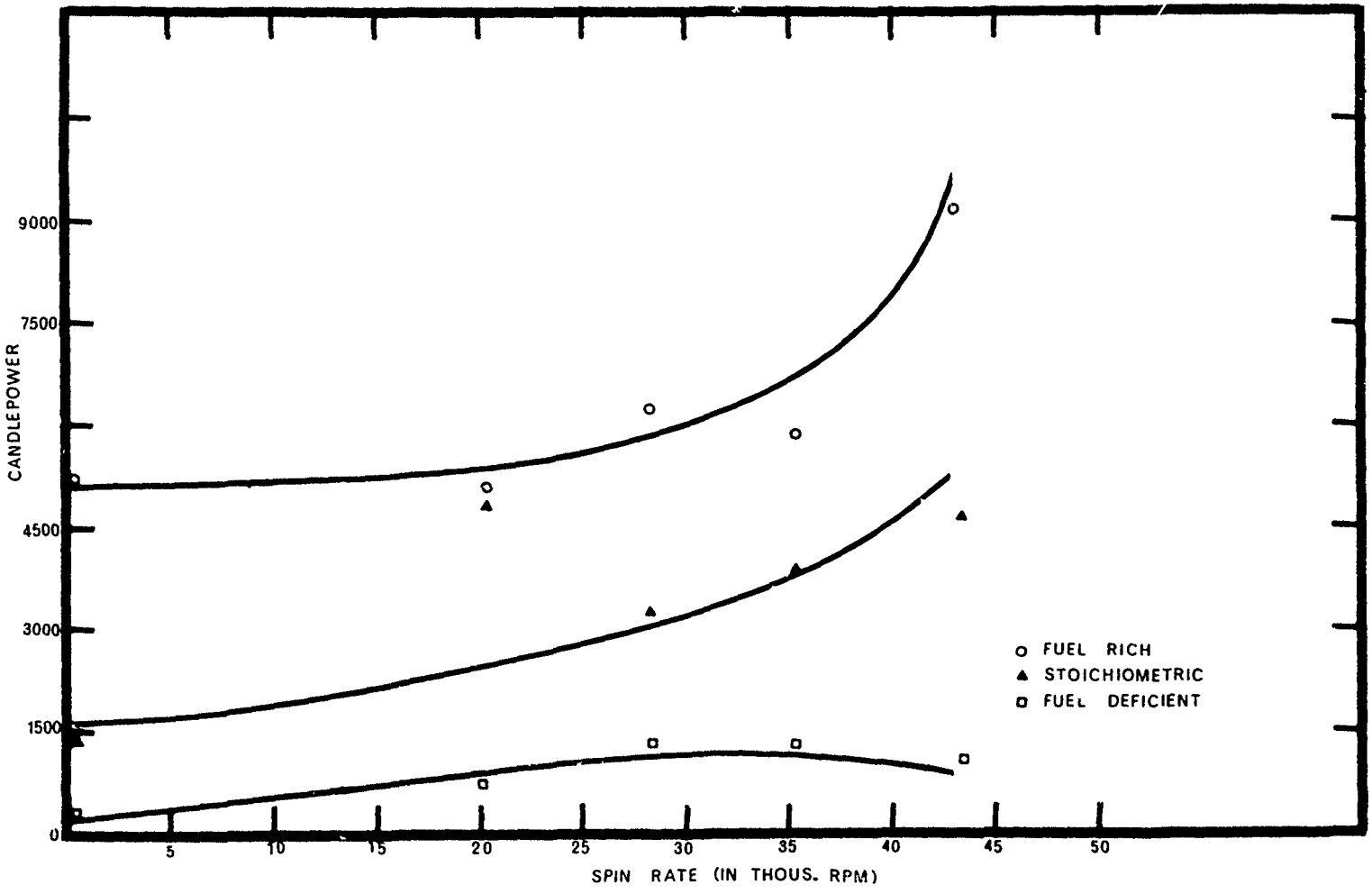

CANDLEPOWER VS SPIN RATE FOR THREE $Mg-Sr(NO_3)_2$ MIXES

Figure 8

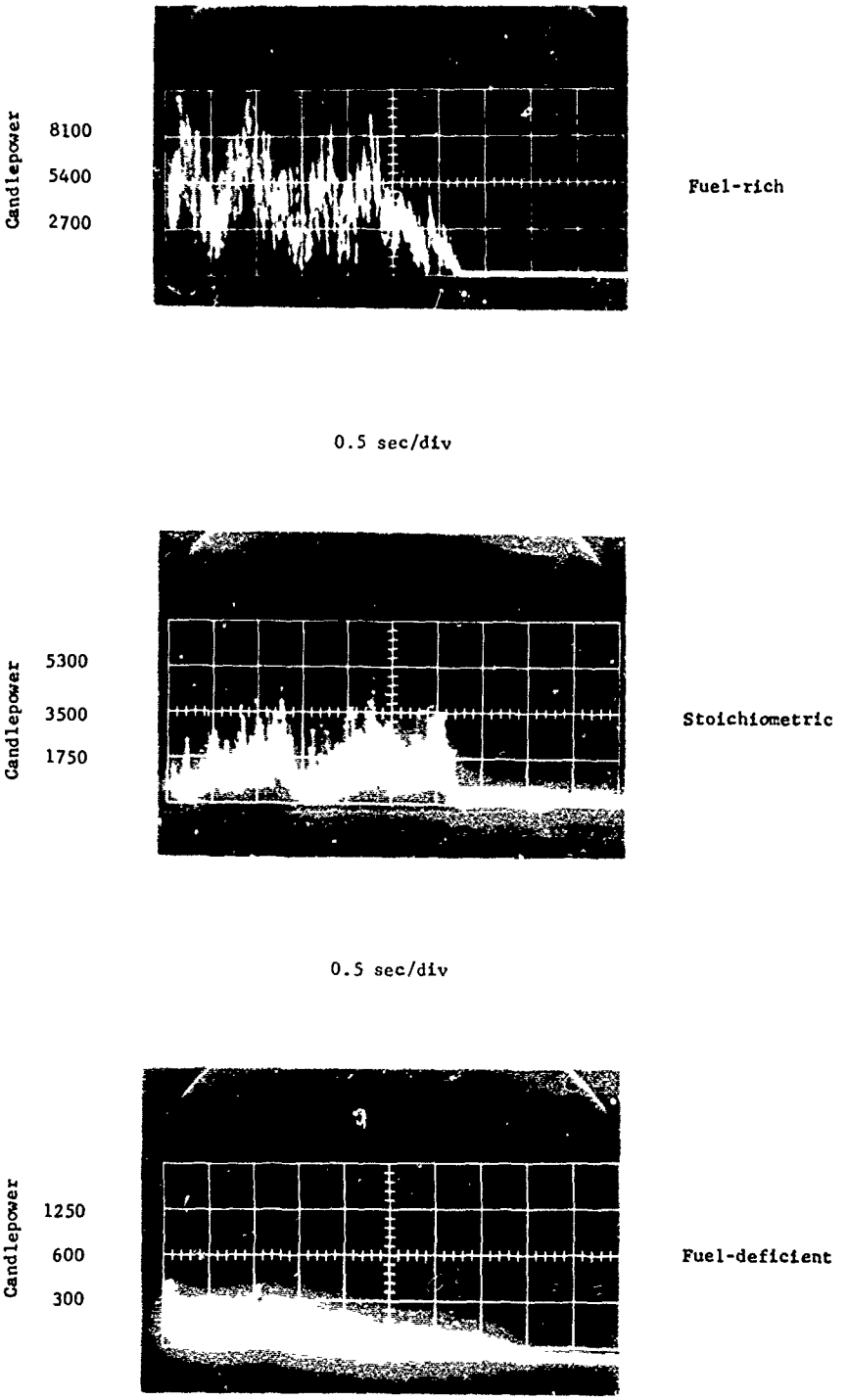

SAMPLE OSCILLOGRAMS OF CANDLEPOWER VS BURNING TIME FOR STATIC CONDITIONS

Figure 9

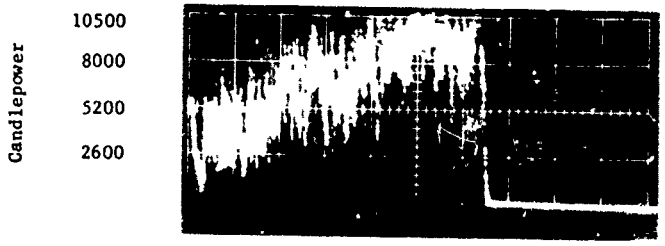

Fuel-rich

0.5 sec/div

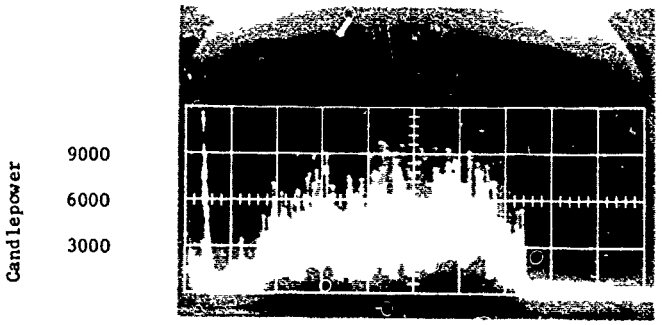

Stoichiometric

0.5 sec/div

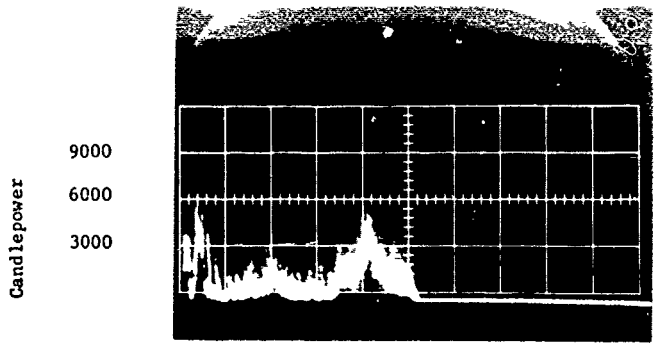

Fuel-deficient

1.0 sec/div

SAMPLE OSCILLOGRAMS OF CANDLEPOWER VS BURNING TIME FOR 43,000 RPM CONDITION

Figure 10

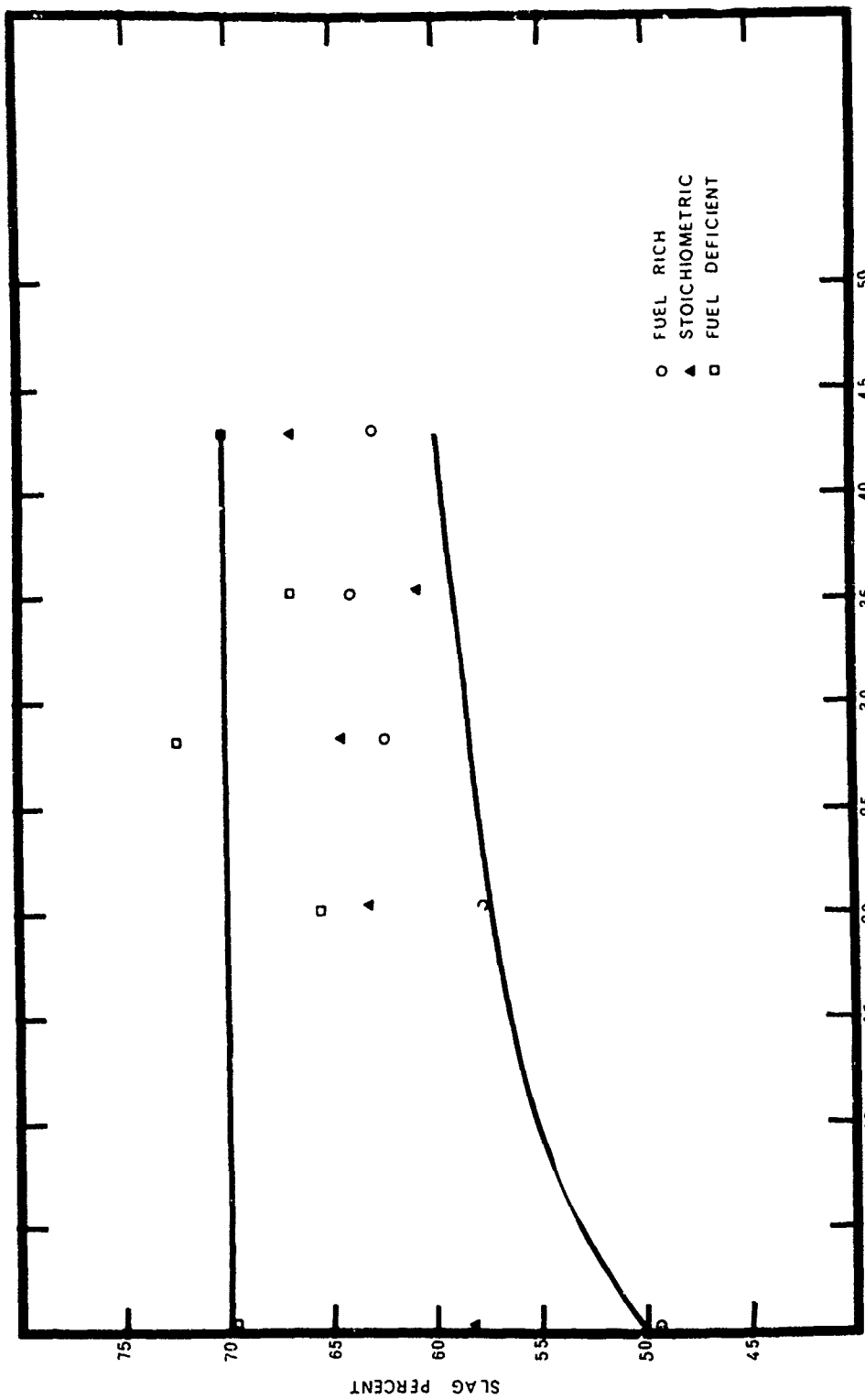

SLAG PERCENT VS SPIN RATE FOR THREE $Mg-Sr(NO_3)_2$ MIXES

Figure 11

REFERENCES

1. Shulman, R., "Factors Affecting Small Arms Tracer Burning", Frankford Arsenal Technical Report R-1287 (September 1955).

2. Shulman, R., "Effect of Cavity Geometry Upon Small Arms Tracer Burning", Frankford Arsenal Technical Report R-1421 (November 1957).

3. Beams, J. W., Pickels, E. G., "The Production of High Rotational Speeds", Rev. Sci. Inst. 6, 299 (1935).

BIBLIOGRAPHY

1. Shidlovsky, A. A., "Fundamentals of Pyrotechnics", Picatinny Arsenal Technical Memorandum 1615 (May 1965).

2. Ellern, H., "Military and Civilian Pyrotechnics", Chemical Publishing Co., Inc., New York, 1968.

3. Proceedings Second International Pyrotechnics Seminar held at Aspen, Colorado, 20-24 July 1970 (Sponsored by Denver Research Institute, University of Denver), pp 101-115, 269-293.

4. Proceedings Third International Pyrotechnics Seminar held at Colorado Springs, Colorado, 21-25 August 1972 (Sponsored by Denver Research Institute, University of Denver), pp 435-444, 445-459.

5. Engineering Design Handbook, Military Pyrotechnic Series, Part One, Theory and Application, AMCP 706-185 (1967).

6. Private Conversations at a Government Sponsored Workshop on Basic Processes in Pyrotechnics, Held at NAD Crane, Ind., 11-14 April 1973.

SMALL-ARMS TRACER STUDIES USING A RAPID SCANNING SPECTROMETER

Peter N. Keliher
(Villanova University, Villanova, Pa.)

Walter J. Puchalski
(Frankford Arsenal, Philadelphia, Pa.)

Abstract

A mechanical rapid scanning spectrometer (RSS) has been used for studies of small-arms tracer phenomena. The RSS scans from approximately 250 nm to 650 nm with a sweep time of 100 milliseconds. Typical burning times for the pyrotechnic phenomena reported in this work are 2 to 5 seconds. Pyrotechnic compositions studied include magnesium-strontium nitrate, magnesium-strontium peroxide, and magnesium-potassium nitrate. A particular complication in the spectroscopic examination of these tracers arises from the very random nature of the burning phenomena itself. Methods to alleviate this problem are suggested in this paper. In addition, some preliminary spectroscopic data are reported.

SMALL-ARMS TRACER STUDIES USING A RAPID SCANNING SPECTROMETER

Spectroscopic characteristics of pyrotechnic phenomena have been studied by many workers including Barrow and Caldin[1], Douda[2-4], and Blunt[5]. It is advantageous to study the spectral characteristics of pyrotechnic phenomena so as to determine which and in what quantities species are responsible for flame coloration. Knowing this, it would be much simpler to develop specific emitters for specific user requirements. It is also advantageous to use spectral studies to determine the role of the flame in pyrotechnic propagation. Since the flame is the major heat source influencing the pyrotechnic reaction, a better understanding of the reactions, species population distributions, and thermal gradients will make for establishing a more realistic burning rate model as a basis for future compositional developments.

Spectral characterization may be accomplished in several ways of which the simplest (and least reliable) is direct visual observation. A second approach would be photographing the flame and comparing colors. This is an improvement over direct visual observation but suffers the drawback associated with non-uniform spectral response of the film. A third approach would be to use a conventional spectrometer; but because of the very transient nature of pyrotechnic phenomena, it is not normally feasible to scan spectra over any reasonable wavelength range with a conventional monochromator and drive motor. For tracer munitions under development the maximum burn time is of the order of five seconds.

There are two main approaches to the gathering of significant spectral information during a short time:

1. A conventional grating spectrograph having reasonable dispersion (at least 15 angstroms per millimeter) may be used. As implied, photographic readout is normally used.

2. A rapid scanning spectrometer, in which a selected portion of the spectrum is scanned on a time scale from several seconds to a few microseconds, may be used. Both mechanical[6,7] and vidicon[8] devices have been used in rapid scan spectrometry. Pardue and coworkers[9] have recently published an excellent review article on rapid scan spectrometry.

For the work reported here, a commercially available mechanical rapid scanning was employed. This instrumentation is a Warner and Swasey Model 501 Rapid Scanning Spectrometer (present manufacturer, Norcon Instruments, 125 Water Street, South Norwalk, Connecticut), utilizing a grating with 258 lines/mm (320 nm blaze) to provide a wavelength coverage of approximately 250-650 nm. The optical principles of the spectrometer are shown in Figure 1.

In the preliminary experiments, output from the spectrometer was displayed on a Tektronix Model 565 Dual-Beam oscilloscope with two Tektronix 3A72 amplifiers. The displayed spectra were photographed with a Polaroid scope camera. Later data were recorded on a Bell and Howell oscillograph.

The Rapid Scanning Spectrometer and the pyrotechnic samples were positioned such that light from the pyrotechnic would be focused on the

Cassegranian entrance slit at a distance of approximately one meter. To calibrate the output displayed on the oscilloscope, a series of vapor discharge lamps and hollow cathode lamps were employed.

Binary (magnesium-strontium nitrate) mixtures were prepared according to standard procedures and ignited in the optical path of the spectrometer. First experiments employing the oscilloscope system were not successful.

Consider that the pyrotechnic burns for (typically) five seconds. As a complete scan with the system is made every 100 milliseconds with a delay time of 25 milliseconds, this means that a total of forty spectra (eight spectra per second times five seconds) will be generated across the oscilloscope during the burn. Manual interpretation of this data with the Polaroid camera is virtually impossible due to the random nature of the phenomenon. Consequently, it was decided to photograph only one or two spectra during a burn to attempt to obtain "representative" spectra; these spectra would be recorded during the "middle" of the burn. To accomplish this, a photocell was hooked into another oscilloscope with a delay trigger output. Knowing the approximate burning time of the sample, it was only necessary to decide at what point the scan should be recorded. Upon ignition, the photocell is triggered. When the auxiliary scope reaches the proper burn-time point, a pulse to the dual-beam oscilloscope gates the Model 565 to display the next <u>complete</u> scan. Although this is an improvement over attempting to interpret forty spectra, there is no guarantee that the spectra photographed is representative.

With this approach, spectra were obtained which could be interpreted in terms of the lines, bands and continua; however, reproducibility using this approach, even with apparently identical phenomena was still very poor.

It was recognized, at this time, that some system capable of "adding" and "averaging" all of the spectra obtained during the short burning time would be very advantageous. Two approaches were investigated. A Bell & Howell oscillograph was introduced into the system. With this it is possible to record all of the spectra and to observe variations of the event during the burn time.

There are three galvanometers used in this system, two high frequency response galvonometers for spectral readout (high and low wavelength ranges) and one low-frequency response galvonometer for the scan time marker output. Using the scan time marker as a start signal, there is no need to be concerned with variations in response time of the rapid scanning spectrometer or the chart paper speed, since each sweep will have an individually marked start point.

Another approach considered is some type of signal averaging system. As of this point in time, we are awaiting delivery on a Nicolet Instruments Model 1083 system. Using this system, in conjunction with the oscillographic recording, it should be possible to correlate composition with spectral information. Figure 2 illustrates the relationship between the Rapid Scanning Spectrometer and the three read-out devices.

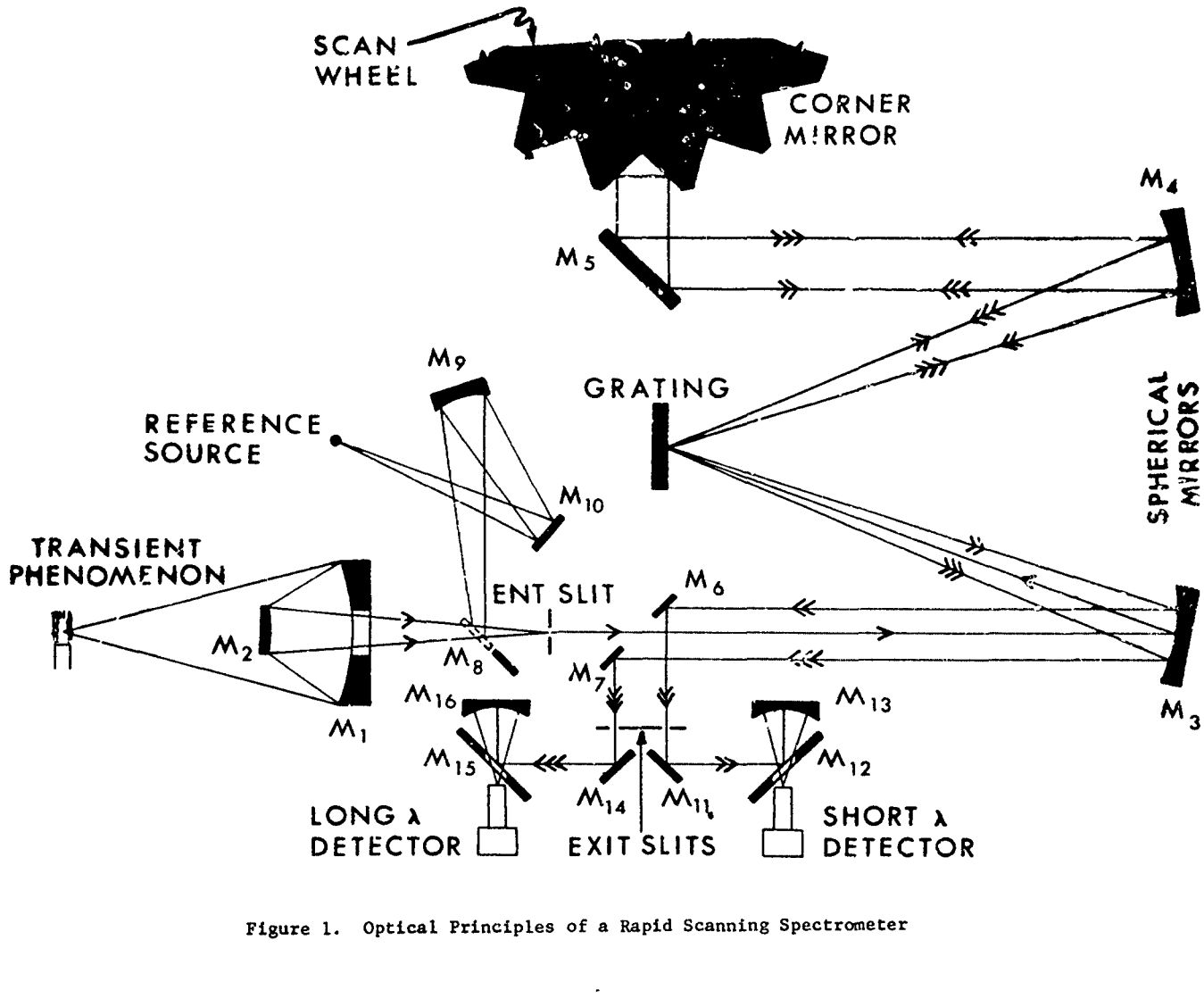

Figure 1. Optical Principles of a Rapid Scanning Spectrometer

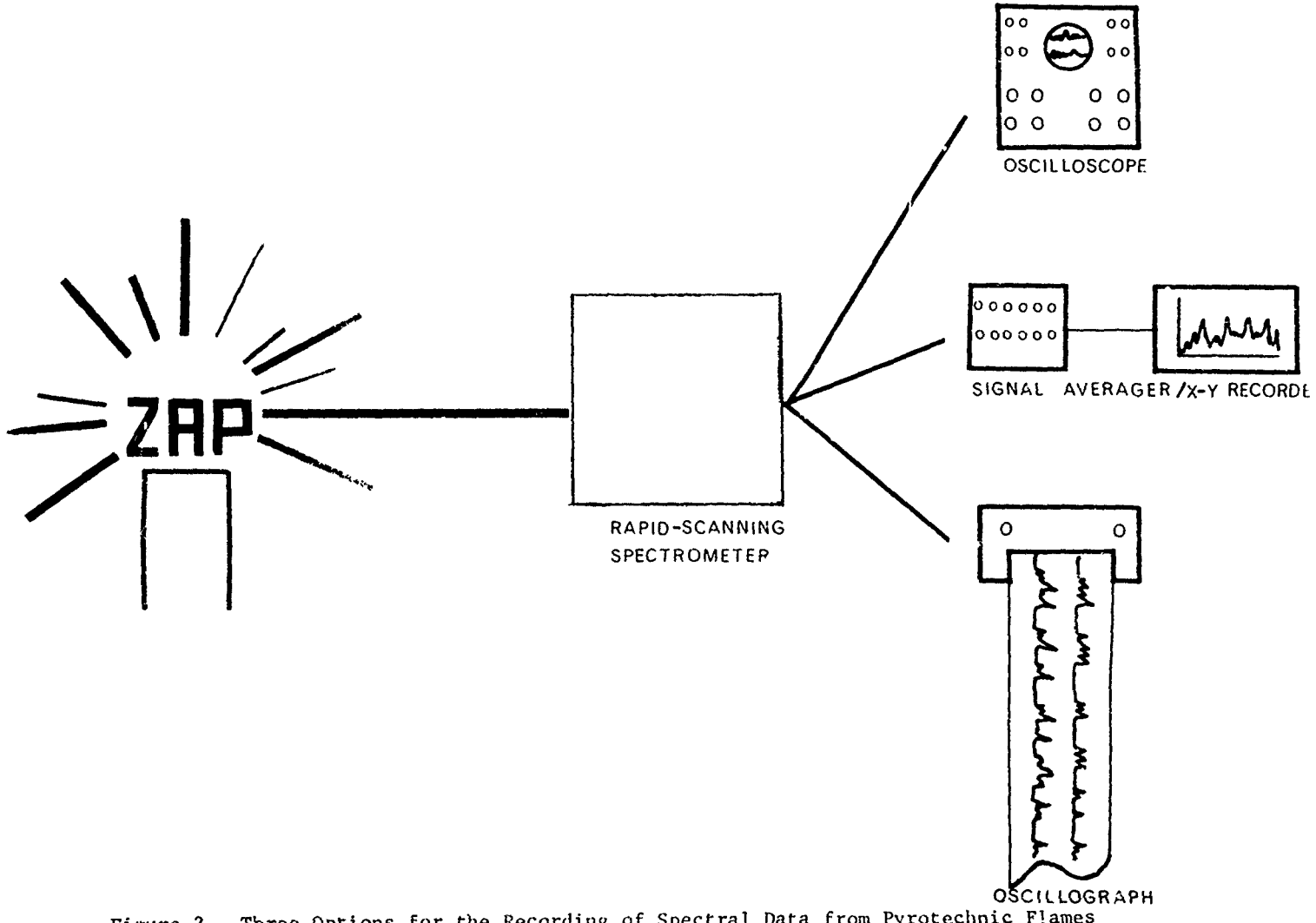

Figure 2. Three Options for the Recording of Spectral Data from Pyrotechnic Flames

REFERENCES

1. R. F. Barrow and E. F. Caldin, Proc. Phys. Soc. (London) B62, 32 (1949)

2. B. E. Douda, Paper presentated at the High Temperature Inorganic Chemistry Symposium at Carleton University, Ottowa, Canada, September 4, 1964

3. B. E. Douda, Paper presented at the First Pyrotechnic Seminar, Estes Park, Colorado, August 1968. Paper Number 5

4. B. E. Douda, J. Opt. Soc., Amer., 55, 787 (1965)

5. R. M. Blunt, "Spectral Distribution of Different Regions of Illuminating Flare Flames", July 1972. Naval Ammunition Depot, Research and Development Department, Crane, Indiana, RDTR Number 220.

6. H. J. Babrov and R. N. Tourin, Appl. Opt., 7, 2171 (1968)

7. J. W. Stroject, G. A. Gruver, and T. Kuwana, Anal. Chem., 41, 481 (1969)

8. K. W. Busch, N. G. Howell, and G. H. Morrison, Anal. Chem., 46, 575 (1974)

9. R. E. Santin, M. J. Milano, and H. L. Pardue, Anal. Chem., 45, 915A (1973)

RADIATION POLYMERIZATION OF PYROTECHNIC COMPOSITIONS

Gerald B. Franklin
Frankford Arsenal, Philadelphia, Pa.

Clyde F. Parrish
Vego Chemical Corporation, Terre Haute, Indiana

ABSTRACT

One approach to eliminating or reducing the ballistic mismatch between the ball and tracer flechettes in the Serial Flechette Rifle System was to undertake the development of an "external" tracer, where externally applied pyrotechnic material burns while the projectile is in flight. With this approach, the ball and tracer projectiles would have similar shapes and centers of gravity. Standard metal/oxidizer tracer compositions initially containing varying amounts of monomer/polymer binders were either polymerized by conventional means with curing agents, or radiation-polymerized with a cobalt-60 source. The present paper discusses this latter procedure. During the course of the investigation, some fifty candidate formulations were evaluated as coating agents externally applied to flechette tracer projectiles. Results in the form of ignition reliabilities and visible trace ranges indicate the feasibility of this approach.

RADIATION POLYMERIZATION OF PYROTECHNIC COMPOSITIONS

With advances in small caliber weapon technology, performance specifications for ammunition proposed for new weapon systems can be more difficult to meet. One example of this is the Serial Flechette Rifle (SFR), a micro-caliber weapon, which due to the small projectile size, has an inherent ballistic mismatch between the ball and tracer rounds. In order to achieve a workable tracer for this weapon system, it was necessary to increase the size of the basic ball projectile and alter its configuration (to provide room for a tracer cavity). This step increased the weight of the projectile and led to a corresponding decrease in velocity and ballistic performance. One means of eliminating or reducing the ballistic mismatch arising between the ball and tracer projectiles (or flechettes) was to develop an "external" tracer, whereby the pyrotechnic tracer material is applied to the external surface of a projectile which more closely matches the configuration of the ball projectile.

One approach to obtaining an external trace is that of using an epoxy binder admixed with standard pyrotechnic compositions.[1] Thirty percent acceptable trace function was obtained with this technique; however, severe setback forces experienced in the weapon during the ballistic cycle require higher bonding strengths than epoxy binders can render. The net result is that such formulations breakup in the weapon on firing, with ejection of pyrotechnic material from the projectile and resultant muzzle flashes. An alternate method of increasing bonding strength is through the use of radiation-induced polymerization.

It is generally known that ionizing radiation can significantly alter the properties of polymers. Furthermore, it is possible to polymerize many common monomers to obtain a product having properties not obtainable by normal catalytic means. Initial investigations on radiation-induced polymerization date back to the 1930's. Only recently have commercial applications made use of this technology[2]. Radiation processing has been recently applied to the formation of binders as used in pyrotechnic flare compositions[3-5].

There are two common sources of ionizing radiation which have commercial potential: electron accelerators, such as Van de Graaff generators and linear accelerators; and electromagnetic sources, such as isotopes and x-rays. These sources have energies far in excess of normal chemical bond energies, which are typically in the range of 10 ev. Because of these high energies and intensities associated with radiation sources, there is concern that degradation of pyrotechnic compositions will occur during the radiation process. Experience has shown, however, that doses required to yield 100% conversion of monomer to polymer are usually less than 10 rads (one rad corresponds to the absorption of 100 ergs/gm of material). Degradation of common explosives and pyrotechnics formulations is not significant below 10^3 Mrads[6].

This means that no change in characteristics should be detectable in the pyrotechnic mix from radiation doses necessary to effect a 100% cure of the polymeric binder.

The use of radiation processing to cure binder compositions has several advantages over thermal or catalytic systems. The principle advantages are: a) the rate of initiation of polymerization may be easily controlled, and b) the reaction may be run at low temperatures. These factors are inherent safety advantages unobtainable in catalytic or thermally initiated polymerizations. It is possible to interrupt or even halt the conversion process of most radiation-induced polymer systems with no detrimental effects on end item characteristics. Cost studies[7,8] indicate that radiation processing is more economical than conventional methods in many applications.

Experimental

All monomers used in this study were of standard commercial grade. No attempt was made to remove inhibitors usually present to prevent polymerization on storage. This better simulated commercial production conditions.

Slurries of a pyrotechnic composition containing a monomer and/or polymer were prepared (for exact compositions of combinations studied, see Appendix A). The projectiles were hand dipped to obtain a uniform coating, placed in a sealed container and then irradiated to a dose sufficient to yield 100% conversion of monomer to polymer. Figure 1 offers a comparison of the type 10, internal tracer (item a) with several different external tracer configurations. Projectiles (b) and (c) represent the tracer formulations in which thermally cured epoxy resin was used[9]. For projectile (b), the pyrotechnic composition was applied by hand, cured, and then hand-filed to the final configuration. For projectile (c), the tracer mixture was fabricated in a transfer mold and then cured. Projectile (c), appears here in the "as molded" condition.

Samples (d) through (f) represent various radiation polymerized configurations. Projectile (d) was unsatisfactory due to the physical limitations of the sabot, which is a molded fiberglass shoe used to hold the projectile in place as it travels along the barrel of the weapon. Projectiles (e) and (f) represent two configurations of projectiles having externally applied pyrotechnics; these were used in the majority of the lots which were further tested.

Irradiations were performed in a nominal 10,000 curie, cobalt-60 facility. This facility is of a "cave-type" design and has been described previously[10]. The cobalt-60 in its normal configuration is located on a platform which may be raised or lowered into a water well, thus permitting both modification of the source configuration and entry into the radiation chamber. Since irradiations are performed in the chamber it is easy to control the temperature and other experimental

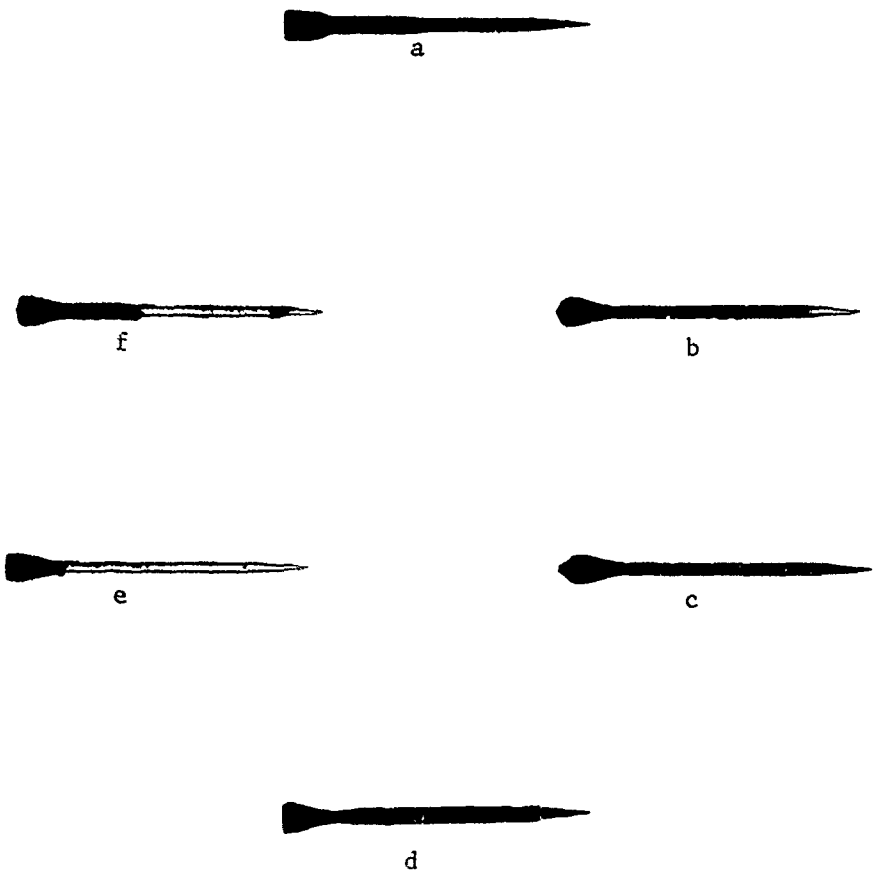

Figure 1. SFR Tracer Projectiles: a) Type 10 Internal; b) External-hand fabricated and filed (epoxy); c) Molded (epoxy); d) Radiation Polymerized (shaft only); e) Radiation Polymerized (fins only); f) Radiation Polymerized (fins and shaft)

conditions. The dosimetry was determined with a standard Fricke dosimeter having $G(FE^{+3}) = 15.5$.[11]

After irradiation, the projectiles were loaded into primed cartridge cases and charged with approximately 20 grains of propellant. The complete loaded rounds were fired from a mounted test weapon at the outdoor firing range facilities, Fort Dix, New Jersey, where tracer ignition and function characteristics were determined. Results of these observations are included in Appendix A.

Discussion and Results

After irradiation the samples generally appeared hard to the touch. In particular, the recoated samples had a glossy appearance. When tested, sporadic trace function was observed in all lots except lot numbers 24, 42 and 46. These lots contained $Zr/KClO_4$ and trimethlol propane trimethacrylate, trimethylol propane triacrylate, and ethylene glycol dimethacrylate with PMMA/MMA respectively. The results indicate that a high binder concentration is necessary to yield necessary strength to withstand high g-forces set up on launch. It was initially believed that an optimum binder should be a highly crosslinked matrix which had some resilience. Such resiliency was difficult to introduce into the system. In the limited number of systems studied, no highly resilient compositions resulted. Additional studies may be necessary in order to obtain this characteristic.

Another factor which appeared to be important was the quantity of pyrotechnic mix coated onto the projectile. Large quantities generally produced bright muzzle flashes with no tracing. In the three systems that exhibited some trace function, only a small amount of mix (100 - 150mg) was present in the fin area. These systems did not trace brightly or to a desired distance, indicating that the optimum balance between luminous output and bonding strength was not yet achieved.

Conclusions

The feasibility of utilizing radiation processing techniques to produce external tracer rounds has been demonstrated. Results indicate that systems which produce highly cross-linked binders with the resulting resilient properties should give optimum performance. The quantity of material applied to the fin area is critical, with a balance existing between desired trace characteristics and bonding strength required for retention of the pyrotechnic charge during firing.

REFERENCES

1. R. Bruce Young, SFR Tracer Ammunition Development, Final Report, AAI Corporation, Baltimore, Md., Contract DAAA25-70-C-0688 (March 1971).

2. W. E. Mott, V. T. Stannet, Isotope Radiation Technology, 6, 263 (1969).

3. C. K. Schaab, T. R. Davis, J. F. Hannig, E. Raeser, F. J. Northan, and P. K. Ase, AFATL-TR-68-35 (March 1969).

4. W. T. Biggs, C. F. Parrish, J. Appl. Polymer Sci., 16, 1779-1789

5. C. F. Parrish, J. E. Short, Jr., W. T. Biggs, Radiation Polymerization Binder for MK-48 Decoy Flare, NAD Crane, RDTR No. 232, February 1973.

6. J. F. Riley, Literature Survey on Effects of Radiation on Explosives, Report LMSGA-30-65-2, Lockheed Missiles & Space Co., Sunnyvale, California.

7. Harmer, David E., Ballantine, David S., Radiation Processing, Chem. Engr., April 1971.

8. A. G. David, Plastic Impregnation of Fibrous Materials: An Analysis of the Economics of Various Curing Methods, Atomic Energy Report AECL - 3327 (1969).

9. R. Bruce Young, SFR External Type Tracer Study, Final Report. AAI Corporation, Baltimore, Md. Contract DAAA25-73-C-0205.

10. C. F. Parrish, paper presented at the 153rd Meeting of the Amer. Chem. Soc., Miami Beach, Florida, E-15, April 1967.

11. J. L. Haybittle, R. D. Saunders, A. J. Swallow, J. Chem. Phys., 25, 1213 (1956).

APPENDIX A. CHARACTERISTICS AND PERFORMANCE OF TRACER COMPOSITIONS

Lot* Number	Tracer Mix	Binder Comp.	Trace Functions
2-1	70% Zr* 30% $KClO_4$	Acrylonitrile, no polymer, radiation dose 5 Mrad	Blind***
2-2	70% Zr 30% $KClO_4$	Acrylonitrile with ~ 10% PMMA**** Dose 5 Mrad	"
2-3	70% Zr 30% $KClO_4$	Acrylonitrile with ~ 10% PMMA after ~ 3 Mrad Coated with--5% PMMA in MMA□ and irradiated for ~ 1 Mrad More	1-50
2-4	70% Zr 30% $KClO_4$	1:1 copolymer with acrylonitrile and vinyl acetate with --10% PMMA, radiation dose ~ 4 Mrad	Blind
2-5	70% Zr 30% $KClO_4$	1:1 copolymer of acrylonitrile and vinyl acetate with --10% PMMA added. Irradiation stopped after ~ 4 Mrads and system coated with mixture of 5% PMMAin MMA and then irradiated for another 1 Mrad.	2-25 m+
2-6	70% Zr 30% $KClO_4$	1:1 copolymer of styrene and acrylonitrile with ~ 10% PMMA	not loaded due to poor adhesion of mixture
2-7	70% Zr 30% $KClO_4$	1:1 mixture of styrene and acrylonitrile with approximate 10% PMMA. Irradiation stopped after ~ 4 Mrad and system coated with 5% PMMA/MMA and irradiated for another 1 Mrad	Blind
2-8	1:1 Boron/$NaNo_3$	Vinyl acetate	1-50-100 m
2-9	Boron/$NaNO_3$	A solution of 5% divinylbenzene/PMMA and MMA irradiated to a dose of ~ 4 Mrads	Blind

* 20 round per lot
** 3m-5m particle size Zr
*** No trace function - includes muzzle flashes
**** Poly-(Methyl methacrylate)
□ Methyl methacrylate

Sample Number	Tracer Mix	Binder Comp.	Trace Functions
2-10	1:1 Boron $NaNO_3$	Vinyl Acetate/5% Divinyl benzene. Irradiation dose ~ 5 Mrads	Blind
2-11	1:1 Boron $NaNO_3$	MMA	1 - 50 m+
2-12	1:1 Boron $NaNO_3$	~ 10% Divinyl benzene, vinyl acetate	Blind
2-13	70% Zr 30% $KClO_4$	10% PMMA/Vinyl acetate	3 - 25 m+
2-14	70% Zr 30% $KClO_4$	10% PMMA/Styrene, Radiation dose ~ 5 Mrads	Blind
2-15	70% Zr 30% $KClO_4$	10% PMMA/Styrene. Dose 5 Mrads Coat 5% PMMA in MMA then irradiate 1 Mrad	Blind
2-16	70% Zr 30% $KClO_4$	Copolymer Styrene/MMA with 10% PMMA ~ 4 Mrads	1 - 50 m+
2-17	70% Zr 30% $KClO_4$	Copolymer of Styrene/MMA with 10% PMMA Dose 4 Mrads. Then coated with 5% PMMA in MMA and irradiate 1 Mrad.	2 -25 - 100 m+
2-18	70% Zr 30% $KClO_4$	10% PMMA/MMA Irradiate to ~ 5 Mrads	2 - 50 m+ 1 - 100 m+ 2 - 300 m+
2-19	70% Zr 30% $KClO_4$	10% PMMA/MMA Irradiate to dose ~ 5 Mrads Coat with 10% PMMA in MMA and 30% TMPTMA□□. Irradiate to 1 Mrad.	1 - 25 m+
2-20	70% Zr 30% $KClO_4$	MMA/10% Trimethylol propane trimethacrylate with 10% PMMA Irradiate to ~ 4 Mrads	2 - 50 m+
2-21	70% Zr 30% $KClO_4$	MMA/10% TMPTA□□□.Irradiate ~ 4 Mrads then coat with solution of 10% PMMA 30% TMPTMA□□ and irradiate to dose of 1 Mrad.	Blind

□□ Trimethylol propane trimethacrylate
□□□Trimethylol propane triacrylate

Sample Number	Tracer Mix	Binder Comp	Trace Functions
2-22	70% Zr 30% $KClO_4$	MMA/10% TMPTA ~ 10 Mrads	Blind
2-23	70% Zr 30% $KClO_4$	TMPTA	2 - 25 m
2-24	70% Zr 30% $KClO_4$	TMPTMA Dose 10 Mrads	5 - 25 m - 50 m 9 - 100 m - 200 m 2 - 250 m+
2-25	70% Zr 30% $KClO_4$	Styrene/5% divinylbenzene/10% polystyrene Dose 2 Mrads	1 - 25 m
2-26	70% Zr 30% $KClO_4$	Styrene/10% polystyrene, 5% divinylbenzene Dose 2 Mrads. Coat with solution styrene 10% polystyrene, 15% divinylbenzene. Dose 1 Mrad.	Blind
2-27	70% Zr 30% $KClO_4$	Styrene/10% polystyrene, 5% divinylbenzene Dose 5 Mrads	1 - 25 m+
2-28	70% Zr 30% $KClO_4$	MMA/10% TMPTMA 5% PMMA Dose ~ 3 Mrads	1 - 25 m+
2-29	70% Zr 30% $KClO_4$	MMA/10% TMPTMA 5% PMMA Dose 3 Mrads. Coat same solution. Dose 1 Mrad.	1 - 50 m 2 - 100 - 200 m 1 - 250 m+
2-30	70% Zr 30% $KClO_4$	Styrene/5% Polystyrene 10% Divinylbenzene 5 Mrads Coat same system Dose 1 Mrad	1 - 100 m+
2-31	70% Zr 30% $KClO_4$	MMA/10% TMPTMA 5% PMMA Dose 5 Mrads	Blind
2-32	70% Zr 30% $KClO_4$	MMA/10% TMPTMA/5% PMMA Dose ~ 5 Mrads	Blind
2-33	70% Zr 30% $KClO_4$	Styrene/10% Divinylbenzene 5% polystyrene 4 Mrads	1 - 50 m 2 - 100 m
2-34	70% Zr 30% $KClO_4$	Styrene/10% Divinylbenzene 5% Polystyrene 4 Mrad Same mix coat Dose 1 Mrad	1 - 50 m 1 - 150 m

Sample Number	Tracer Mix	Binder Comp	Trace Function
2-35	70% Zr 30% $KClO_4$	MMA/10% TMPTMA 5% PMMA 4 Mrads	1 - 150 m
2-36	70% Zr 30% $KClO_4$	MMA/10% TMPTMA 5% PMMA 4 Mrads Coat with above solution Irradiate dose 1 Mrad	2 - 25 m - 50 m 1 - 150 m 1 - 200 m+
2-37	70% Zr 30% $KClO_4$	TMPTMA Dose 5 Mrads	Blind
2-38	70% Zr 30% $KClO_4$	TMPTMA with PMMA/MMA 25% binder 5 Mrads	3 - 50 m - 100 4 - 150 m
2-39	70% Zr 30% $KClO_4$	EGDMA□□□□□ 10 Mrads	Blind
2-40	70% Zr 30% $KClO_4$	30% EGDMA/30% MMA 40% PMMA Dose ~ 10 Mrads	Blind
2-41	70% Zr 30% $KClO_4$	TMPTA Dose ~ 10 Mrads	Blind
2-42	70% Zr 30% $KClO_4$	Increased amount of TMPTA to Tracer Mix Dose ~ 10 Mrads	3 - 100 m - 150 m 1 - 200 m 3 - 250 m 2 - 300 m+
2-43	70% Zr 30% $KClO_4$	40% PMMA 45% MMA very high ratio to tracer mix ~ 40% Dose ~ 5 Mrads	4 - 50 - 150 1 - 250+
2-44	70% Zr 30% $KClO_4$	45% PMMA/45% MMA/10% TMPTMA Dose ~ 5 Mrads	6 - 100 m - 150 m
2-45	70% Zr 30% $KClO_4$	50% EGDMA + higher concentration of PMMA in MMA Dose ~ 5 Mrads	1 - 200 m 1 - 350 m
2-46	70% Zr 30% $KClO_4$	50% EGDMA + even higher concentration PMMA/MMA Dose ~ 5 Mrads	11 - 100 m - 200 m 8 - 200 - 250 1 - 350 m

□□□□□ Ethylene glycol dimethacrylate

Sample Number	Tracer Mix	Binder Comp.	Trace Function
2-47	70% Zr 30% $KClO_4$	Very high mixture; 40% binder with PMMA/MMA/TMPTMA + Butyl Stearate ~ 5% Dose ~ 5 Mrads	3 - 100 - 200
2-48	70% Zr 30% $KClO_4$	Very high binder concentration 40%/40% EGDMA 30% PMMA/25% MMA 5% Butyl stearate Dose 5 Mrads	Blind
2-49	[illegible]	Very high PMMA in MMA 30% Binder Dose ~ 5 Mrads	Blind
2-50	AlH_3	High PMMA/MMA a 30% Binder + Butyl stearate Dose ~ 5 Mrads	Blind

NON-EXPLOSIVE DESTRUCTION OF TNT WITH HYPERGOLS

by

A. J. Tulis, J. N. Keith, and W. K. Sumida

IIT Research Institute, Chicago, Ill. 60616

and

D. C. Heberlein

U.S. Army MERDC Fort Belvoir Virginia 22060

ABSTRACT

The ignition of the TNT charge of land mines can be effected very rapidly by the use of hypergolic reagents. Active hypergols such as metal alkyls are very effective in small quantities, but these reagents are sensitive to air and moisture, which will complicate the delivery problem. An interesting alternative has been found in amine-type hypergols. TNT is very sensitive to nucleophilic attack by strong bases, and the reaction appears to be greatly enhanced by the presence of certain high dielectric solvents such as ketones and nitriles. With sufficiently basic amines, hypergolic ignition occurs with 50 grams or less of the reagent. The best amine systems for hypergolic ignition of cast TNT were found to be pyrrolidine in acetonitrile and ethylenediamine in acetone. Laboratory scale screening and field testing are described.

INTRODUCTION

We have recently completed an 18 month research program on the investigation of methods for neutralizing TNT-based land mines by direct chemical attack on the explosive charge. Two approaches were used, involving a chemical reaction - dissolution technique, on which we have reported elsewhere;[1,2] and hypergolic methods, which are the subject of this paper.

TNT is an exceptionally stable explosive, highly resistant to chemical attack by acids and conventional oxidizers. It is attacked, however, by the very powerful interhalogens, and is susceptible to many reducing agents. It is also extremely susceptible to attack by nucleophilic reagents. Since our previous work had shown that the reactions of TNT with amines in certain solvents are extremely exothermic, it was expected that it would be possible to attain ignition of TNT castings by the use of very small amounts of sufficiently reactive amines.

Since the purpose of this work was to investigate the hypergolicity of TNT with candidate reactants, many of which are highly reactive with air or moisture, effort was directed at distinguishing between reaction in air and in an inert atmosphere such as dry nitrogen. Results of this work could then be extended with credibility to buried TNT castings, which are air-starved for practical considerations.

The definition of hypergolicity-ignition on contact-implies a very short time delay to ignition. However, hypergolicity is a distinct function of temperature; at sufficiently low temperatures there are no hypergolic systems whereas at sufficiently high temperatures paper is hypergolic with air. Hypergolicity also generally involves highly exothermic reactions. Thus, the criteria for hypergolic

destruction of TNT in this work was hypergols that, when contacted with a large TNT casting in a small quantity, would caused rapid reaction and temperature rise to achieve autocatalytic decomposition of the total TNT casting, in as short a period of time as practicable.

EXPERIMENTAL APPARATUS AND PROCEDURE

Because of the extremely hazardous nature of most of the candidate hypergols and the associated increased hazard of explosion when subjecting TNT to these reactants, three levels of experimental evaluation were conducted.

The first level of investigation, termed small-scale laboratory experiments, were conducted with quantities of TNT up to about 2-gm maximum. The purpose of these experiments was for large-scale screening of candidate hypergols and for subsequent measurement of fundamental properties, such as time delay and effect of temperature, of promising candidate hypergols.

The second level of investigation, termed intermediate-scale tests, were conducted at IITRI's explosives test facility and involved TNT castings of about 100 gm; i.e., about 50 times larger than the small-scale laboratory experiments and 50 times smaller than the full-scale, 10-lb TNT castings. The aspect ratio of the cylindrical castings was maintained at about 4:1, diameter to thickness. The purpose of these tests was parametric evaluation of the candidate hypergols and final selection of the best systems. Factors such as minimal amounts of hypergol to attain autocatalytic decomposition, effect of system temperature, rates of reaction, thermal stability of products, etc. were of particular interest.

The third and final level of investigation, termed full-scale field evaluation, involved tests with nominally 10-lb TNT castings under various field conditions; i.e., surface

emplaced, enclosed in a container, and buried under several inches of soil. Only the best candidate hypergols were so tested; it should be noted that for hypergolic ignition relatively small amounts of hypergol were required to cause ignition and lead to auto-catalytic decomposition, the latter being independent of the hypergol utilized once achieved. The major variants were TNT casting emplacement and temperature.

Preliminary laboratory experiments were conducted with 0.25-gm samples of powdered TNT placed in a 300-ml Pyrex flask which was then evacuated and cooled or heated to a desired temperature. About one ml of a candidate hypergol was then introduced into the flask. Results were qualitative, and ranged from an instantaneous flash of light and total decomposition to no interaction. Some experiments were performed under nitrogen.

The most convenient and accurate method of predicting the useability of a hypergol at low temperature is the measurement of the time delay to ignition over a range of temperatures. Figure 1 illustrates the apparatus that was utilized. A 50 mg sample of TNT was placed on a small watch glass in the central cavity of the aluminum cell. After positioning of the copper-Constantan thermocouple and fiber optics, the cell was closed, swept with dry argon, and brought to the desired temperature by external heating or cooling. A positive flow of argon was maintained throughout the experiment.

The drops of hypergol triggered the oscilloscope by breaking the light beam passing above the TNT sample. Light output from ignition of the sample was monitored by means of a phototransistor light detector, connected to the sample cell by another fiber optic aimed directly at the TNT.

Dry nitrogen was used to purge the hypergol feed line and control the discharge of the hypergol liquid drops. Experiments were conducted at -30°C, 0°C, 25°C, 55°C, and 75°C.

Two techniques were used for evaluating hypergolic ignition of intermediate-scale TNT castings; (1) inert-atmosphere and (2) open atmosphere tests. In the open atmosphere tests the hypergolic liquid was simply discharged from a graduate, through a funnel, into a 3/4-in. diameter by 1/2-in. hole in the 100-gm TNT casting. In the case of inert-atmosphere tests the hypergolic liquid was discharged from a syringe, loaded previously in a dry, inert-atmosphere chamber, through the cover of a closed glass jar, purged with dry nitrogen, vented through a vent hole in the lid. Both systems were operated remotely and results were photographed with a 16-mm camera, using color film.

Full-scale field tests were conducted utilizing 10 lb castings, both surface emplaced, and buried under a few inches of soil. The hypergolic liquids tested were generally encapsulated in frangible glass containers which were set in place upon the casting surface and broken from a remote location, using a steel cylinder that dropped through an alignment tube. The main purpose of these tests was to confirm scaling effects determined from the 100 gm tests, to assess the total neutralization time, determine minimal amounts of hypergol, and the effect of temperature, and to establish the non-explosive nature of this method.

EXPERIMENTAL RESULTS

Laboratory Experiments

Although white phosphorous (WP) ignites cast TNT, such ignition must be attributed to its pyrophoricity and subsequent incediary characteristics with materials exposed to air. It is a solid, melting at 44°C and must be heated in

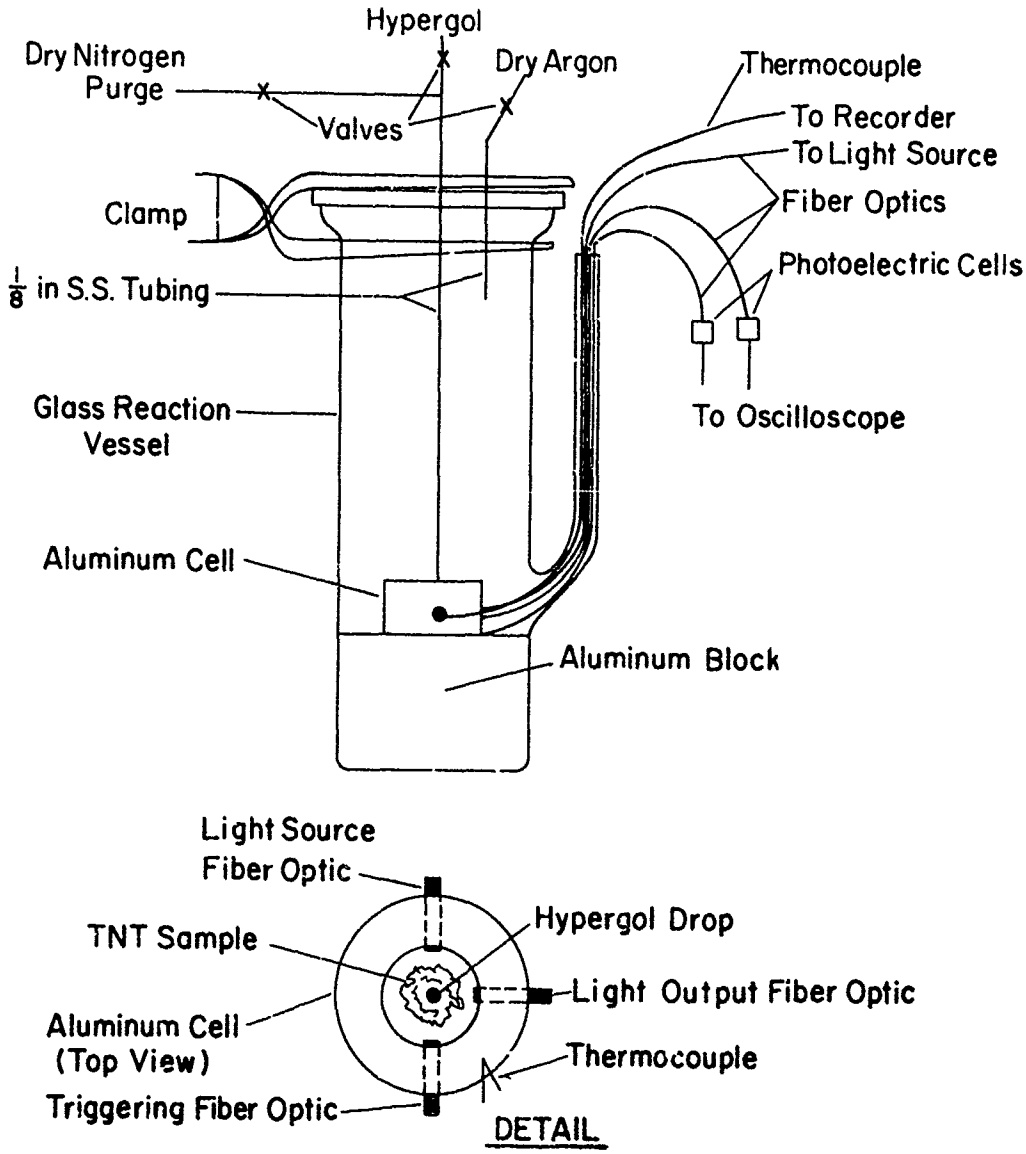

Figure 1: Inert-Atmosphere Apparatus for Evaluating Hypergolic Ignition of TNT

order to achieve delivery as a liquid. Initially, powdered TNT was dropped onto molten WP at 50°C in an evacuated flask. No visible evidence of reaction was observed at 50°C nor upon heating to 100°C. At the latter temperature both WP and TNT were in the liquid state and appeared to be immiscible. After an hour at 100°C, sublimation of WP was observed upon the upper surfaces of the flask. The WP was destroyed by filling the flask with copper sulfate solution and the TNT was recovered. Differential Thermal Analysis (DTA) confirmed that the TNT was unreacted. The obvious conclusion was that WP is not hypergolic with TNT and its use for igniting TNT would be restricted to its incendiary characteristics in the presence of air.

The more reactive metal alkyls, such as triethylaluminum (TEA), triethylboron (TEB), and diethylzinc (DEZ), are extremely reactive pyrophoric liquids and as such have found numerous applications as chemical igniters. These metal alkyls, in addition to several others such as triisobutyl-aluminum (TIBA) and ethylaluminum dichloride (EADC), were evaluated for hypergolicity with TNT. Typical preliminary experiments were conducted as follows. A 0.25 - gm TNT powder sample was placed in a rotatable side arm of a flask which was then evacuated. About one ml of TEA was admitted to the flask and the side arm was then rotated to drop the TNT powder into the liquid TEA. A flash of light was instantly observed and the flask filled with brown smoke. This experiment was conducted at ambient temperature. In repeating the experiment at 0°C, only a mild reaction occurred on the surface of the TNT powder. Upon thawing to ambient temperature no violent reaction was observed, although the TNT was converted to a dark-brown solid. At -30°C, very little reaction could be observed, except that the color of the TNT turned dark yellow.

The boron alkyls are unique amongst the metal alkyls in that they are inert with water whereas metal alkyls in general react explosively upon contact with water. Therefore TEB was considered since, if it were hypergolic with TNT, its use would alleviate the additional hazard of handling under high moisture and/or wet conditions. Unfortunately, TEB was determined to be non-hypergolic with TNT at ambient conditions.

Similar experiments were conducted with DEZ. Results proved DEZ to be hypergolic with TNT powder at 0°C and even at -30°C, although at the latter temperature there was a time delay of several seconds. Of all the hypergols evaluated only DEZ reacted spontaneously with TNT powder at -30°C.

Table I illustrates the major results of these preliminary experiments with metal alkyls and powdered TNT under vacuum conditions.

All these experiments were conducted with powdered TNT since surface area is of great consequence where hypergolic reaction between a liquid and a solid is concerned. Thus, under an inert atmosphere at ambient temperature the following results were obtained upon contacting TEA with 0.25 gm of TNT in various forms: (1) with powdered TNT, flame-flash ignition and complete decomposition; (2) with flake TNT, flame-flash ignition upon contact, without sustained decomposition; and (3) with cast TNT, only copious liberation of smoke without any evidence of a flame. Thus, the hypergolicity of metal alkyls and TNT was dependent on the: (1) type of metal alkyl, (2) form of TNT, and (3) temperature.

Three interhalogens, bromine trifluoride (BrF_3), bromine pentafluoride (BrF_5), and chlorine trifluoride (ClF_3), were evaluated as hypergolic candidates for TNT. Preliminary experiments consisted of contacting 0.25 gm of powdered TNT

Table I

HYPERGOLICITY OF TNT POWDER AND METAL ALKYLS UNDER VACUUM

Metal Alkyl	Temperature °C	Flame Ignition	Reaction
TEB	25	No	None
TEA	25	Yes	Violent
TEA	0	No	Mild
TEA	-30	No	Discoloration
DEZ	25	Yes	Violent
DEZ	0	Yes	Violent
DEZ	-30	Yes	Violent *
TIBA	25	Yes	Violent
EADC	25	Yes	Violent

* delayed by several seconds

with various amounts of these interhalogens, under both inert and open-air atmospheres. The presence of oxygen was immaterial; in all cases the TNT dissolved in the interhalogen. In the experiments with BrF_5 and ClF_3 TNT was reprecipitated upon evaporation of the interhalogen; DTA indicated that no chemical changes occurred in the TNT. However, in the experiments with BrF_3, a fizz-type reaction with some heat evolution occurred. The reaction residue appeared as a white-grey material and subsequent DTA confirmed that the material was no longer TNT.

When the more reactive amines, such as pyrrolidine (PYR) or ethylenediamine (EDA) were added to powdered TNT, purple smoke accompanied by light output (detected with the use of fiber optic probes in conjunction with phototransistor light detectors) resulted and generally led to total TNT decomposition.

The two most promising metal alkyl hypergols, TEA and DEZ, along with the two most promising amines, PYR and EDA, were then evaluated for time delay to reaction as a function of temperature in the test apparatus previously described and illustrated in Figure 1. The results are tabulated in Tables III, IV, and V, and graphically illustrated in typical Arrhenius-type plots in Figures 2, 3, 4, and 5 for TNT-DEZ, TNT-TEA, TNT-PYR, and TNT-EDA, respectively. For the TEA and DEZ hypergols, time delay was to initial light output; for the PYR and EDA hypergols, time delay was to initial smoke output. The reaction producs of TNT-PYR had a strong amine smell and those of TNT-EDA had a burnt smell. Both products were readily soluble in water.

The anomalous behavior of TNT with metal alkyl hypergols for flame ignition in the vicinity of 55°C was not resolved and was attributed to a crystalline-plastic transition that TNT undergoes in that temperature range[3].

Table II

IGNITION TIME DELAY FOR TNT-DEZ

Time Delay, sec, at Specified Temperatures, °C					
-30	0	25	55	55*	75
4.0	0.81	0.21	0.01	0.01	0.028
5.8	0.84	0.21	0.01	0.02	0.030
22	0.88	0.25	0.05	0.065	0.032
>20	1.04	0.25	0.05	0.082	0.032
>50	1.15	0.27	0.90	0.148	
	1.40	0.29	0.12	0.245	
	1.45	0.32	0.20	0.30	
		0.37	0.25		
			0.26		
			0.32		
			0.37		
			0.42		
			0.62		
Average					
10.6	1.08	0.27	0.22	0.12	0.030

* Pre-heated to 75°C before testing.

Table III

IGNITION TIME DELAY FOR TNT-TEA

Time Delay, sec, at Specified Temperatures, °C			
25	40	55	75
.35	.046	.010	.008
>1.00	.050	.010	.010
*	.164	.018	.012
*	*	.031	.020
	*	.033	.020
		.050	.020
		.077	.021
		>.200	
		>.500	
		*	
		*	
		*	
Average			
.350	.105	.033	.015

*No light output observed.

Table IV

SMOKE REACTION TIME DELAY FOR TNT-PYR

Time Delay, sec, at Specified Temperatures, °C				
0°*	20°	40°	55°	75°
>20	2.52	1.78	0.91	0.56
9.0	2.59	1.86	1.05	0.58
8.7	2.63	1.87	1.28	0.63
	2.92		1.41	0.69
	3.16			
	3.19			
	3.21			
	3.26			
	3.49			
	3.60			
	3.62			
	4.09			
Average				
9.4	3.19	1.84	1.19	0.62

*When PYR was also at 0°, no ignition occurred.

Table V

SMOKE-REACTION TIME DELAY FOR TNT-EDA

Time Delay, sec, at Specified Temperature, °C			
20°	40°	55°	75°
2.35	1.73	1.14	0.78
2.78	1.77	1.15	0.78
2.95	1.84	1.16	0.82
2.97	1.85	1.18	0.83
3.01			
3.10			
3.17			
3.47			
Average			
2.98	1.80	1.16	0.80

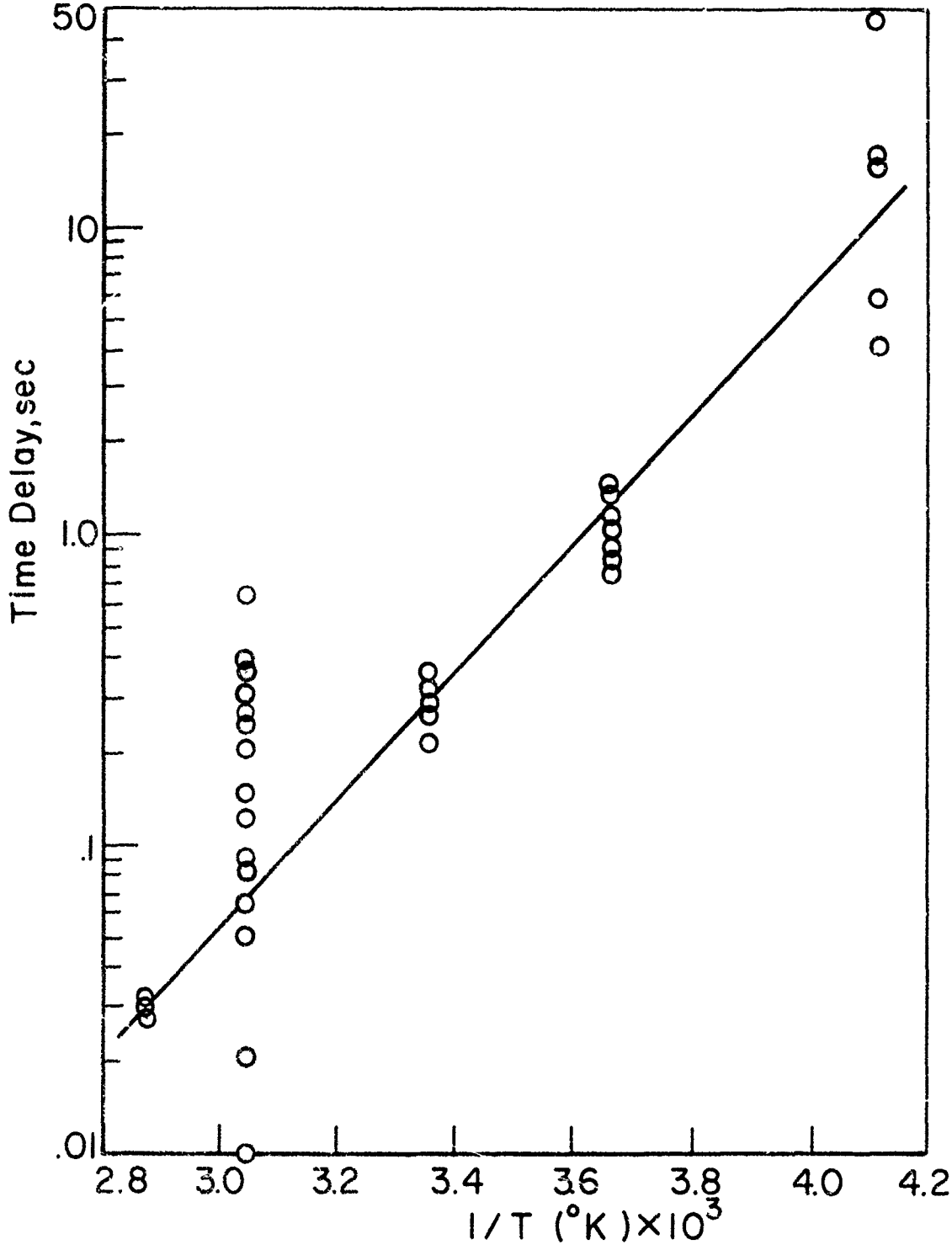

Figure 2 : Ignition Delay for TNT-DEZ

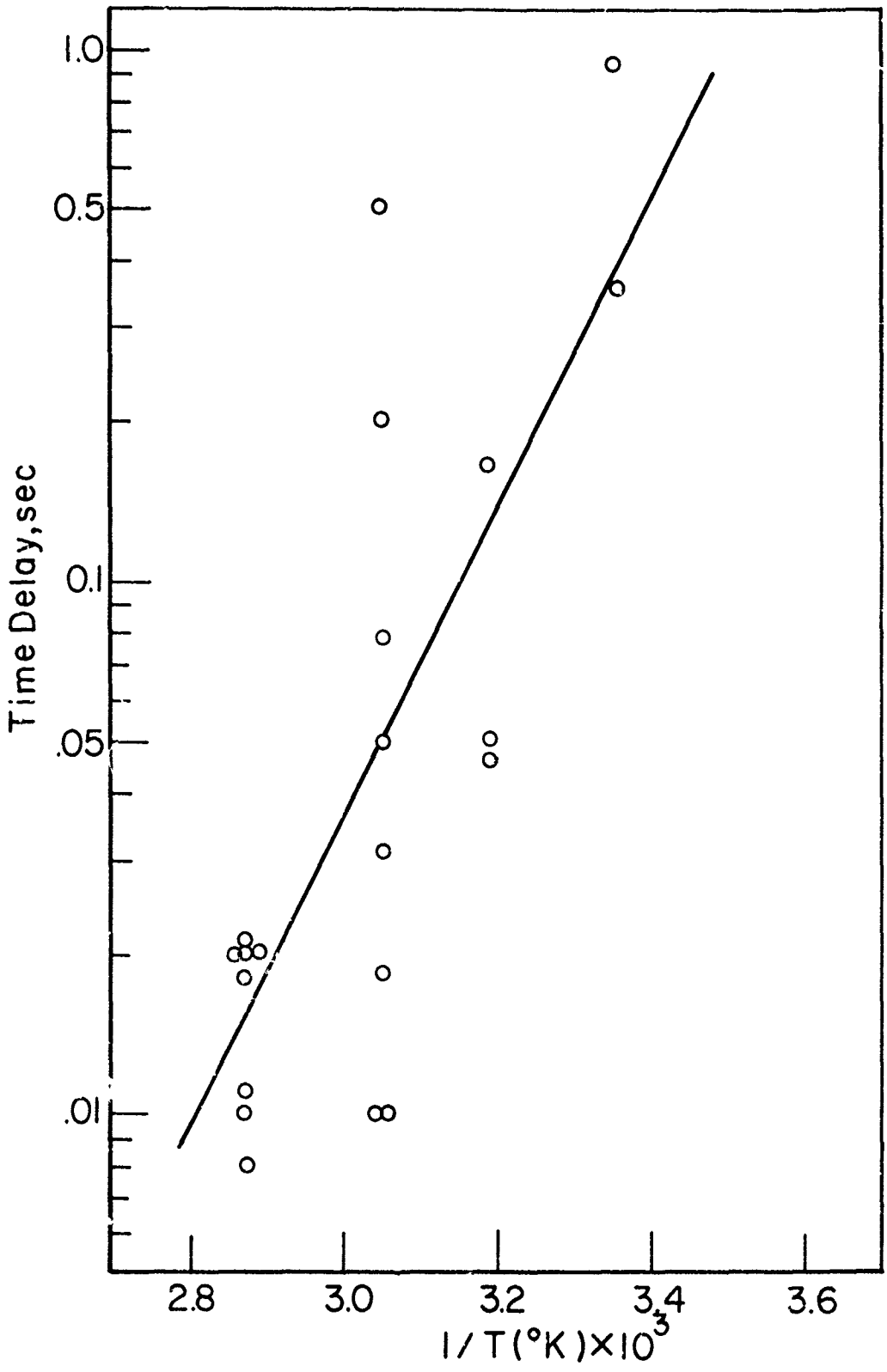

Figure 3 : Ignition Delay for TNT-TEA

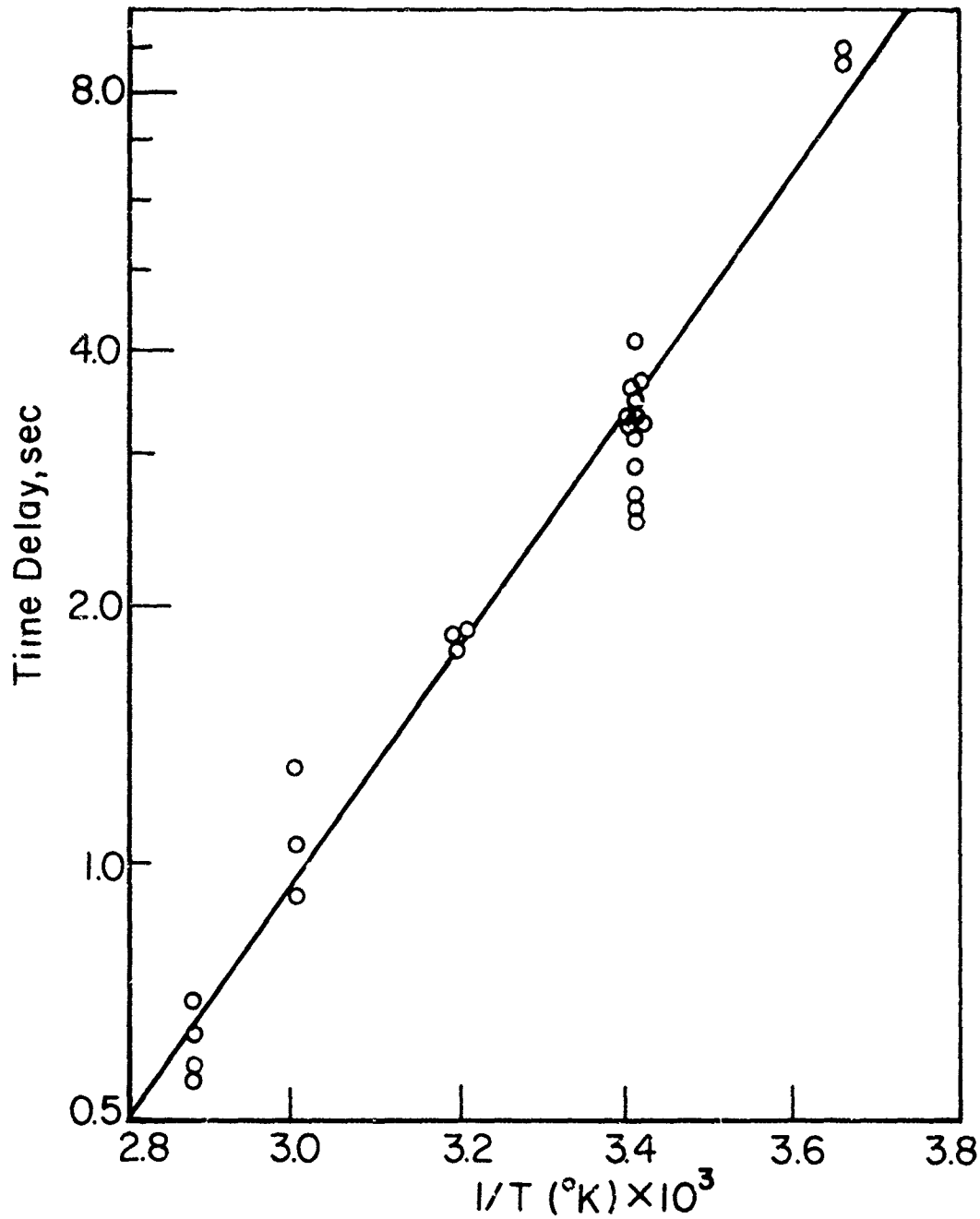

Figure 4: Ignition Delay for TNT-PYR

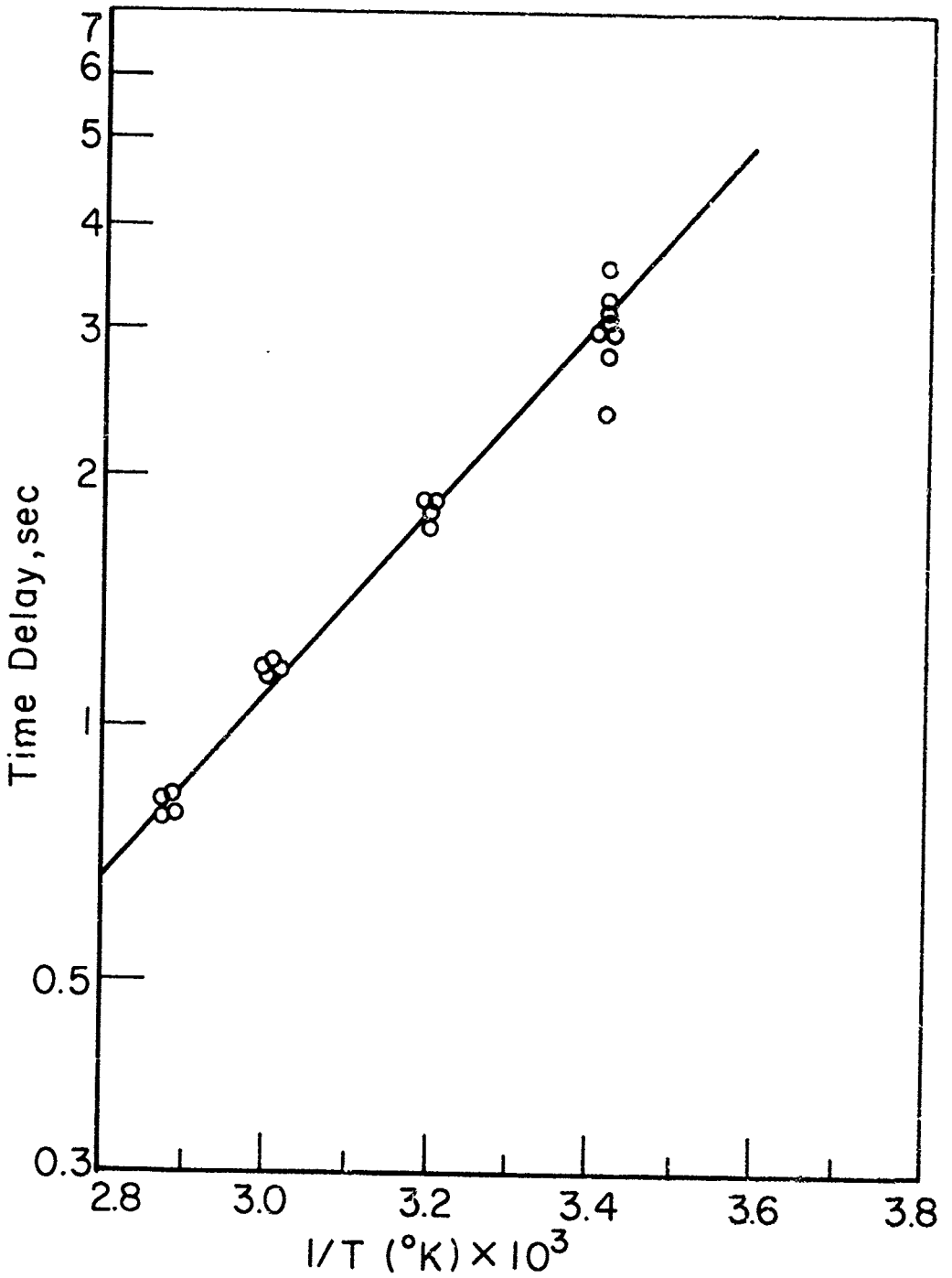

Figure 5. Ignition Delay for TNT-EDA

Field Experiments, Intermediate

Intermediate-scale experiments, were conducted to assess parameters such as time delay, amount of hypergol required to achieve ignition leading to self-sustained decomposition, effect of environment and effect of ambient temperature. Since only a relatively small amount of hypergol was required for ignition, over a relatively small portion of the casting, these experiments were sufficient to consider overall scaling factors-except such as might be dependent on the auto-catalytic self decomposition of the total casting.

With PYR either 5 or 10 ml of the liquid produced boiling and vigorous fuming within five minutes and the entire casting was consumed. When the same experiment was performed in air; ignition occurred a short time after the vigorous fuming began.

When 10 ml EDA were placed into the hole in the 100-gm TNT casting, under nitrogen, very little evidence of reaction, other than the usual color change, occurred for several minutes. The sample was therefore set aside while other experiments were in progress. However, the temperature was being monitored and rose slowly during the next 40 minutes to 56°C. A short time later boiling and fuming commenced, rapidly becoming very vigorous, until an autocatalytic reaction was achieved which caused the jar to crack open with subsequent flame ignition of the material.

Two types of intermediate-scale experiments were conducted with the amine hypergols. In the first a relatively large volume of the hypergol amine was used; i.e., 100 to 200 ml in a tall-form beaker. In the second a small quantity, 10 ml or less, was delivered by means of the hypodermic syringe into the hole in the surface of the TNT castings; the results of these experiments are presented in Tables VI to X. The large-volume data indicated that with a sufficiently large volume of solution, ignition could be attained reliably

down to -5°C. Considerable variation was obtained in the time delays, probably due largely to non-uniformity of the castings. The trend to longer time delays at lower temperatures is seen in the comparable 32°C and 9°C data, although the -5°C data do not seem to fit this pattern in all cases. The optimum concentrations appear to be 30 to 40 percent PYR-AN and 40 to 50 percent EDA-AC. PYR-AC and the other polyamines were slower than these, and were therefore eliminated from further consideration.

In the small-volume experiments an effort was made to determine the minimum amount of hypergol required to ignite the 100-gm TNT casting to self-sustained decomposition. The data in Table IX indicate that ignition cannot be obtained with less than 2 ml of undiluted PYR, and the time delays are comparable to those of Table VI with PYR-AN. A problem concerning micro-crystalline cavities in some of the TNT castings became apparent during these experiments, and accounted for the exceedingly short time delays to ignition in some cases. An improved casting and sample preparation procedure minimized this problem in subsequent experiments. Variance due to evaporative cooling was also minimized by covering the top of the beakers after delivering the amine.

With PYR the time delays obtained at 25°C were comparable to those obtained with PYR alone. In a number of cases the heat of the reaction caused the solution to boil too vigorously and it splashed out of the hole, dissipating the heat which had been building up. The 9°C experiments probably would have resulted in ignition had it been possible to avoid this loss of heat. The time delay for the single experiment at this temperature which did ignite was 7 minutes, much better than the 13.5 minutes obtained with PYR alone.

EDA-AC results were erratic, producing no ignition in most cases, but a very rapid ignition in a single experiment with 10 ml of solution. The experiment with 5 ml EDA produced ignition in about twice the time required with 10 ml. EDA-AC

Table VI

INTERMEDIATE-SCALE (100-GM) PHASE III FIELD TESTS OF AMINE HYPERGOLS, LARGE VOLUME

SYSTEM: PYRROLIDINE-ACETONITRILE

Solution Vol. ml	Amine Vol. %	Ambient Temp °C	Time Delay min	Preignition Temp, °C
200	30	32	7.1	152
200	30	9	12.0	132
200	30	9	12.6	182
200	30	9	a	(95)
200	40	32	6.2	172
200	40	9	10.2	172
200	40	9	11.8	132
200	40	-5	7.0(6.0)b	na
200	50	9	~30.	na
200	50	9	17.0	132
100	20	8	a	(62)
100	30	3	a	(98)
100	30	8	7.0	185
100	40	9	6.3	144
100	40	8	7.0	122
100	40	3	10.4	200
100	40	-5	20.0(14.0)b	na
100	50	9	10.5	182
100	50	8	10.4	122
100	50	3	15.4	192
100	60	9	12.6	182

[a]No ignition. Maximum temperature given.

[b]Time required to dissolve casting.

na= not available.

Table VII

INTERMEDIATE-SCALE (100-GM) PHASE III FIELD TESTS OF AMINE HYPERGOLS, LARGE VOLUME

SYSTEM: ETHYLENEDIAMINE-ACETONE

Solution Vol. ml	Amine Vol. %	Ambient Temp °C	Time Delay min	Preignition Temp, °C
200	10	32	a	(93)
200	20	32	12.1	149
200	20	32	16.3	152
200	20	8	a	(75)
200	30	32	7.8	177
200	30	32	a	(32)
200	30	9	12.6	137
200	40	9	5.3	162
200	40	-5	8.0(6.5)[b]	na
200	50	9	4.0	172
200	60	9	13.3	177
100	20	9	29.4	127
100	30	8	6.0	134
100	30	3	6.3	172
100	40	9	4.0	172
100	40	9	5.8	147
100	40	8	7.1	160
100	40	-5	a	c
100	50	9	3.3	184
100	50	8	a	(55)
100	50	8	3.8	182
100	50	3	4.9	202
100	50	3	a	(47)
100	60	9	9.2	182
100	60	8	a	(47)

[a]No ignition. Maximum temperature given.

[b]Time required to dissolve casting.

[c]Solution remained cold and the casting did not dissolve.

na= not available.

was not examined at the lower temperature.

Tests with the metal alkyls were conducted mostly under nitrogen cover, except for a few which were exposed to the air. Delivery was by syringe, but at 3°C a sealed ampule was used. Although no flame was observed in any of these tests, ignition occurred immediately on contact. In the first 10-ml TEA tests, excessive pressure build-up burst the glass jar, scattering the residual TNT, which did not continue to decompose. Pieces of this sample, up to 1 gm in size, were recovered up to 50 feet from the test site. In subsequent experiments, an extra vent hole was provided in the lid of the jar to prevent excess pressure. Data for TEA and DEZ are presented in Table XI.

With 5 ml of TEA or DEZ profuse fuming commenced immediately and continued for 2-3 minutes. Upon cessation of the smoke, the vessel was purged with air to assure complete consumption of the metal alkyl, and the jar was opened. Although the entire surface of the casting was blackened, only about 5 percent of the casting had been consumed. With 10 ml of metal alkyl, however, sustained autocatalytic decomposition was obtained and consumed the entire casting in a matter of minutes. Evidently 10 ml of the hypergolic liquid is required to produce selfsustained decomposition under these conditions.

In the 3°C experiments, ignition was obtained with 5 ml (2 ml in one case), but the decomposition was not sustained. The cover blew off in one case. In another 5-ml DEZ experiment air admitted after the reaction stopped reignited the residual hypergol and the casting then burned to completion in air. In a 5-ml TEA experiment, the jar burst and most of the TNT was recovered from the remains of the jar.

In tests conducted in opern air, flame ignitions occurred immediately with as little as 1 ml of TEA or DEZ and the casting burned to completion.

Table VIII

INTERMEDIATE-SCALE (100-GM) PHASE III FIELD TESTS OF AMINE HYPERGOLS, LARGE VOLUME

SYSTEM: PYRROLIDINE-ACETONE

Solution Vol. ml	Amine Vol. %	Ambient Temp °C	Time Delay min	Preignition Temp, °C
200	30	32	23	192
200	40	32	15	222
200	50	32	25	222
100	30	9	a	(79)
100	40	9	21.4	157
100	50	9	a	(25)
SYSTEM: DIETHYLENETRIAMINE-ACETONE				
200	30	32	14.3	142
SYSTEM: TRIETHYLENETETRAMINE-ACETONE				
200	30	32	17.8	142

[a]No ignition. Maximum temperature given.

Table IX

INTERMEDIATE-SCALE (100-GM) PHASE III FIELD TESTS OF AMINE HYPERGOLS, MINIMUM VOLUME[a]

SYSTEM: PYRROLIDINE

Volume Used ml	Ambient Temp °C	Ignition Time Delay min
5	25	<0.2[b]
5	25	c
3	25	<0.2[b]
3	25	c
3	25	5.0
3	25	4.9
2	25	3.7
2	25	7.3
2	25	3.0
2	25	0.07[d]
1	25	<0.2[b]
1	25	~0.07
1	25	c,e
1	25	c,e
1	25	c,e
1	25	c,e
1	25	c,e
5	9	c
5	9	13.5
3	9	c
3	9	c

[a]Although temperatures were monitored, the results were erratic. Therefore, temperature data is not listed in this table.

[b]Defective casting

[c]No ignition.

[d]Several 1/32-in holes drilled into the interior of this casting. prior to testing.

[e]Vigorous reactions producing smoke, sometimes purple-colored which generally preceded ignition in tests where ignition resulted.

Table X

INTERMEDIATE-SCALE (100-GM) PHASE III FIELD TESTS OF AMINE HYPERGOLS, MINIMUM VOLUME[a]

HYPERGOL: PYRROLIDINE IN ACETONE

Volume Used ml	Amine Volume %	Ambient Temp °C	Ignition Time Delay min
5	20	9	b,c
5	30	9	b,c
5	40	9	7.0
5	40	9	b,c
5	40	25	b,c
5	40	25	b,c
5	50	25	2.0
5	50	25	2.5
5	70	25	5.7
5	80	25	8.0
5	100	25	8.0
5	100	25	5.5
3	20	9	b,c
3	30	9	b,c
3	40	9	b,c
	HYPERGOL: ETHYLENEDIAMINE IN ACETONE		
10	30	25	2.35
10	50	25	b
5	20	25	b
5	30	25	b
5	100	25	85.0

[a]Although temperatures were monitored, the results were erratic. Therefore, temperature data is not listed in this table.

[b]No ignition.

[c]The reactions were so vigorous that the liquid boiled violently and was thrown out of the hole, resulting in no further reaction.

Table XI

COMPARISON OF HYPERGOLS AT 32°C and 3°C
100-GM TESTS

Hypergol	Volume ml	Temp, °C	Atmosphere	Reaction type	Ignition %	Casting Consumed
TEA	5	32	N_2	fume	No	~5
TEA	10	32	N_2	fume	Yes	~0[a]
TEA	10	32	N_2	fume	Yes	100
TEA	5	32	air	flame	Yes	100
DEZ	5	32	N_2	fume	No	0
DEZ	10	32	N_2	fume	Yes	100[b]
BrF_3	10	32	N_2	frothing	No	~0
BrF_3	20	32	N_2	frothing	No	~0
BrF_3	5 + 15	32	air	frothing	No	~0
EDA	10	32	air	fume	Yes	100[e]
PYR	10	32	air	fume	Yes	100
PYR	5	32	N_2	fume	Yes	100
PYR	5	32	air	fume	yes	100[d]
TEA	5	3	N_2	fume	No	~0
TEA	1	3	air	flame	Yes	100[e]
DEZ	5	3	N_2	fume	No	~0[f]
DEZ	5	3	N_2	fume	No	100
DEZ	2	3	N_2	fume	No	~0
DEZ	1	3	air	flame	Yes	100

[a]Pressure build-up in the glass jar system exploded scattering unreacted TNT pieces.

[b]BrF_3 exploded - about 75% of the TNT casting remained intact.

[c]After 40 minutes.

[d]TEA exploded breaking the creme jar - unreacted TNT remained but broken into pieces.

[e]Cover blew off admitting air to reignite casting.

[f]Burned to completion when reignited with air.

Table XII

FULL-SCALE FIELD EVALUATION HYPERGOLIC IGNITION
of 10-LB TNT CASTINGS

Hypergol	Casting Emplacement	Volume ml	Ambient Temp °C	Flame Ignition	Time Delay min	Maximum Temp °C
TEA	exposed	10	10	Yes	immediate	
DEZ	buried[a]	10	10	Yes	2-3	
BrF_3	foil[b]	100	-7	No	5[c]	
40% PYR-AN	foil[b]	100	7	Yes	54	
40% PYR-AN	exposed	110	10	No		10
40% PYR-AN	cast in jar	700	-5	No		62
50% PYR-AN	buried	20	7	Yes	15	
100% EDA	buried	100	10	No		10
30% EDA-AC	foil	50	10	No		100
40% EDA-AC	exposed	110	10	No		22
40% EDA-AC	foil	50	10	Yes	6.5	
50% EDA-AC	buried	100	7	No		112
50% EDA-AC	foil	100	7	Yes	1.5	

[a]Casting covered by about 2 inches of sand.

[b]Casting wrapped in aluminum foil, then covered with sand.

[c]Casting exploded, but fragments were recovered.

Tests with BrF_3 were conducted in covered glass jars like those with the metal alkyls to minimize loss of BrF_3 by evaporation. Delivery was made by pouring from a graduated cylinder, remotely operated. In the 10-ml experiment very little seemed to happen immediately but frothing began in the BrF_3 contained in the hole in the casting in a few minutes. In 10 minutes the BrF_3 which had overflowed to the bottom of the jar began to froth and expanded, eventually covering the casting. Several minutes later ignition occurred near the top of the casting and a brilliant flame filled the jar. The lid blew off and the remainder of the casting, about 75 gm, was recovered about 20 feet from the site.

In the 20-ml experiment, the progress of the reaction was similar, except that no ignition occurred and the reaction gradually subsided after a short time. The excess BrF_3 boiled off, leaving a residue similar to those obtained in the 2-gm tests.

When 5 ml of BrF_3 were used in the open air nothing seemed to happen except that some of the TNT was dissolved in the interhalogen. An additional 10 ml of BrF_3 produced frothing and some bromine fumes, but this reaction soon subsided without leading to ignition.

Full Scale Field Evaluation

Candidates for the full-scale (10-lb) experiments consisted of two metal alkyls, TEA and DEZ; one interhalogen, BrF_3; and two amines, PYR and EDA. The hypergolic liquids were placed in small holes drilled in the upper surface of the castings or in the dish-shaped depression caused by shrinkage during cooling of the cast TNT. Film coverage was obtained of all of the experiments in which ignition occurred, and temperatures were monitored by thermocouples placed at the point of delivery of the hypergol. Results are presented in Table XII. Castings were exposed above

ground, buried under several inches of sand, or wrapped in aluminum foil and buried (to simulate mild confinement). In one case (40% PYR-AN) TNT was cast in the bottom of a battery jar which was then covered with aluminum foil to minimize evaporative cooling. In this test the solution was delivered in four portions: 100 ml, 100 ml, 250 ml and 250 ml. No temperature increase was noted until the third portion was added and then it was insufficient to produce a violent reaction of any kind. With the castings buried under soil, liquid was delivered by pouring through a piece of glass tubing sealed to the surface of the TNT.

In all cases where ignition occurred the casting was completely consumed. Time delays and maximum temperatures (for those experiments not culminating in ignition) are given in the last column. Performance of the metal alkyls was very good, 10 ml being quite sufficient to initiate sustained decomposition, as in the 100-gm tests. BrF_3 produced an explosion a few minutes after delivery and again unreacted TNT was recovered, most of it in a large fragment at the reaction site. The amine hypergols were susceptible to evaporative cooling, with very little temperature increase being observed in exposed tests. EDA did not react significantly with a buried TNT casting. However, EDA-AC solutions ignited buried TNT castings which were wrapped in aluminum foil, with very short time delays. The time delay for 50% EDA-AC at 1.5 minutes was especially short, while the time delay for 40% PYR-AN, on the other hand, was surprisingly large, in view of the 100-gm tests. The experiment with 20 ml of 50% PYR-AN gave about the expected result and indicated that relatively small volumes of amine hypergol would be effective at this scale.

The decomposition were first observed visually by the smoke issuing from the hole through which the hypergol was delivered. As the reaction proceeded and became more vigorous, flames appeared and the smoke generation diminished. In several cases, with the autocatalytic decomposition well under

way, the reaction was nearly smokeless and the flame was nearly white, evidently intensely hot. In no case was detonation or explosion the result of any ignition except the BrF_3 experiment.

CONCLUSIONS

Hypergolic ignitions by several types of reactants have been examined. Laboratory-scale tests indicated that white phosphorous did not react with TNT, even above the melting point of the latter. TEA and DEZ were examined and found to be hypergolic and with powdered TNT, time delay studies indicated that ignition occurred in fractions of a second from 0 to 75°C. Arrhenius-type correlations of the data were quite good, except for the data in the vicinity of 55°C in both cases, where it proved impossible to obtain reproducible results. No completely satisfactory explanation is offered for this anomaly, but it is felt that the "plastic transformation" in this region may be involved. Erratic results were obtained whether the sample was specially dried, anealed at 75°C, or heated in dry nitrogen for periods varying from 20 to 120 minutes.

Intermediate-scale tests indicated that 10 ml of either metal-alkyl hypergol was required to ignite cast TNT and that once ignition had been effected the casting was completely consumed, even in a nitrogen atmosphere. No flame occurred with the castings unless air was present, although in the small-scale tests light output had been observed with the powder. Samples smaller than 10 ml reacted with the cast TNT, but only a small amount was consumed before extinguishment. In the presence of air, however, self-sustained decomposition was effected by as little as 1 ml of either TEA or DEZ, with complete consumption of the 100-gm castings. Full-scale field evaluation with 10-lb castings demonstrated that 10 ml of either hypergol would ignite a casting to

self-sustained decomposition within a matter of seconds, and that the entire casting was consumed whether it was exposed or buried under several inches of soil.

Examination of several amine candidates in 2-gm tests showed that the best of these were PYR in AN and EDA in AC. Time-delay studies with undiluted amines indicated that, with powdered TNT, both amine reactions were slower by about an order of magnitude than those of the metal alkyls. No light output was observed in any of these reactions and flame was not observed in any larger-scale tests unless air was present. In 100-gm field tests, 10 ml of PYR or EDA ignited cast TNT, although the latter reaction was extremely slow. As little as 2 ml of PYR would ignite the castings at 25°C and time delays with PYR were comparable with those obtained for PYR-AN, on the order of a few minutes. Time delays for EDA-AC were similar. More reliable ignition at low temperatures (0-10°C) were obtained with larger volumes of solution (100-200 ml).

Full-scale field tests demonstrated that, if the castings were covered with aluminum foil and buried to reduce evaporative cooling, ignition could be obtained with PYR-AN EDA-AC, with surprisingly short time delays in the latter case (6.5 and 1.5 min). In all cases where ignition occurred (evidence by smoke evolution) the entire casting was consumed.

BrF_3 was the only interhalogen compound which reacted irreversibly with TNT under the conditions of our experiments. In small-scale laboratory experiments both ClF_3 and BrF_5 dissolved TNT without reaction, but BrF_3 apparently caused fluorination, even when no violent reaction occurred. Reactions at the 2-gm scale were always mild with little exothermicity. Relatively mild reactions were obtained in 100-gm experiments also, with, however, considerably more frothing. In one experiment, in particular, fairly vigorous

frothing culminated in ignition of the TNT and bursting of the reaction vessel, although most of the TNT was recovered intact. A similar result was obtained with a 10-lb casting. Most of the casting was recovered in one piece after an explosion. In none of the explosions was there any evidence of detonation of the TNT. The vigor of the reaction simply exploded the sample and scattered the TNT.

Thus, the hypergolic candidates evaluated produced the following useful hypergols for cast TNT: the two amine types, PYR in AC and EDA, in AC; and the metal alkyls, TEA and DEZ. Other amines, such as DETA and TETA can also be used, but probably with some loss of performance, as can other metal alkyls. The four listed are the most reactive hypergols of their types.

Hypergolic ignition of TNT can be reliably effected by two fundamentally different types of reactants: the amines and the metal alkyls. Small volumes of reactant are required 10 ml of the metal alkyls and 20-50 ml of the amine solutions. In the absence of air, ignition by metal alkyls produces flame with powdered TNT, but not with cast TNT, and time delays of fractions of a second are obtainable with the former. The reactions with the amines are slower, both with powdered and cast TNT, time delays of the order of a few seconds with powder and several minutes with castings being obtained. With the amines, no flame occurs unless air is present. In all cases where sufficient hypergol is used to produce ignition, the burning is rapid and complete and no explosions or other untoward incidents occur. In the open air, TNT burns with a very smoky flame, but when hypergolically ignited under confinement the non-flame autocatalytic decomposition rate builds up rapidly until an intense, white-hot flame simulating a rocket exhaust emanates from the delivery opening, with very little smoke. Evidently a mechanistic decomposition shift occurs so that the reaction

products are much hotter and very little, if any, uncombusted carbon is liberated. Both detection and pollution are minimized in this manner.

Except for the differences in the time delays, the behavior of the amines and the metal alkyls with 10-lb castings is rather similar. Although no attempt has been made to date to develop delivery systems for these chemical reagents, it is anticipated that the amines will have considerable advantage over the pyrophoric and moisture-sensitive metal alkyls in being much easier to store and handle. Mainly for this reason, the amine hypergols are believed to show greater promise for neutralization of land mines.

ACKNOWLEDGEMENT

This work was sponsored by the U.S. Army Mobility Equipment Research and Development Center, Mine Neutralization Division, Fort Belvoir, Va., under Contract No. DAAK02-72-C-0466, whose support is gratefully acknowledged.

REFERENCES

1. Tulis, A.J., Keith, J.N., Sumida, W.K., and Heberlein, D.C., "Technology Investigation on Mine Explosive Neutralization and/or Destruction Utilizing Chemical Attack-Phase 1" ADPA, Pyrotechnics and Explosives Applications Annual Meeting, Seattle, Wash., December 5, 1973.

2. Keith, J.N., Tulis, A.J., Sumida, W.K., and Heberlein, D.C., "Chemical Neutralization of Explosives" Eighth Symposium on Explosives and Pyrotechnics, Los Angeles, California., February 5-7, 1974.

3. Jefremov, N.N. and Khaibashev, O.K., Naucho - issl. roboty Kim. Inst. Akad Nauk, 79 (1945); Isvest. Sektora Fiz. Khim. Anal. Akad. Nauk. 17, 130 (1949).

DISPERSION AND DETONATION OF EXPLOSIVE DUSTS

by

A. J. Tulis and R. F. Remaly

IIT Research Institute
Chicago, Ill.

ABSTRACT

The devastating effects of dust-cloud explosions of combustible materials, such as starch dust in starch-processing plants and coal dust in coal-mining operations, are legion. The work discussed here concerns (1) investigation and development of solid-particle dispersal techniques to simulate dust clouds extant in dynamic situations where dust-lofting or other explosive dispersal mechanisms are associated with an explosion and (2) evaluation of explosion and/or detonation characteristics of such clouds.

The major problem in the rapid dispersal of solid particles into a dust cloud involved the agglomeration of the powder. In this work we have utilized hydrophobic Silanox to eliminate this problem and additionally to (1) neutralize electrostatic charges, (2) reduce inter-particle friction and (3) increase bulk density. A statistically-designed parametric study was conducted with a simulated explosive powder to determine the effect of (1) particle size, (2) dispersal pressure and (3) dispersal nozzle size.

Preliminary experiments were conducted utilizing TNT and PETN explosive dusts. These explosive dusts were dispersed inside cylindrical plastic bags at concentrations of 1 to 2 gm per liter and an explosive booster charge of tetryl was detonated inside one end of the explosive-dust cloud. Detonation of both explosive dusts was achieved, confirmed by both 16-mm Fastax film and light detector monitors at a number of stations within the cloud. The detonation velocity

in both cases was about 1800 meters per second. To the best of our knowledge, this is the first time explosive dusts have been dispersed and detonated and instrumentally confirmed.

INTRODUCTION

The devastating effects of dust-cloud explosions of combustibe materials, such as starch dust in starch-processing plants and coal dust in coal-mining operations, are legion. Generally these explosions are sub-sonic. However, detonations of two-phase, fuel-air systems are possible and are of great interest at present by military agencies, although major emphasis has been on liquid fuel-air systems. Briefly, this latter system involves explosively disseminating a liquid, such as propylene oxide, to form a cloud of droplets. Explosive packages are then injected into the cloud and upon their detonation a strong shock is created. This shock wave interacts with the droplets in a very complicated "droplet shattering" process to create a micro-mist, which subsequently allows the flame speed to become supersonic. The result is a detonation of the two-phase, fuel-air system.

In the case of two-phase, solid-gas systems it is evident that the particle size has to be sufficiently small to allow for combustion consumption at supersonic velocity because extensive particle shattering is improbable. In such cases attainment of detonation is profoundly dependent on system parameters such as type of fuel, concentration, particle size, and particle interaction. However, detonations are certainly possible; coal dust has been shown to detonate in a mine shaft, achieving a flame velocity of 1080 m/sec, about three times sonic velocity (Ref. 1).

Our initial approach to investigation of two-phase, solid-gas detonation was to utilize explosives for the solids dust. Thus, the effect of particle size and concentration would not be as dominant as in the case of a hydrocarbon fuel. The primary consideration was the fundamental question: Could low density explosive clouds be made to detonate?

TECHNICAL DISCUSSION

The major problem for the rapid dispersal of solid particles into a dust cloud involves the agglomeration of the powder. It is absolutely essential that the powder be free flowing and that all particles separate sufficiently to allow attainment of proper concentration. In the case of explosive powders the latter restriction is not absolutely essential for functioning, but it is desireable for uniform distribution and constant propagation.

Calcium stearate and aluminum silicate have been utilized in the food industry as conditioners to prevent agglomeration (Ref. 2). The mode of action of these conditioners in inhibiting agglomeration and improving flowability was explained in three ways:

(1) As a solid barrier between the powder particles; reducing their attractive forces;

(2) As lubricants of the solid surface, reducing the friction between the particles; and

(3) As neutralizers of electrostatic charge.

Another excellent solution to this problem was developed by Dow Corning Corporation (Ref. 3), by converting a hydrophilic silica aerogel to a hydrophobic colloidal silica by reacting it with hexamethyldisilazane. This product is commercially available under the trade name Silanox. This product has been utilized to prepare a free-flowing, readily dispersable powder of CN (tear gas), an oily, sticky solid with a low boiling point (Ref. 4).

After some preliminary experimentation, our selection was Silanox. The advantages are many; (a) this powder has an exceedingly light bulk density; (b) the particle size is about 10^{-3} μ, (c) the powder can be pre-mixed before milling and will allow milling of waxy materials such as nitroguanidine, (d) the treated powder becomes water repellant, even if initially hygroscopic like ammonium perchlorate, (e) on

a weight basis, less than 1% is often adequate, and (f) the resultant powder generally has a higher bulk density after adding the Silanox than before it was added.

This latter point is exemplified in Figure 1. The simulant pow is Borax, approximately 6 liters (5905 gm) initially. The graduate contains 2 liters (100 gm) of Silanox. When the Silanox is added to the Borax, the total volume is about 8 liters initially. However, after mixing (without milling) for about 15 minutes the overall volume for the mixture becomes less than that of the Borax alone, initially. Dependent on particle size and other factors, bulk-density increases of up to 50% have been obtained with as little as 2% (by weight) additive of Silanox.

The fluidity of this powder is amazing. When agitated, it appears to be a liquid and gives the illusion of surface tension existing. This material has been utilized with nitroguanidine, ammonium perchlorate, PETN, and TNT with excellent results in all circumstances.

EXPERIMENTAL APPROACH

The major experimental apparatus utilized to assess feasibility of this concept was a polyethylene "stack" 2 ft in diameter and 10 ft high. The side supports were six 1/2-in thin-wall conduits. In one of these tubes, holes were drilled at one foot intervals into which fiber optic probes, monitored by photoelectric light detectors, were inserted. A 6-mil polyethylene sleeve, open at the top and bottom, was placed over this apparatus. The apparatus was placed upon a heavy 1-in thick steel plate and secured using three guy-ropes from the top to the ground. The whole experimental apparatus was placed in the field about 250 feet from the control building.

The initial dispersal technique utilized air pressure to disperse the powder from a 3-necked flask or flasks, either 500 ml or 1000 ml size. The air pressure inlet was

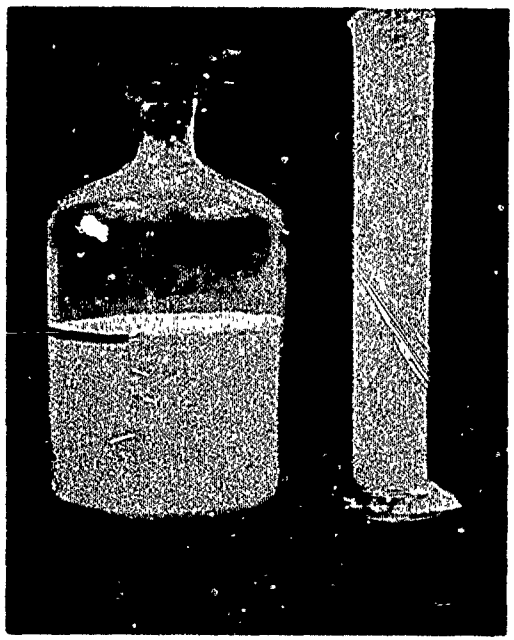

5905 gm Borax powder and 100 gm Silanox in the 2 liter graduate

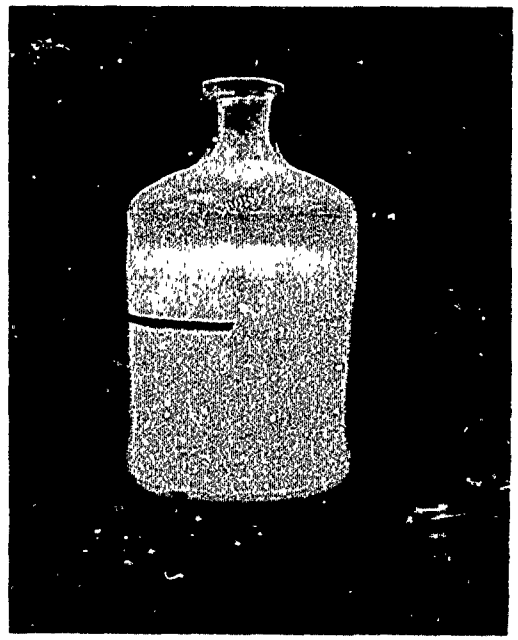

2 liters of Silanox on top of about 6 liters of Borax powder net volume 8 liters.

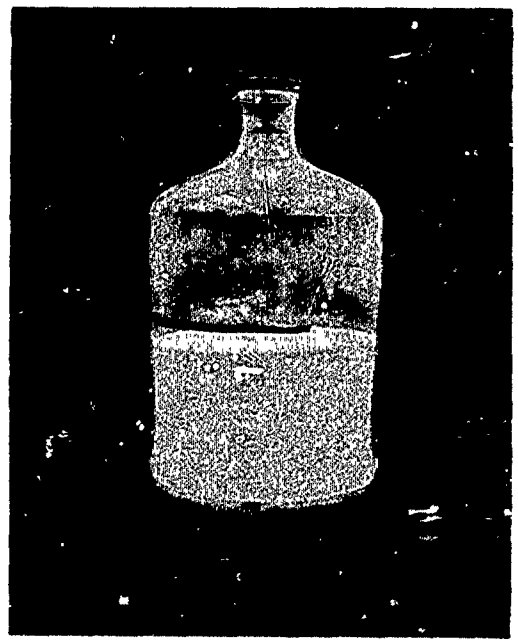

Mixing the Silanox with the Borax powder to obtain non-agglomerating free-flowing powder. Note that the overall volume has decreased to considerably less than 6 liters.

Figure 1: Adding Hydrophobic Silanox to Borax for Fluidity.

from the two side necks, through copper tubing into the bottom of the flask, opposing each other so as to create a cyclone effect. Dispersal time was about sixty seconds.

An alternative, smaller-scale experimental apparatus was also utilized, using a 1/4-in thick plastic tube, 8-in diameter and 6-ft high. Fiber optic probes were implemented at 10-in intervals. All experiments were monitored by cine photography, in most cases using a Fastax camera at 5000 f/sec and 16-mm color film.

There was considerable difficulty in generating a suitable cloud sufficiently fast to neglect powder fall out. Subsequent effort was directed to a self-contained dispersal technique, using a pressurized vessel with the powder pre-loaded; i.e., comparable to a fire extinquisher. A parametric study was conducted, utilizing the Borax simulant, to evaluate (1) particle size, (2) dispersal pressure and (3) dispersal nozzle size.

To effect detonation of the explosive-dust cloud, second-event explosive charges ranging from 5.5 gm tetyl to about 1/4-lb sheet explosive were utilized.

EXPERIMENTAL RESULTS

Results of experiments with the pressurized vessel and Borax-powder simulant indicated that 1000 gm of powder could be dispersed in 2 to 4 seconds, dependent upon the parameters. Higher pressures, larger nozzles, and smaller particle sizes led to fast discharge times. On the other hand, larger particle sizes led to higher concentrations, although of lesser surface areas. Although other factors such as particle shape, density, and vessel configuration are pertinent, sufficient information has been obtained on the tested parameters to allow relatively good control of size of cloud, time to form the cloud, cloud concentration, and surface area.

Results of experiments to detonate explosive dust clouds are summarized in Table 1. Figure 2 illustrates a sequence of Fastax film frames from the detonation of PETN dust. The height of the vessel was six feet and the booster explosive, 11 gm of tetryl, was located at the 5-ft level. The time interval between frames was about 200 μsec.

CONCLUSION

The detonation velocity of the flame front was determined from both Fastax film and the light detector probes monitor. The last experiment in Table 1, illustrated in Figure 2, resulted in the most conclusive data in that the flame front propagation could be observed through a number of frames on the film and a comparable amount of stations for the light-detector fiber optic probes. The resultant detonation velocity, 1700-1800 m/sec, is exceptionally close to the detonation velocity of liquid fuels in fuel-air explosions. The significance of this result will be of future interest and is presently under study.

To the best of our knowledge, this is the first time explosive dusts have been dispersed and detonated and instrumentally confirmed.

ACKNOWLEDGEMENT

This work was conducted by IIT Research Institute under Internal Research & Development Programs. The authors wish to acknowledge the valuable consultation afforded by M. Nusbaum and E. Bergman and the experimental effort of D. Baker.

Table 1

Data For Detonation of Explosive Dusts

Apparatus (diam x ht) ft	Explosive Powder (type) (concentration) gm/l		Detonator type (gm)	Detonation Velocity (Fastax) mm/μ sec (light)	
.42 x 3	PETN	2	tetryl 5.5	———	———
2 x 10	TNT	1	sheet ~100	2.0	1.5
.69 x 6	PETN	1.4	tetryl 11	1.8	1.7

Frame 1, 0 μsec

Before detonation of second event explosive charge, 11 gm tetryl, at 5-ft level (can be seen). Apparatus is 6 ft high and 10 in. in diameter.

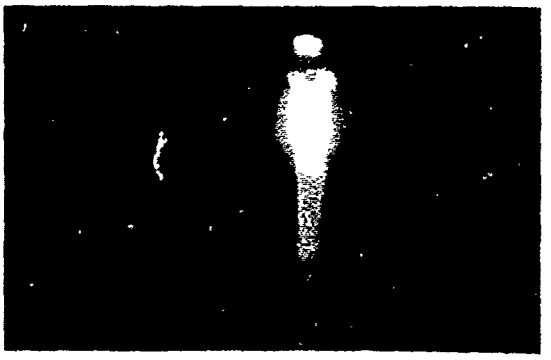

Frame 2, 200 μsec

Detonation of second-event tetryl charge. Framing speed is 5000 frames per second.

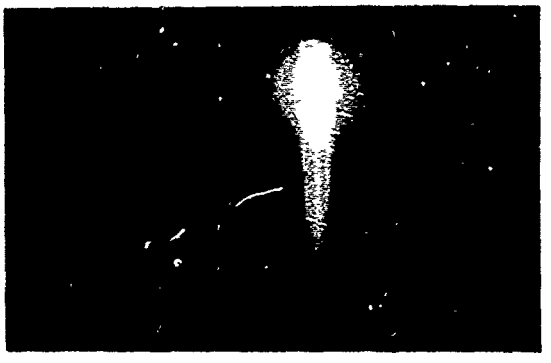

Frame 3, 400 μsec

Flame front exists at top and propagates downward.

Figure 2: Sequence of Fastax frames for the Detonation of Air-Dispersed PETN Dust at About 1.4 Gm per Liter.

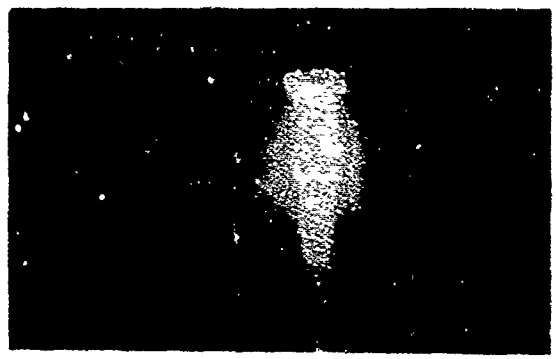

Frame 4, 600 μsec

Flame front continues to propagate downward at about 1.8 mm/μsec.

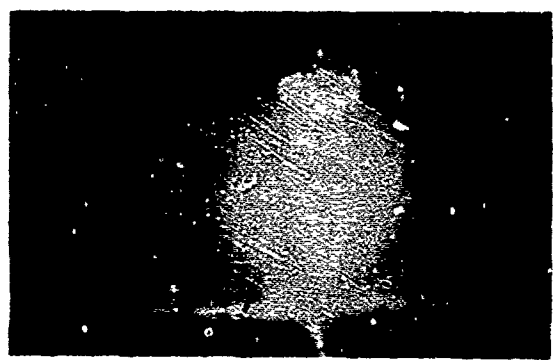

Frame 5, 800 μsec

Flame front almost reaches bottom of vessel

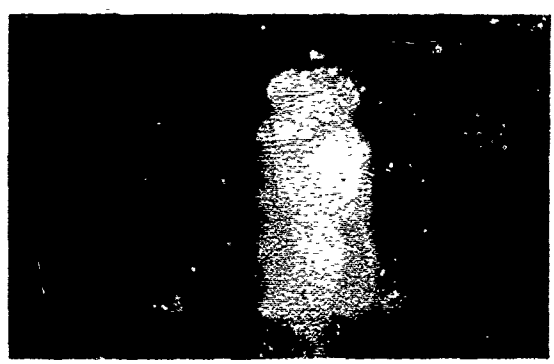

Frame 6, 1000 μsec

Flame front has reached the bottom of the vessel

Figure 2: Continued

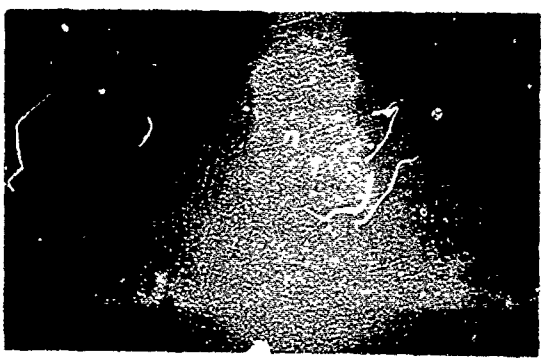

Frame 7, 1200 μsec

Detonation product gases expanding outward at about 0.9 mm/μsec.

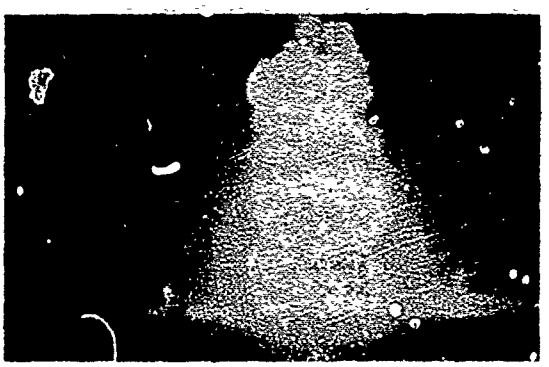

Frame 8, 1400 μsec

Detonation product gases continue expanding outward at supersonic velocity.

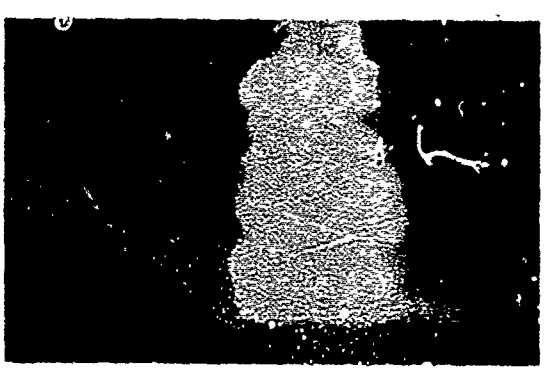

Frame 9, 1600 μsec

Detonation product gases continue exapnding outward at supersonic velocity.

Figure 2: Concluded

REFERENCES

1. Meerbach, Hans, "Progress of Coal Dust Explosions in Underground Experimental Sections and Testing of Measures for Explosion Control," Staub-Reinhalt Luft, Vol. 31, No. 11, November, 1971, pg. 23.

2. Peleg, M. and Mannheim, H., "Effect of Conditioners on the Flow Properties of Powdered Sucrose," Powder Technology, 7, 1973, pgs.45-50.

3. Rauner, L. A. and Maynard, W. J., "Hydrophobic Silica as a Grinding Aid," U.S. Patent 3,333, 776, August 1, 1967.

4. Wilcox, J. D. and Klein, J.M., "A New Concept in Preparation Techniques of Powders," Powder Technology, 5, 1971-72, pgs. 19-24.

IGNITION BY SHOCK

P. CHOTARD

Aerospatiale/Les Mureaux France

1. INTRODUCTION

This study was undertaken in the context of a contract from D.T.En (French Missiles Agency) to Aerospatiale.

The experiments were made in the Aerospatiale's Pyrotechnical Laboratory in Les Mureaux.

The definition of the main component, Squib Ignited by Shock or SS was subcontracted to the D.T.A.T./E.F.A.B. (French Agency for Army Weapons, BOURGES manufacturing Center).

2. OBJECTIVE OF THE WORK

Thanks to a lot of experiments on real boosters, we wanted to show the feasability of a new ignition process. This process uses the shock wave carried by a detonating cord as input for a new squib ignited through a bulkhead which is not destroyed after burn out, to replace the conventional electrical squib.

3. EXPERIMENTAL PROGRAM

3.1 State of Art

The use of detonating cords to carry inputs to pyrotechnical functions from only one electro explosive device, is now frequent on Ballistic Missiles. The detonating cord used is manufactured by S.N.P.E. (Société Nationale des Poudres et Explosifs - Propellant and high explosive). Its main characteristics are 2 mm diameter and linear charge 0.8 g/m RDX.

The Technology selected to cancel outside effects is to put the detonating cord inside a stainless steel tube 6 mm diameter, and to use a standard adaptation load A.L. for each break in the detonating cord. This adaptation is a cone-shaped charge of about 50 mg RDX.

./.

From that standard Technology we took as an example showing the feasibility of the process, the ignition of a real booster usually used in Ballistic Missiles. The characteristics of the booster's main load are:

- propellant: double base homogeneous powder
- weight of propellant: 170 g
- specific impulse: 40 N x s
- average thrust: 4 000 Newton

The characteristics of the pyrotechnical train to ignite the propellant in the conventional booster are:

- electrical squib loaded with 100 mg of Ammonium perchlorate with Aluminium (French MI 9)
- intermediary load of 4.5 g Potassium perchlorate with Aluminium (French PAL 00) in 16 capsules

For the experiments, the main load was kept and the pyrotechnical train replaced by the new squib SS.

3.2 Program

From this data the program was:

- study of a new component SS able to transform the shock wave given to AL by the detonating cord into an energy able to ignite the main load under good conditions, guaranteeing at the same time impermeability when the main load is burning. This component must be designed to be ignited through a bulkhead which remains intact after burning.
- realisation of a lot of experiments with the new pyrotechnical train: detonating cord - AL - SS - Main load.

4. STUDY AND EXPERIMENTS

4.1 The research undertaken by D.T.A.T./E.F.A.B. led to the definition of 2 SS's

- SS 1 made of a completely closed casing of stainless steel 15 mm in lenght and 6 mm in diameter, loaded with 291 mg of ignition composition (exact nature not available). On the side of the AL component SS 1 has a metallic bulkhead through which the squib is ignited, thickness 1.5 mm $\pm$ 0,1, and on the main load side a very thin welded plate.
- SS 2 same component as SS 1 except 25 mm in lenght and loaded with 582 mg ignition composition.

./.

These components SS need no special precision manufacturing 200 experiments of this component have shown:

- distance required between AL and SS (d_1) for good initiation of SS: 0-3 mm
- post fire integrity: 500 bar without leaking
- operating temperature range - 100° C + 100° C
- the bulkhead remained intact after each experiment.

The following figure shows the flame produced by SS 1 when initiated by a detonating cord and A.L.

4.2 The five experiments done with real boosters with live main loads are explained by:

- figure 1: experimental configuration
- figure 2: output type curve and parameters recorded
- figure 3: results

4.3 Conclusions

- We succeeded in reducing the too long level at P_1 recorded in the 1st experiment.
- T is shorter with SS 2 than with SS 1 but R has the same values with both SS 1 and SS 2.
- Outputs recorded in the 4th and 5th experiments are very close to the output obtained with conventional pyro train.
- To improve the output it would be necessary to increase the weight of ignition composition up to 1 or 2 g without reaching 4.5 g (PAL 00 in the conventional pyro train), and to add a perforated cover on the SS in order to spread the gas flow and to protect the main load from violent mechanical effects of SS.
- No bulkhead was broken after firing.

5. ADVANTAGES OF THE NEW PROCESS COMPARING TO THE CONVENTIONAL ONE

- Less weight of live materials in the pyro train for ignition of the main load is obtained.
- Assembling of the pyro train is simplified and impermeability easy to obtain with SS.
- A non electric stimulus is needed to ignite the booster.
- General safety of the booster is reinforced thanks to the use of RDX and the technology of the casing in which the ignition composition is enclosed, which cancels all the RF hazards.

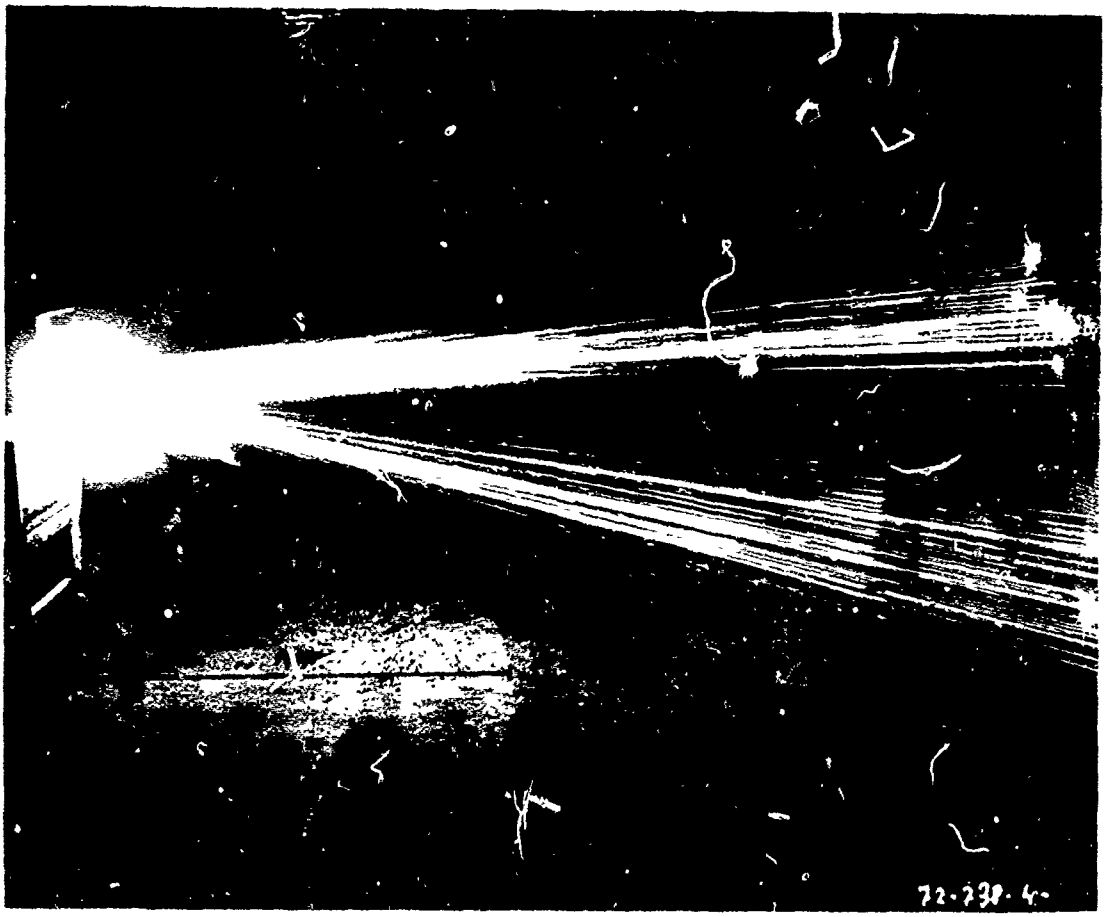

Photographie montrant la flamme produite par SS 1

Figure showing the flame produced by SS 1

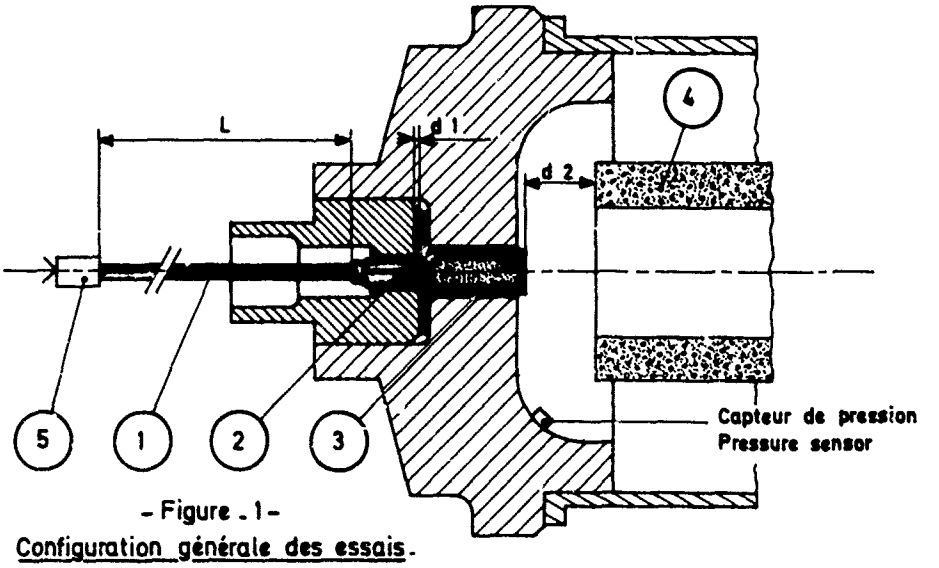

- Figure . 1 -

Configuration générale des essais.
General experimental configuration.

(1) Cordeau détonant Ø 2
Detonating cord 2 mm diameter

(2) Relais 50 mg hexogène
Adaptation load A.L 50 mg RDX

(3) Inflammateur initié par choc, type 1 ou 2 suivant les essais
Squib ignited by shock SS1 or SS2 according to the experiments

(4) Charge principale
Main load

(5) Inflammateur électrique classique
Classical electrical squib

d1 Jeu entre relais et inflammateur, compris entre 0 et 3 mm
Distance between A.L and SS always within 0 and 3 mm

d2 Distance entre inflammateur et charge principale variable suivant les essais
Distance between SS and main load depending on the experiments

L Longueur de cordeau environ 1500 mm
Detonating cord lenght about 1500 mm

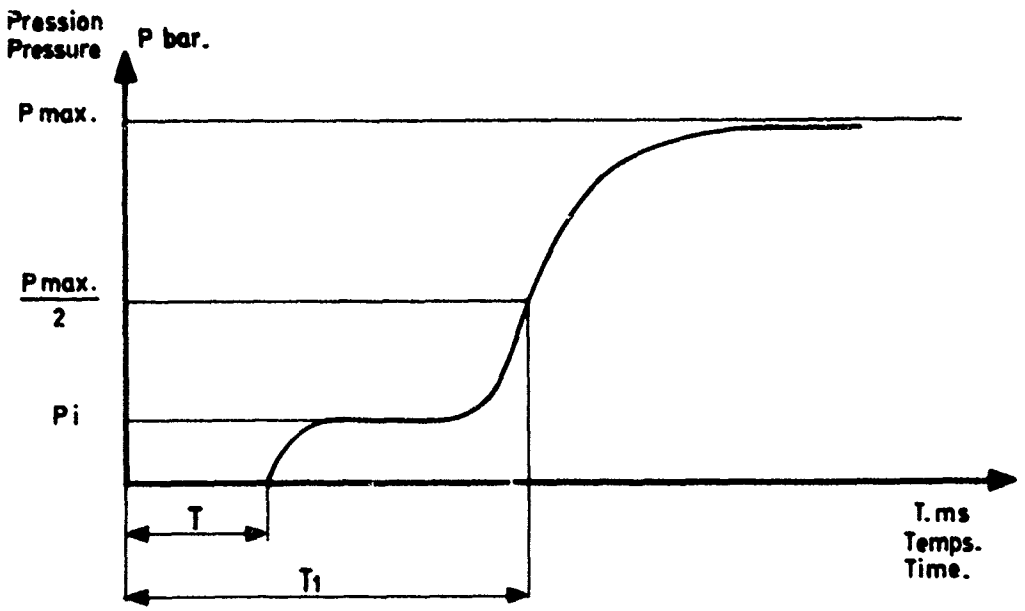

- Figure - 2 -

- Courbe type et définition des paramètres relevés.
- Type Curve and definition of the parameters recorded.

T - Temps entre ordre électrique donné à (5) et apparition de la pression.
Time between electrical imput on (5) and rising of pressure.

T1 - Temps à 1/2 P max.
Time to reach $\frac{P max.}{2}$

Pi - Pression d'allumage.
Ignition Pressure.

R - Rapidité de montée en pression.
Rate of increasing pressure.

N° Exp.	- Configuration -	T ms	Pi bar	T_1 ms	P bar	R bar/ms	- Courbe - - Curve -	
1	d2 = 12,5 mm 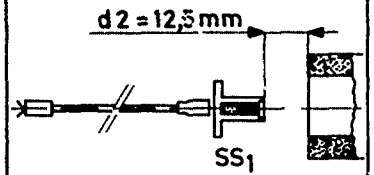 SS_1	2,6	13	47	201	14	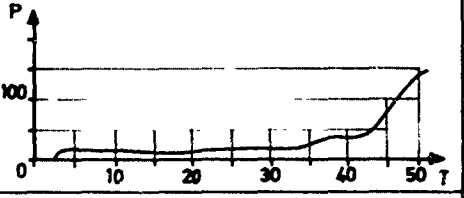	Long palier instable à Pi. Too long unstable level at Pi.
2	d2 = 1,5 mm 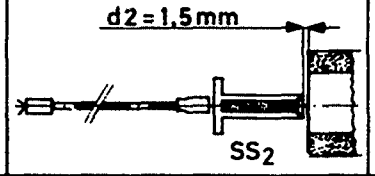 SS_2	0,4	12,5	18,5	203	12	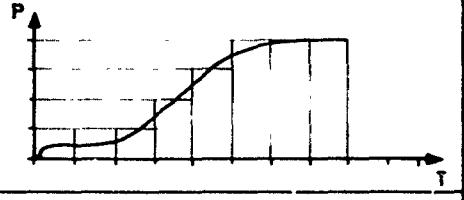	
3	d2 = 1,5 mm 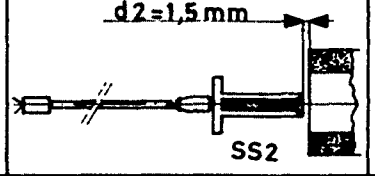 SS2	0,4	11	18,5	199,5	11,5	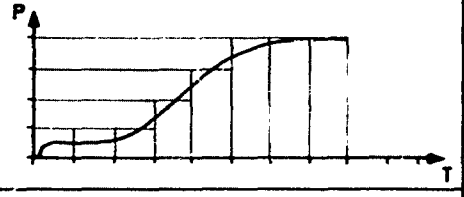	
4	d2 = 22,5 mm 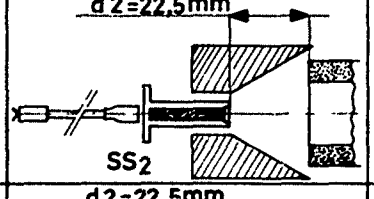 SS_2	1,4	14	10,6	203	14	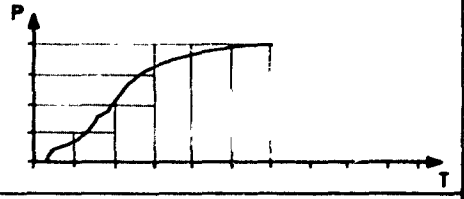	SS2 avec une pièce conique pour améliorer l'écoulement. SS2 with a cone shaped part to improve the gas Flow.
5	d2 = 22,5 mm 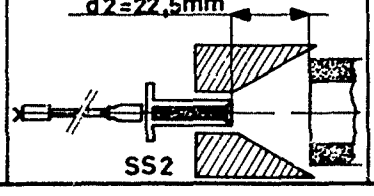 SS2	1,7	11,5	12,5	193	12	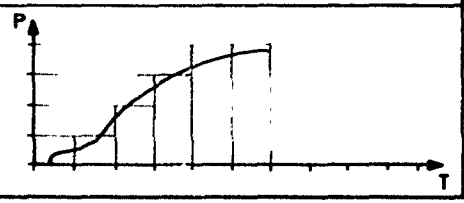	SS2 avec une piece conique pour améliorer l'écoulement. SS2 with a cone shaped part to improve the gas Flow.

Figure : 3 - Résultats des essais - - Results of the experiments -

SLA-74-5165(A)

Thru-Bulkhead Ignition of Pyrotechnics: An Analytical and Experimental Investigation

E. A. Kjeldgaard, D. W. Larson, D. J. Gould
Sandia Laboratories, Albuquerque, NM 87115

ABSTRACT

The feasibility of igniting a highly thermally conductive pyrotechnic material through a high pressure stainless steel barrier by means of heat generated by a gasless pyrotechnic has been demonstrated. An analytical model coupled with experimental measurements has been used to predict the performance and thermal response characteristics of the system. Experimental data were used in conjunction with theoretical predictions to determine the film heat transfer coefficients. The model can be used to design parameter studies to optimize the thermal ignition system.

NOTE: Author will distribute copies of the paper at the Seminar.

THRESHOLDS FOR THE INITIATION OF PYROPHORIC SPARKING

W. W. Hillstrom

Ballistic Research Laboratories
Aberdeen Proving Ground, Maryland

ABSTRACT

Pyrophoric metals such as cerium, titanium, and zirconium show experimental kinetic energy thresholds for the initiation of sparking. The thresholds for cylinders projected against targets of aluminum and steel are an order of magnitude higher than impacts of glowing metals in a drop weight impact apparatus. Relatively non-pyrophoric metals such as steel and copper had thresholds for sparking several orders of magnitude higher than the pyrophoric metals.

THRESHOLDS FOR THE INITIATION OF PYROPHORIC SPARKING

W. W. Hillstrom

I. INTRODUCTION

Sparks have been used to start fires for untold years. Flint and steel have given way to modern cigarette lighter flints and sensitive primers and igniters. Only a few metals have been found to produce vigorous sparks. The long term objective of this work is to investigate the nature of pyrophoric sparking and the factors that increase or decrease pyrophoricity. The immediate objective is to determine the thresholds of kinetic energy for sparking. These thresholds may then be used to estimate the relative pyrophoricity of different materials.

Pyrophoric materials are defined by Webster as those that (1) ignite spontaneously and/or (2) emit sparks when scratched or struck. Many materials ignite spontaneously in oxidizing atmospheres as a result of their extreme reactivity. Examples of such materials are metal hydrides and alkyls such as lithium hydride and trimethyl aluminum. Dusts of very small diameter metal particles may also ignite when exposed to air at room temperature. The ignition temperatures of these dusts usually vary with particle size and surface history.[1,2,3]

In this exploratory study, we are concerned primarily with the second definition where bulk metal pieces spark profusely when ground, abraded, impacted, or otherwise subjected to mechanical shock. Cerium, zirconium and uranium are most commonly described as pyrophoric metals in terms of the above definition. Some of the chemical and physical properties of these metals are shown in Table I. Cerium is the major constituent of misch metal which is used in the manufacture of lighter flints. The ease of sparking of lighter flints is well known.

Table I. Properties of Pyrophoric Metals

	Zr	Ce	U
Atomic Number[4]	40	58	92
Electronic Structures[5]	$4d^2 5s^2$	$4f^1 5d^1 6s^2$	$5f^3 6d^1 7s^2$
Specific Gravity (20°C)	6.506	6.771	18.95
M.P., °C[4]	1852	798	1132
B.P., °C[4]	4377	3257	3818
Heat of Comb., K cal/g[6]	2.8	1.9	1.09[7]
Heat of Comb., K cal/cm^3[6]	18	13	20.4[7]
Spontaneous Ignition Temperature, °C[8]	150	150-180	20

An empirical correlation predicts whether a metal is pyrophoric from two properties: (1) the standard free energy of formation per oxygen atom in the metal oxide and (2) the metal oxide volume compared with metal volume.[9] The free energy of formation of the oxide indicates the relative metal reactivity with oxygen. It is also a good indicator of the heat given off by reaction of the metal with oxygen. The other parameter in the correlation is oxide expansion. The violent expansion of metal during its oxidation may be one cause of the explosive cascading, or "popcorning" observed with pyrophoric sparks.

Sufficient data were available for 60 elements to estimate their pyrophoricity according to these criteria. Some 14 elements possess properties that suggest pyrophoric behavior. The elements that fit this pyrophoricity criteria are: aluminum, beryllium, cerium, hafnium, lanthanum, neodymium, plutonium, praseodymium, samarium, thorium, titanium, uranium, yttrium, and zirconium.

Sparks from pyrophoric metals easily ignite combustible fuel-air mixtures as demonstrated by the various cigarette lighters. Since pyrophoric metals are by nature reactive with air and the reactions are very exothermic, the sparks must heat up considerably in flight. D. Rae has estimated temperatures of 2700° C for friction sparks of titanium and misch metal.[10]

II. EXPERIMENTAL

Metal samples were used as obtained from the suppliers. Pure zirconium (Johnson Matthey Chemicals, Ltd., Specpure Grade) was purchased from Fisher Chemical Co., Pittsburgh, Pa. Analysis showed less than 600 ppm impurities, including less than 200 ppm hafnium. Sponge (irregular, fractured lumps), solid rod, and dust samples of zirconium as Commercial Grade 11 were supplied by Amax Specialty Metals, Inc., Akron, New York. Analysis showed the major contaminants to be iron and chromium at 0.18% total, with zirconium and hafnium at greater than 99.5%. Rods of 4.77 mm diameter misch metal alloys were purchased from Ronson Metals Corporation, Newark, N.J. Misch metal grades, 75M2 (75% rare earths, 23% iron, 2% magnesium), 95M (95% rare earths, 5% magnesium), and 100 X (97.5% rare earths and 2.5% magnesium) were used. A typical analysis of the rare earths in misch metal is 53% cerium, 24% lanthanum, 16% neodymium, 5% praseodymium, 2% other rare earths. Pure cerium (99.9%) ingots were purchased from Research Organic/Inorganic Chemical Corp., Sun Valley, Calif., and carefully machined to the desired shapes. Pure titanium, aluminum, and copper rods were obtained locally. Irregular lumps of titanium metal were purchased from Fisher Scientific Company as fused titanium metal, C.P.

Rods of 3 mm, 4.77 mm, and 7.6 mm (caliber .30) diameters were fired against targets using two separate guns for low and high velocities. Firings at velocities less than 300 meters/sec were made with a caliber .50 compressed gas, smooth bore gun using nitrogen. Velocities up to 3274 ft/sec were achieved with a caliber .30 smooth bore propellant gun. The metal projectiles were saboted in either lexan or wood positioners and their velocities were measured accurately with spaced printed circuit paper screens. The time interval between breakage of the two screens was recorded by a TSI Model 385R interval counter.

The target and projectile hardnesses are summarized in Table II. In most cases the values were obtained from the supplier, but those of mild steel, pure titanium, and hard copper were measured.

Table II. Target and Projectile Hardnesses

Metal	Hardness
Targets	
Dural, 2024-T3	BHN 120*
Mild Steel	BHN 140
Rolled Homogeneous Steel Armor	BHN 500
Projectiles	
Hard Copper	BHN 96
Misch Metal, 95M	BHN 107
Pure Zirconium	(BHN 140)
Misch Metal, 75M2	BHN 160
1095 Steel	BHN 170
Grade 11 Zirconium	BHN 180
Pure Titanium	BHN 210

* BHN, Brinnell Hardness

III. SPARKING UPON IMPACT

A. Thermal Sensitization

The behavior of bulk metal pieces on heating is quite different from that of powders of the same metals. For example, 75M2 misch metal was heated at 200°C in air for 3 days without glowing, burning, or sparking. It only corroded or oxidized slowly. This is in contrast to its reported autoignition temperature of 150-180°C. When the misch metal was heated at higher temperatures (600-1000°C) in air, it glowed bright orange, but still no flames, sparks, or burning were seen. In an argon atmosphere the misch metal did not glow brightly when heated at 830°C. The same piece glowed brightly when subsequently exposed to air. Thus, the glowing results from an oxidation reaction.

The pyrophoric metals examined here spark much easier when impacted while glowing than at room temperature. The length of time to the beginning of glowing was measured at different furnace temperatures.

The minimum temperature at which glowing is seen is called the Lower Glow Temperature. Small rods of 75M2 misch metal, 4.77 mm diameter by 12.7 mm length, were set in a combustion boat in the hot furnace and the time measured for the onset of a bright orange glow. At temperatures below about 400°C no bright orange glow appeared. This is the Lower Glow Temperature. Shorter times to the beginning of bright glowing were observed for 95M misch metal, but the Lower Glow Temperature is about the same as that found for 75M2 within the experimental error.

Pure cerium pellets with the same geometry began to glow faster than 75M2 and 95M. For example, at 600°C pure cerium began to glow in only 27 seconds compared with 98 seconds for 75M2 and 50 seconds for 95M.

Zirconium and titanium sponge gave similar results although two stages of glowing were observed. First, an orange glow is seen, then the particles become incandescent white when heated at temperatures above the Lower Glow Temperature. Since the white incandescent state was required for sparks on impact, the Lower Glow Temperature is 580°C for zirconium. Similarly, the Lower Glow Temperature for titanium sponge is 870°C.

Kinetic energy thresholds for sparking were determined in the impact apparatus shown in Figure 1. A drop weight of 169.2 grams was dropped from varied heights onto the glowing pellets on the anvil of the apparatus. Photographs of 75M2 misch metal sparks from 10, 20, 30 and 39.1 cm drops are shown in Figure 2. From these tests it is apparent that a kinetic energy of at least 0.332 newton meters is needed for extensive sparking from the glowing pellets.

Higher energies were estimated for glowing zirconium and titanium sponge. They would not spark in the impact apparatus, apparently due to handling delays between the initiation of the white incandescence and impact. A quick hammer blow to the glowing pellets generated a large number of vigorous sparks. The necessary impact with the hammer was somewhat more than that needed for the misch metals and pure cerium.

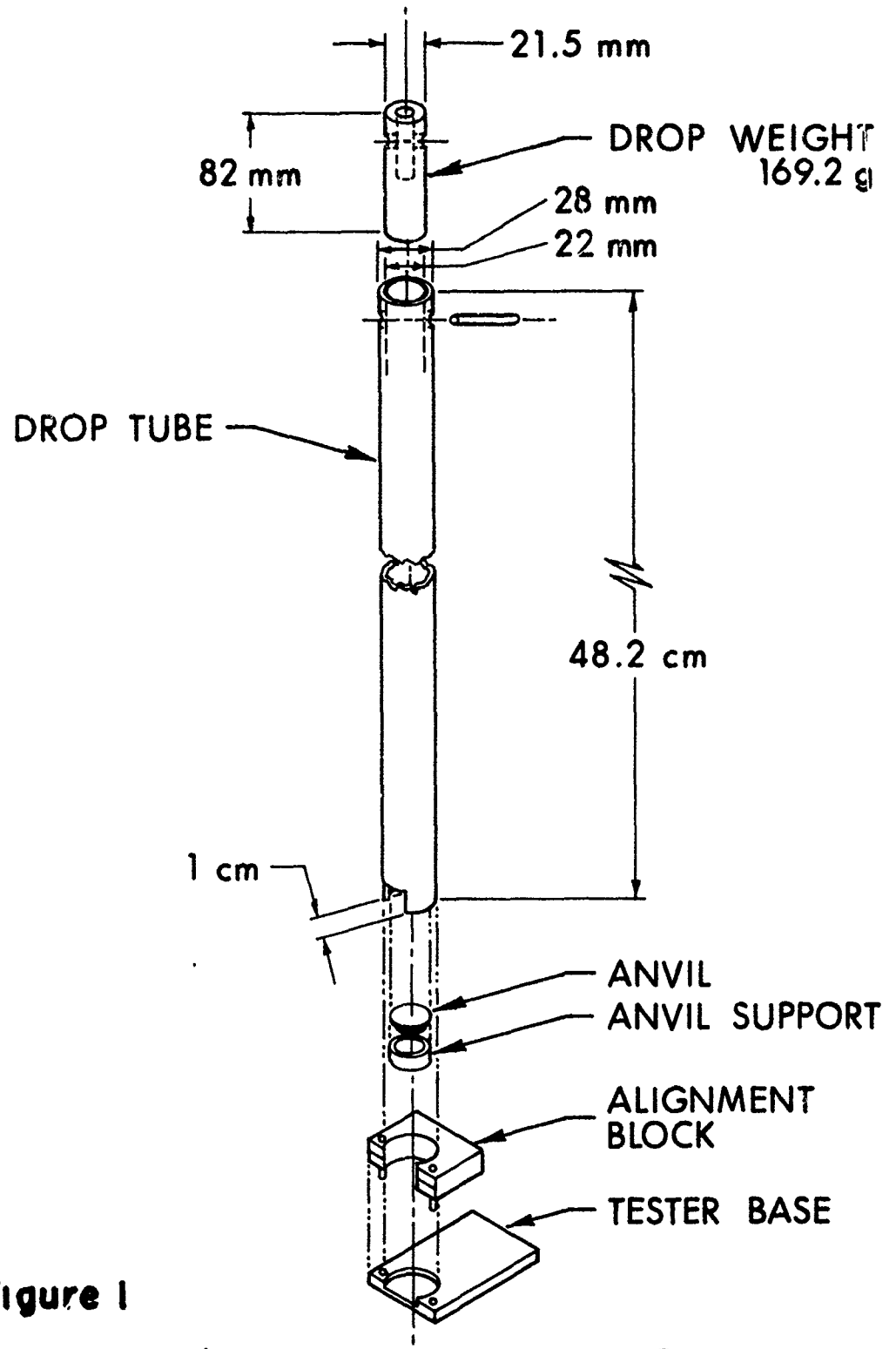

Figure 1

Drop Weight Impact Apparatus Dimensions.

A. 10 cm DROP
(0.166 newton m)

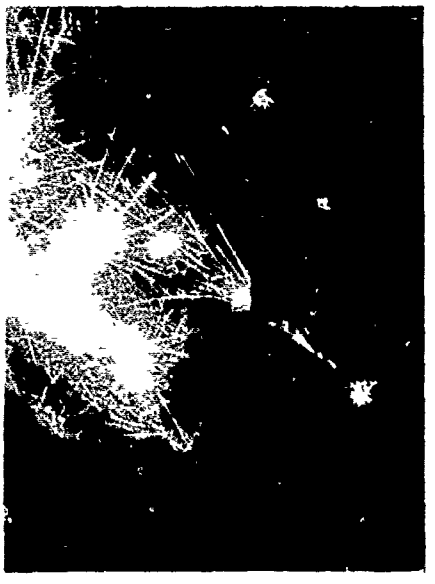

B. 20 cm DROP
(0.332 newton m)

C. 30 cm DROP
(0.498 newton m)

D. 39.1 cm DROP
(0.647 newton m)

Effect of Drop Height on Spark Formation.

Figure 2

B. Gun Firings

1. Misch Metal and Cerium

Cylinders of the misch metal alloys (4.77 mm diameter and up to 12.7 mm length) and a 12.7 mm diameter hemisphere of pure cerium attached to a wooden dowel were projected against 2024 Dural Sheets and a cold rolled, mild steel brick. The results are shown in Table III.

Table III. Misch Metal Impacts on Dural and Steel

Run No.	Projectile	Mass, Grams	Velocity, Ft/Sec	Velocity, Meters/Sec	Kinetic Energy N-met.	Target	Sparks
1	75M2	0.16	893	272	5.9	Dural	Some
2	75M2	1.22	815	248	41.5	Dural	Yes
3	75M2	1.39	2496	761	402	Dural	Yes
4	Pure Cerium	-	674	205	-	Mild Steel	Yes
5	75M2	0.26	367	112	1.6	Mild Steel	Some
6	75M2	0.210	795	242	6.1	Mild Steel	Yes
7	75M2	1.44	695	212	32.3	Mild Steel	Yes
8	95M	1.42	718	219	34.1	Mild Steel	Yes
9	100X	1.43	707	215	33.1	Mild Steel	Yes

The kinetic energy threshold for sparking of 75M2 on Dural (0.16 grams at 272 meters/sec) is on the order of 5.9 newton meters. The threshold against mild steel is somewhat lower, 1.6 newton meters (0.26 grams at 112 meters/sec). These results are an order of magnitude higher than the temperature sensitized impacts reported in the previous section.

2. Zirconium

Cylinders of pure zirconium and Grade 11 zirconium (3 mm and 4.77 mm diameter, respectively) were projected against 2024 Dural, mild steel, and steel armor. The results are shown in Table IV.

Table IV. Zirconium Impacts on Dural and Steel

Run No.	Projectile	Mass, Grams	Velocity, Meters/Sec	Kinetic Energy N-met.	Target	Sparks
1	Grade 11	1.31	247	40	Dural	No
2	Pure Zirconium	.30	192	5.6	Dural	No
3	Pure Zirconium	.64	264	22	Dural	No
4	Pure Zirconium	.64	397	50	Dural	Some
5	Pure Zirconium	.30	592	52	Dural	Some
6	Pure Zirconium	.61	804	197	Dural	Some
7	Pure Zirconium	.57	245	19	Mild Steel	No
8	Pure Zirconium	.57	258	20	Mild Steel	Some
9	Pure Zirconium	.60	358	38	Mild Steel	Yes
10	Pure Zirconium	.60	816	20	Mild Steel	Yes
11	Pure Zirconium	.58	250	18	Steel Armor	Some
12	Pure Zirconium	.57	319	28	Steel Armor	Yes
13	Pure Zirconium	.56	664	123	Steel Armor	Yes

The kinetic energy threshold of sparking for zirconium against Dural is 50 newton meters. Thresholds against mild steel and steel armor are 19 and 18 newton meters, respectively. When impacted above the thresholds, the sparks from zirconium do not appear as numerous or intense as those from misch metal.

3. Other Metals

Cylinders of pure titanium (3 mm diameter) 1095 steel (3.00 and 4.77 mm diameter) and hard copper (7.60 mm diameter) were projected against Dural and steel armor.

The results are shown in Table V.

Table V. Titanium, Steel, and Copper Impacts on Dural and Steel

Run No.	Projectile	Mass, Grams	Velocity, Ft/Sec	Velocity, Meters/Sec	Kinetic Energy N-met.	Target	Sparks
1	Pure Ti	0.39	530	162	5.1	Steel Armor	Some
2	Pure Ti	0.39	1307	398	31	Steel Armor	Yes
3	1095 Steel	1.94	2431	741	532	Dural	No
4	1095 Steel	1.94	3274	998	966	Dural	Some
5	1095 Steel	.66	2100	640	135	Steel Armor	Some
6	1095 Steel	.66	2761	842	234	Steel Armor	Yes
7	Copper	1.91	1591	484	224	Dural	No
8	Copper	1.89	3000	914	789	Dural	Some

From these results it can be seen that pure titanium has a somewhat lower sparking threshold (5.1 newton meters) against steel armor than zirconium (18 newton meters). For impacts of 1095 steel on Dural, kinetic energy impacts of 966 newton meters are needed for sparking. For 1095 steel on steel armor, the threshold drops to 135 newton meters. For the relatively soft copper cylinders against Dural Sheets, the threshold is 789 newton meters which is on the order of steel against the same target.

IV. CONCLUSIONS

Thresholds of sparking were measured for both pyrophoric and non-pyrophoric metals projected against targets of aluminum and steel. The measured thresholds are higher than temperature sensitized impacts of pyrophoric metals in a drop weight apparatus. For example, 75M2 misch metal sparked when impacted with a kinetic energy of 0.332 newton meters while glowing, but the same metal at ambient temperature needed 1.6 newton meters when projected against a mild steel plate.

Impacts against a slightly softer material such as 2024 Dural had a slightly higher threshold. Thus, the same misch metal, 75M2, had a sparking threshold of 5.9 newton meters against Dural compared with 1.6

newton meters against mild steel. Similarly, zirconium against Dural needed 50 newton meters for sparking, but only 20 against mild steel.

The relatively non-pyrophoric metals such as steel and copper had thresholds of 966 and 789, respectively, against Dural compared with misch metal and zirconium which gave 5.9 and 50 respectively. Thus, the distinction between pyrophoric and non-pyrophoric metals shows up in orders of magnitude for ambient impacts.

ACKNOWLEDGMENT

The author wishes to thank C. Roop and E. Donnelly for their assistance in projecting the rods against the targets.

REFERENCES

1. I. Hartmann, J. Nagy, and M. Jacobson, "Explosive Characteristics of Titanium, Zirconium, Thorium, Uranium and Their Hydrides," BMRI 4835, (1951).

2. B. Kopelman and V. B. Compton, Metal Progress, 63(2), 77 (1953).

3. C. R. Schmitt, J. Fire and Flammability, 2, 157 (1971).

4. "Handbook of Chemistry and Physics," The Chemical Rubber Co., Cleveland, Ohio, 53rd Edition (1972).

5. U. Kask, "Chemistry: Structure and Changes of Matter," Barnes and Noble, Inc., New York, 1969.

6. H. Ellern, "Military and Civilian Pyrotechnics," Chemical Publishing Co., Inc., New York, 1968.

7. G. E. Zima, "Pyrophoricity of Uranium in Reactor Environments," AECHW-62442 (1960).

8. J. R. Gibson and J. D. Weber, "Handbook of Selected Properties of Air - and Water-Reactive Materials," U.S. Naval Ammunition Depot, Crane, Indiana, RDTR No. 144, AD 699427, (1969).

9. W. W. Hillstrom, "Formation of Pyrophoric Fragments," BRL MR 2306, AD 765447, (1973).

10. D. Rae, "A Measurement of the Temperature of Some Frictional Sparks," Combustion and Flame, 5, 341 (1961).

A STUDY OF FAST BURNING TUNGSTEN DELAY COMPOSITIONS IN SMALL COLUMN DIAMETERS

Scranton G. Nesbitt

ABSTRACT:

The ability of four relatively fast burning tungsten delay compositions (MIL-T-23132, Series I) to burn in small column diameters was studied. The compositions tested had specification burning rates which ranged from 0.379 sec/in to 2.759 sec/in. In this study column diameters of 0.039 in. to 0.055 in. and column lengths of 0.100 in. to 1.000 in. were used. The burning rates of the four compositions were measured in several column diameter-column length combinations at ambient and extreme temperatures. In general, changes in column diameter affected the magnitude and uniformity of burning rates less than the changes in column length. Extreme temperatures did not produce major changes in burning rate uniformity. Results indicate that the use of such delay compositions is feasible in small diameter components such as might be employed in miniaturized explosive trains.

A STUDY OF FAST BURNING TUNGSTEN DELAY COMPOSITIONS IN SMALL COLUMN DIAMETERS

Scranton G. Nesbitt
Naval Ordnance Laboratory
White Oak, Silver Spring, Maryland

INTRODUCTION

The purpose of this study was to evaluate the abilities of four Series I, MIL-T-23132[1], tungsten delay compositions to propagate in small column diameters. This work was confined to studying fast burning Tungsten delay compositions in bodies which constituted extremely large heat sinks. The effects of column diameter, column length, and extreme temperatures on the delay burning rates are presented.

In many weapon designs minimization of fuze or explosive train weight and size is of great interest. Studies such as the one reported here can provide information to assist weapon and fuze designers in selecting designs and materials which are feasible for miniaturized applications.

Unfortunately, in general, miniaturization cannot be accomplished by direct downscaling of normal sized explosive items. Smaller columns and smaller quantities of explosives and pyrotechnics, reduced confinement, and alignment difficulties often bring about changes in sensitivity, reliability, and safety, which cannot be accurately predicted. Materials, such as delay compositions, with relatively slow chemical reactions are of particular concern in small column diameters, because the reaction zone is particularly vulnerable to excessive heat loss[2]. For this reason it was of particular interest to establish the feasibility of using this group of Tungsten delay compositions in small column diameter components.

The four tungsten compositions used in this study were purchased from Pyrotechnic Specialties, Inc., Byron, Georgia.* The specification burning rates, as certified by the manufacturer, are given in Table 1 for room temperature and -54°C. The composition numbers were assigned for identification and go from the fastest burning composition, #1-W, to the slowest burning, #4-W.

APPARATUS AND METHOD

All burning rate measurements were made with the delay compositions loaded in bodies of the same material and outside diameter as required for the specification burning rate test. Figure 1-A shows cross sections of the body required for the specification test[3] and all bodies used in this study. They were all machined from 2024-T4 aluminum with a 0.498-inch O.D. The inside diameters or column diameters used in this study (0.055, 0.047, and 0.039 inch) are very small compared to the 0.261-inch I.D. for the specification burning test. The first burning rate tests were conducted

*Discussion of specific commercial products does not imply either endorsement or criticism of them by the Naval Ordnance Laboratory.

using bodies 1.060 inches long with 0.055-inch I.D. Because of difficulties in drilling smaller diameter holes as true as desired in 1.060-inch long bodies, the body length was reduced to 0.460 inch. The 0.160-inch long bodies (of Figure 1) were used to check the effect of short delay column lengths on the burning rate.

The lengths of the delay bodies allow space for a 0.060-inch long increment of A-1A ignition mix in addition to the desired delay column length. Figure 1-B shows a typical loaded delay body. In all cases the A-1A and the delay composition were loaded at 30,000 psi. The delay compositions were loaded in increments so that the ratio of increment length to the column diameter was always within the limits of 1.0 to 1.4. A small spot of basic lead styphnate was placed on the output end of each delay column to provide a bright flash when the burning front reached the end of the delay column.

Delay column burning times were measured electronically; Figure 2 is a diagram of the test arrangement. An electric match was used to initiate the A-1A ignition mix, which in turn ignited the tungsten delay column. Light from the match was transmitted by a Crofon Light Guide or light pipe to a photomultiplier which started an electronic timer. When the burning front reached the end of the delay column, the basic lead styphnate spot charge emitted a flash of light which was transmitted by another light pipe to a photomultiplier which stopped the timer.

Thus, the timer measured the burning time of the delay column plus the small A-1A increment. The burning rate of the tungsten delay composition was determined from the measured burning time by subtracting an average A-1A burning time and dividing by the delay column length. It should be noted that all burning rates will be given in seconds per inch.

TESTS AND RESULTS

Burning rate tests were conducted using 0.055-inch diameter delay columns 1.000 inch long at room temperature, -54°C, and +71°C. Fifteen samples were tested at each temperature. The hot and cold samples were conditioned at their respective temperatures for at least three hours and were fired within twenty seconds after being removed from the conditioning chamber. The average burning rates and coefficients of variation are shown in Table 2. At -54°C the delay compositions burned from 9.5% to 17% slower than at room temperature. This can be compared to changes of 4% to 9% in the specification test data supplied by the manufacturer (see Table 1). At 71°C they burned from 11% to 13% faster than at room temperature. Figure 3 is a plot of the average burning rates as a function of temperature; the range of experimental measurements is shown for each test. The burning rate data from Table 1 (0.261-inch column diameter) are also plotted for comparison. The small column diameter and the large heat sink bodies caused a greater difference in the extreme temperature burning rates of the slowest burning composition (#4-W) than for the faster ones.

However, the observation that all four propagated reliably at -54°C was considered significant and encouraging. It is not known why the burning rates of #s 2-W, 3-W, and 4-W measured by the manufacturer in the 0.261-inch column diameters are slower than these measured in small diameter columns.

Tests were conducted at room temperature to study the effect different column lengths would have on burning rate. Burning rates were determined for 0.055-inch diameter delay columns 1.000-inch long, 0.400-inch long, and 0.100-inch long. The burning rates and coefficients of variation are shown in Table 3. The greatest percentage change was observed between the 0.400-inch and the 0.100-inch long delay columns. The compositions burned from 19% to 26% slower in 0.100-inch columns than in 0.400-inch columns. This apparent effect of column length on burning rate is an unusual observation, since the burning rate of a delay composition is generally thought to be independent of the length of the column. Realizing that variations in the burning times of the 0.060-inch long increments of A-1A would have a greater effect on the burning rate calculations for short columns than longer columns, calculations were performed to determine if the large change in burning rates could be accounted for by observed variations in A-1A burning rates. Though it is possible some of the difference in delay burning rates could be accounted for by variations in A-1A burning rate, the data of this study do not justify totally discounting the observed relation between column length and burning rate on the basis of variations in A-1A burning rates.

It may be possible to explain the slower burning rates for short delays by considering the heating of the delay bodies by the burning A-1A and delay compositions. Even with the heat liberated from the A-1A ignition charge, it is possible that the delay composition and body immediately preceding the burning front will not reach a thermal equilibrium relative to the burning front until the front has propagated some distance. The distance required would probably depend on parameters such as column diameter, delay burning rate and heat output, thermal conductance and heat capacity of the body, and initial temperature. Such an effect may not be as obvious for delays with relatively large column diameters or in relatively thin wall bodies, since in such cases a thermal equilibrium would be established much sooner relative to the burning front.

Though all tests in this study were conducted using small column diameter delays, it was of particular interest to determine the effect changes in column diameter might have on burning rates. It was also of interest to determine at what column diameter failures would be observed. Table 4-A shows average burning rates and coefficients of variation for groups of samples with delay columns 0.400-inch long and diameters of 0.055-inch, 0.047-inch, and 0.039-inch. Table 4-B provides a comparison of the cross sectional areas of the three column diameters. The values of the diameters may seem relatively close together; however, from the cross sectional areas it is apparent that they represent significant changes. As for the effect column diameter changes had on burning rates, it was not possible from these tests to identify any clear relationship between column diameter and burning rate.

The most significant result shown in Table 4 is that three of five samples of the slowest burning delay composition, #4-W, failed to burn the full length of the 0.039-inch diameter columns. Thus, 0.039 inch is very close to the effective failure diameter of that composition in the type body used. However, the burning rates for the two samples that did burn the full length of the column were 2.68 sec/in and 2.68 sec/in; these are within 1% of the average burning rates for the larger diameter samples.

Since failures had been observed for the slowest burning composition in 0.039-inch diameter columns, it was of interest to determine if the other three compositions could propagate reliably in this diameter column at a reduced temperature. Five samples of each delay composition were conditioned at -40°C for at least three hours and were fired within twenty seconds after being removed from the conditioning chamber. Average burning rates and coefficients of variation are given in Table 5 for the three faster burning delay compositions in 0.039-inch diameter columns, 0.400-inch long, at -40°C and room temperature. These data with the range of measurements for each test are plotted in Figure 4 along with corresponding data for 0.055-inch diameter, 1.000-inch long columns from Figure 3. The slopes of the lines for the 0.039-inch diameter samples are not significantly different from those for the 0.055-inch diameter samples. Thus, there is no particular evidence of marginal performance for these three Tungsten delay compositions in 0.039-inch diameter columns in thermodynamically massive bodies at -40°C. It is believed that the shift in the data (0.039-inch samples burning at a slower rate than the 0.055-inch samples) is primarily caused by the difference in column length rather than column diameter.

As previously noted, all burning rates given have been corrected for the 0.060-inch long A-1A ignition mix increment in each sample. Tests to measure the burning rate of A-1A were conducted using bodies of the same type used for the delay testing. Column diameters of 0.055-inch and 0.039-inch were used. The spreads in the data were rather large with coefficients of variation as high as 21% (for the 0.039-inch diameter group). The average burning rate of the A-1A was taken to be 0.300 sec/in. Thus, 0.018 second was subtracted from each delay composition burning time measurement when calculating the corrected burning rates.

SUMMARY AND CONCLUSIONS

The four relatively fast burning Series I, MIL-T-23132, Tungsten delay compositions tested, all propagated reliably at room and extreme temperatures in columns 0.055-inch in diameter. However, the differences in burning rates from room temperature to -54°C were found to be greater than the differences determined by the manufacturer for 0.261-inch diameter columns. The burning rates of all four compositions were found to be significantly slower in short (0.100-inch) column lengths than for longer columns. In the small column diameters studied (0.055-inch to 0.039-inch), no correlation between column diameter and burning time was observed. The slowest burning delay composition did not propagate reliably in the

0.039-inch diameter column (3 of 5 failed). At -40°C the other three compositions still performed satisfactorily (5 of 5 burned) in 0.039-inch diameter columns. The burning rate of A-1A, in small column diameters, was found to be approximately 0.30 sec/in.

Relatively fast burning, Series I, Tungsten delay compositions, like those studied, can be considered for miniaturized applications based on the results of this study. The severe thermal penalties imposed in this study (bodies which were very large heat sinks and low temperature testing) allow reasonable confidence that such compositions could be used reliably in properly designed miniaturized systems.

TABLE 1 BURNING RATES CERTIFIED BY MANUFACTURER*

Delay Composition Number	Burning Rate in sec/in and (Coefficient of Variation)	
	Room Temperature (24.4°C)	-54°C
#1-W	0.3792 (6.11%)	0.4024 (6.006%)
#2-W	0.9084 (0.413%)	0.9889 (0.797%)
#3-W	1.6543 (0.449%)	1.800 (1.302%)
#4-W	2.7588 (2.533%)	2.8584 (3.575%)

* Burning rates measured using 0.261 inch diameter delay columns 1.00 inch long.

TABLE 2 EFFECT OF TEMPERATURE EXTREMES ON BURNING RATES

Temperature of Delay Bodies (°C)	Burning Rate and (Coefficient of Variation)			
	#1-W (sec/in)	#2-W (sec/in)	#3-W (sec/in)	#4-W (sec/in)
-54	0.49 (2.05%)	0.92 (2.90%)	1.63 (1.95%)	2.73 (1.88%)
+24 (room temperature)	0.42 (3.25%)	0.82 (2.24%)	1.46 (2.54%)	2.50 (1.81%)
+71	0.37 (1.32%)	0.72 (2.83%)	1.30 (2.14%	2.22 (2.40%)

All samples had 0.055-inch diameter and 1.000-inch long delay columns.

All burning rates have been adjusted to account for burning time of A-1A.

TABLE 3 EFFECT OF CHANGES IN COLUMN LENGTH ON BURNING RATES

Delay Column Length (Inches)		Burning Rate and (Coefficient of Variation)			
		#1-W (sec/in)	#2-W (sec-in)	#3-W (sec/in)	#4-W (sec/in)
1.000	(1)	0.42 (3.25%)	0.82 (2.24%)	1.46 (2.54%)	2.50 (1.81%)
0.400	(2)	0.42 (2.15%)	0.81 (3.48%)	1.59 (4.45%)	2.69 (1.83%)
0.100	(1)	0.52 (5.57%)	1.02 (3.41%)	1.88 (6.14%)	3.25 (4.72%)

All samples had 0.55-inch column diameter.

All tests were conducted at room temperature.

All burning rates have been adjusted to account for burning time of A-1A.

(1) Each burning rate is an average from 15 samples.

(2) Each burning rate is an average from 5 samples.

TABLE 4A EFFECT OF CHANGES IN COLUMN DIAMETER ON BURNING RATE

Delay Column Diameter (inches)		Burning Rate and (Coefficient of Variation)			
		#1-W (sec/in)	#2-W (sec/in)	#3-W (sec/in)	#4-W (sec/in)
0.055	(2)	0.42 (2.15%)	0.81 (3.48%)	1.59 (4.45%)	2.69 (1.83%)
0.047	(1)	0.46 (3.45%)	0.87 (3.46%)	1.64 (1.94%)	2.71 (1.50%)
0.039	(2)	0.44 (3.39%)	0.87 (3.15%)	1.56 (2.39%)	(3)

All burning rates have been adjusted to account for burning time of A-1A.
All tests were conducted at room temperature.
All samples had 0.400-inch long delay columns.

(1) Each burning rate is an average from 15 or 16 samples.
(2) Each burning rate is an average from 5 samples.
(3) Three of five samples did not burn the full length of the delay columns.

TABLE 4B CROSS SECTIONAL AREAS OF DELAY COLUMNS

Column Diameter (inches)	0.055	0.047	0.039
Cross-Sectional Area (square inches)	0.002376	0.001735	0.001195
% of largest area	100%	73%	50%

TABLE 5 BURNING RATES OF 0.039-INCH COLUMN DIAMETER SAMPLES AT ROOM TEMPERATURE AND -40°C

Temperature of Delay Bodies (°C)	Burning Rates and (Coefficient of Variation)		
	#1-W (sec/in)	#2-W (sec/in)	#3-W (sec/in)
-40	0.49 (14.51%)	0.97 (3.81%)	1.70 (2.28%)
24	0.44 (3.39%)	0.87 (3.15%)	1.56 (2.39%)

All samples had 0.400-inch long delay columns.
All burning rates have been adjusted to account for burning time of A-1A.
Each burning rate is an average from 5 samples.

FIGURE 1

A. DELAY BODIES

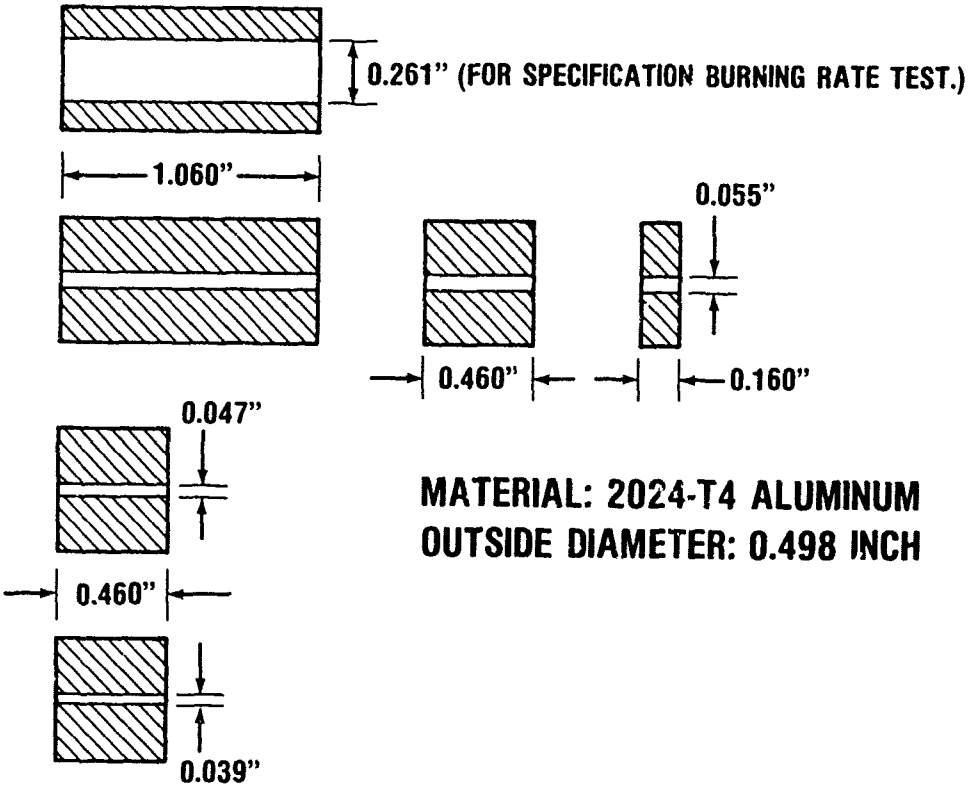

MATERIAL: 2024-T4 ALUMINUM
OUTSIDE DIAMETER: 0.498 INCH

B. DELAY BODY LOADING

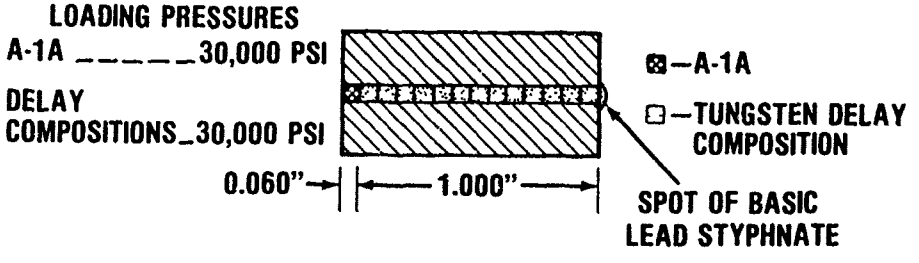

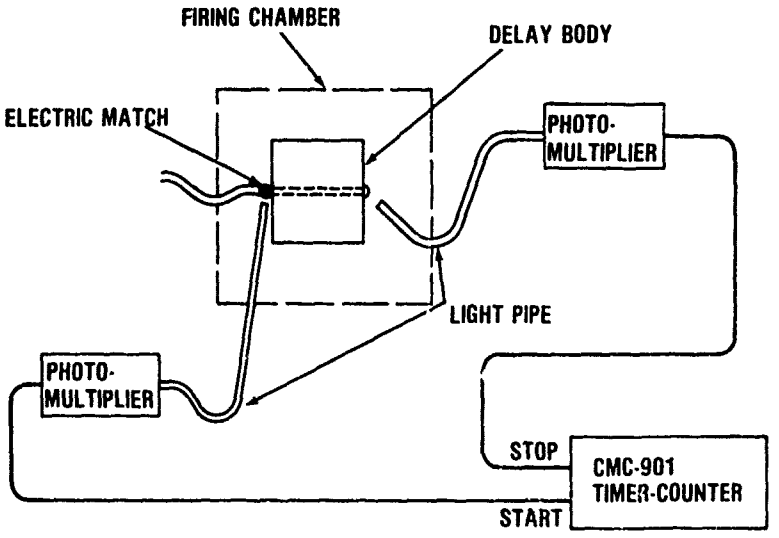

FIGURE 2 ARRANGEMENT FOR MEASURING DELAY BURNING TIMES

FIGURE 3 TEST TEMPERATURE VS BURNING RATE FOR 0.055 INCH AND 0.261 INCH DIAMETER COLUMNS

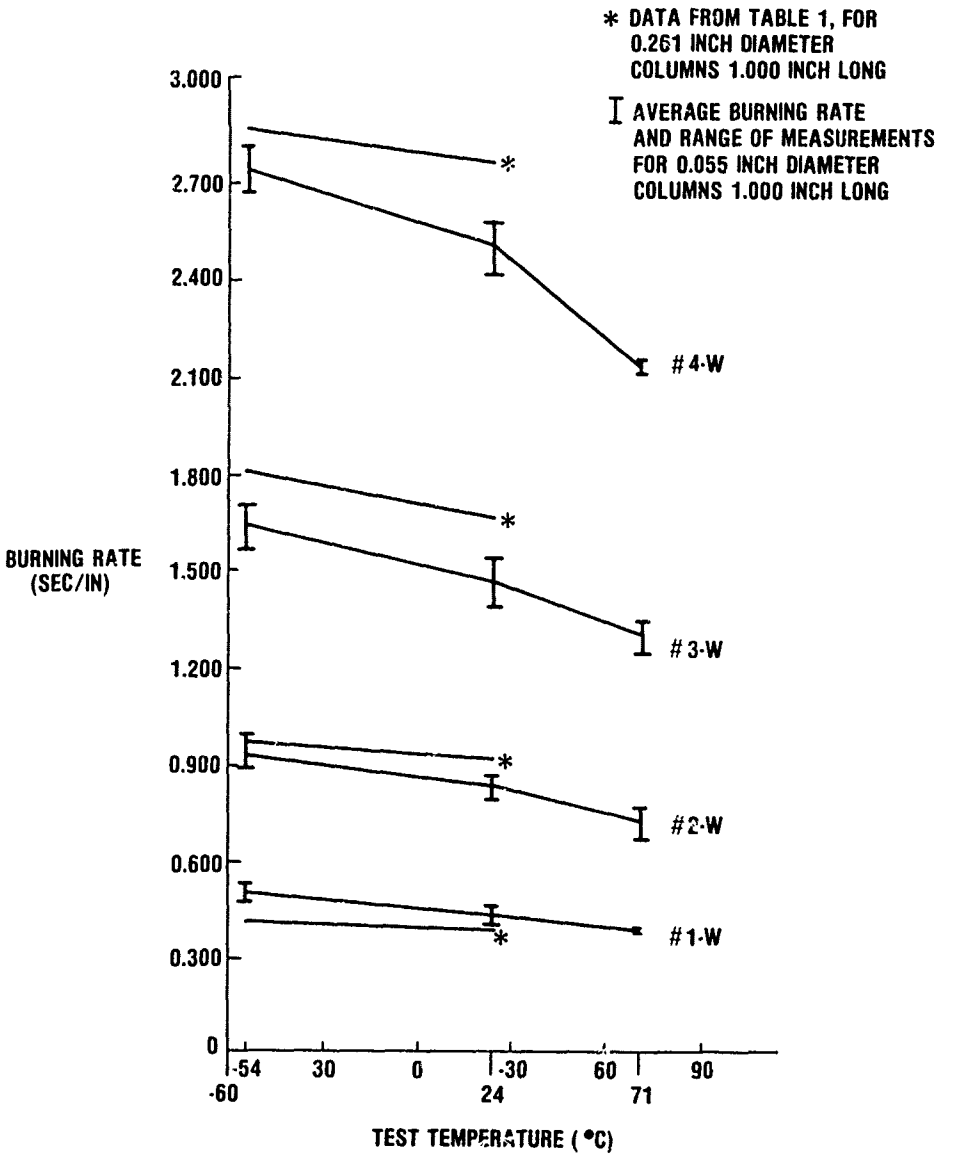

FIGURE 4 TEST TEMPERATURE VS BURNING RATE FOR SMALL DIAMETER COLUMNS

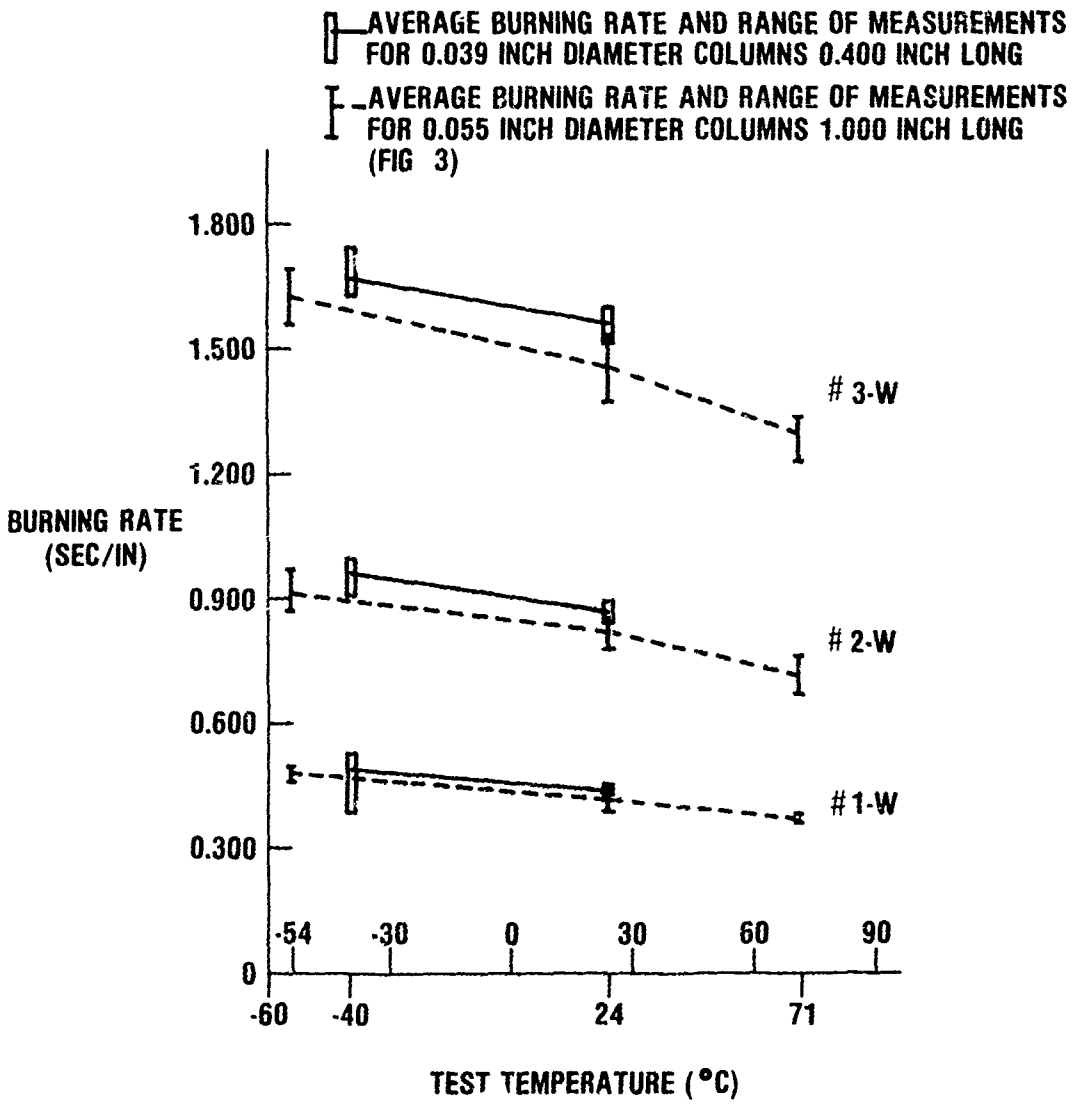

A Pyrotechnic Fuze Timer with Selectable Settings

by

W. Keith Gallant
Honeywell Inc.

Abstract

Selectable times of from 3 to 60 seconds in increments of one second can be provided by a timer module incorporating pyrotechnic delay cord. The timer, which consists of a potted delay module and a rotor containing a primer and a relay, can be functioned from either a percussion primer or a stab firing pin. The timer has been packaged in a cylinder .55 inch high and 1.71 inch in diameter.

In the evaluation phase of the design effort, a total of seven batches of delay cord was obtained from three vendors. The cord was processed into timer modules; however, between each length required for a module, a ten inch length was set aside. The ten inch lengths were tested at room temperature with excellent reproducibility. The spread of the coefficient of variation (C.V.) of the burning rate of the ten inch strands for the several batches tested was a maximum of 1.95 percent and a minimum of 0.75 percent. Testing of delay modules at various temperatures resulted in C.V.'s of from 2.0 to 4.2 percent.

The effect of temperature on burn rate was quite small ranging from 7.4×10^{-4} to 1.4×10^{-3} second/inch/°F over the range of -65°F to +165°F for two batches.

Limited environmental testing was conducted and indicated that requirements for transportation vibration and storage at +165°F can be met. Eighteen (18) rounds ballistically tested at shock levels up to 10,000 g's showed no shock damage.

TRACER MUNITIONS USING INTERMETALLIC REACTIONS

by

A. P. Hardt

Lockheed Palo Alto Research Laboratory, 3251 Hanover Street
Palo Alto, California 94304

ABSTRACT

The use of intermetallic reactions for tracer munitions was demonstrated on a coarse mixture of titanium powder with amorphous boron. Methods of improving the charge retention and factors affecting the trace visibility are described. The results confirm the findings made in preceding studies on the mechanism and rates of gasless reactions and suggest that in certain tracer applications intermetallic reactions may constitute a new and promising type of pyrotechnic system.

Section 1
INTRODUCTION

CHARACTERISTICS OF INTERMETALLIC REACTIONS

When certain powdered metals are mixed with powdered elements of the transition subgroups of the periodic table and subjected to an intense heat pulse, a strongly exothermic reaction may take place which results in an alloy or intermetallic compound. This reaction occurs without gas formation and therefore resembles gasless redox systems such as thermites. The study of intermetallic reactions for possible application in pyrotechnic devices is of recent origin (Refs. 1,2), and the findings have brought about an improved understanding of gasless pyrotechnic reactions (Refs. 3 to 5). Intermetallic reactions occur in a self-sustained manner only when the adiabatic reaction temperature exceeds the melting temperature range of the alloy. In practice, such reactions occur in mixtures of boron, carbon, or aluminum with nickel, palladium, platinum, titanium, and zirconium as well as in some mixtures with alkali and alkaline earth metals. For most applications, aluminum containing systems require excessively high initiation energies and good thermal insulation to prevent quenching, whereas the initiation energies of alkali metal mixtures are so low as to present a safety hazard. The addition of intermetallic reaction mixtures to some pyrotechnic systems has brought about improved performance and reliability (Refs. 6 and 7). Table 1 lists some properties of intermetallic reaction mixtures.

OBJECTIVE

This study was undertaken to test the feasibility of using intermetallic reactions in tracer bullets. The high reaction temperature and the brilliant display suggested their employment to improve the visibility of the tracers and hence to increase their range.

Table 1

PROPERTIES OF SOME INTERMETALLIC REACTIONS

Intermetallic Product	Heat of Reaction (cal/g)	Computed Adiabatic Reaction Temperature (°C)	Measured Brightness Temperature (°C)
TiB_2	1155	3770	3300
ZrB_2	690	3400	3240
TiC	737	3600	2050
ZrC	461	3800	1540
NiAl	329	1639	–
PdAl	327	2380	–
PtAl	216	2300	–

Section 2
FACTORS AFFECTING THE VISIBILITY OF TRACER BULLETS

The visibility of tracers depends on the brightness of the background as well as on the illuminance of the tracer on the eye. Each background brightness has an associated threshold illuminance for the human eye. The values of the threshold illuminance under average day and night conditions are given in Table 2.

Table 2
MINIMUM COLOR SENSITIVITY OF HUMAN EYE (Ref. 10)

Color	Illuminance (lm/m^2)	
	Day Time	Night Time
Red	0.5×10^{-3}	0.8×10^{-6}
Green	0.9×10^{-3}	1.2×10^{-6}
Yellow	1.0×10^{-3}	2.0×10^{-6}
White	1.5×10^{-3}	3.0×10^{-6}

The illumination E, of a spherical surface of radius r, enveloping a point source of intensity I is given by

$$E = \frac{I}{r^2} \quad lm/m^2 \tag{1}$$

The luminous intensity of a burning tracer bullet depends on the temperature and the psychophysical standard visibility function. These have been computed (Ref. 10) for the temperature interval between 1000 and 5000°K. We have assumed that crimping the bullet will reduce the exposed area by 55 percent and that the emissivity correction is inherent in the use of the brightness temperature. These data are plotted in Fig. 1

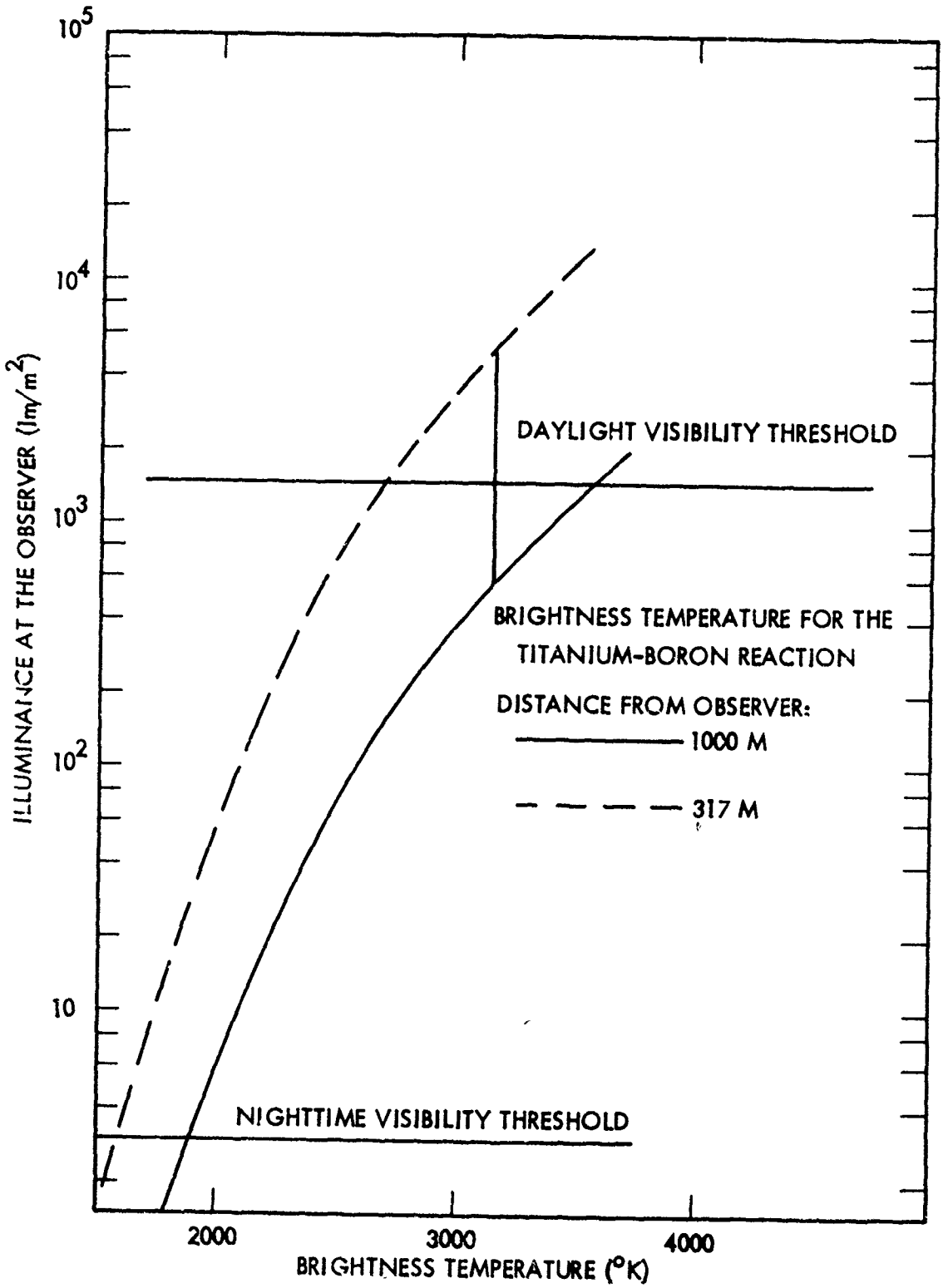

Fig. 1 Luminous Intensity of Crimped Tracer Bullet

for a distance r of 1000 m and 317 m from the observer. It is evident that a titanium-boron mixture reacting with a (experimentally determined) brightness temperature of 3300°K will not be visible in daylight at distances much in excess of 300 m. In reality, one must expect that the trace intensity will be reduced further by heat losses to the bullet and by the inevitable presence of a wake and smoke.

One would therefore conclude that daylight visibility of intermetallic reaction tracers would be insufficient unless some effort is devoted to providing for smoke generation. It may not be possible to combine good daylight visibility and good nighttime visibility in the same tracer munition.

Figure 1 also shows the nighttime visibility threshold. As long as the bullet has a brightness temperature of 1900°K, the bullet will be visible at night. We have measured the temperature-time history of stationary bullets and found that, by a graphical analysis (Fig. 2), intermetallic reaction tracers should be visible for 700 to 800 m, depending on composition and particle size of the constituents.

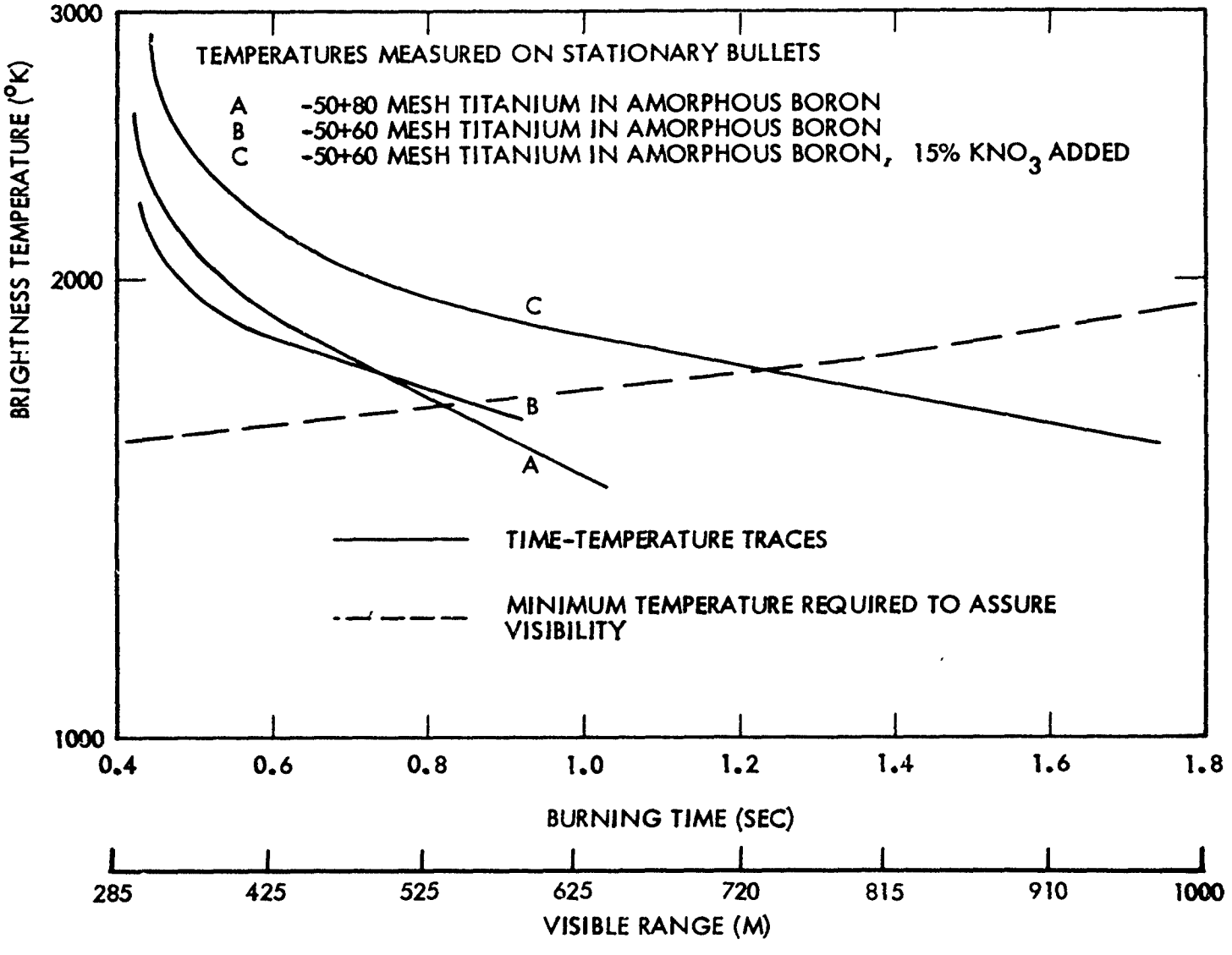

Fig. 2 Prediction of Intermetallic Reaction Tracer Nighttime Visibility

Section 3
APPARATUS AND PROCEDURE

Based on the preceding analysis titanium-boron mixtures were selected for testing in tracer bullets. Empty 30-caliber tracer bullets were filled with intermetallic reaction mixture and pressed to 100,000 psi. One grain each of an igniter and a dim trace igniter was then added, followed by a second pressing to 100,000-psi and slight crimping. The appearance of the completed bullet is shown in Fig. 3. No metal base closure was employed.

All materials were procured from commercial sources as shown in Table 3 and used without further treatment except for the titanium powder which was passed through a 60 mesh screen in order to remove the fine particles. The igniter was a mixture of 40% CuO, 10% Al, 45% $BaCrO_4$, and 5% B. The dim trace igniter consisted of 10% calcium resinate and 90% SrO_2.

Table 3
PROPERTIES OF MATERIALS

Material	Mesh or Particle Size	Supplier
Titanium (Ti)	-50 +60 mesh	Atlantic Equipment Engineers -50 +100 mesh grade received
Zirconium (Zr)	2 μm G Grade	Foote Mineral Company
Aluminum (Al)	10 μm	Atomized, Class 400, Organic-Inorganic Research Chemicals, Inc.
Boron (B)	0.1 μm	U. S. Borax, 95% Grade
Barium ($BaCrO_4$) Chromate	-325 mesh 98% 0.7 μm	Ceramic Chemical Manufacturers MIL B 550-A
Cupric Oxide (CuO)	2 μm	Harshaw Chemical Company MIL C 13600

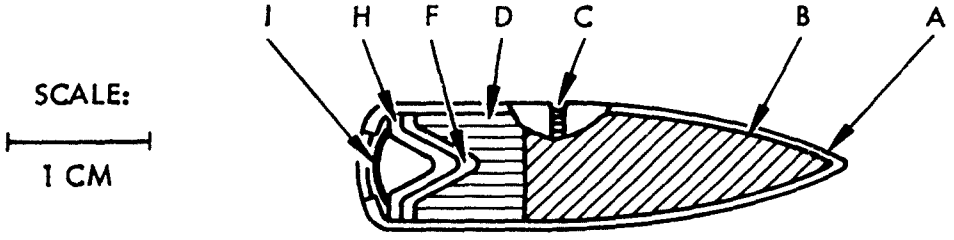

(a) TRACER BULLET, NATO 7.62 mm

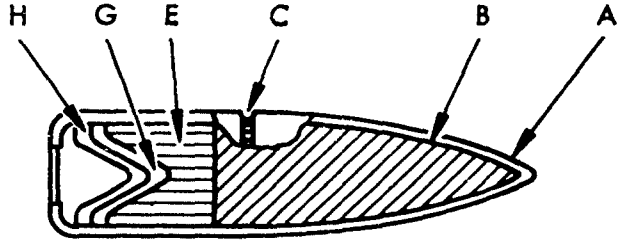

(b) INTERMETALLIC REACTION TRACER BULLET

LEGEND:

A	GILDING METAL CLAD STEEL JACKET	F	SUBIGNITER I-280
B	LEAD POINT FILLER	G	IGNITER CABB 50
C	CANNILURE	H	DIM TRACE IGNITER I-136
D	TRACER COMPOSITION R-284	I	CUP CLOSURE
E	INTERMETALLIC REACTION MIXTURE		

Fig. 3 Schematic Drawing of Tracer Bullets

The static burn tests were performed by contacting the back of the bullet with a hot Nichrome wire. The burn was observed with an Infrared Industries TD 11S pyrometer. The output was displayed on a Type 556 Tektronix oscilloscope and recorded on Polaroid film. The pyrometer was calibrated in the high-temperature region against the melting points of molybdenum, tantalum, and tungsten; in the low-temperature region a Bureau of Standards standard lamp was used. The threshold for detection was about 1000°C. No emissivity corrections were required in this study because the luminous output was measured in terms of brightness temperatures.

Sample rounds were prepared by handloading primed cartridges.

The rifle range studies were performed with a M14 rifle. The traces were recorded on B&W film at 100 f/s using a Millikan Model S framing camera. The trace duration was analyzed on a Vanguard film analyzer. When a frame count was used to determine the visibility range of intermetallic reaction tracers any differences in sensitivity between film and the human eye in discerning the trace were ignored. Interpretation of tracer visibility was aided by the placement of an observer about 500 m downrange from the weapon. In general the observer's reports agreed with those of the test personnel stationed at the firing stand. It appears as if the visible range might be somewhat greater than the value obtained from a frame count.

Tests were conducted at Fort Ord, Monterey, California, where the range was in excess of 1000 m.

Section 4
RESULTS OF RIFLE RANGE TESTS

Preliminary tests had shown that fine metal powder would give rise to muzzle flash and subsequent break-up of the tracer charge downrange. Intermetallic mixtures other than titanium-boron were found to be distinctly inferior for tracer applications so that the main effort was devoted to perfecting the titanium-boron tracer concept. By using metal powder in excess of 200 μ, the problems of muzzle-flash and spillage were virtually eliminated. Figure 2 also shows that in laboratory tests significant improvement in visibility was attained when an oxidizing additive was added. Therefore, the titanium was resieved onto a 60-mesh screen and nitrates of strontium, cesium, potassium, and sodium were added. Further improvement in performance can be expected for titanium grades coarser than 50 mesh. Table 4 shows the improved formulations, some of which had a visible range of better than 550 m. The trace durations were obtained from a frame count of the motion-picture records, and a range table for 7.62-mm M62 tracers. While the improved traces were reliable and reproducible, the visibility did decrease with distance. The maximum visible range may not be limited as much by the rate of reaction or by any possible effect of spin on the molten lead as by the small size of the luminous surface.

Table 4

FORMULATIONS FOR INTERMETALLIC REACTION TRACER BULLETS[a]

Intermetallic Reaction Mixture -50 +60 Mesh Titanium, 95% Amorphous Boron	Approximate Range (m)[b]
90% Ti/2B, 10% Sr $(NO_3)_2$	500
85% Ti/2B, 15% Sr $(NO_3)_2$	500
80% Ti/2B, 20% Sr $(NO_3)_2$	Some breakup
85% Ti/2B, 15% $CsNO_3$	275
85% Ti/2B, 15% KNO_3	530
85% Ti/2B, 15% $NaNO_3$	550

(a) All bullets were loaded with 0.46 ± 0.015 g of intermetallic reaction mixture, tapped, charged with 0.065 g of Igniter, and compressed to 100,000 psi; then 0.065 g of dim trace igniter was added. The total charge was then compressed again to 100 Kpsi. For both compressions, a plunger with a teat was used. The loaded bullet was then crimped slightly.

(b) Average of 5 tests.

Section 5
DISCUSSION OF EXPERIMENTAL RESULTS

Table 1 lists some of the intermetallic reaction characteristics which were determined in a previous study (Ref. 1). The results of this study confirm the predictions which were made on the basis of these data. The quantity which controls the visibility of an intermetallic reaction tracer is the brightness temperature. Figure 2 shows that the maximum visible range will be about 720 m, but that somewhat improved performance might be expected from a still coarser mixture. These figures are in acceptable agreement with the observed visibility ranges of 550 m as shown in Table 4. These numbers are somewhat less than the visible ranges predicted from the brightness temperature alone because of radiative and conductive heat losses and because of the fact that the reaction in coarse mixtures is not completed within the time frame. Furthermore, adiabatic reaction temperatures are determined by the fusion temperatures of the products and therefore reflect the presence of an isothermal heat reservoir, while no such reservoir exists if temperatures are lowered because of heat losses or reaction inefficiencies.

It was found empirically that the visibility of the trace improved significantly when an oxidizer was added to the mixture. Calculation of the heats of reaction showed, however, that heat output was increased only negligibly over the starting mixture. It was therefore necessary to look for an explanation elsewhere. Brewer (Ref. 8) has reported that in a reducing atmosphere, B_2O_3 will vaporize as BO. For example, a mixture of B and B_2O_3 should produce 1 atm partial pressure of BO at about 1100°K. BO is stable enough so that even the most stable oxides can be reduced by boron under vacuum conditions. It appears that the luminous signature of the intermetallic tracer reaction is not due to the high grey-body temperature but due to the presence of reaction products which are luminous when they disproportionate in the vapor phase.

An alternative approach would be to select an additive which produces a volatile solid oxide such as SrO. Tests showed no advantage of strontium nitrate as oxidizer over sodium or potassium nitrate. Sodium nitrate produces a higher heat of reaction than does the potassium nitrate as shown in Table 5. It is believed that the corresponding

Table 5

CALCULATED HEATS OF REACTION OF INTERMETALLIC REACTION TRACER MIXTURES

Mixture	Heat of Reaction (cal/g)
Ti/2B + 15% KNO_3	1183
Ti/2B + 15% $NaNO_3$	1240
Zr/2B + 15% KNO_3	785
Zr/2B + 15% $NaNO_3$	826

higher volatility of BO is the main reason for the high visibility of the sodium nitrate containing mixture and not the presence of the Sodium D line in the flame. It will be recalled that titanium forms nitrides and hydrides as readily as oxides and that therefore even with added sodium or potassium nitrate the systems do not act as gas generators except as through the formation of BO. This argument could be demonstrated by repeating the test when the source of the oxygen was a solid oxide such as Fe_2O_3.

COMPARISON OF INTERMETALLIC REACTION TRACERS WITH CONVENTIONAL TRACERS

The performance of the tracer bullets developed in this program was compared with that of standard 7.62-mm tracer bullets. These have a cavity of 11.1 mm and an inside diameter of 6 mm (see Fig. 3). The visible range of these bullets is 775 m as observed in this study. The ignition reliability of current NATO tracers is about 98 percent. The loading is described in Table 6. The NATO tracer also has a thin copper base closure cap which is meant to act as a moisture seal but which does not seem to affect ignition or the existence of a muzzle flash.

Table 6

LOADING OF STANDARD 7.62-mm NATO TRACER BULLET (REF. 9)

Charge	Weight (mg)	Approximate Compression KPSI	Composition (wt%)				
			$Sr(NO_3)_2$	Mg	PVC	Ca Resin Na	SrO_2
Main Charge R-284	422	84	55	28	17		
Subigniter I-280	23	18		15		8.5	76.5
Igniter I-136	65	90				10	90

The purpose of the igniter is to delay initiation of the luminous main charge so as to ensure an initial dim trace. The color of the main trace is red, and the burning rate varies with spin rate. The high degree of compression serves mainly to secure the charge in the cavity against breakup upon launch. The mechanism of the burning rate dependence on spin is not clearly understood, and it has been made, in part, the subject of a current study (Ref. 11). It has been suggested that one reason for the spin dependence is the increase in cavity pressure due to constricted gas flow (Ref. 9).

In conventional tracers the range has been extended by the addition of PVC as well as by the addition of magnesium. The reason for this increased range arises from the creation of a fuel-rich reaction mixture which retards the burning rate and enhances the secondary combustion in the plume.

Similar attempts at extending the range of intermetallic reaction tracers by the addition of diluents to the reaction mixture have failed, because diluents will reduce the reaction temperature and consequently reduce the luminous intensity of the tracer and so shorten the visible range. The relationship between the luminous intensity and the range has been examined in greater detail in Section 2.

It will be noted that in conventional tracer bullets a larger part of the tracer mixture is expelled upon burning and that tracer bullets generate a plume which effectively eliminates the low-pressure vortex in the rear of the bullet, which is one of the characteristic ballistic phenomena that adversely affect the range. Both effects, namely, the elimination of the vortex and the loss of mass during flight, increase the range of the tracer bullets over that of conventional bullets so as to give rise to an accuracy mismatch which is detrimental when tracers are interspersed with conventional bullets in an extended range application. These effects may be to a large degree absent in intermetallic reaction tracers.

Because the reaction mixture in conventional tracers is expelled upon burning, the bullets remain comparatively cool and the lead remains solid. On the other hand, in intermetallic reaction tracers the heat is retained within the bullet so as to cause the lead to melt and to be distributed annularly about the bullet walls under the spin effect.

The bullet tends to discolor in laboratory tests, showing that the mean temperature of the bullet exceeded the oxidation temperature of the gilding metal. Heat transfer from such a bullet in flight is a complex problem which has been examined only in a preliminary way.

Conventional tracers can be tracked from both the rear and from the side because of the highly visible plume. This visibility may either be detrimental when the munition is to be used covertly or it can be beneficial when it is used to direct and orient friendly forces. Intermetallic reaction tracers are not always visible from the side because the luminous source remains contained within the bullet. The covert use of intermetallic reaction tracers depends also on the availability of a suitable detector.

Both conventional and intermetallic reaction tracers tend to generate a display upon impact and ricochet. Intermetallic reaction tracers, moreover, tend to have spotting characteristics when impact is not much in excess of 250 m from the observer as shown by a bright display when the bullet impacts on a hard surface. Whether this display is sufficient to ignite volatile liquids is not known.

Section 6
SUMMARY AND CONCLUSION

Intermetallic reaction tracer munitions were shown to be feasible. Visibility diminishes with distance, although most of heat of reaction is retained by the bullet. For this reason the use of intermetallic reaction tracers in covert action applications appears to be of potential interest. If approximately 15 percent of potassium or sodium nitrate are added to a stoichiometric mixture of titanium and boron, ranges of better than 550 m can be achieved. Titanium coarser than 80 mesh tends to prolong the trace duration and to minimize the breakup of the charge in flight. Coarse titanium-boron mixtures require an igniter if the reaction is to function as a tracer. The igniter may be delayed by the use of a conventional dim trace igniter. The trace color is white, as any coloring addition which acts as an energy sink tends to lower the luminous intensity and hence the visible range.

ACKNOWLEDGMENT

This research was conducted under Contract DAAA25-72-C-0319 for the U.S. Army, Frankford Arsenal, Philadelphia, Pennsylvania. Mr. Dennis J. Mancinelli was the program scientist. The author is thankful for the Army's support and permission to publish these results.

REFERENCES

1. A. P. Hardt, Incendiary Potential of Exothermic Intermetallic Reactions, AFATL-TR-71-87, Jul 1971 AD 889403L

2. J. Cohn, "Fuze Member and Method of Making the Same," U. S. Patent 2911504, 1959

3. A. P. Hardt, Development of Improved Incendiary Ignition Systems, AFATL-TR-73-99, Apr 1973 AD-773847

4. A. P. Hardt and P. V. Phung, "Propagation of Gasless Reaction in Solids," I. Analytical Study of Exothermic Intermetallic Reaction Rates, Combustion and Flame, Vol. 21, 1973, pp. 77 – 89
   See also:
   A. P. Hardt and R. W. Holsinger, II. Experimental Study of Exothermic Intermetallic Reaction Rates, Ibid., Vol. 21, 1973, pp. 91 – 97

5. P. V. Phung and A. P. Hardt, "Ignition Characteristics of Gasless Reactions," Combustion and Flame, to be published in 1974

6. R. L. McKenney, Jr., Development of Experimental Intermetallic Forming Starter System for the M1 Smoke (HC) Canister, AFATL-TR-71-136, Oct 1971

7. H. H. Helms, Jr., and A. G. Rozner, Pyronol and Associated Pyrotechnic Devices, Magnesium and Metallurgy Division (211), Naval Ordnance Laboratory, Silver Springs, Md., Jun 1970

8. L. Brewer, "The Thermodynamic Properties of the Oxides and Their Vaporization Processes," Chemical Reviews, Vol. 52, No. 1, 1953, pp. 2 – 75

9. J. J. Caven and T. Stevenson, Pyrotechnics for Small Arms Ammunition, Report R-1969, Frankford Arsenal, Jul 1970

10. M. Hone, "Simulation of Intermetallic Tracer Reactions," Calculation of the Necessary Light Intensity of Intermetallic Tracer Reactions, BCL-D Task Order 72-666

11. A. P. Hardt, Study of Reaction Mechanisms in Tracer Munitions, DAAA 25-73-C-0675, LMSC-D356878, Mar 1974

POLLUTION ABATEMENT
RECLAMATION OF RED PHOSPHORUS SMOKE COMPOSITIONS

Clarence W. Gilliam
and
Duane M. Johnson
Naval Ammunition Depot
Applied Sciences Department
Crane, Indiana 47522

ABSTRACT

Results are presented on a number of methods for the ecologically permissible disposal and reclamation of smoke compositions containing red phosphorus as the principle ingredient. The methods investigated included acid dissolution, wet oxidation and flotation techniques based on density differences. The results indicated that an acid dissolution process was the most likely candidate for pilot plant scale-up. In addition to these results, several interesting technical reactions of pyrolusite (the other major ingredient in these compositions) were observed. The physical and chemical properties were compared with those of pure MnO_2.

INTRODUCTION

Most industrial and military processes create unusable materials, defective units, and units which deteriorate in performance which must be disposed of in some manner.

Our increasing concern for preventing pollution of the environment compelled us to investigate and develop new and/or novel non-polluting methods for pyrotechnic waste disposal or reclamation techniques which would provide a cost savings for the Navy.

This report covers an exploration of the physical and chemical processes involved in the reclamation and/or disposal of the ingredients of Navy pyrotechnic devices. This year's work was specifically directed at devices containing red phosphorus compositions such as the Mk 25, Mk 58 and Mk 57 Marine Location markers. A typical red phosphorus composition is as follows:

	% Wt
Red Phosphorus	53
Pyrolusite ("MnO_2")	34
Magnesium	7
Zinc Oxide	3
Linseed Oil	3
	100

SOURCES OF WASTE AND DISPOSABLE MATERIALS

As mentioned in the introduction, processes are not completely efficient and materials do not last forever. Accordingly, we were tasked to investigate new methods of disposal of waste pyrotechnic compositions. Since our specialty is formulation of pyrotechnic composition, we should have the most knowledge about how to dispose of or reclaim these items. Figures 1, 2 and 3 are cutaways of three red phosphorus smoke signals, the Mk 7 and Mk 58 Mod, and Mk 25 Marine Location markers. These are examples of the types of signals which will need disposal due to either of the reasons mentioned earlier.

Currently the Navy has many tons of phosphorus smoke composition from scrap and non-functional pyrotechnic ordnance items such as the Mk 25, Mk 27, Mk 58 and Mk 18.

DISCUSSION

During FY 72, the primary mission of this task was disposal but in FY 73 the mission statement was modified to include reclamation. Therefore, our approach necessarily included a serious effort to reclaim the materials such that they could be reused or sold.

Had our interest during this investigation been primarily the separation of red phosphorus from the pyrotechnic composition, a 10% hydrochloric acid solution treatment for two hours at 90°C would yield 99+% red phosphorus. But our plans were to separate the composition into its respective parts: Mg, ZnO, P, and MnO_2. We investigated a two step acid process for further separation of this mixture. In theory, a 6% acetic acid solution heated to 90° for two hours should dissolve 10% of the mixture by the following reaction path:

$$Mg + 2H^{+} \rightarrow Mg^{++} + H_2 \qquad (1)$$

$$ZnO + 2H \rightarrow H_2O + Zn^{++} \qquad (2)$$

Actually 9% of pyrolusite is dissolved in 6% acetic acid solution which strongly suggests that pyrolusite is not MnO_2. Also, theory suggests that 13% red phosphorus smoke composition should dissolve in this solution. Actually, 12.8% of the sample was dissolved in the 6% acetic acid solution. If the two-step process is used and one desires to recover manganese, about 90% of the manganese present in pyrolusite is recoverable leaving a red phosphorus residue. Other methods in RDTR No. 267, which is a part of the preceding package, are one-step-acid process,[1] wet oxidation process, differential densities, and nitric acid dissolution. The presence of pyrolusite in the composition confounded all of the methods to the extent that no clear cut method of separation yielded the same results on replicate samples. Again we refer you to the Pyrolusite section of RDTR No. 267 for a description of the composition of pyrolusite versus reagent grade manganese dioxide which points out some of the characteristics of this high grade ore which complicated the separation technique.

From the experimental results, we decided upon the nitric acid process whose end product is a usable soil additive (see Fig. 4).

EXPERIMENTAL

Nitric Acid Dissolution Process

Samples of red phosphorus smoke composition were treated with aqueous solutions of nitric acid (HNO_3) ranging in concentration from 10% HNO_3 up to 70% HNO_3 ("concentrated" HNO_3). Normally, the reactions with the HNO_3 solutions were carried out at temperatures near or above 100° Centigrade for at least thirty minutes.

At levels of concentration below 20% HNO_3, incomplete sample dissolution occurred. Above 20% HNO_3 concentrations, sample dissolution occurred more completely as HNO_3 concentration was increased. However, it was discovered that if concentrations of 45% HNO_3 or greater were employed, spontaneous fires occurred quite regularly as the HNO_3 solution was added to the samples. This hypergolic reaction could be accounted for by the following reactions:

(1) The hydrolysis of red phosphorus

$$2P_4 + 12\ H_2O \xrightarrow{HNO_3} 3\ H_3PO_4 + 5\ PH_3$$

(2) The rapid oxidation of phosphine

$$2\ PH_3 + 4\ O_2 \rightarrow P_2O_5 + 3\ H_2O$$

This latter reaction is catalyzed by HNO_3, steam in the presence of metal catalysts, and NO and NO_2 gases which would be present from the thermal decomposition of HNO_3 in the first reaction.[2]

From extensive laboratory tests,[3] the optimum dissolution of the red phosphorus smoke composition (RPC) occurred when an 8-gram sample was mixed with 53 milliliters of 35% nitric acid and heated at 105°C for a duration of 75 minutes to 120 minutes. The time of heating varied in somewhat direct proportion to the size of the largest RPC aggregate in the 5-gram sample.

Care needs to be taken that the RPC is not added too rapidly to the acid solution. The very exothermic reaction between the magnesium and acid produces a rapid rise in the temperature of the acid solution. The excessive foaming that one observes is due to hydrogen gas evolution. Proper venting of the hydrogen gas in a pilot plant process will be necessary to eliminate the potential explosive mixture of hydrogen and air. Hydrogen-air mixtures have a very wide range of explosive limits. A potentially explosive mixture exists with as little as 5% hydrogen in air.[4]

The dissolution of the sample occurs with an open beaker where a reduction in solution volume can occur or under reflux conditions where no moisture loss can occur. If the "open beaker" technique is used, it is important that the solution volume is not reduced by more than 40% since insoluble materials begin to precipitate.

The dissolution is complete when the red color of the phosphorus is no longer visible in the solution.

The chemistry involved is straightforward with the one exception being the pyrolusite.[5]

(1) $Mg + 2H^{+} \rightarrow Mg^{++} + H_2 \quad \rightarrow$

(2) $ZnO + 2H^{+} \rightarrow Zn^{++} + H_2O$

(3) $P_4 + 6\ H_2O \rightarrow 2\ HPO(OH)_2 + 2PH_3$

$HOP(OH)_2 + H_2O \rightarrow OP(OH)_3 + H_2$

$PH_3 + 4\ H_2O \rightarrow OP(OH)_3 + 4H_2$

The pyrolusite, which normally is considered to be manganese dioxide (MnO_2), reacts in the following manner.

Half-cell reactions:

(4) $MnO_2 + 4H^+ + 2e^- \quad Mn^{++} + 2\ H_2O$

(5) $P_4 + 12\ H_2O \quad 12e^- + 20\ H^+ + 4\ HPO_3^=$

Overall:

(6) $6\ MnO_2 + 4H^+ + P_4 \quad 6\ Mn^{++} + 4\ HPO_3^=$

Normally, one would not expect the pyrolusite to be dissolved in nitric acid[6] but, in the presence of the red phosphorus, the redox reaction (6) occurs.

CONCLUSIONS

Several processes were investigated and presented here and in RDTR No. 267 which offer various possibilities as means to reclaim certain ingredients in waste red phosphorus smoke composition or to convert the waste composition to usable and/or ecologically "clean" by-products.

With the current fertilizer shortage that exists, the nitric acid dissolution process seems the most feasible approach. This process produces a solution which, when adjusted to pH = 8 using concentrated ammonium hydroxide solution, provides a soil additive solution which contains approximately 4.4% P_2O_5 (phosphoric anhydride) and 1.8% N_2 (soluble nitrogen)[4] as well as the metallic ions of manganese[2] (0.8%), magnesium (0.25%) and zinc (0.1%). Ten gallons of this solution was tested by a Purdue University agronomist, Dr. Eldon Hood, at the Southern Indiana Agriculture Center (SIPAC), Dubois, Indiana on 20 March 1974.

REFERENCES

1. C. W. Gilliam and D. M. Johnson, *Pollution Abatement: Reclamation of Red Phosphorus Composition*, RDTR No. 267, Naval Ammunition Depot, Crane, Indiana (April 1974), pp. 9 and 10.

2. J. W. Mellor, *Inorganic and Theoretical Chemistry* (Wiley-Interscience Publishers, New York, 1971), Vol. VIII, Supplement III, p. 282.

3. Reference 1, pp. 3-6.

4. M. K. Niemiller, *Mk 45 Aircraft Parachute Flare Malfunction Investigation of accidental End Cap Ejections*, RDTR No. 221, Naval Ammunition Depot, Crane, Indiana (January 1973), p. 57.

5. J. R. VanWazer, *Phosphorus and Its Compounds* (Interscience Publishers, Inc., New York, 1958), Vol. I, p. 100.

6. N. A. Lange (Ed.), *Handbook of Chemistry* (McGraw-Hill Book Company, New York, 1967), 10th Ed., pp. 286-7.

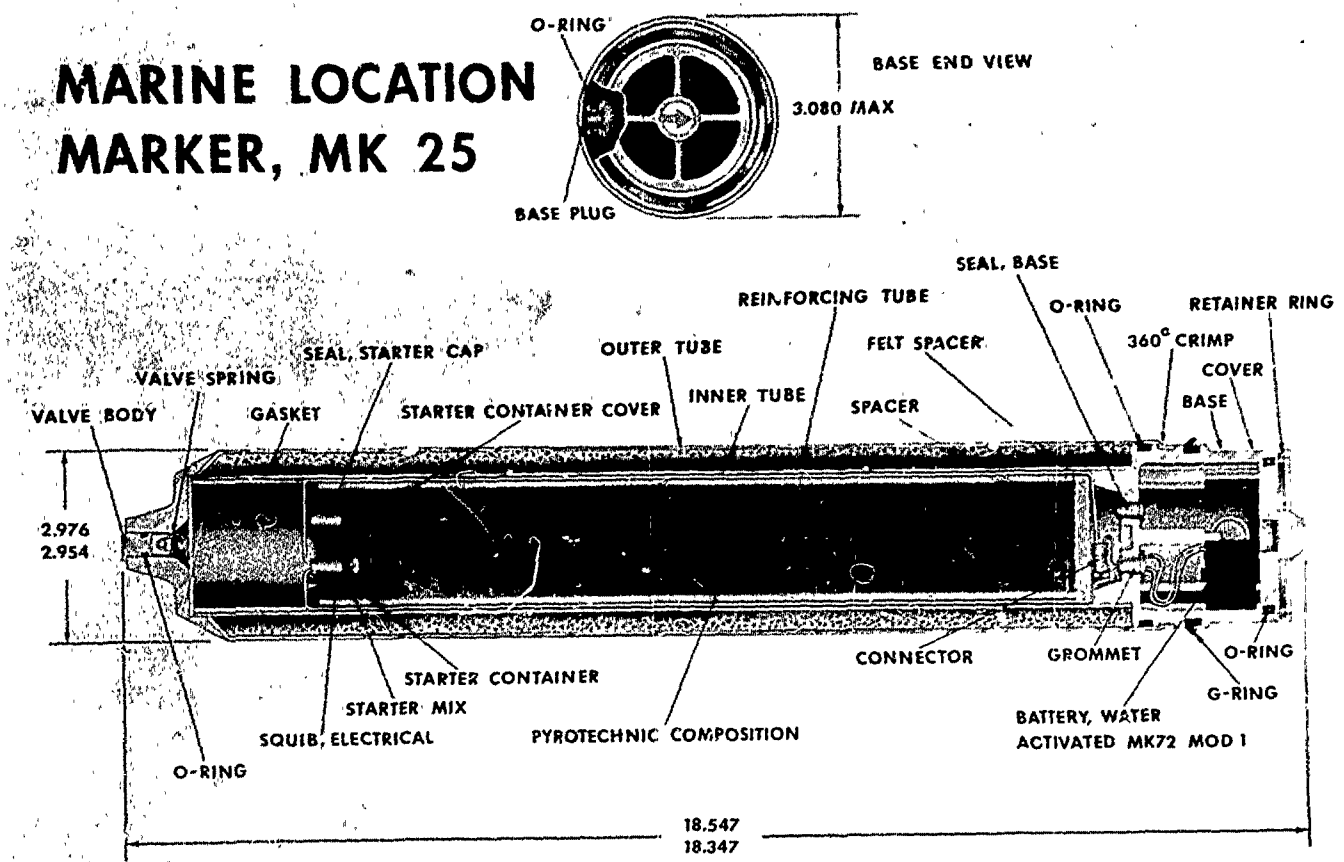

FIG. 3. Cross section of a Mk 25 Mod 0 Marine Location Marker

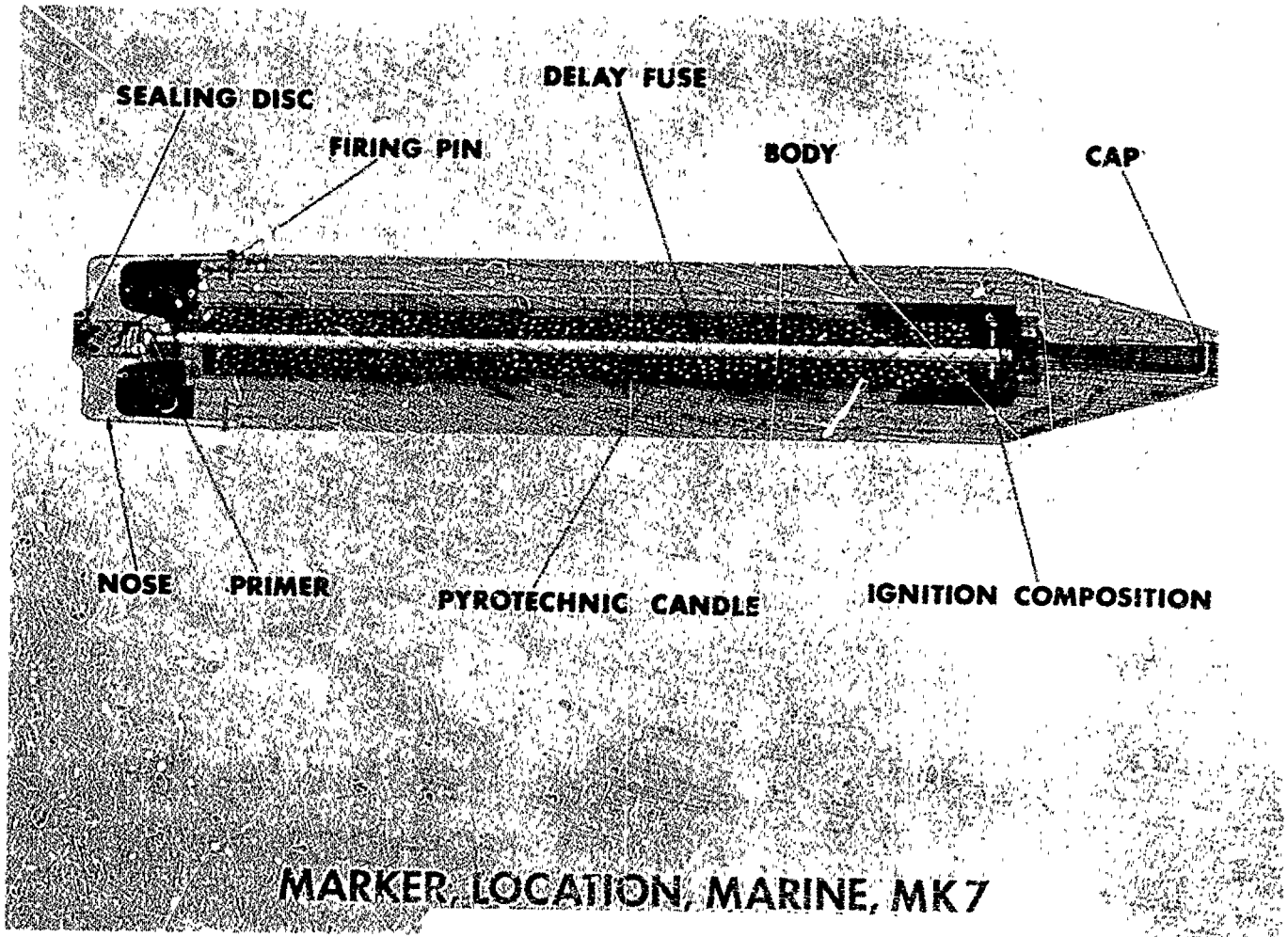

FIG. 1. Cross section of a Mk 7 Marine Location Marker

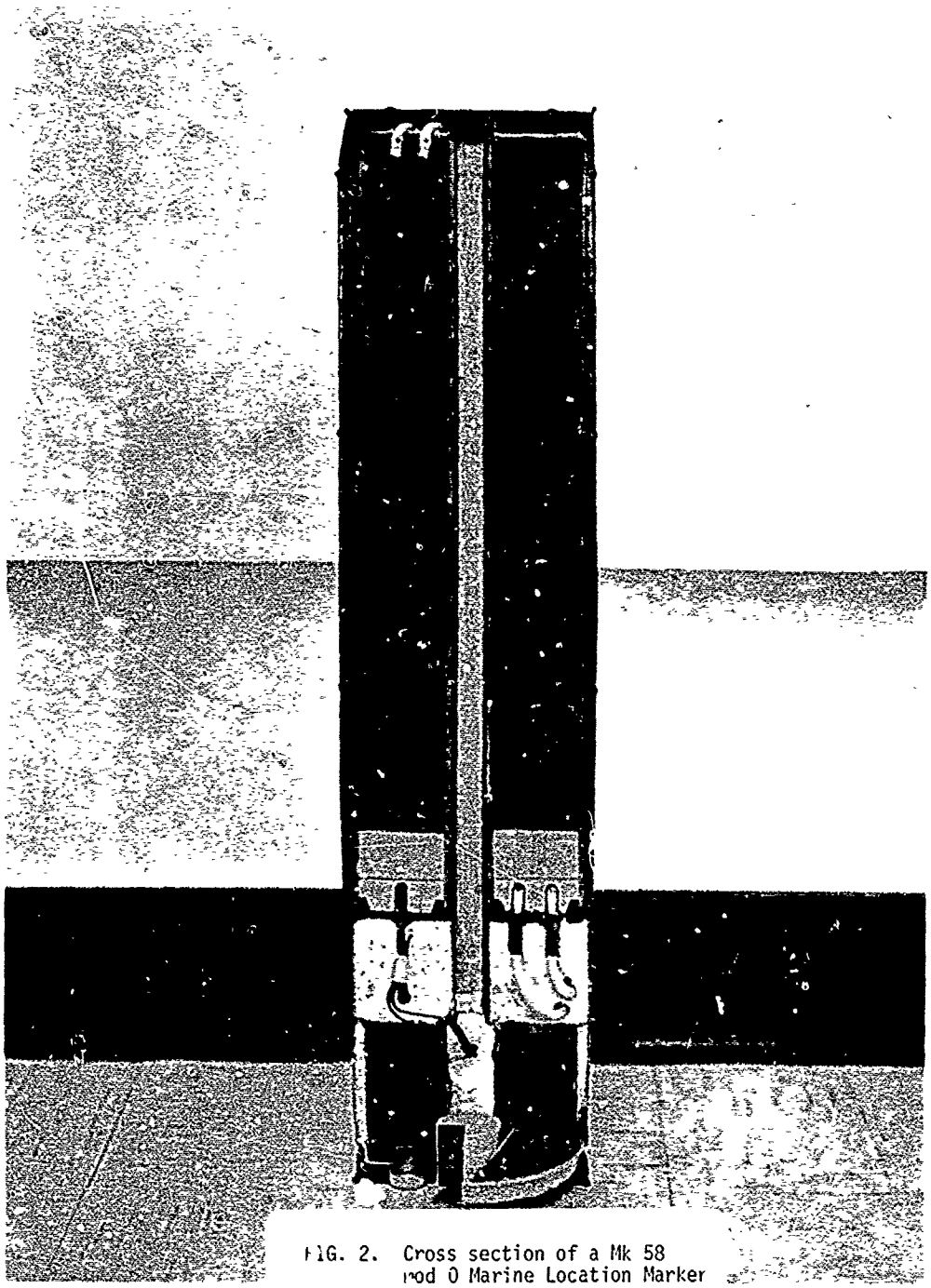

FIG. 2. Cross section of a Mk 58 mod 0 Marine Location Marker

FIG. 4. Grasses treated with neutralized red phosphorus waste from the nitric acid digestion process. Located at Southern Indiana Purdue Agriculture Center (SIPAC)

DEVELOPMENT OF POUR CASTABLE SMOKE COMPOSITIONS

by

G. Couture and R.E. Kluchert

DEFENCE RESEARCH ESTABLISHMENT VALCARTIER

P.O. Box 880, Courcelette, P.Q.

CANADA

ABSTRACT

By the application of existing technology, associated with castable composite propellants, pour castable smoke compositions were developed, based on a commercially available polybutadiene prepolymer. This report outlines the initial research work carried to achieve a truly pour castable composition at a binder concentration of 15% using granulated dyes. Smoke volume output was optimized by selecting a centrally vented and bottom ignited candle layout. With the addition of a burn-rate catalyst a composition was developed that exhibited the necessary properties of low exhaust gas temperature (325°C), good colour quality and high smoke volume output.

INTRODUCTION

The work reported in this paper was carried out at the Defence Research Establishment Valcartier (DREV) from August 1971 to December 1973. The prime objective of this development programme was to develop pour-castable and cool burning orange smoke formulations that could be applied to search and rescue signals, and that would minimize the risk of starting grass or bush fires. Furthermore it was mandatory that the mix remain pour-castable for at least one hour after completion of the mixing operation to allow time for the filling operation for the smoke signals. Also the performance should be at least equivalent or better than conventional, pressed powder formulations. For reasons of cost effectiveness it was thought desirable that all chemical ingredients should be commercially available and that the processing equipment be similar to existing rocket propellant processing equipment. Long term storage stability and low sensitivity to impact, shock, friction and electrostatic discharge were also included on the list of mandatory objectives. Lastly it was planned that, upon completion of the development of a satisfactory castable orange smoke formulation, further development of other coloured smoke formulations for smoke grenades would be undertaken.

The reason why research in this field was even considered was that modern technological advances in castable propellants and explosives had indicated that certain advantages could be gained by going to polymer bonded, castable smoke formulations. Namely, mass production of large quantities (50,000 and above) of pyrotechnic devices filled with castable formulations can be cheaper, handling of the liquid mixes is usually much safer and cleaner, and the final cured product is usually more stable from the explosive

safety point of view. Furthermore the mechanical properties are usually better than for pressed powder formulations. The fact that castable compositions are easily filled into any shape or configuration also gives added design flexibility when applying them to military devices.

FORMULATION DESCRIPTION

In the initial phase of this study the chemicals listed in Table 1 were extensively utilized. The solid phase of the formulation consisted of 40 to 49% 1-Amino anthraquinone (1-AAQ) dye, 20 to 26% potassium chlorate oxidizer, 5 to 9% lactose fuel and 2 to 3% sodium bicarbonate as a coolant and stabilizer. Special precautions were taken to eliminate moisture and to deagglomerate the potassium chlorate. The binder blend was based on a commercially available polybutadiene prepolymer. At a later stage a polypropylene glycol (PPG) based binder was evaluated, but it did not give a low enough end of mix (EOM) viscosity or any significant improvement in smoke performance.

The average particle size of the solid powder ingredients (Table II) was determined by Fisher Sub-Sieve analysis for the fine powders and by Tyler Screen analysis for the granulated dyes. Particle size distributions for the powdered ingredients were determined with the MSA liquid sedimentation technique, the Alpine Jet analyser and the Tyler Screens. The fine dye powders, however, could not be evaluated reliably for particle size distribution because of the long needle shape of the particles.

TABLE I

CHEMICALS FOR DREV CASTABLE FORMULATIONS

DYE (ORANGE)	1-AMINO-ANTHRAQUINONE
OXIDIZER	POTASSIUM CHLORATE
FUEL	LACTOSE
COOLANT/STABILIZER	SODIUM BICARBONATE
BINDER	POLYBUTADIENE

TABLE II

AVERAGE PARTICLE SIZE (μm) OF SOLID INGREDIENTS

POTASSIUM CHLORATE	–	10 μm[a]
LACTOSE	–	12 μm[a]
1 – AAQ DYE		
COMMERCIAL	–	14 μm[a]
GRANULATED TYPE II	–	620 μm[b]
GRANULATED TYPE III	–	550 μm[b]

a = Fisher Sub Sieve Analyzer
b = Tyler Screens

ESTABLISHMENT OF MIXING CYCLE

Prior to commencing actual mixing operations, Differential Scanning Calorimetry (DSC) and Thermo Gravimetric Analysis (TGA) were carried out with a Mettler Thermoanalyzer on various combinations of the ingredients to check for explosively hazardous blends. This study indicated that special precautions were necessary to avoid highly concentrated combinations of $KClO_3$ and lactose, and also of $KClO_3$ and the binder curing agent. Both mixes produced explosion exotherms at 330°C, near the melting point of potassium chlorate. On occasions an explosion exotherm was noted also at 210°C for a 50/50 mix of potassium chlorate and lactose (melting point of lactose is 222.8°C). Combinations of potassium chlorate and 1-AAQ and also of potassium chlorate and the polybutadiene prepolymer produced exotherms in the 350°C region, but not with explosive characteristics. In fact for the latter mixture the indicated melting point of potassium chlorate seemed to shift from 356°C to 360°C, indicating a very stable mixture.

These data were used to establish a safe mixing cycle with the following order of adding ingredients:

a) add prepolymer, plasticizer and wetting agent, and mix for 5 minutes;

b) add lactose, sodium bicarbonate and mix for 15 minutes;

c) add 2/3 of 1-AAQ and mix 25 minutes;

d) add $KClO_3$ and mix 15 minutes;

e) add curing agent and mix 5 minutes;

f) add remaining 1/3 of 1-AAQ and mix 30 minutes.

One third of the dye was incorporated at the end of the cycle to keep the viscosity at a low value and to ensure a good dispersion of $KClO_3$ and the curing agent.

MIXING AND FILLING OPERATION

The production of smoke candles was carried out on a pilot plant scale, using existing rocket propellant processing facilities. The first mixes were prepared using a standard 1.8kg shaftless "Z" blade horizontal mixer. Because of the low density (approx $1.5 g/cm^3$) and high viscosity of the smoke compositions, it became evident that the equipment was not suitable.

The mixing problem was resolved, however, with the availability of a high shear, vacuum mixer (Atlantic Research Vertical Helicone 4CV mixer) that can handle viscosities over 5,000,000 centipoises (5×10^3 N·s/m^2). Figure 1 gives a schematic representation of the processing flowchart for our castable smoke formulations, indicating the vertical cone mixer and the casting bell beneath it. On completion of the mixing operation a valve at the bottom of the mixer was opened and the mixture pushed out by the extruding action of the helical blades. With the assistance of a mechanical vibrator the composition was gravity cast directly into the smoke cannisters or tubes located below in a revolvable bell, which was also maintained under vacuum (0.4 KPa pressure). With the more recently developed low viscosity mixes (<300,000 centipoises) the need for vacuum may be entirely eliminated, but for mixes having EOM viscosities of 300,000 centipoises or higher vacuum processing will still be necessary since air entrapment is a problem with these low density mixtures.

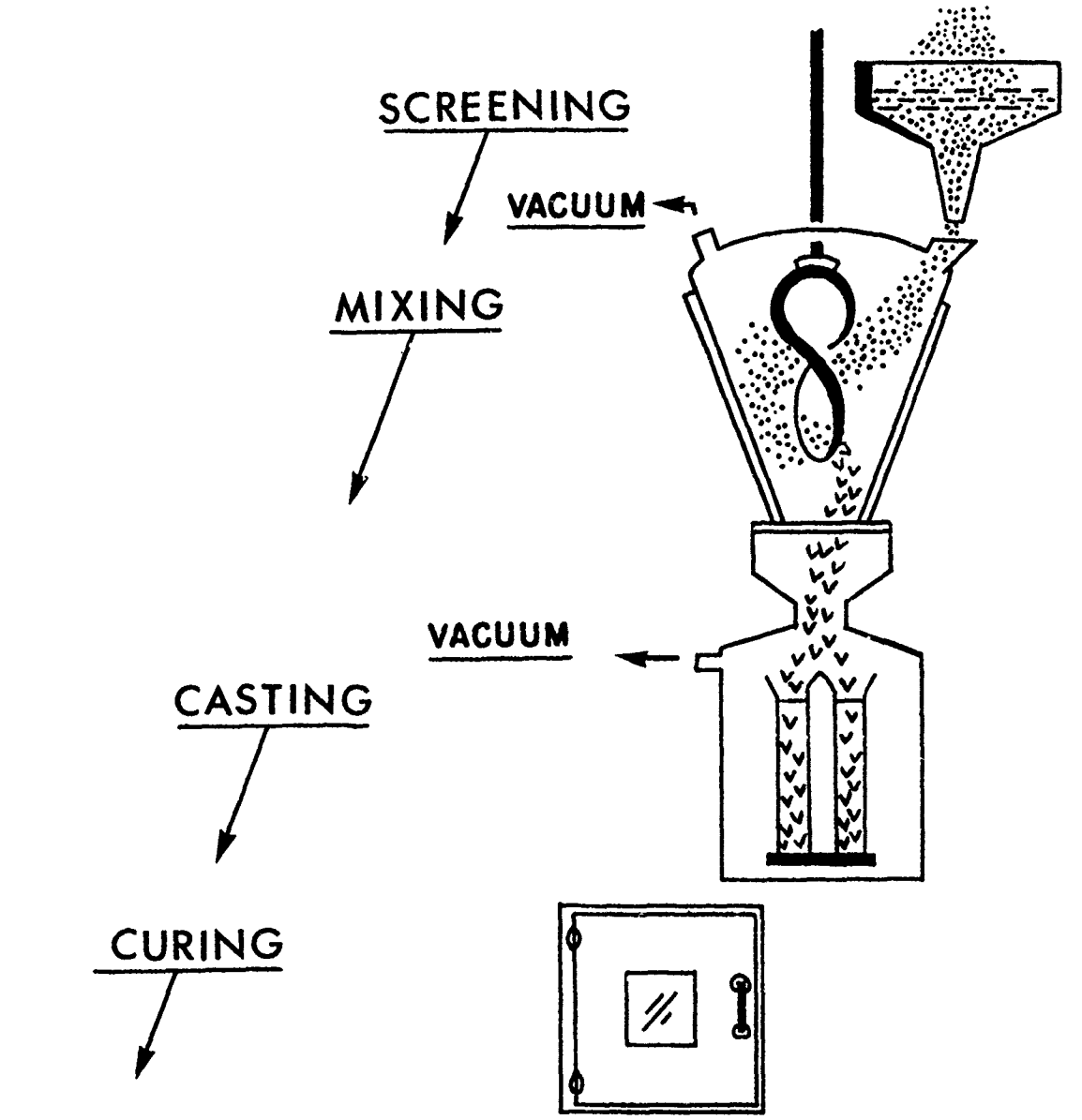

FLOWCHART FOR CASTABLE PYROTECHNICS

FIGURE 1

During mixing the wall temperature of the mixer was maintained at 60°C with a hot water jacket, but no excessive overheating in the mixture was recorded when actual temperature measurements of the mix were taken (max mix temperature was 65°C). In other words, the heat generated by the polymerization reaction of the binder is minimal; however, the curing period for the polybutadiene bonded mixes and the polypropylene-glycol bonded mixes takes up to 5 days at 60°C. This long cure period obviously is undesirable since production with these formulations would entail the need for large curing facilities, thus raising capital costs.

END OF MIX VISCOSITY OPTIMIZATION

Viscosties were determined at the mixing temperature of 60°C, using a HAT type Brookfield viscometer with a T-type spindle. In the early investigations, when fine dye powders were used, discouragingly high EOM viscosities resulted. The polybutadiene bonded formulation (A in Table III) had a high EOM viscosity of 2,400,000 centipoises at a 25% binder concentration and similarly formulated PPG bonded mixes (B and C in Table III) had EOM viscosities in excess of 3,000,000 centipoises. As a result, PPG formulations with their shorter pot life (see viscosity vs time characteristics in Figure 2) were eliminated at an early stage in the programme.

Another approach for reducing the EOM viscosity would be to modify the average particle size of the powdered ingredients. Increasing the average particle size of either the potassium chlorate or lactose was quickly ruled out because this would only serve to reduce the already too slow burn rate; besides, both of these chemicals are present in relatively

TABLE III

EOM VISCOSITIES (60°C)
POLYBUTADIENE AND POLYPROPYLENE GLYCOL FORMULATIONS

	A	B	C
% 1-AAQ	40.15	40.15	40.15
% $KClO_3$	22.81	22.81	22.81
% LACTOSE	8.21	8.21	8.21
% $NaHCO_3$	1.83	1.83	1.83
% CATALYST	2.0	2.00	2.00
% BINDER	25	25	25
TYPE	PB-57	PPG-35	PPG-41
EOM VISCOSITY CENTIPOISES	2,400,000	TOO THICK	3,150,000

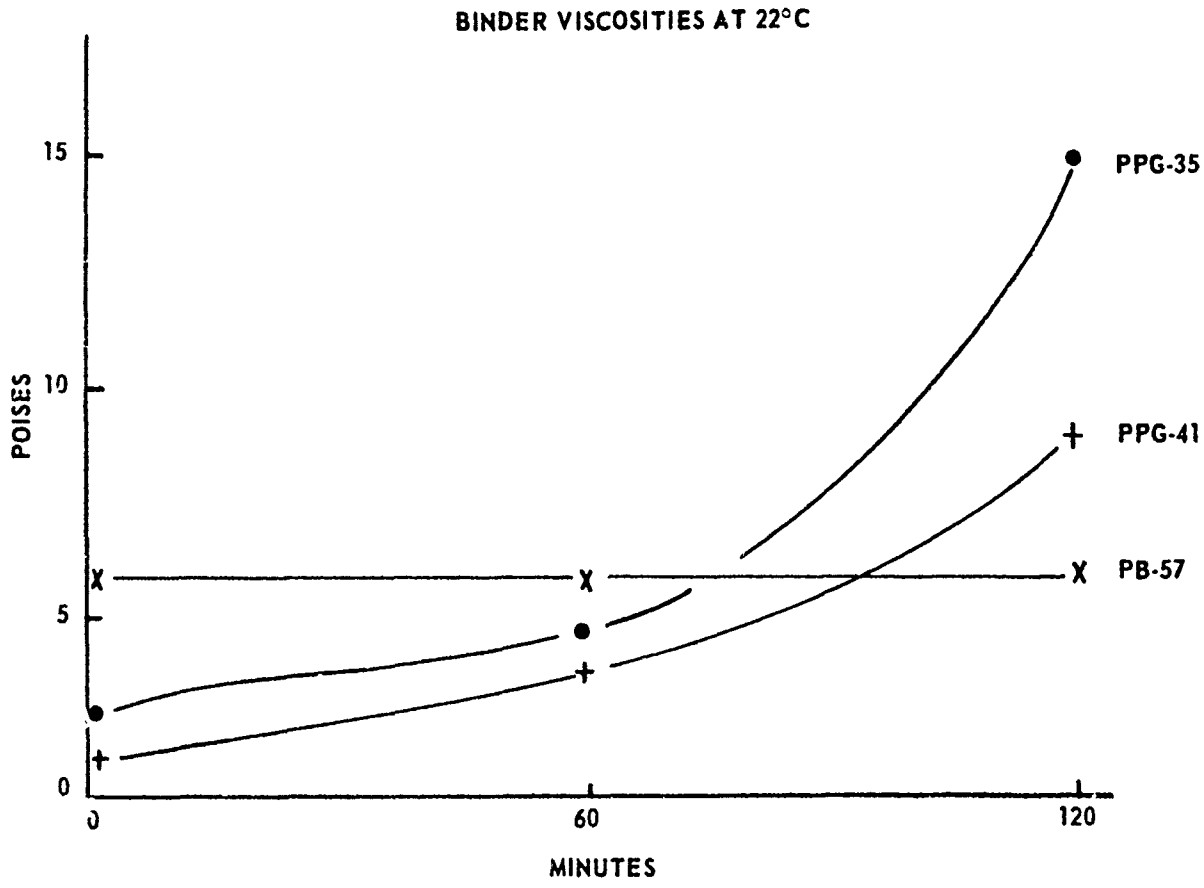
BINDER VISCOSITIES AT 22°C
15
10
5
0
POISES
PPG-35
PPG-41
PB-57
0
60
120
MINUTES

FIGURE 2

small concentrations compared to the more significant concentration of the dye. The 40 to 50% by weight concentration of fine dye particles (avg size 14μm) has by far the greatest influence on the EOM viscosity. Furthermore, their low crystaline density ($\sim$1.5g/cm^3) and needle-like shape yield a maximized surface area, thus requiring excessive quantities of binder to coat these particles. Also, the needle shaped dye particles prevent a tight packing arrangement of the powders, thus increasing the void space and correspondingly demanding a larger amount of binder to fill these voids.

Accordingly techniques of granulating dye powders were studied and several granulated powders, prepared by different granulations methods, were evaluated. A dramatic reduction in EOM viscosity was possible when granulated 1-AAQ dyes Type II and Type III were used (Table IV). Formulation D, which contained fine (ungranulated) 14μm dye, had a near pour-castable EOM viscosity of 720,000 centipoises at a 25% binder concentration. In comparison, formulations E and F which both contained 49% granulated dye (average particle size 620μm and 550μm respectively), yielded EOM visocisities of 500,000 centipoises and 240,000 centipoises respectively at binder concentrations of only 15%. A minor modification to the granulation technique, Type II, made possible the additional 50% reduction in EOM viscosity for formulation F. It has been estimated tha the cost for granulation will be as low as $0.40 (Canadian) per pound of dye, based on a production of 50,000 lbs of granulated dye.

TABLE IV

EOM VISCOSITIES (60°C)

	D	E	F
% 1-AAQ	42[1]	49[2]	49[3]
% $KClO_3$	21	24	24
% LACTOSE	7	8	8
% $NaHCO_3$	2	2	2
% CATALYST	2	2	2
% BINDER	25	15	15
EOM VISCOSITY CENTIPOISES	720,000	500,000	240,000

NOTES: 1. Avg Particle Size 14 μm

2. Avg Particle Size 620 μm
   Granulation Type II

3. Avg Particle Size 550 μm
   Granulation Type III

CANDLE LAYOUTS AND BURN RATE OPTIMIZATION

For early formulations, using fine dye powders and a 25% binder concertration, very slow burn rates (i.e. poor smoke volume) were achieved with an end burning cylindrical layout. Furthermore it was noted that with this layout the smoke colour tends to become progressively paler as the combustion zone moves down the candle (see Figure 3A). This colour fading is mainly due to the increasingly thick layer of hot coke through which the heat sensitive dye vapours are forced to diffuse. As a consequence several modified layouts were evaluated of which the most successful is shown in Figure 3B. The illustration shows a 500g candle, with a 12.7 cm (5 inch) long and a 7cm (2.75 inch) diameter grain. The candle is bottom ignited and vented centrally via a 2.54cm (1 inch) diameter chimney. A perforated phenolic/kraft paper tube (2.54cm I.D) is located in the upper 2/3 portion of the chimney to prevent it from plugging up due to expanding hot coke residue and to control or prevent a progressively faster combustion rate. With bottom ignition and central venting, unburned composition above the combustion zone is preheated by the hot gases flowing up the center. This arrangement assures a fast smoke build-up and a maximized burn rate, thus maximizing smoke volume output. This layout also minimizes dye breakdown (colour fading) since the lateral diffusion path through the hot coke layer is shorter than for a end burning candle layout. The cone shaped interface (Figures 3B) between the coke residue and unburned composition gives a good approximation of the actual profile in the candle and has been confirmed by placing thermocouples at exact locations in the candle grain.

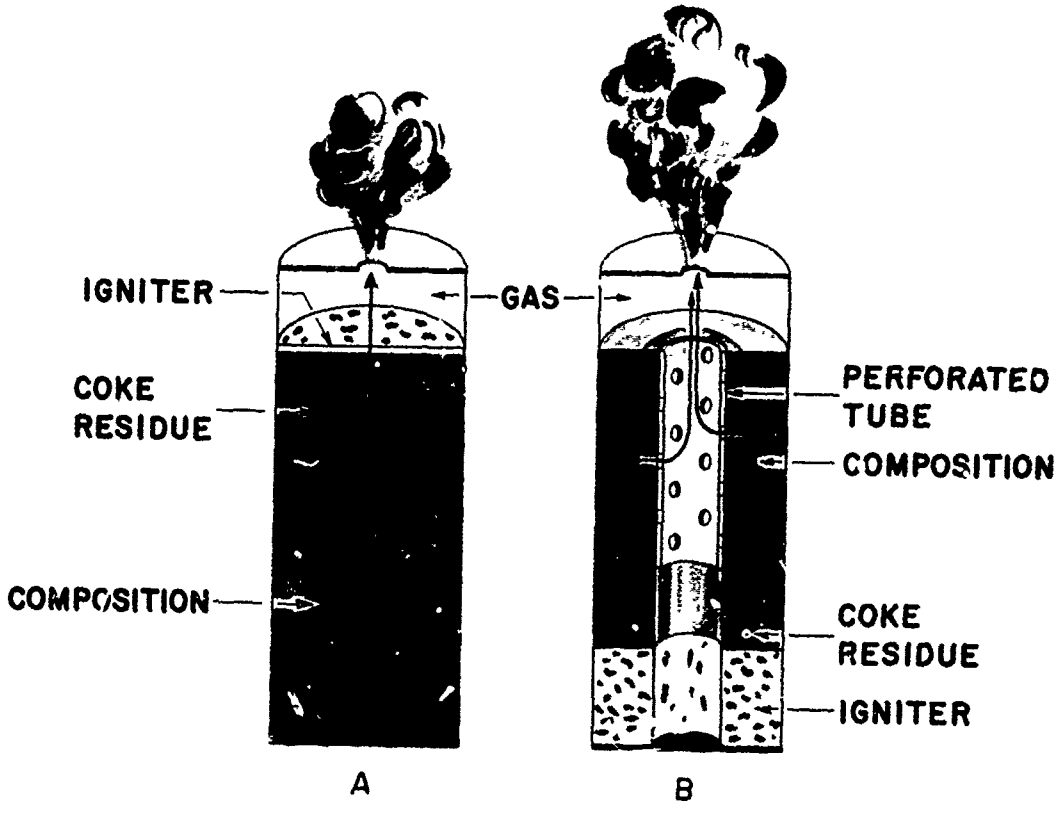

COMBUSTION PROFILES OF CANDLES

FIGURE 3

INSTRUMENTATION AND TEST CONFIGURATION

In Figure 4 a fully instrumented test candle is shown. The test unit is located on a "Weightloss Transducer" that allows measurement of weight changes as the burn progresses. Thus burn rate in the units grams per minute is calcuable and can be related directly to smoke volume output. Two thermocouples are used: one to record the internal temperature in the composition as the combustion zone passes through, and the other to record the exhaust gas temperature for the duration of the burn.

Low exhaust gas temperatures are obviously of prime importance since the orange smoke compositions that are being developed are intended for search and rescue markers that will be used over a variety of terrain (i.e. dry bush, prairie grass and tundra). Temperatures as low as 325°C (625°F) were thought to be realistic objectives; this compares to exhaust gas temperatures of about 500°C (932°F) for most conventional pressed powder formulations.

EFFECT OF BURN-RATE CATALYST

In order to augment the burn rate further without causing excessive increases in the exhaust gas temperature, a study was carried out with a known burn rate catalyst. Four formulations were prepared having constant weight ratios for the solid ingredients (43/21/7/2 for 1-AAQ/$KClO_3$/lactose/$NaHCO_3$ respectively) and a constant binder concentration of 25%. The catalyst concentrations were selected at 0, 1, 2 and 3% for the four mixes. From the data in Table V it is evident that a catalyst concentration of about 2% has a maximized effect on burn rate. Composition I (2% catalyst) achieved nearly twice the burn rate (85g/min) than Composition G (0% catalyst, 47g/min).

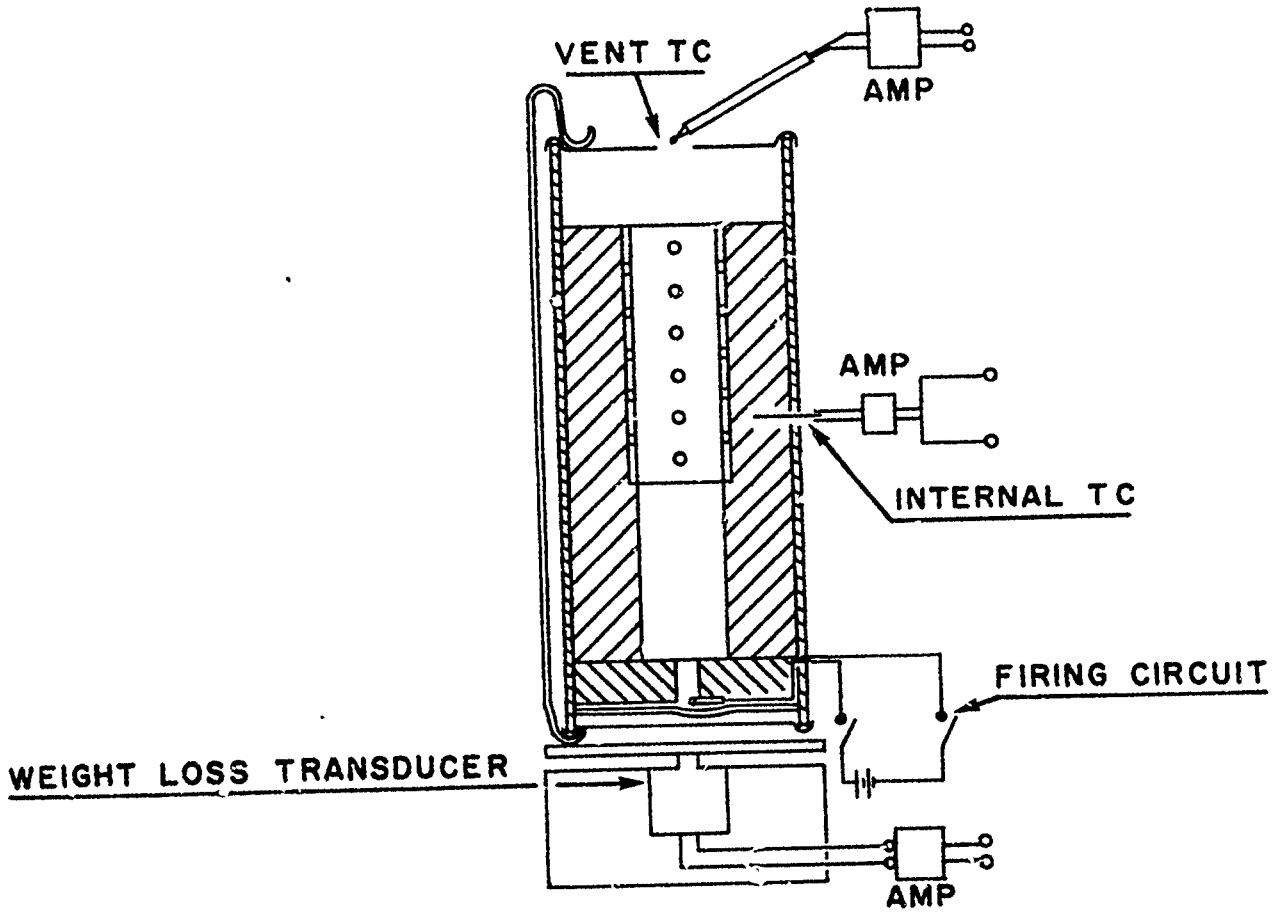

TEST CONFIGURATION AND INSTRUMENTATION

FIGURE 4

TABLE V

EFFECT OF CATALYST ON BURN RATE

	H	I	J	K
% 1-AAQ	44.8	43.59	43	42.4
% $KClO_3$	21.58	21.29	21	20.7
% LACTOSE	7.19	7.10	7	6.9
% $NaHCO_3$	4.05	2.02	2	2
% CATALYST	0	1	2	3
% BINDER	25	25	25	25
LINEAR BURN RATE cm/min	–	0.399	0.434	0.391
AVG WEIGHT LOSS RATE gm/min	47.04	70.47	85	68

INFLUENCE OF GRANULATED DYE ON COMPOSITION PERFORMANCE

As indicated earlier the use of granulated dye has the desirable effect of significantly reducing the EOM viscosity; by the same token the use of granulated dye has a pronounced influence on burn-rate and smoke colour performance.

Since the binder has poor combustion properties and since pour-castable formulations are now possible with 10% less binder (from 25% down to only 15%) the overall effect of this reduction is a significant increase in burn rate. Furthermore, since the dye also behaves as a very poor fuel, but is now concentrated in larger granules, its interference with the potassium chlorate/lactose combustion reaction is minimized. Thus in effect, the use of granulated dye has a dual influence on the increase in burn rate. In addition, the improved burnrate made possible a further increase in dye concentration, and this led to a further decrease in the exhaust gas temperature.

These changes are reflected in the data of Table VI where three formulations are compared having progressively improved performance (these formulations are identical to those in Table IV). Composition D with its high 25% binder concentration and 43% fine dye powder content has an average burn rate of only 80g/min, only a fair smoke colour and an exhaust gas temperature of 416°C (780°F); in comparison, composition E with a low 15% binder concentration and 49% dye (granulated, 620μm) content has an improved burn rate of 266g/min, a good smoke colour and an exhaust gas temperature of only 329°C (624°F). Composition F, having the same

TABLE VI

BURN DATA

	D	E	F
% 1-AAQ	43	49	49
% $KClO_3$	21	24	24
% LACTOSE	7	8	8
% $NaHCO_3$	2	2	2
% CATALYST	2	2	2
% BINDER	25	15	15
BURN RATE gm/min	80	266	263
COLOUR	FAIR	GOOD	GOOD
VENT TEMP °C	410	329	255.8

formulation but using differently granulated dye, gives a nearly identical performance as Composition E, but the very low exhaust gas temperature of 255.8°C (493°F) must still be verified. It is suspected that the measuring thermocouple was not always centered in the wavering exhaust gas stream, which tends to change in exit angle as the orifice plugs up with residue and dye.

DEVELOPMENT OF RED, YELLOW, AND GREEN FORMULATIONS

Development work has commenced recently on castable coloured smoke formulations for smoke grenades. Granulated samples were prepared from red, yellow, violet and green dyes. Table VII describes 4 identical formulations using 46% granulated dye (avg. particle size ∿600μm) and a 20% concentration of a polybutadiene binder. From the EOM viscosity data it is apparent that no processing difficulties will occur for the violet, yellow and green formulations. Burn results have been also satisfactory for these three formulations in terms of colour and smoke volume. However, for the red smoke formulations, which contain 1-methyl-amino-anthraquinone (MAAQ) dye, difficulties are being encountered with high EOM viscosities and poor burn performance. The high viscosities with the red formulations are attributed to the very fragile properties of the MAAQ dye granules. During the high shear mixing operation the granules break up into a fine powder, thus canceling the beneficial effects of granulation. Furthermore, since MAAQ has one of the lowest densities of all the dyes, 1.3g/cm^3, its greater bulk demands larger quantities of binder to maintain low EOM viscosities.

TABLE VII

EOM VISCOSITIES (60°C) FOR COLOURED SMOKE FORMULATIONS

	VIOLET	YELLOW	GREEN	RED
% DYE (GRAN)	46	46	46	46
% $KC10_3$	23	23	23	23
% LACTOSE	8	8	8	8
% $NaHCO_3$	3	3	3	3
% BINDER	20	20	20	20
EOM VISCOSITY CENTIPOISES	136,000	336,000	290,000	3,720,000

SURVEILLANCE TESTING

Recently completed surveillance tests, carried out with orange (1-AAQ) formulations, resulted in a 9% decrease in burn rate (measured in grams per minute) after the smoke candles had been stored for 56 days at 60°C (140°F). After 84 days at 60°C (140°F) the average burn rate dropped from 102g/min to 70g/min, a 31% decrease. Surprisingly, the linear burn rate was not affected since the total burn time of the test candles remained at approximately 2.4 minutes. Candles stored for 168 days at room temperatures did not appear to suffer any significant change in burn rate. For these, only a 4.5% drop in weight loss rate was recorded. An additional surveillance test with 5g of orange smoke composition that was stored in a Paar Bomb for 3 months at 49°C (160°F), 100% R.H. indicated no pressure increase whatsoever. However, noticeable swelling of the 5g sample was apparent. This was attributed to water entering the sample and was confirmed by thermogravimetric analysis. However, DSC analysis of a 5mg sample did not show the characteristic exotherm at 210°C that is attributed to the reaction between potassium chlorate and lactose.

Both surveillance tests were somewhat severe and do not reflect a normal storage environment. However, no ready explanation could be given for the drop in burn rate after 84 days at 60°C (140°F). One possible explanation may be a decrease in the available oxidizer by a redox reaction between potassium chlorate and one of the organic ingredients (possibly lactose).

CONCLUSIONS

Initial development work with 1-AAQ dye and a polybutadiene binder has indicated the feasibility of producing pour-castable orange smoke formulations having EOM viscosities of less than 500,000 centipoises at 15% binder concentration. Low exhaust gas temperature (~329°C) together with a good smoke colour and high volume output were also achieved. Existing propellant processing equipment and commercially available chemicals were used in the preparation of the formulations. Pour-castable formulations were achieved when the particle size of the fine dye powder was increased by a granulation technique to approximately 600μm. Introduction of a burn rate catalyst aided the development of cool burning compositions.

Further development work with violet, green, yellow and red smoke formulations indicated pour-castable formulations are achievable for the first three but that the red (MAAQ-dye) formulations are excessively viscous due to the fragile properties of the MAAQ granules, which break up into fine particles during the high shear mixing process.

A surveillance test of a pour-castable orange smoke formulation indicated that some decrease in smoke performance (weight loss rate) will take place depending on the storage temperature. Only minor changes in weight loss rate were noted for the test formulations stored for 168 days at room temperature, but a 31% decrease in weight loss rate was noted for the test formulation stored for 84 days at 60°C (140°F).

CHEMICAL EFFECTS OF DOPING ON THE LITHARGE SILICON SYSTEM

Charles A. Lipscomb, Jr.
Applied Sciences Department
Naval Ammunition Depot, Crane, Indiana 47522

ABSTRACT

Litharge may experience noticeable and drastic alterations in its reaction with silicon depending on the presence, extent and nature of dopant species in either or both the litharge and the silicon. Reactivity differences were measured as enthalpy of the following reaction $PbO + Si \rightarrow SiO + Pb$ which reaction is confirmed by X-ray diffraction of product species.

CHEMICAL EFFECTS OF DOPING ON THE LITHARGE SILICON SYSTEM

BACKGROUND

In pyrotechnics, as in other areas of solid state chemistry, one of the most important tasks has been and continues to be the preparation of solid materials having a definite chemical reactivity. By chemical reactivity, one includes such measurable properties as heats and rates of reaction, and the ease of initiation or sensitivity.

For instance, one may wish to obtain a more energetic ignition mix or a first fire than those which are readily available. Faced with this situation, the pyrotechnic designer usually searches for another ignition mix or alters the formulations of those readily available. Alternatively, suppose that a routine check of a production line delay element indicates that the delay is burning too fast; this problem is usually fixed on the production line by altering the formulation of the materials in the delay composition.

In the first example, it is conceivable that the pyrotechnic designer's problem could be solved if he had tailor

made materials at his disposal. In the second example, the problem often arises from the variability[1,2] of the materials received for use on the production line, and that problem could be solved in the same manner.

Thus, our approach is one which leads away from the artful mixing of pyrotechnic ingredients to one which formulates from ingredients of tailor made reactivity prepared by chemical doping.

This effort was funded by Naval Ordnance Systems Command under their Task Assignment Number ORD 332-004/060-1/UF17-546-301.

THEORY

Nature of Dopant Defects

There are two possible ways in which the specific dopant can become incorporated into the host crystal lattice:

Vacancies - these defects result when either cation or anion vacancies are created. If a cation vacancy is created, the material acquires a p-type character, and if an anion vacancy is created, an n-type material results. If anion and cation vacancies are equal in number, the defect is Shottky type.

Interstitials - these defects result when either a host or a dopant anion or cation occupies an interstitial position within the crystal lattice. If the interstitial element is an anion, the material becomes p-type, whereas, if the interstitial is a cation, the material will be n-type. If the situation exists where one has an interstitial ion with vacancies where the majority of both interstitials and vacancies are cations, then the defect structure is Frenkel type.

Chemical Effects of Doping

The discussion of these effects will be limited to oxidation-reduction (Red-Ox) reactions. Red-Ox reactions can be explained in terms of a transfer of electrons from the reducing agent to the oxidizing agent. One particular type of Red-Ox reaction, though it is seldom thought of in this manner, is that involved in the n-p junction of two semiconductor materials. In this instance, electrons are permitted to flow from the n-type material to the p-type material when a potential is applied. Thus, the n-type material may be thought of as the reducing agent and the p-type material may be regarded as the oxidizer.

It is possible to enhance the nature of n and p-type semiconductor materials by varying the concentration of certain impurities or dopants in these materials,[3] and thus the chemical potential available to effect the transfer of electrons is altered by the amount of dopant in the materials[4] (See Fig. I). Thus, by increasing the concentration of dopant that causes a material to be n-type,

the material will be more n-type and will become a better donor of electrons. Likewise, if the amount of dopant that causes a material to be p-type is increased, then the material will become a better acceptor of electrons. The converse is also true.[3,5]

Just as in the case of semiconductors then, one may argue that Red-Ox reactions in general and pyrotechnic reactions, in particular, may be affected in the same manner.

The potential energy for the transfer of electrons may be represented by the Faraday Equation which states that the potential energy for the transfer of electrons is proportional to: (1) n, the number of electrons transferred, and (2) E, the electropotential in volts (electro-negativity difference) through which the electrons transfer, or

$$\Delta G = -n F E \qquad (1)$$

where F is the value of the Faraday 96,500 coul/gm. equiv. and ΔG is the Gibbs free energy (also referred to as the thermodynamic potential or reaction potential).

Following McLain's[6] treatment for an n-doped fuel F_n as compared to the undoped fuel F, if the number of electrons in the Fermi level are increased, the Fermi level will be higher in F_n than in F or

$$E_{F_n} > E_F. \qquad (2)$$

In a Red-Ox reaction between the fuel F (or F_n) and an oxidizer A, the free energy for the system F_n + A will be greater than in the system F + A, i.e.,

$$\Delta G_{F_n} > \Delta G_F \qquad (3)$$

provided the two reactions

F + A → Products (a)

F_n + A → Products (b)

proceed by the same mechanism. Therefore, the energy of

activation for reaction (a) will be greater than reaction (b), i.e.,

$$\Delta Ea_F > \Delta Ea_{F_n} \qquad (4)$$

by the same amount that

$$\Delta G_F < \Delta G_{F_n} \qquad (5)$$

or

$$\delta\Delta G = -\delta\Delta Ea \qquad (6)$$

Dividing both sides of equation (6) by RT, one obtains, after integration,

$$\frac{\Delta G}{RT} = a\,\frac{Ea}{RT} + \text{Const.} \qquad (7)$$

where a is proportionality constant. Since

$$\Delta E_a = -\frac{\ln K}{RT} \qquad (8)$$

and

$$\Delta G = - \frac{\ln k}{RT} \qquad (9)$$

we get

$$\ln k = a \ln k + \text{const} \qquad (10)$$

Evans and Polanyi[7] point out that for equation (10) to apply, the reactions must be "similar-different but closely analogous reactions." Such is definitely the case with the system studied by Schwab[8]

$$Ge + 2\ MoO_3 \rightarrow GeO_2 + 2\ MoO_2 \qquad (11)$$

where the germanium fuel was doped with various dopants to make it either n-type or p-type (see Fig. II). Golinkin[9] has applied this relationship to the solvolysis of benzyl chloride in different but similar aqueous alcohol solutions at various temperatures. There are numerous citations of

the series of papers presented by Evans and Polanyi.[10,11] That work includes, for example, the following references by Glasstone, Laidler, and Eyring,[12] and Hammett[13] -- upon whose own work[14] Evans and Polanyi had initially drawn.

Hammett's[14] proposal of equation (10) and its interpretation as applying to a "group of reactions" actually predates that of Evans and Polanyi but is strictly empirical. Burkhardt[15] observes that equation (10) applies to various types of substituted benzene derivatives, and Rock[16] presents a treatment of the relationship between the rate constants and the equilibrium constant that is analogous to equation (10) but in differential form.

Physical Effects of Doping

Another factor which must be considered is when there is a significant disparity in ionic size between the dopant and host species, it is possible to introduce strains in the crystal bonds, and this will generally have the effect of increasing the chemical reactivity of the doped material

relative to that of the undoped.

It is possible to cause severe rupture of the interior crystal bonds which result in internal cracks and fissures (Smekal cracks). Such cracks may reach even to the surface as grain boundaries and alter surface characteristics such as surface area and bond energies.

The nature of these effects may be summed up under the general term mechanical activation. Usually mechanical activation results when some external source of energy such as grinding or milling is applied to a material.

The term mechanical activation and the scientific fundamentals of the concept originate with Smekal[17] who notes that plastically deformed diamonds and calcite became more susceptible to attack with dilute acid. Naeser and Scholz[18] report that Fe_2O_3, $CaCO_3$, or MoO_3, when mechanically activated in a rolling mill, sometimes exploded violently.

They report Fe_2O_3 was worked in a steel ball mill for several hours at room temperature. The Fe_2O_3 was activated

mechanically in the presence of iron to the extent that it was reduced to Fe_3O_4 and that the decomposition temperatures of mechanically worked NiO , MoO_3, and WO_3 were noticeably lowered from the values of unworked NiO , MoO_3, and WO_3.

Obviously, these mechanical effects can alter what we have addressed as chemical reactivity. So, regardless whether this mechanical activation arises from the material being subjected to an external source of mechanical energy such as grinding or to an internal source of mechanical energy such as doping -- the result is the same. Potential energy is imparted to the material as stress and strain which is indicated by an altered physical structure, thereby increasing the potential energy of the reacting system, and thus the activation energy is decreased according to the former argument. What results is a more reactive material.

MATERIALS

Silicon

The Silicon used for this work was purchased from Dow.

The material was received in the following approximate range of resistivities:

n-type	10 ohm • cm
n-type	100 ohm • cm
n-type	2000 ohm • cm
p-type	10 ohm • cm
p-type	100 ohm • cm
p-type	3000 ohm • cm

The materials were then individually ground in a jar mill for periods of up to 200 hours and screened through a 325 mesh sieve.

Litharge

The following reagent grade starting materials were used in the preparation of both the doped and undoped samples of litharge:

Lead Nitrate	$Pb(NO_3)_2$
Ammonium Oxalate	$(NH_4)_2\ C_2O_4 \cdot H_2O$
Lithium Hydroxide	Li OH
Chromium Nitrate	$Cr(NO_3)_3$

(1) Lead Nitrate is dissolved in distilled water.

(2) In another container (beaker, flask, etc.) is dissolved the Ammonium Oxalate.

(3) The dissolved Ammonium Oxalate is then poured with constant agitation into the Lead Nitrate solution resulting in the precipitation of very fine Lead Oxalate.

(4) The Lead Oxalate is then collected on a filter paper and washed with hot distilled water.

(5) The Lead Oxalate is then transferred from the filter paper into a crucible and dried at 80°C for 24 hours.

(6) The dried Lead Oxalate is then transferred in a crucible to a furnace at 350°C for 16-24 hours. The Lead Oxalate converts to Lead Carbonate.

(7) The Lead Carbonate is then heated at 700°C for 24 hours and is converted to litharge.

Lithium Doped Litharge

The preparation of the Lithium doped Litharge is the same as that of the undoped with the exception that in step (1), 95 weight percent Lead Nitrate and 5 weight percent Lithoum Hydroxide are dissolved in distilled water.

Chromium Doped Litharge

The preparation of the Chromium doped Litharge is the same as that of the undoped with the exception that is step (1), 95 weight percent Lead Nitrate and 5 weight percent Chromium Nitrate are dissolved in distilled water.

General Statement on Metal Oxide Doping Procedures

Metal Oxides may be conveniently prepared by a wide variety of techniques, one of which involves the decomposition of metal oxy-salts such as: sulfates, carbonates, nitrates, hydroxides, phosphates, oxalates, tartrates, acetates, etc. If the oxy-salt is dissolved in a solvent containing a selected dopant which is also in solution and then precipitated as low solubility oxy-salt, the doped precipitate can then be decomposed to yield the doped metal oxide. Hauffe[19] indicates that Zinc Oxide may be made n-type by doping with Ga^{+++} and that TiO_2 made n-type by doping with W^{+6}. Similarly, NiO can be made p-type or n-type by doping with Li^{+} or Cr^{+3}, respectively,[20,21] Thus, for a divalent metal oxide,

one might suspect an n-type oxide to result with the addition of a cation dopant having a valence greater than two, and that a p-type oxide would result from the addition of a cation dopant having a valence less than two. Anion dopants may also be used such as SO_4^{-2} ions. Krylov, Rogenskii[21] and Zhabrova[22] show the effects of various dopants on the activation energy of adsorption of O_2 on ZnO for various impurities. The SO_4^{-2} impurity increases the activation energy linearly with concentration within the limits studied and the Li impurity decreases the activation energy.

Since Lead was a divalent metal in the oxide being prepared-- and following the above rules-- the dopants selected were the Li^+ and Cr^{+3} for the p-type and n-type PbO, respectively.

EXPERIMENTAL RESULTS

Heats of combustion for the lead oxide plus silicon mixtures listed in Table 1 were obtained. The amount of mixture was, in each case, 0.40 gm; this amount was placed in a weighed Coors crucible. The general operating procedure for the Parr Oxygen Bomb Adiabatic Colorimeter was then followed with the exception that an atmosphere of 30 P.S.I.G. Argon.was used.

A potentiometric titration of the unreacted lead oxide was made. The bomb reaction products were washed into glass bottles with 25 ml of H_2O. One ml of 10% Acetic Acid was added, and the bottle closed and agitated on a wrist action shaker for at least one hour. The bottle contents were then washed into a 400 ml beaker and diluted to 300 ml with distilled H_2O. The titration was performed on this volume of material using 0.05 N K Cr_2O_7. The conductivity was then determined as a function of the amount of $K_2Cr_2O_7$ to a point well beyond the end point; the minimum on this plot is the end point. See Fig. III for example.

There was surprisingly little difference in the amount of unreacted lead oxide from test to test, and this correction can be omitted if desired, but with some sacrifice in accuracy.

SUMMARY

The results of this study indicate that the heats of reaction, and hence $\bar{Q}$ values as measured in kilocalories per mole of oxidizer, are dependent upon the following factors:

1. Type of Si used. The n-type Si is in each case more reactive than the p-type Si which is in agreement with the foregoing theory.

2. Resistivity of Si used. All mixtures of p-type Si + PbO show increasing values for $\bar{Q}$ with resistivity (decrease in $\bar{Q}$ with conductivity) and in its reaction with PbO$_{Li}$ shows decreasing $\bar{Q}$ values with resistivity, which is consistent with Theory. The remaining data do not obey this portion of that Theory. See Figs. IV, V, and VI.

3. Type PbO used. The Lithium doped PbO, which is p-type, is consistently more reactive than the Chromium doped PbO, which is n-type. This is consistent with Theory. However, there are two disturbing observations which can be made. Firstly, the Chromium doped PbO is more reactive than the undoped PbO, whereas, Theory predicts that it would be less reactive;

this can possibly be explained if one considers the disparity in ionic radius[23] between the Cr and Pb ions which are 0.52 Å and 0.84 Å, respectively, which gives a ration of R = 1.61. Since the Chromium doped PbO is n-type, the Chromium must enter the PbO lattice to occupy a Pb ion, thus creating an interstital Pb ion. Strain can thus occur from Pb occupying an interstitial position. This possible strain energy could possibly exceed any reduction of the chemical potential, thus, causing the Chromium doped PbO to be more reactive than the undoped PbO. However, this interpretation is inconsistent with thermal analysis data which reveal that the pre-ignition reaction (PIR) for the reaction between PbO_{Cr} + Si is higher than that for PbO undoped + Si. Secondly, the Lithium doped PbO is extremely more reactive than the undoped. One might argue that this indicates a difference in mechanism. However, preliminary investigation of Fig. VII reveals that the mechanism is likely the same in only two instances each reaction apparently proceeds according to:

$$PbO + Si \rightarrow SiO + Pb \qquad (13)$$

except for the Cr-doped PbO + Si reaction.

4. X-ray powder diffraction data, obtained on the reaction products of the plain PbO + Si reaction, indicates the presence of Pb, some unreacted Si, and nothing else. SiO_2 and Silicates should have produced pronounced peaks, whereas, amorphous SiO would produce none. Equation (13) is apparently substantiated.

ACKNOWLEDGEMENTS

The author greatfully acknowledges the assistance of Treva M. Smith, Clyde F. Parrish and William T. Biggs in the conduct and completion of this work.

REFERENCES

1. W. L. Ripley and C. A. Lipscomb, *A Preliminary Investigation of the Reactivity of Amorphous Red Phosphorus*, RDTR No. 110, NAD Crane (1968).
2. Ibid, *A Preliminary Investigation of the Reactivity of Lead Dioxide*, RDTR No. 114, NAD Crane (1968).
3. A. J. Dekker, *Solid State Physics*, Prentice-Hall, Inc., 310-314 (1957).
4. G. M. Schwab and J. Gerlach, Z. Physik, Chem. N. F., 56, 121 (1967).
5. P. J. Holmes, *The Electrochemistry of Semiconductors*, Academic Press, 24-26 (1962).
6. J. A. Altham, J. H. McLain, and G. M. Schwab, Z. Physik. Chem. N.F. 74, 139-145 (1971).
7. M. G. Evans and M. Polanyi, Nature, 530-531,(28 Mar 1936).
8. G. M. Schwab and J. Gerlach, Z Physik, Chem. N. F., 56,121 (1967).
9. H. S. Golinkin, I. Lee, and J. B. Hyne, J. Am. Chem. Soc.,89, 1307-1312 (1967).
10. M. G. Evans and M. Polanyi, Trans. Faraday Soc., 31, 875-894 (1935).
11. Ibid., 32, 1333-1360 (1936).
12. S. Glasstone, K. J. Laidler, and H. Eyring, *The Theory of Rate Processes*, McGraw-Hill, 466-470 (1941).
13. L. P. Hammett, Trans. Faraday Soc., 34, 156-165 (1938).
14. Ibid, Chem. Rev., 17, 125 (1935).
15. G. N. Burkhardt, W. G. K. Ford, and E. Singleton, J. Chem. Soc., 17-25,(Jan. 1936).
16. P. A. Rock, J. Chem. Educ., 44, 104-108 (1967).

17. A. G. Smekal, Proc. of the International Symposium on Reactivity of Solids, S131 (Gotenberg, 1952).

18. G. Naeser and W. Scholz, Kolloid-Zert, 156, 1-8 (1958).

19. K. Hauffe, Ange. Chem., 68, 776-784 (1956).

20. G. M. Schwab and Block, Reunion de Chimie, Paris, (June 1954).

21. O. V. Krylov and S. Z. Roginskii, Kinetika and Dataliz, 1, 15-21 (1960).

22. G. M. Zhabrova, V. I. Vladimirova, and O. M. Vinogradova, Dokl. Akad, Nauk, SSSR, 133, 1375 (1960).

23. L. Pauling, *The Nature of the Chemical Bond*, Third Edition, Cornell University Press.

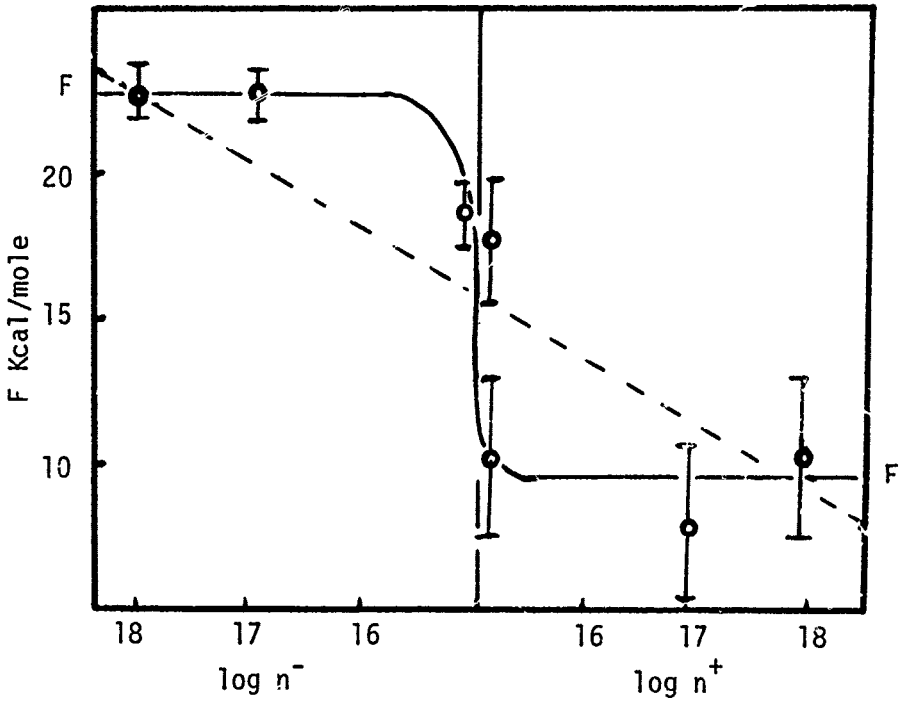

Fig. I. The change of the activation energy of dehydration of C_2H_5OH on Ge as a function of basic charge carriers: donor (log n^-) and acceptor (log n^{-1}) dopants. The change of position of the Fermi level FF with dopant concentration and type is represented by the dashed line (from ref. 4).

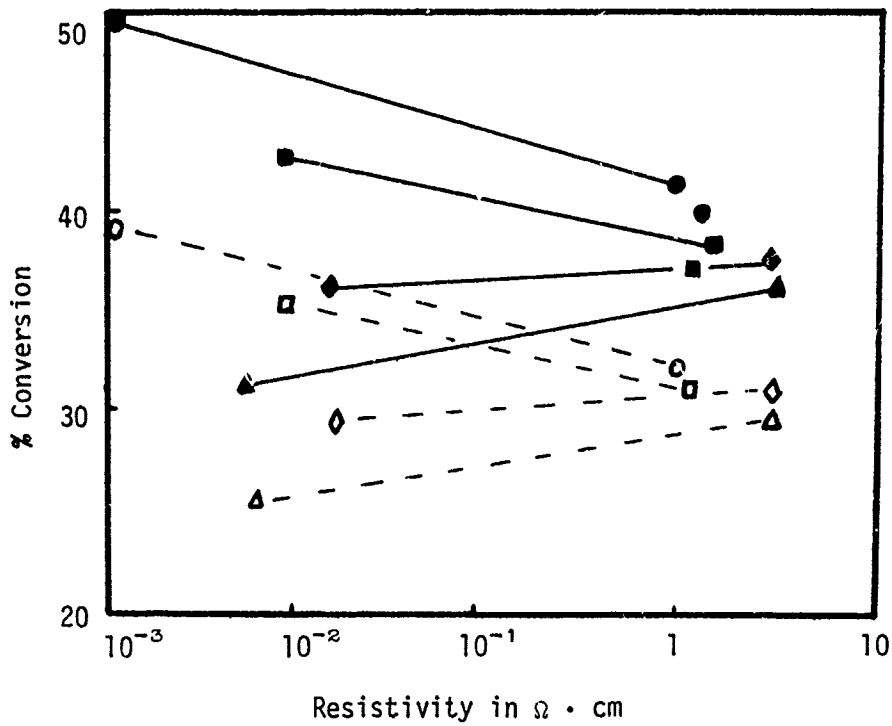

Fig. II. This figure represents the percent conversion to products of the reaction Ge + MoO_3 → GeO_2 + MoO at 496°C for periods of time

----- 10 hr.

——— 20 hr.

The Ge has been doped n-type with ○ As and ▫ Sb and p-type with ◊ In and △ Ga. The MoO_3 has not been doped (from ref. 8).

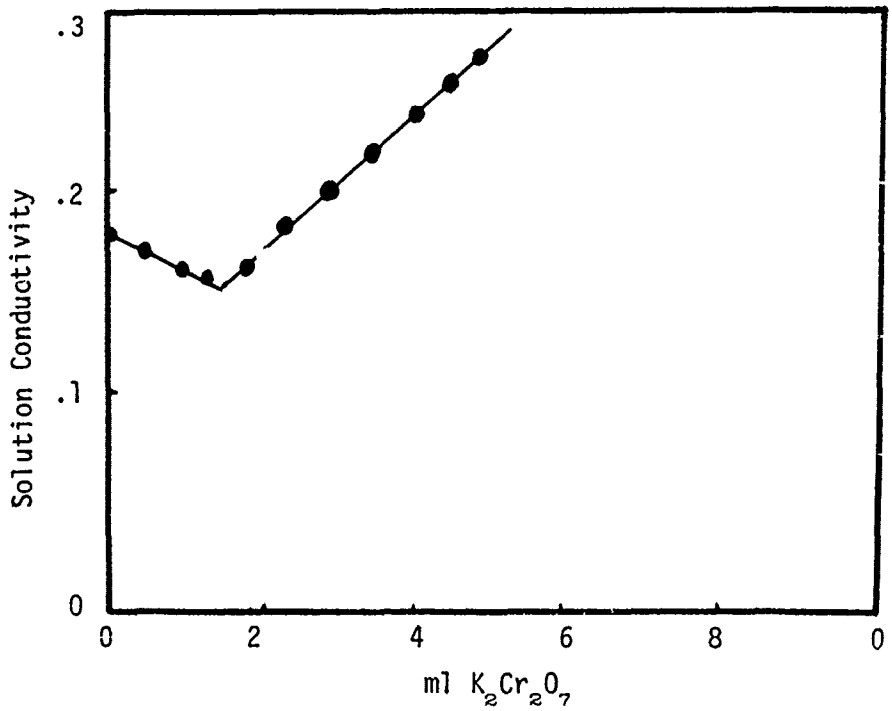

Fig. III. Typical conductimetric titration for lead with .05 N $K_2Cr_2O_7$. Recovered combustion products of Cr^{3+} doped PbO here indicate 89+% conversion of PbO to Pb in the combustion process for a combustion efficiency of 0.97+ for 12:88 Si:PbO

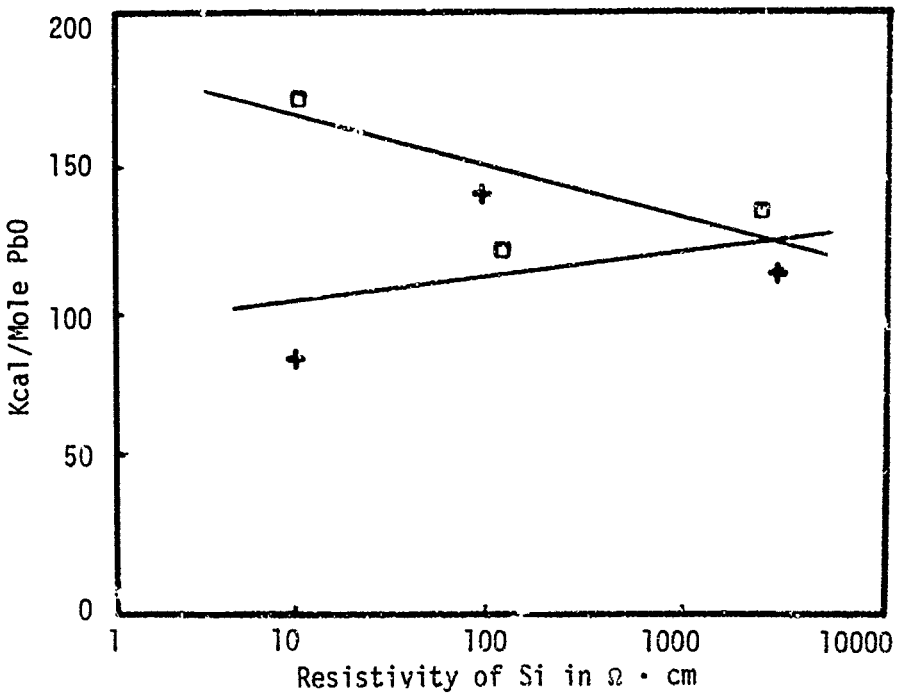

Fig. IV. Effect of type and amount of dopant in Silicon in reaction with 5% lithium doped PbO upon the heat of reaction.

□ n-type Silicon

\+ p-type Silicon

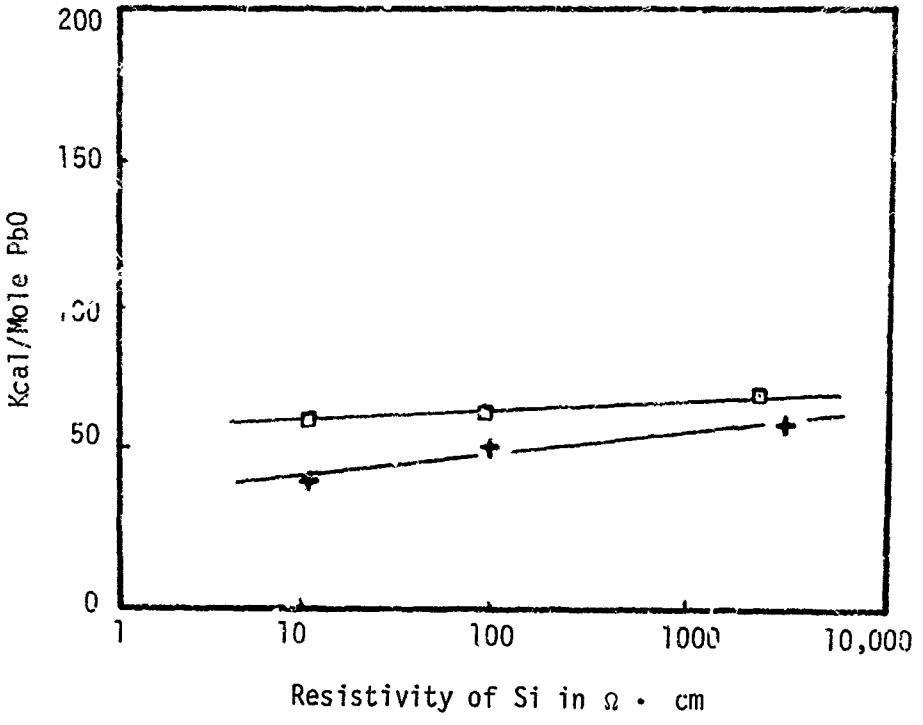

Fig. V. Effect of type and amount of dopant in Silicon in reaction with 5% chromium doped PbO upon the heat of reaction.

□ n-type Silicon

\+ p-type Silicon

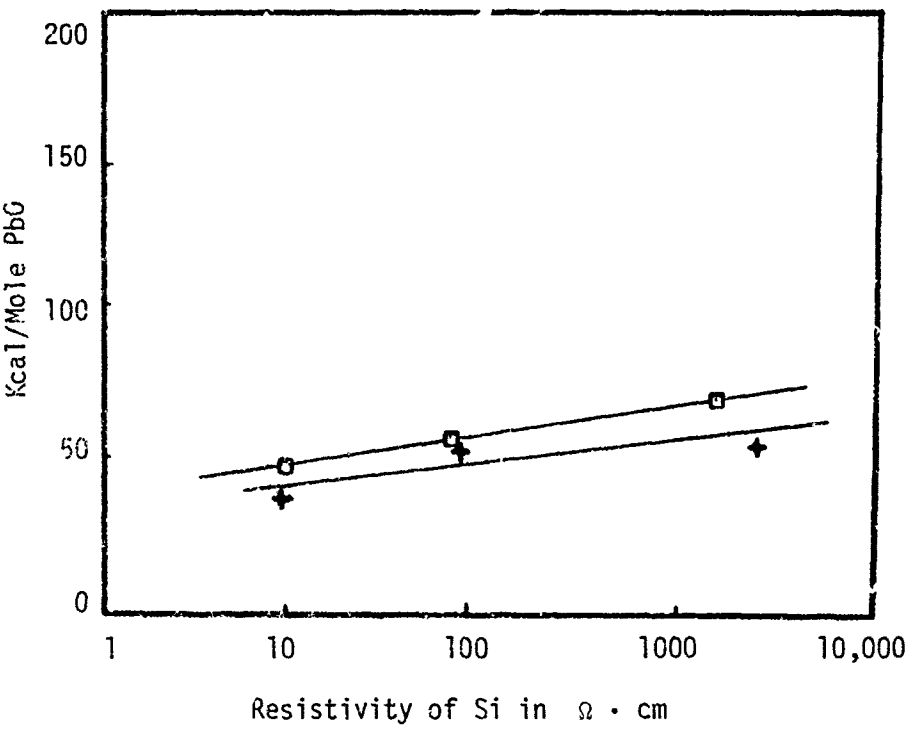

Fig. VI. Effect of type and amount of dopant in Silicon in reaction with undoped PbO upon the heat of reaction.

□ n-type Silicon

\+ p-type Silicon

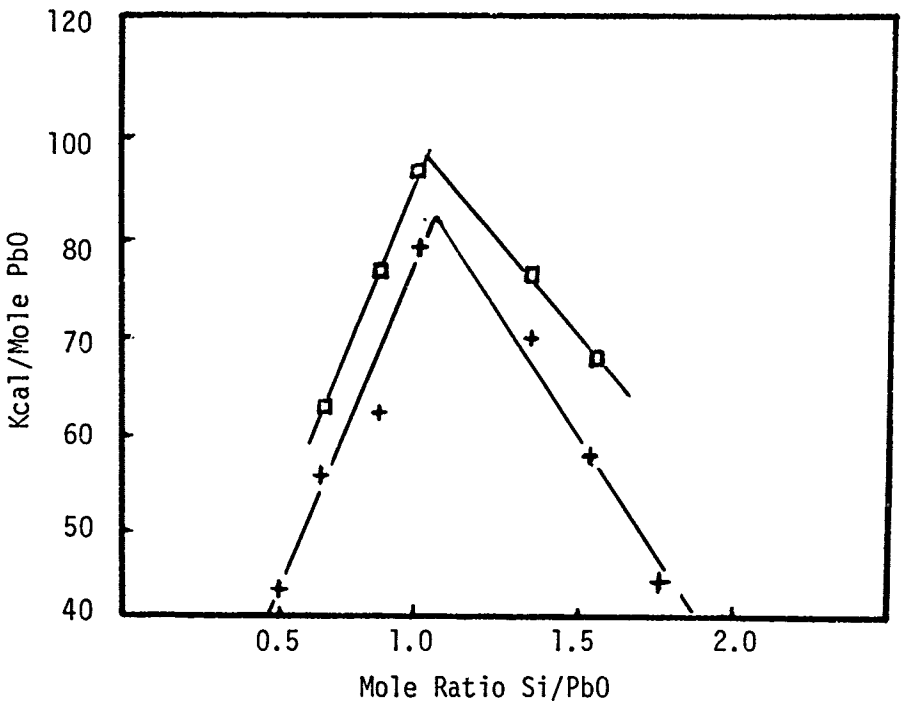

Fig. VII. Effect of dopants on the molar heat of combustion for the reaction PbO + Si → SiO + Pb

\+ Commercial Litharge and Silicon

□ Lightly Lithium doped Litharge and Silicon n-type 10 Ω · cm resistivity.